University of Alberta
Department of Civil Engineering

Structural Engineering Report No. 194

EXPERIMENTAL INVESTIGATION OF THE COMPRESSIVE BEHAVIOR OF GUSSET PLATE CONNECTIONS

by

Michael C.H. Yam

and

J.J. Roger Cheng

September 1993

Structural Engineering Report No. 194

EXPERIMENTAL INVESTIGATION OF THE COMPRESSIVE BEHAVIOR OF GUSSET PLATE CONNECTIONS

by

Michael C.H. Yam

and

J. J. Roger Cheng

Department of Civil Engineering

The University of Alberta

Edmonton, Alberta, Canada T6G 2G7

September 1993

ABSTRACT

Gusset plate connections are commonly used in bridge trusses and braced steel frames to transfer forces from one structural member to another. Due to the complexity of these connections, it is extremely difficult to evaluate the strength of gusset plate connections. Hence, the compressive behavior and ultimate strength of gusset plate connections was examined by testing full-scale diagonal bracing connections. A total of twenty-one tests were conducted on nineteen specimens. The test parameters included gusset plate thickness, size, brace angle (30° and 45°) and out-of-plane restraint boundary conditions. In addition, the effects of frame action on the compressive behavior of gusset plate connection was also investigated by applying beam and column moment to the specimens. Out-of-plane loading eccentricity, which happens frequently in tubular bracing member with a slotted-in splice plate, was also examined by testing three eccentrically connected specimens. In general, the gusset plate specimens failed by sway buckling of the connection. However, for the specimens tested with out-of-plane restraint local buckling of the free edges was observed. The failure mode of the eccentrically loaded specimens was yielding of the splice member at the conjunction of gusset-to-splice. In general (except the EP type specimens), the test results indicated that significant yielding of the gusset plate specimens was observed prior to reaching the ultimate load. However, for the specimens with a plate thickness of 6.5 mm only slight yielding was observed. The ultimate load of the specimens increased with increasing plate thickness and decreased with increasing plate size. The out-of-plane restraint boundary condition had negligible effects on the ultimate load of the compact specimens (500 x 400), however, the ultimate load of the slender specimens (850 x 700)increased when out-of-plane restraint was applied. Slight decreased in ultimate load of the specimens was observed when a 30° brace was used instead of a 45°. The beam and column moment only had negligible effects on the ultimate load of the specimens , however, yielding of the specimens was detected at a load level significantly

lower than that predicted by the Whitmore method. The out-of-plane loading eccentricity reduced the ultimate load of the specimen significantly.

TABLE OF CONTENTS

1. Introduction

1.1 General

Gusset plate connections are frequently used in bridge trusses (Fig. 1.1) and braced steel frames in heavy industrial buildings. Typical braced frames, which are designed to resist lateral loads produced by wind and/or earthquake loads, are shown in Fig. 1.2. Depending on the particular connection detail, gusset plate can be either bolted or welded to the diagonal bracing member and to the main framing members. The diagonal bracing member may transfer either tensile or compressive load to the gusset plate according to the type of bracing system. Even though it is usually assumed that members of a gusset plate connection are loaded in their axial direction, however, the delivery of these loads from the bracing member to the framing members through the gusset plate will produce bending, shear and normal force in the gusset plate.

Although gusset plate connections are widely used in a variety of steel structures, current Canadian bridge design standard CAN/CSA-S6-88 only provides design philosophy and have no specific methods and formulas to design gusset plates. The conventional method of designing gusset plate (Kulak et al. 1987) is based on beam formula and elastic analysis together with the engineer's intuition, past practice and experience. Recently, both the CAN/CSA-S16.1-M89 and AISC -LFRD specification (1986) provide a set of formulas developed by Hardash and Bjorhovde (1985), which are based on block shear concept, to design gusset plates subject only to tension.

Recent research on the behavior and design of gusset plate connections (Hardash and Bjorhovde 1985, Williams and Richard 1986) concentrated on gusset plates loaded in tension. When gusset plates are subject to compressive loads; local buckling of the gusset plate free edges and local crippling of the gusset plate area near the end of the diagonal bracing member have to be examined. Due to the geometry of the connection, the

boundary conditions and complicated by the fact that stability failure may occur in the gusset plate caused by compressive loading applied to the connection, the compressive strength of the gusset plate connection is extremely difficult to evaluate. To date (1993) only limited amount of research work on the compressive behavior of gusset plate connections (Hu and Cheng 1987, Gross 1990, Chakrabarti and Richard 1990, Cheng, Yam and Hu 1993) is available. Both experimental and analytical research work are still insufficient to provide a complete design guideline and recommendations for designing gusset plate connections loaded in compression. Hence, a research program was initiated to investigated the compressive behavior and strength of gusset plate connection.

1.2 Objective and Scope

Based on the above discussion, it can be seen that much research work has to be done in the area of compressive strength and behavior of gusset plate connections in order to provide rational design guidelines and recommendations to the design engineer. Therefore, a research program was initiated to investigate experimentally the strength and behavior of gusset plate connection subject to compressive loads. The objectives of the program are following:

1) To provide experimental data for the behavior of gusset plate connection loaded in compression.

2) To evaluate the effects of the following variables on the compressive behavior and ultimate strength of gusset plate connections:

i) gusset plate size and thickness

ii) out-of-plane restraint at base of test frame (refers to test setup scheme I in chapter 2)

iii) brace angle

iv) beam and column moments

v) out-of-plane loading eccentricity.

3. To examine the inelastic as well as elastic compressive behavior of gusset plate connection.
4. To compare the test results to the current design methods.
5. To identify specific areas for further experimental investigation.

A total of twenty-one tests are performed on nineteen specimens. Due to the significant number of test parameters, the scope of the program is limited to the following:

1. Single gusset plate connections of a braced steel frame were considered.
2. Three gusset plate thicknesses (13.3 mm, 9.8 mm and 6.5 mm) and two bracing angles (45° and 30°) were examined.
3. Only gusset plate with a rectangular shape was investigated. A practical size of 500 mm x 400 mm gusset plate was chosen to study the effects of various test parameters. A larger plate size of 850 mm x 700 mm was included for comparison.
4. The effect of framing members on the compressive behavior of gusset plate was examined. However, the influence of the axial force in the framing members was neglected. Two beam and column moment levels were considered and the ratio of column moment to the beam moment was kept at 0.5.

1.3 Literature Review

Prior to the investigation by Whitmore in 1952, gusset plates were designed on the basis of simple beam theory combined with experience, general practice and engineers' intuition. Whitmore (1952) performed tests of gusset plates prototype of a bottom chord connection in a Warren truss as shown in Fig. 1.1. He investigated the elastic stress distribution in the gusset plate by using wire-bond strain gauges, brittle lacquers and photoelastic procedures. He found from the tests that the maximum tensile and compressive stresses in the gusset plate were near the ends of the tension and compression diagonals, respectively. He also concluded that the use of simple beam theory to analyze gusset plate led to erroneous

predictions as shown in Fig. 1.3. Based on the tests results, Whitmore proposed the well known effective width concept to approximate the maximum normal stresses existed near the ends of diagonal members. The effective width of the gusset plate was defined as the length of the line passing through the bottom row of fasteners and intercepted by two 30° lines originated at the outside fasteners of the first row of the diagonal. The maximum normal stress was then calculated on the effective width. This concept is illustrated schematically in Fig. 1.4. This method of analyzing gusset plate connection is widely used in practice today. For this particular report, the Whitmore load is defined as the static yield strength of the material multiplied by the effective width and the thickness of the gusset plate.

Additional experimental work on gusset plate were made by Irvan (1957) and Hardin (1958). Irvan investigated the general stress distribution in a double gusset plates prototype of a Pratt truss. He basically had similar findings as Whitmore except that he modified slightly the Whitmore's effective width concept. He proposed to extend the 30° lines from the center of gravity of the rivet group instead of from the outside fasteners of the first row of bolts as suggested by Whitmore (1952). Hardin's work in 1958 substantiated the findings by Irvan. Davis (1967) and Vasarhelyi (1971) used the finite element method to analyze the gusset plate connection. Davis's results confirmed Whitmore's experimental findings. Vasarhelyi tested a lower chord joint in a simple Warren truss. He then employed the finite element method to analyze the test specimens. He found that maximum normal stresses evaluated by various simplified methods were only slightly different from the analysis. However, the location of those maximums might vary quite significantly.

Analytical work performed by Struik (1972) involved the use of elastic-plastic finite element program which could take into account the gusset plate behavior in the inelastic range. To estimate the effects of bolt holes in the gusset plate, Struik included the linear

portion of the load deformation relationship of the fasteners in the analysis. The result of his studies indicated that current design procedures produced a large and variable margin of safety against the ultimate gusset plate capacity. Bjorhovde (1985) performed full-scale testing of diagonal bracing connection to evaluate the behavior and ultimate strength of gusset plate in tension. A total of six tests were performed with two different thickness (3 mm and 9 mm) and three different angles of bracing (30°, 45°, and 60° measured from the beam axis). He observed from the tests results that the primary failure mode was tearing across the last row of bolt holes of the gusset plate at the end of the splice plates. He also found that plate buckling due to secondary effects might be a significant factor in developing the design criteria for gusset plates

Richard et al. (1983) performed finite element analysis to model the diagonal bracing used in Bjorhovde's experimental work. To include both the material and geometric nonlinearity of the complete connection, load deformation relationships of the fasteners, bolts, weldments and double framing angles determined from physical tests were used in the finite element analysis. The measured strains from the tests compared well with the analytical predictions at areas of low strain gradients. However, the predictions at areas of high strain gradient differed significantly from the test results. This difference might be attributed to the improper mesh size in the finite element model.

Hardash and Bjorhovde (1985) performed a series of gusset plate tests aimed at developing an ultimate strength design criteria for gusset plate connection loaded in tension. Based on the test results, they modified the block shear concept of coped beam-to-column connections into the ultimate tensile strength model for gusset plate. This modified block shear concept incorporated the ultimate tensile stress on the net area between the bolts of the last row and an uniform effective shear stress on the gross area along the outside bolt lines as shown in Fig. 1.5.

So far, the above discussions mainly concern the in-plane stress distribution and tensile behavior of gusset plate connections. When gusset plate is subject to compression, the problem of instability must be addressed. Williams and Richard (1986) performed elastic buckling analysis of gusset plates. They investigated the compressive behavior of gusset plate by excluding the beam and column framing members from the analysis. They assumed that the bracing member would not buckle and the brace-to-gusset connection was restrained from out-of-plane translations. The parameters examined were types of bracing (single brace and K brace), brace angle, edge support, finite element mesh size and plate size. They concluded from the finite element analysis that fixed edge supports increased the buckling strength of gusset plate significantly when comparing with simply supported edge conditions. They also found that K-bracing gussets had higher buckling strength than single-bracing gussets. Typical buckled shapes of a 45^{o} angle single-brace gusset plate are shown in Fig. 1.6. They also demonstrated that frame action could affect the behavior of gusset plate significantly.

Hu and Cheng (1987) investigated the compressive behavior of gusset plate connections in the elastic range by testing full-scale diagonal bracing similar to Bjorhovde's tests (1985). A schematic of the test setup is shown in Fig. 1.7. As can be seen from this figure, the effects of the framing members on the gusset plate were neglected in the testing program. The test series consisted of six specimens with plate thickness and plate size as primary variables. The plate thicknesses examined were 6.7 mm and 3.11 mm and the plate sizes examined were 850 x 550 and 850 x 700. The effects of load eccentricity were also investigated in this program by testing six eccentrically loaded specimens. The test results showed that for the concentric loading cases the primary failure mode for the gusset plate was elastic buckling of the longer free edge of the plate. Depending on the out-of-plane restraints of the framing members, either local buckling or overall buckling of the gusset plate might occur. For the eccentric loading cases, failure was initiated at the splice plate

due to excessive yielding. The beam-column formulas of a rectangular section,

$$\left(\frac{P}{P_y}\right)^2 + \left(\frac{M_{pc}}{M_p}\right) = 1.0 \qquad [1.1]$$

where P is the applied axial load, P_y is the yield load of the section, M_{pc} is the applied bending moment and the M_p is the plastic moment capacity of the section, was employed to evaluate the strength of the ecccentrically loaded specimens. Reasonable predictions of the strength of the specimens were obtained by the beam-column formula.

The maximum elastic normal compressive stress in the gusset plate obtained from the tests agreed quite well with Whitmore's predictions. However, using Whitmore's effective width concept to predict the test results would produce unconservative estimates since the primary failure mode of the gusset plate was elastic buckling. The finite element program BASP was used to investigate analytically the elastic compressive behavior of gusset plate. The finite element solutions showed reasonable agreement with the test results. It was also found from the parametric studies by BASP that the rotational restraint from the boundary elements, the bending stiffness of the splice plates and the distance between the end of the splice plate and the beam-column boundary affected the elastic buckling strength of gusset plate significantly.

Cheng et al. (1993) performed additional analysis of the test results from Hu and Cheng (1987). The finite element program ANSYS was employed to perform the analysis. Reasonable predictions of the elastic buckling load of the test specimens were obtained. It was also found from the analytical results that the elastic buckling strength of the specimens increases with increasing splice member connection length or splice member thickness. In addition, a large deflection analysis was performed on the specimen with a plate thickness of 3.11 mm. It was found from the large deflection analysis that postbuckling strength existed in the specimen and the analytical load deflection curve agrees well with that of the test.

Recently, Yamamoto et al. (1988) investigated the buckling strength of gusseted truss joint of the Warren type. Eight specimens with four different types of gusseted truss joints were tested. Strain gauges, rosette gauges and photoelastic coatings were used to measure the development of the plastic zone and strain distribution in the gusset plate. It was shown in the test results that all specimens yielded before reaching the buckling load. The buckling load in these particular tests was estimated at the load which caused strain bifurcation to occur in the gusset plate due to bending. Based on this test observation, they concluded that the buckling strength of the gusset plate specimens could be evaluated by only considering the elastic buckling load of a triangular area of the gusset plate which remained in elastic range prior to buckling with various boundary conditions. The buckling analysis was then performed by the finite element method which utilized the eigenvalue formulation. A design equation for the test specimens was then proposed based on the analytical study. The test results also showed that the ratio of ultimate load to initial buckling load varied from 1.2 to 1.7 which was attributed to the postbuckling strength of the gusset plate connection.

The most recent (1990) experimental investigation of full-scale gusseted connections loaded in compression was performed by Gross. The testing program consisted of three diagonally braced steel subassemblages as shown in Fig. 1.8. All the gusset plate specimens were 6.35 mm thick. The two main objectives of the testing program were:

1. to investigate the interaction between the intersection of the beam-column centroidal axes and the line of force in the diagonal member.
2. to investigate the orientation of the column strong axis in relation to the plane of the braced frame.

As can be seen in Fig. 1.8, Gross test setup took into account the effects of the framing members on the gusset plate. According to Williams and Richard (1986), frame action influenced the gusset plate behavior significantly. However, the test setup did not permit

the out-of-plane translation of the bracing member which might have significant effect on the buckling strength of gusset plate. The test results showed that the primary failure mode of the gusseted connection was gusset plate buckling. Gusset plate tearing was observed only in the weak axis column connected specimen. All specimens exhibited yielding before reaching the ultimate load. The first yield load of the specimens agreed well with Whitmore's predictions. For specimens failed in plate buckling, the ratio of the ultimate load to the first yield load ranged from 2.08 to 2.32. Fung and Richard (1987) analyzed the test specimens by an inelastic finite program, INELAS. The analytical solutions compared well with the measured stress distribution. No attempt was made to determine the inelastic buckling strength of the gusset plate specimens by the finite element method. To estimate the inelastic buckling load of the specimens, Gross used the procedure proposed by Thornton (1984) which will be discussed later in this review. Nevertheless, the buckling loads of the gusset plates evaluated by Thornton's method were very conservative. The ratio of the ultimate load to the predicted buckling load for the two specimens were 1.5 and 1.7.

1.4 Current Design Methods

As mentioned earlier, the current design specifications (S16.1 and S6) do not have any specific formulas to evaluate the compressive strength of gusset plate load in either in tension or compression. However, some design provisions are recommended in the S6 standard. The conventional method of designing gusset plate is to assume that load distribution among the fasteners are equal, hence, the required number of fasteners can be determined. The gusset plate configuration is then selected to accommodate all the connecting elements and fasteners. Then, stresses are checked at the weakest and critical sections by beam formulas (Gaylord 1992). The normal stress in the gusset plate should also be checked by the Whitmore's effective width concept.

In CAN/CSA-S6-88 the factor shear resistance (V_r) of gusset plate is determined by the following equation:

$$V_r = 0.50\phi A_g F_y \qquad [1.2]$$

where ϕ is resistance factor, A_g is gross area and F_y is the specified minimum yield strength of the material. The CAN/CSA-S6-88 also states that gusset plate shall have ample thickness to resist shear, direct stress and flexure at the most weakest and critical section. It also includes a provision to limit the ratio of the unsupported edge of the gusset plate to its thickness to $945/\sqrt{F_y}$ in order to avoid local buckling of gusset plate subjected to compression.

An alternate method proposed by Thornton (1984) to evaluate the buckling load of gusset plate is to consider an imaginary fixed-fixed column strip of unit width below the Whitmore effective width in the gusset plate as shown in Fig. 1.9. The buckling strength of the gusset plate is estimated to be the compressive resistance of the imaginary column strip. The length of the column strip is the maximum of L_1, L_2 and L_3. Once the length of the column strip has been established, the compressive resistance of the column strip can be evaluated according to CAN/CSA-S16.1-M89. The effective length factor, k, was recommended to be 0.65. The gusset plate will not buckle if the compressive resistance is greater than the normal stress on the Whitmore effective area. It should be noted that the Thornton method does not take into account the effects of plate action since a column buckling formula was employed. Besides, this method would not be appropriate if significant yielding occurs generally in the plate prior to buckling because the column buckling formula only considers the column strip underneath the effective width.

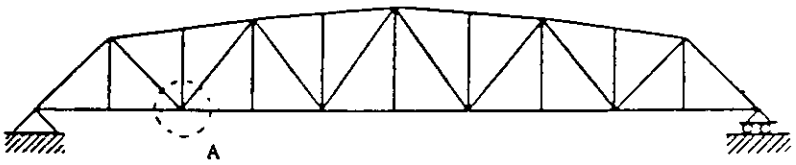

Truss Outline

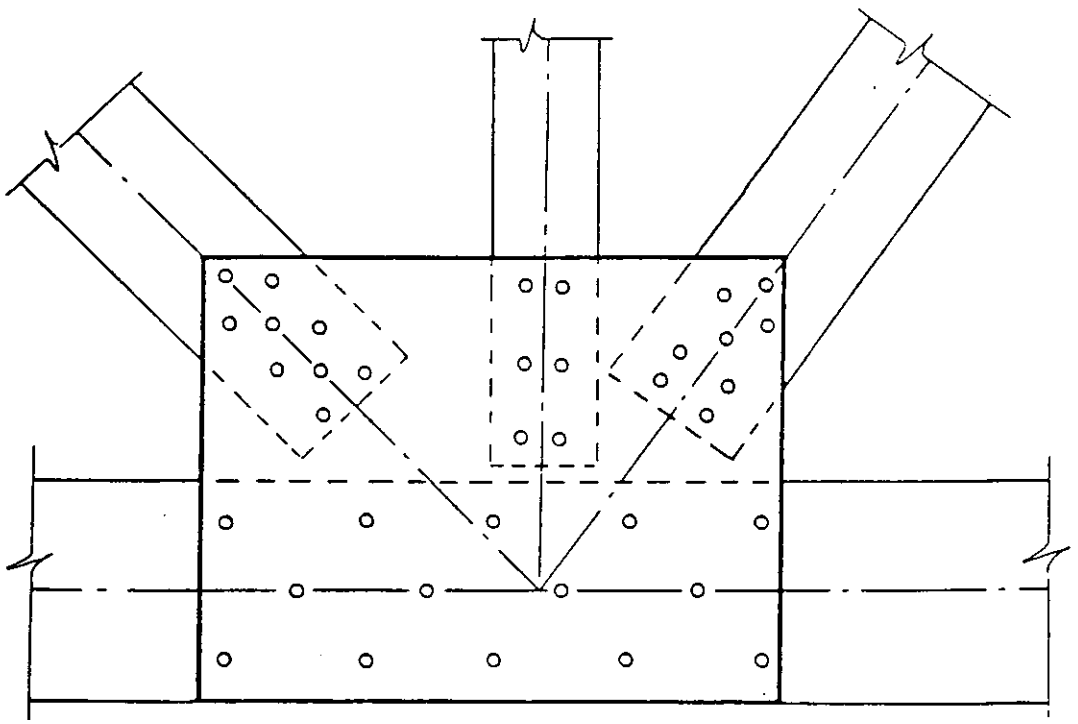

Connection A

Fig. 1.1 Typical Gusset Plate Connection in a Warren Truss

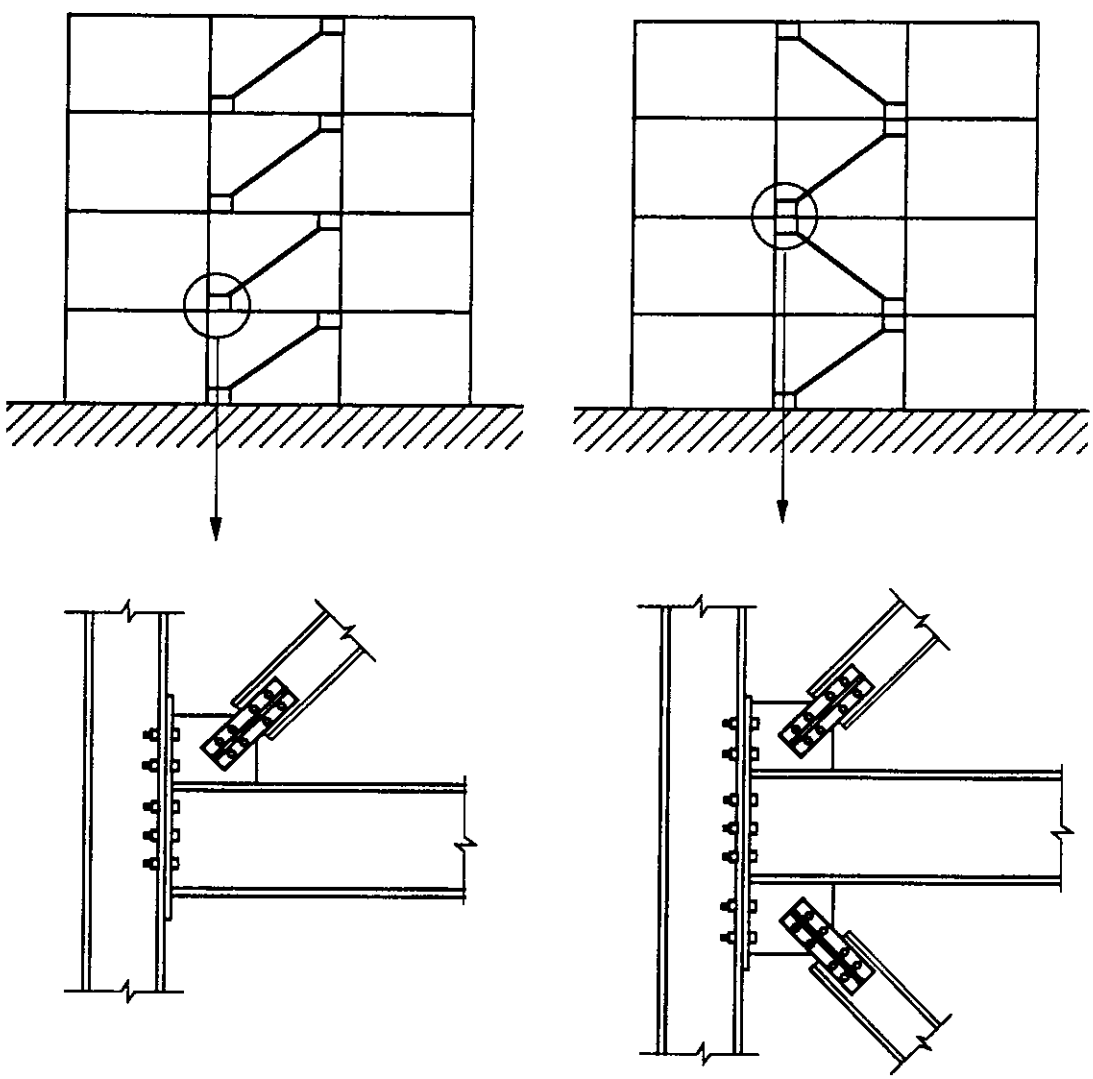

Fig. 1.2 Typical Braced Frames

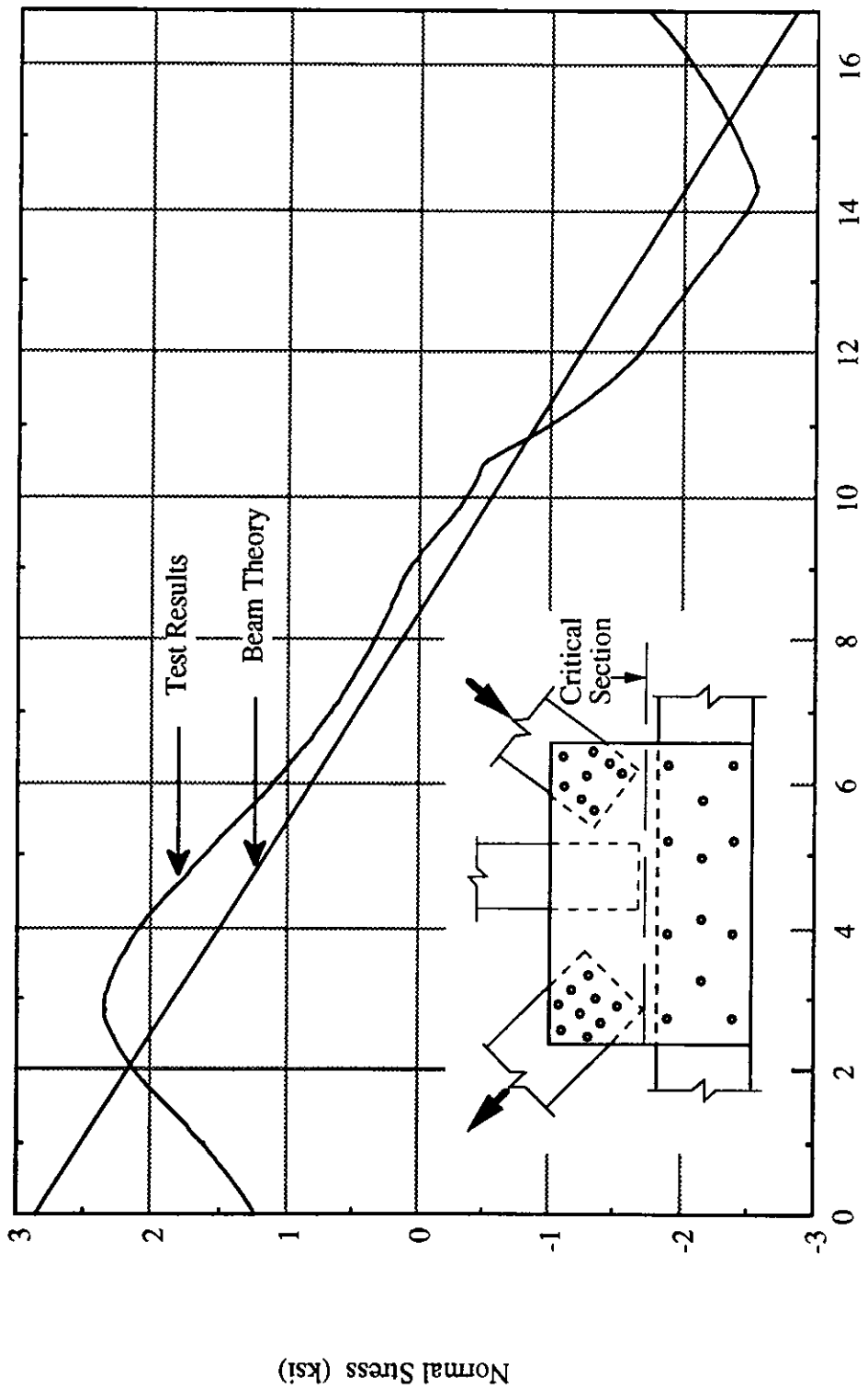

Fig. 1.3 Vertical Normal Stress Distribution Along the Critical Section

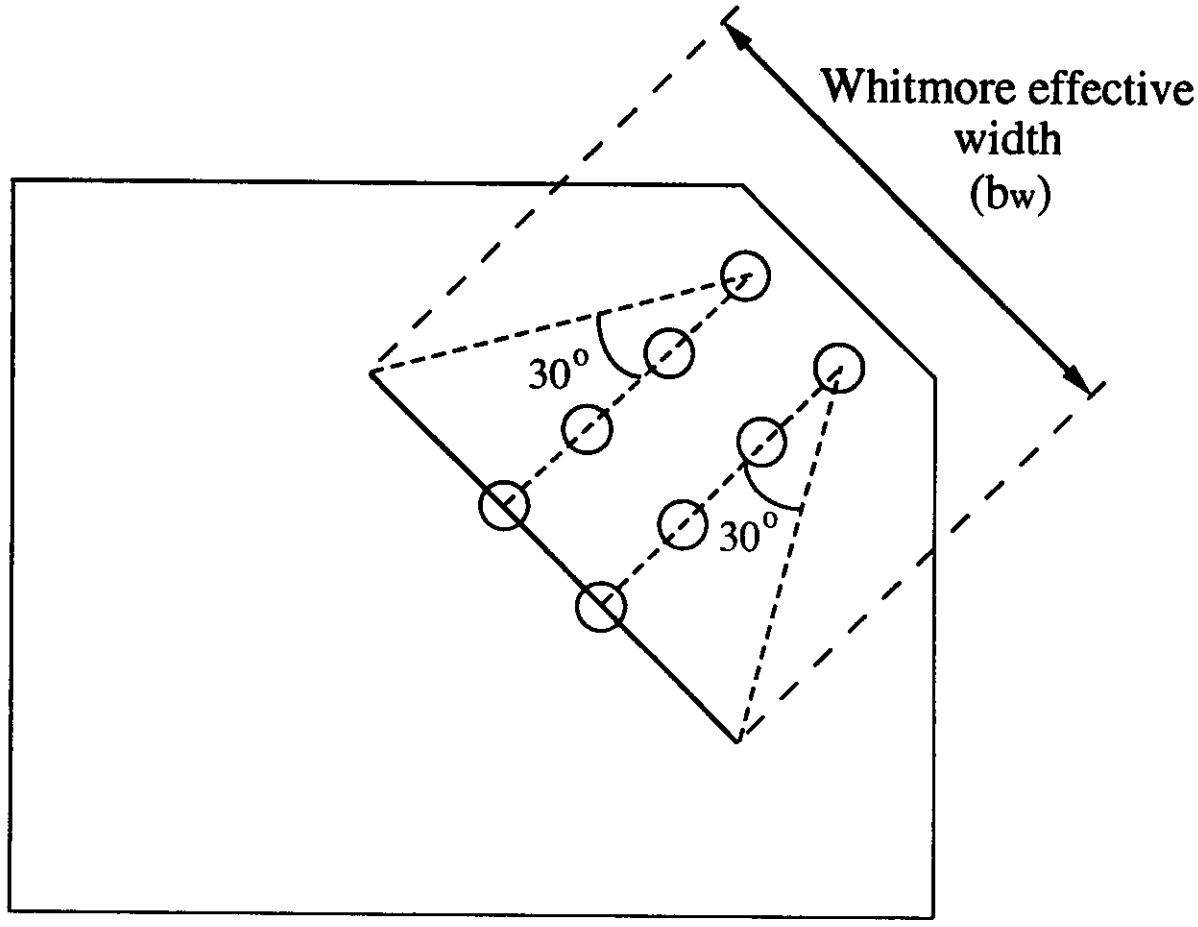

Fig. 1.4 Whitmore Effective Width Concept

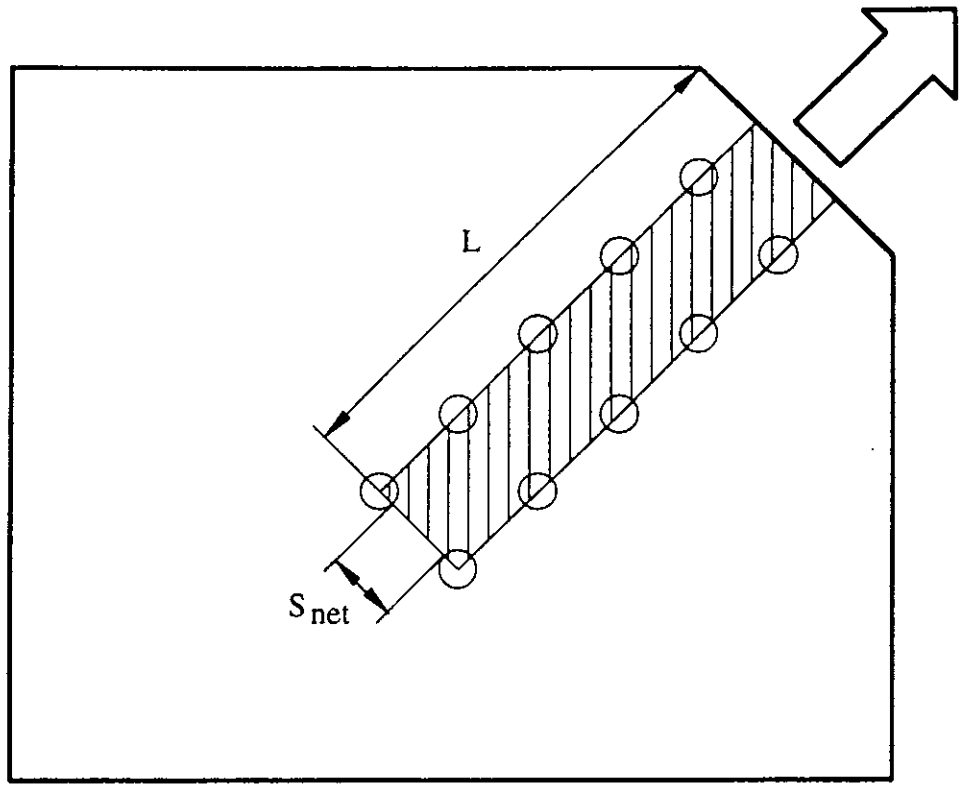

Ultmate Tear-out Resistance, R_n :
(Hardash and Bjorhovde, 1985)

$$R_n = F_u S_{net} t + 1.15 F_{eff} L t$$

Fig. 1.5 Block Shear Tear-out Model

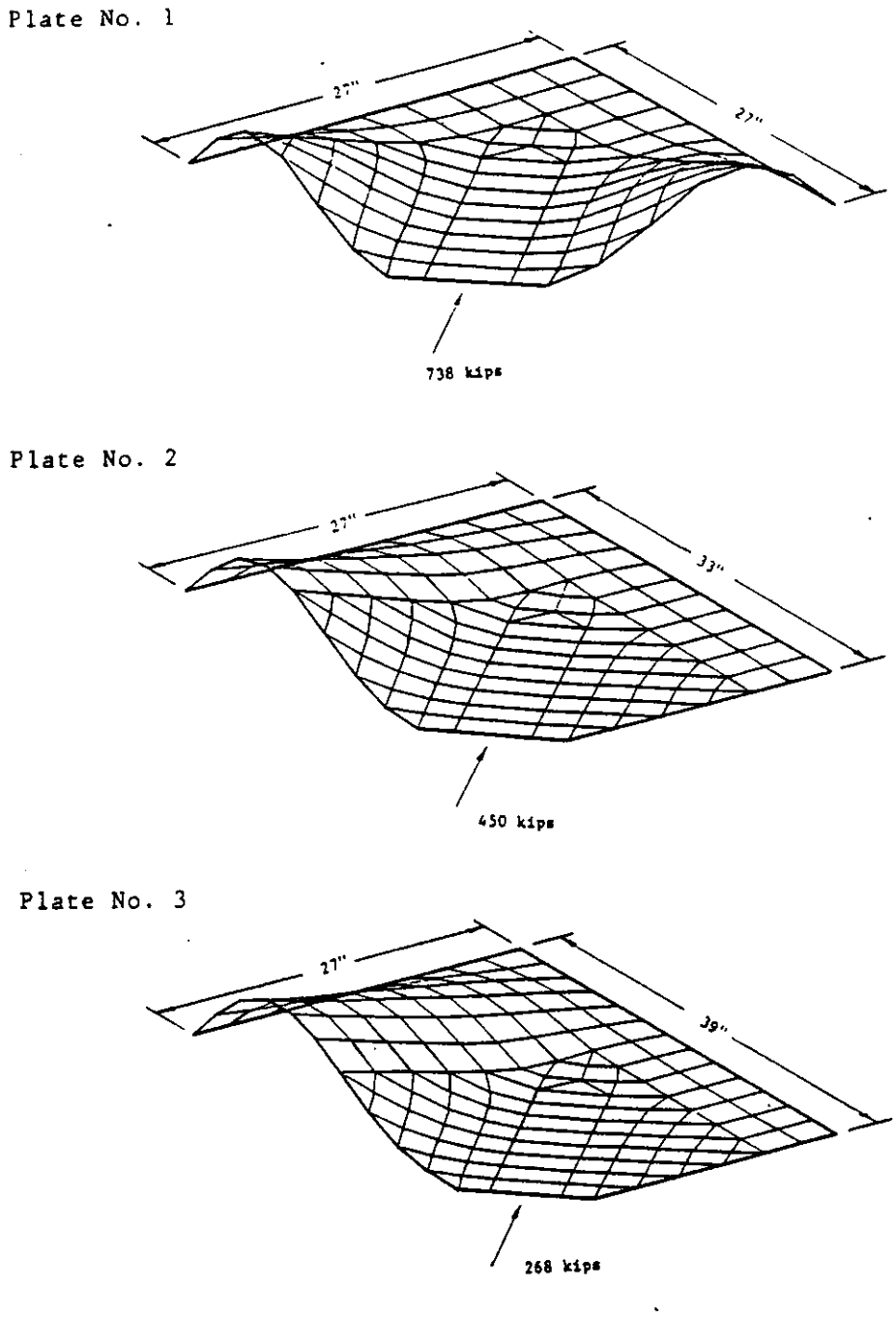

Fig. 1.6 Typical Buckled Shapes for 45° Single Bracing Gusset

(Williams and Richard 1986)

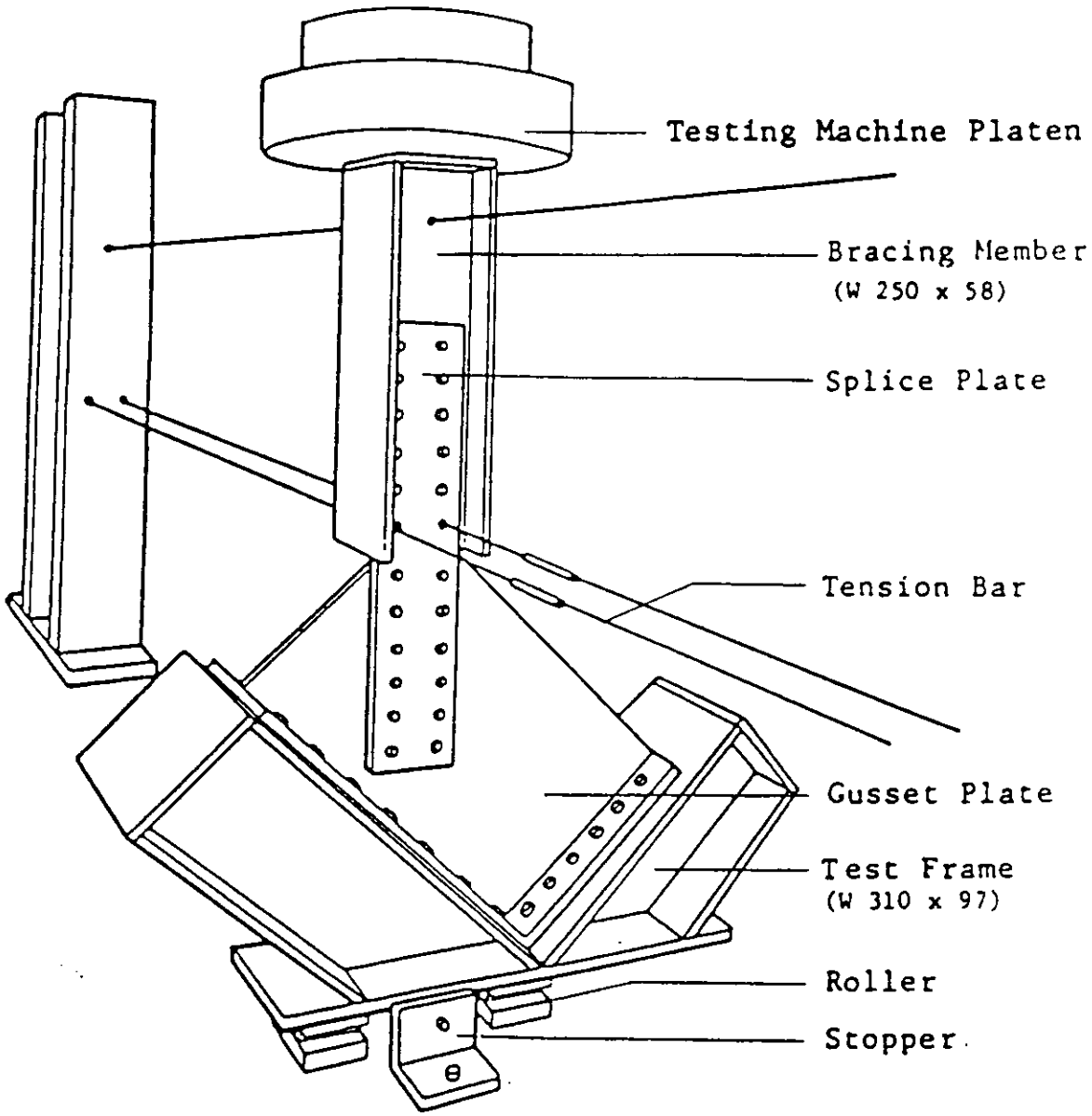

Fig. 1.7 Schematic Test Setup (Hu and Cheng 1987)

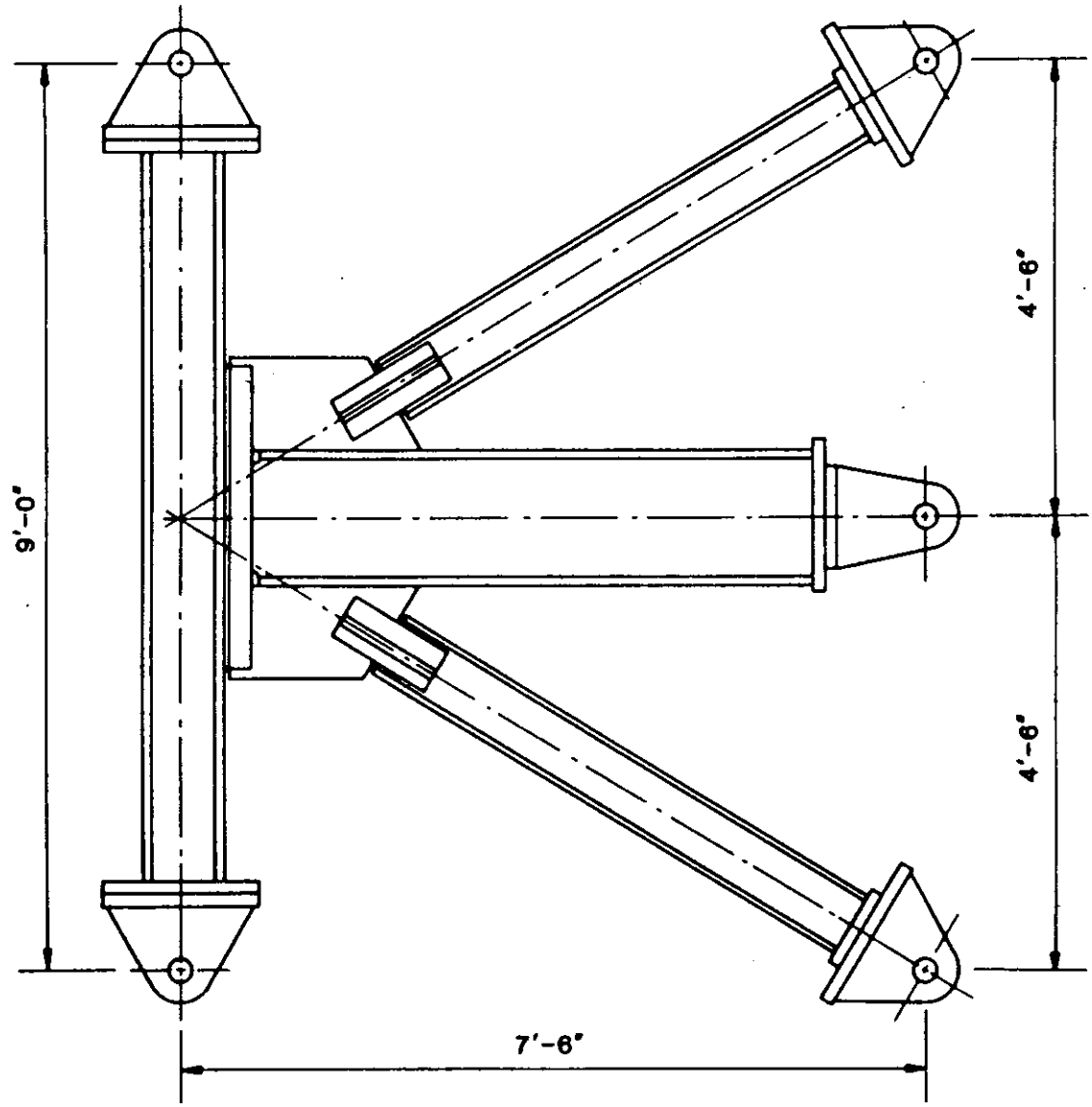

Fig. 1.8 Schematic Test Setup and Specimen Configuration (Gross 1990)

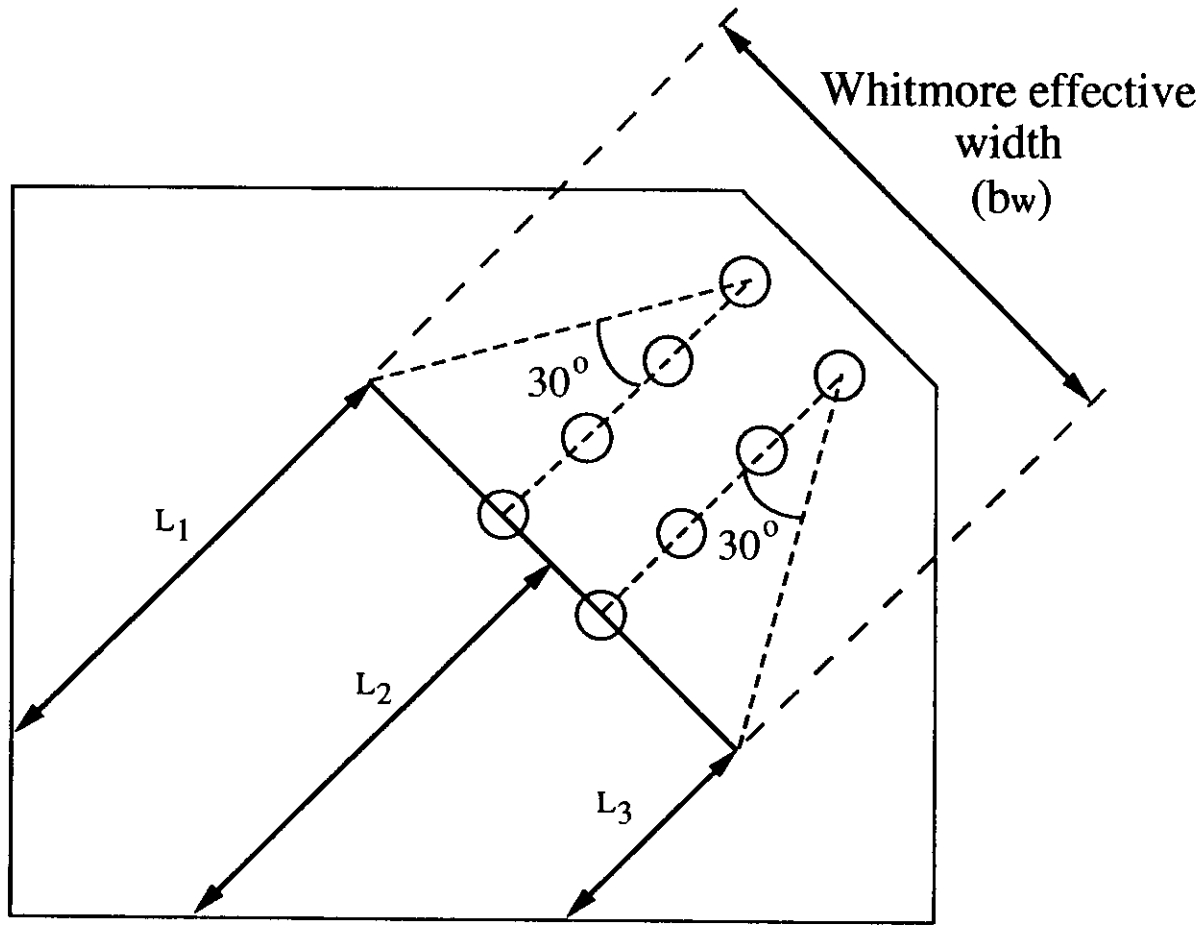

Fig. 1.9 Thornton Method

2. Experimental Program

2.1 Introduction

The design of a bracing system must consider the strength of the framing members, the diagonal bracing members and the gusset plate connections. If the applied load to the bracing system is such that compression exists in the diagonal bracing member, the stability of the gusset plate connection must also be investigated. In this case the gusset plate may fail in buckling of the free edges, local buckling and/or crippling at the gusset plate area directly beneath the splice member. The ultimate compressive strength of the diagonal bracing member can be readily evaluated using the CAN-3-S16.1-M89. However, it is very difficult to evaluate the ultimate compressive strength of the gusset plate due to the complexity of the connection. When the ultimate compressive strength of the gusset plate is significantly lower than that of the diagonal bracing member, buckling of the gusset plate may occur prior to the stability failure of the bracing member. Hence, the bracing member may behave as a restraining member and provide rotational restraint to the gusset plate. It is assumed in this testing program that the bracing member provides infinite rotational restraint to the gusset plate connection and the gusset plate fails before the ultimate strength of the bracing member is reached.

2.2 Scope

The main purpose of this testing program was to examine the compressive behavior of gusset plate connections. In order to simulate the actual behavior of gusset plate connections, full-scale testing on diagonal bracing connection was employed. Due to the complexity of the problem, only one gusset plate configuration was chosen in the testing program as shown in Fig. 2.1. A total of twenty-one tests were run on nineteen specimens in the entire experimental program. All the specimens were fabricated using CSA G40.21-M87 300W steel. In general, the experimental program consisted of two groups of

specimens. The first group of the specimens only considered the "isolated" compressive behavior of gusset plate connections. That is, the framing members, to which the gusset plate was attached, was excluded from the test parameters. The test variables included in this group were the gusset plate size and thickness, brace angle, out-of-plane restraint at the conjunction of gusset-to-splice, and the out-of-plane loading eccentricity. Two out-of-plane restraints were considered, namely; the "without-restraint" condition and the "with-restraint" condition. These two boundary conditions will be discussed in the section of test setup. The out-of-plane loading eccentricity is produced by loading the gusset plate eccentrically with respect to its own plane which happens frequently in tubular bracing member with a slotted-in splice plate as shown in Fig. 2.2. The actual configuration of these connections will be discussed in later section. A 45° brace angle was used for all the specimens except for the specimens which considered brace angle as a test parameter.

The second group of specimens took into account the effects of the framing members on the compressive behavior of gusset plate connections. However, only the beam and column moments were considered. It was assumed that the axial force in beam and column had negligible effects on the behavior of the gusset plate. The test variables in this group of specimens included the beam and column moment levels and gusset plate thickness. The ratio of the column moment to the beam moment was chosen to be 0.5.

2.3 Specimen Description

In general, there are five specimen designations used in the testing program; namely, GP, SP, AP, MP, and EP. The first alphabet of each designation represents the test variable for each type of specimens. These test variables are G-General, S-Size, A-Angle, M-Moment and E-Eccentricity.

For specimens which only considered the "isolated" compressive behavior of gusset plate connection, two gusset plate sizes and three thicknesses were examined as shown in

Table 2.1. Schematic of the specimens are shown in Figs. 2.3. Similar plate aspect ratio of about 1.25 was maintained for both plate sizes of 500 x 400 and 850 x 700. As can be seen from Table 2.1 that a relative compact gusset plate section was selected for GP type specimens (500 x 400) to ensure that the specimens failed in the inelastic range. These specimens were employed to examine the general compressive behavior of gusset plate connection particularly in the inelastic range. The GP type specimens and plate thickness tested in this program also represent practical gusset plate dimensions. For the SP type specimens, a larger plate size of 850 x 700 was used to investigate the size effect. However, only two plate thicknesses were considered (9.8 mm and 13.3 mm). For the specimen with out-of-plane loading eccentricity (EP type) only one gusset plate specimen (500 x 400 x 13.3) was fabricated. However, three tests were conducted with the same specimen by varying the type of splice member used to connect the specimen to the brace. Different types of splice member used with the EP type specimens will be discussed in the following section. The loading eccentricity of the specimens is shown in Table 2.1. A 45° brace angles was used for the GP, SP, MP and EP type specimens. For the AP type specimens, a brace angle of 30° was used. The gusset plate size and thicknesses used for the AP type specimens were identical to that of the GP type specimens. In addition, the effect of out-of-plane restraint conditions at the conjunction of gusset-to-splice was also examined for the GP and SP types specimens. Two restraint conditions were investigated, namely the "without-restraint" condition and the "with-restraint" condition. These restraint conditions will be discussed in the section of Test Setup. To distinguish between these two restraint conditions, a letter R (restraint) was added to the specimen designation. For example, specimen GP1R implied same geometric configuration as specimen GP1 and "with-restraint" condition was incorporated. For the SP type specimens, same specimens were used to conduct the tests of both restraint conditions since it was believed that the tests of the "without-restraint" would not caused significant damage to the specimens.

For the specimens which incorporated the effects of beam and column moments, a specimen size of 500 x 400 was chosen with plate thickness varied from 6.5 mm to 13.3 mm as shown in Table 2.1. These specimens were designated as MP type specimens. The specimen shape was identical to the GP type specimens as shown schematically in Fig. 2.3. As can be seen in Table 2.1, three 6.5 mm thick specimens were used to investigate the effects of moment levels. The applied beam and column moments to the specimens are also shown in Table 2.1. Two moment levels were investigated; namely, beam moments of 250 kN·m and 375 kN·m. The ratio of the column moment to the beam moment was kept as 0.5 for all the tests. A 45° brace angle was used for the MP type specimens and only the "without-restraint" condition was examined.

The arrangements of the splice members for all the specimens are illustrated in Table 2.2. Two tee sections (WT125x22.5) and two 13.0 mm thick plates were used as the splice member for the GP, SP, MP and AP types specimens to ensure that the gusset plate failed before the failure occurred in the splice member. These splice members are shown schematically in Fig. 2.4. This figure also illustrates the direction and orientation of the splice member which are important when examining the test results. For EP type specimens, the splice plate thickness (9.5 mm and 12.7 mm) and type was varied. In particular, specimen EP3 was tested with a splice member consisted of a tee-section (WT125 x 22.5) and a 9.5 mm plate. A schematic of the splice member is shown in Fig. 2.5. This splice member arrangement was employed to simulate the eccentricity produced by a tubular bracing member with a slotted-in splice plate as shown in Fig. 2.2. Eight ASTM A325-M22 bolts were used to connect the splice member to the GP AP, MP and EP type specimens. For the SP type specimens, however, twelve M22 A325 bolts were used. All the bolted connections were installed by an air impact wrench using the turn-of-nut method. All the specimens were directly welded onto the beam and column. After each tests, the failed specimen was flame-cut and the surface of the beam and column was ground smooth before welding on the next specimen.

2.4 Test Setup

2.4.1 General

Two test setups were constructed for this testing program, namely; Scheme I and Scheme II , in order to incorporate all the test parameters mentioned above and facilitate the testing program. Scheme I of the test setup was used to perform tests on specimens which excluded the effects of the beam and column moments. On the other hand, Scheme II of the test setup was employed to conduct tests on specimens which included the effects of beam and column moments. The specimens tested in Scheme I test setup were GP, SP, and EP type specimens. Although AP type specimens did not include the beam and column moments effect, Scheme II test setup was used to facilitate the testing of AP type specimens. The MP type specimens were also tested with Scheme II test setup since the main test parameter for this type of specimens was the effects of beam and column moments.

2.4.2 Scheme I

The concept of this test setup was based on Hu and Cheng (1987). When gusset plate buckling occurred in a braced steel frame, the diagonal bracing member may sway out-of-plane as shown in Fig. 2.6a. This figure shows that the free edges of the gusset plate deform out-of-plane along with the diagonal member while the fixed edges of the plate remain in-plane due to the support from the steel frame. This deformation mode of the gusset plate can be simulated by allowing the steel frame to move out-of-plane instead of the diagonal bracing member as shown in Fig. 2.6b. When comparing Figs. 2.6a and 2.6b it can be seen that both arrangements produce the same out-of-plane deformation mode of gusset plate. In order to simplify the test setup, therefore, the arrangement shown in Fig. 2.6b was used as the basis of designing the test frame.

The setup is shown schematically in Fig. 2.7 and the picture of the test setup is shown in Fig. 2.8. The load was applied to the specimens by the MTS testing machine and stroke control was used for all the tests. The vertical displacement of the specimen was also monitored by the MTS. As can be seen in Fig. 2.7, two W310 x 219 sections were used as the stub beam and column members and the diagonal bracing member (W250 x 67) was fixed in place by four tension rods bolted to a set of columns located approximately four meters from the test frame. Sixteen ASTM A325-M22 bolts were used to connect the splice member to the diagonal bracing member. The stub beam and column were bolted to a distributing beam which sat on three sets of rollers to allow out-of-plane movement. Two channel sections were also bolted to the distributing beam and supported on four sets of rollers to provide lateral stability for the test frame as shown in Fig. 2.8. Stoppers were located at approximately 50 mm from both sides of the distributing beam to avoid sudden kicking out of the test frame.

As mentioned from above, two out-of-plane restraint conditions were examined in the testing program , namely the "without restraint" condition and the "with restraint" condition. For the "without-restraint" condition, the distributing beam was allowed to move out-of-plane while the diagonal bracing member was fixed in place by the tension rods. However, for the "with-restraint" condition both the distributing beam and the diagonal bracing member were restrained from out-of-plane movement. Stoppers, which were located at about 50 mm from the distributing beam to prevent sudden kicking out of the test frame, were used to restrain the out-of-plane movement of the distributing beam by supporting a threaded rod which bear against the bottom flange of the distributing beam. The with-restraint condition was used only in the GP and SP type specimens.

2.4.3 Scheme II

The Scheme II test setup for the testing program must allow the application of beam and column moments and axial load in the bracing member in order to conduct tests on the MP type specimens which included the effects of beam and column moments. To properly accommodate these requirements, a test frame and a loading system were designed based on the actual braced steel frame behavior described previously as shown in Fig. 2.6a. A schematic and a picture of the test setup are shown in Figs. 2.9 and 2.10, respectively. This particular test setup was supported by a reaction frame which was bolted and pretensioned to the strong floor. As can be seen in Fig. 2.9, this test setup consisted of a W310x129 column welded on to a 16 mm thick base plate and a W530x101 beam section welded on to a 16 mm thick end plate. Matching bolt holes were pre-drilled in the end plate and the column flange. The end plate from the beam section was bolted to the column flange by twenty-six ASTM A325-M24 bolts. This complete assemblage was then bolted to the floor beam and the floor beam was welded to two channel sections which were bolted to the strong floor to provide the reaction and lateral stability for the setup. A W200x86 section was used for the bracing member and the gusset plate specimen was welded to the beam flange and the end plate. It should be noted that for the testing of AP type specimens a different floor beam with a 15° (relative to horizontal) inclined flange was used for the setup in order to produce a 30° brace angle as shown in Fig. 2.11.

As can be seen from Fig. 2.9 that this test setup allowed the bracing member to sway out-of-plane when buckling of the gusset plate occurred. To accomplish this behavior and still providing the axial load to the bracing member, a two-hydraulic ram system, which could resist the secondary moment produced by the out-of-plane displacement of the gusset plate when buckling of the plate occurred, was used. This two-hydraulic ram system is shown in Figs. 2.12 and 2.13. In order to employ this loading system, a W310 x 97 distributing beam was welded to the bracing member as shown in Fig. 2.12 to receive the loads from

the 200 ton hydraulic rams which were 700 mm apart. This distance between the hydraulic rams provided the necessary moment arm for the loading system to resist secondary moment. Diagonal stiffeners were also welded to the bracing member and to the ends of the distributing beam to strengthen the loading unit. The applied load from the hydraulic rams were controlled by adjusting the oil pressure in each ram. Each hydraulic ram was controlled by a separate oil pressure supply from a control panel. Since the two hydraulic rams had to maintain equal stroke during testing to simulate the actual loading condition, therefore, a linear variable differential transformer (LVDT) was attached to each hydraulic ram to control the amount of cylinder movement of the ram and the readings of the LVDTs were directly transferred to two voltmeters. A load cell was sat underneath the hydraulic ram to monitor the apply load. Knife edge was also used to properly align the point of load application as shown in Fig. 2.12. Rollers were placed at the top of the hydraulic ram to allow out-of-plane movement of the loading system. These rollers were bear against the bottom flange of the supporting beam which was bolted to the channel sections of the reaction frame as shown in Fig. 2.9.

Lateral bracings were also bolted to the distributing beam to provide lateral support to the loading system. The lateral bracings with roller at the end was supported by the flange of an I beam which was bolted to the reaction frame as shown in Fig. 2.14 A piece of teflon was placed in between the roller and the flange of the I-beam to allow vertical movement of the loading unit as shown in the figure. This lateral bracing system was also stiffened by placing a piece of lumber in between the two lateral bracings and tension rods were then used to tighten the lateral bracings against the lumber such that the whole system could act as a single unit as illustrated in Fig. 2.14.

The beam and column moments were applied by the tension rods as shown in Fig. 2.9. Steel brackets were welded to the ends of the beam and column to provide support for the tension rod. A load cell was placed on the steel bracket and a bearing plate was put on to

the other end of the load cell. The tension rod was then put through the load cell and the bearing plate and secured by a nut at the end. The other end of the tension rod was put through a hydraulic ram which bear against the end plate of a pedestal located away from the reaction frame as shown in Fig. 2.9. Tension was developed in the rod when the cylinder of the hydraulic ram moved outward. The load cell which sat in between the steel bracket and the bearing plate recorded the applied load. Strain gauges located at 1000 mm from the ends of the beam and column were used to monitor the applied moments.

2.5 Instrumentation

LVDTs were used to measure the out-of-plane deflection of the gusset plate free edges. LVDTs were also attached to the gusset plate underneath the splice member to monitor the out-of-plane movement at that region. This region was expected to be highly stressed based on tests by Hu and Cheng (1987). The location of all the LVDTs for specimens GP, MP and SP types are shown schematically in Fig. 2.15. A slightly different arrangement of the LVDTs was used for the EP type specimens to better capture the importance of the test as illustrated in Fig 2.16. This figure shows that more LVDTs were located on the splice members which was expected to be the critical region for these specimens. The schematic of LVDT locations for the AP type specimens is shown in Fig. 2.17. In general, the LVDTs arrangement for the AP type specimens was similar to that of the GP type specimens except on the short side free edge due to a different brace angle. Two LVDTs were attached to the beam and column to record the out-of-plane displacement of the test frame. As shown in Fig. 2.18, the LVDTs attached to the gusset plate were mounted on a frame which was clamped to the beam and column. Hence, the LVDTs measured the out-of-plane displacement of the gusset plate relative to the test frame.

For the MP and AP type specimens, cable transducer was also connected to the distributing beam ,which was welded to the bracing member, to record the out-of-plane movement of the bracing member since the Scheme II test setup was used. The deflection of the beam

due to the apply load was monitored by connecting a brass wire to an LVDT which was located on the pedestal parallel to the tension rod. Identical arrangement of LVDT was used for measuring the column deflection. Vertical deformation of the specimen was recorded by an LVDT attached to the base of the splice member.

Strain gauges and rosettes were used to measure the strain distribution of the specimens and monitor the level of apply beam and column moments for the MP type specimens. Strain gauges location for the GP, SP, and EP type specimens are shown schematically in Fig. 2.19 and Fig. 2.20 shows the strain gauges location for the AP type specimens. All the strain gauges and rosettes were mounted on both sides of the specimen in order to confirm the readings and to detect bending behavior. Strain gauges were also placed at the mid-length of the free edges to capture strain bifurcation when buckling of the gusset plate occurred. Three rosettes were mounted 90 mm under the Whitmore critical section. However, for the EP type specimens only the center rosette was mounted since the critical location of these specimens was expected to be in the splice member. Hence, strain gauges were also mounted on the splice members of the EP type specimens as shown schematically in Fig. 2.21.

Strain gauges locations for the MP type specimens are shown schematically in Fig. 2.22. Again, strain gauges were placed at the mid-length of the plate free edges to detect strain bifurcation. To measure the effects of the beam and column moments on the gusset plate stress distribution, strain gauges were mounted perpendicular to the beam and column boundaries on the specimen as illustrated in Fig. 2.22. Strain gauges were also mounted on the flanges of the bracing member to confirm the apply load.

A data acquisition system was used to collect all the test data and also recorded the MTS load and stroke. A x-y plotter was also used to record the MTS load versus stroke behavior during the tests for specimens tested with Scheme I setup to monitor the loading process. However, for the specimens tested with Scheme II setup the readings of the apply

load and lateral deflection of the specimen were manually input to a computer after each load step to generate a current load deflection plot in order to monitor the loading process. Whitewash was applied to all the specimens to detect yielding process.

2.6 Test Procedure

For the GP type specimens, the test with the "without-restraint" condition was first performed. If the failed specimen had excessive permanent deformation after the test of "without-restraint" condition, this failed specimen would not be used again for the "with-restraint" condition test. In fact, a new specimen of the same type would be fabricated for the test of the "with-restraint" condition. However, for SP type specimens the same specimen was used for the tests of both the "without-restraint" and "with-restraint" conditions since it was expected the permanent deformation would not be significant for these specimens after the "without-restraint" condition test. Again, the SP type specimen was tested with the "without-restraint" condition first and after the test the failed specimen was straightened before performing the "with-restraint" condition test. Only the "without-restraint" condition tests were performed on the AP, MP and EP type specimens.

For the EP type specimens, only one gusset plate specimen (500 x 400 x 13.3) was used. The 9.5 mm thick splice plate was tested first followed by the 13.0 mm thick splice plate using the same gusset plate specimen. Again, any permanent deformation of the gusset plate after each test was corrected before performing the next test. Since it was expected that the tee-section splice member would produce higher ultimate load than the splice plate (and therefore produced more permanent deformation on the gusset plate) therefore the test with tee-section as splice member was conducted last.

In general, the loading process was the same for all the specimens except for the MP type specimens which will be discussed below. An initial load was applied to the specimen to settle the test fixtures. At the initial loading stage, a predetermined load increment was

applied to the specimen and the specimen was allow to stabilize during each load increment. When nonlinear load deflection was observed for the specimen, a smaller load increment was used to capture the nonlinearity. All the experimental observations during the test were recorded. In particular, the yield line pattern and process were recorded in detail to fully understand the load transfer mechanism from the bracing member to the beam and column through the gusset plate connection. The test was terminated when the ultimate load was reached and unloading of the specimen occurred or the physical limit of the LVDT measuring the out-of-plane deflection was reached.

For the MP type specimens, the beam and column moments were applied in two or three increments, however, the moment ratio was always maintained at 0.5. In general, the maximum beam and column moments were applied at an axial load of approximately 25% of the Whitmore load of the specimens. Two moment levels were used in this test phase as shown in Table 2.1. For comparison purpose, a 6.5 mm thick specimen was tested without beam and column moments. As mentioned previously, the level of moments was monitored by the strain gauges mounted on the beam and column flanges. Load was applied carefully to ensure that the stroke of the hydraulic rams were maintained equally by opening and closing the oil pressure valve and observed closely the stroke reading of the hydraulic ram which was measured by an LVDT directly connected to a voltmeter. The beam and column moments were regularly checked and adjusted to maintain the maximum values. After applying the maximum moments, axial load was increased incrementally at a predetermined level. The specimen was allowed to stabilize after each load increment. Again, when nonlinear load deflection was observed for the specimen, a smaller load increment was used to capture the nonlinearity. All the experimental observations were recorded especially the yielding process and pattern. The test was terminated when the ultimate load was reached and unloading occurred or the out-of-plane displacement of the gusset plate specimen reached the physical limit of the measuring device.

2.7 Presentation of Test Results

The test results of each specimen type will be presented in following chapters separately. Test results of GP type specimens are presented first followed by SP, AP, MP and finally EP type specimens (chapters 3-7). Each individual chapter contains the load versus deflection curves, load versus strain gauge readings curves and out-of-plane deflected shapes of the free edges and along the centerline of the specimens. Chapter 8 presents the discussion and comparison of test results. Comparisons with the predictions by the Whitmore and Thornton methods are also included. The summary and conclusion of the test results are discussed in Chapter 9.

Table 2.1. Specimen Description

Specimen Designation	Plate Size (mm x mm)	Plate Thickness (mm)	Loading Eccentricity (mm)	Beam Moment Mb (kN·m)	Column Moment Mc (kN·m)	Brace Angle
GP1	500 x 400	13.3	-	-	-	45°
GP2	500 x 400	9.8	-	-	-	45°
GP3	500 x 400	6.5	-	-	-	45°
GP1R	500 x 400	13.3	-	-	-	45°
GP2R	500 x 400	9.8	-	-	-	45°
GP3R	500 x 400	6.5	-	-	-	45°
SP1	850 x 700	13.3	-	-	-	45°
SP2	850 x 700	9.8	-	-	-	45°
AP1	500 x 400	13.3	-	-	-	30°
AP2	500 x 400	9.8	-	-	-	30°
AP3	500 x 400	6.5	-	-	-	30°
MP1	500 x 400	13.3	-	250	125	45°
MP2	500 x 400	9.8	-	250	125	45°
MP3	500 x 400	6.5	-	250	125	45°
MP3A	500 x 400	6.5	-	375	187.5	45°
MP3B	500 x 400	6.5	-	0	0	45°
EP1	500 x 400	13.3	11.4	-	-	45°
EP2	500 x 400	13.3	13.3	-	-	45°
EP3	500 x 400	13.3	47.2	-	-	45°

Table 2.2. Types of Splicing Members

Specimen Designation	Types of Splicing Member
GP Type	2 x WT 125 x 22.5 2 x Plate 870 x 148 x 13.0
SP Type	2 x WT 125 x 22.5 2 x Plate 870 x 148 x 13.0
AP Type	2 x WT 125 x 22.5 2 x Plate 870 x 148 x 13.0
MP Type	2 x WT 125 x 22.5 2 x Plate 870 x 148 x 13.0
EP1	Plate 870 x 148 x 9.5
EP2	Plate 870 x 148 x 13.0
EP3	WT 125 x 22.5 Plate 870 x 148 x 9.5

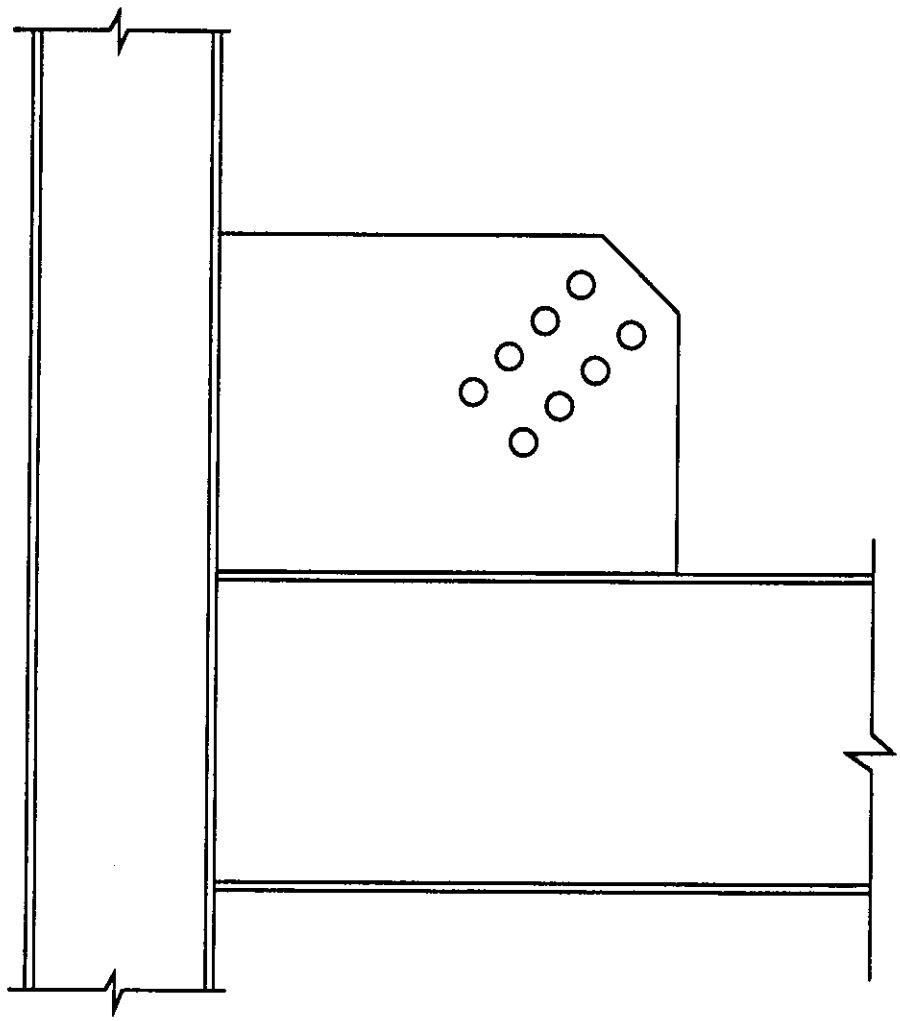

Fig. 2.1 Typical Gusset Plate Configuration

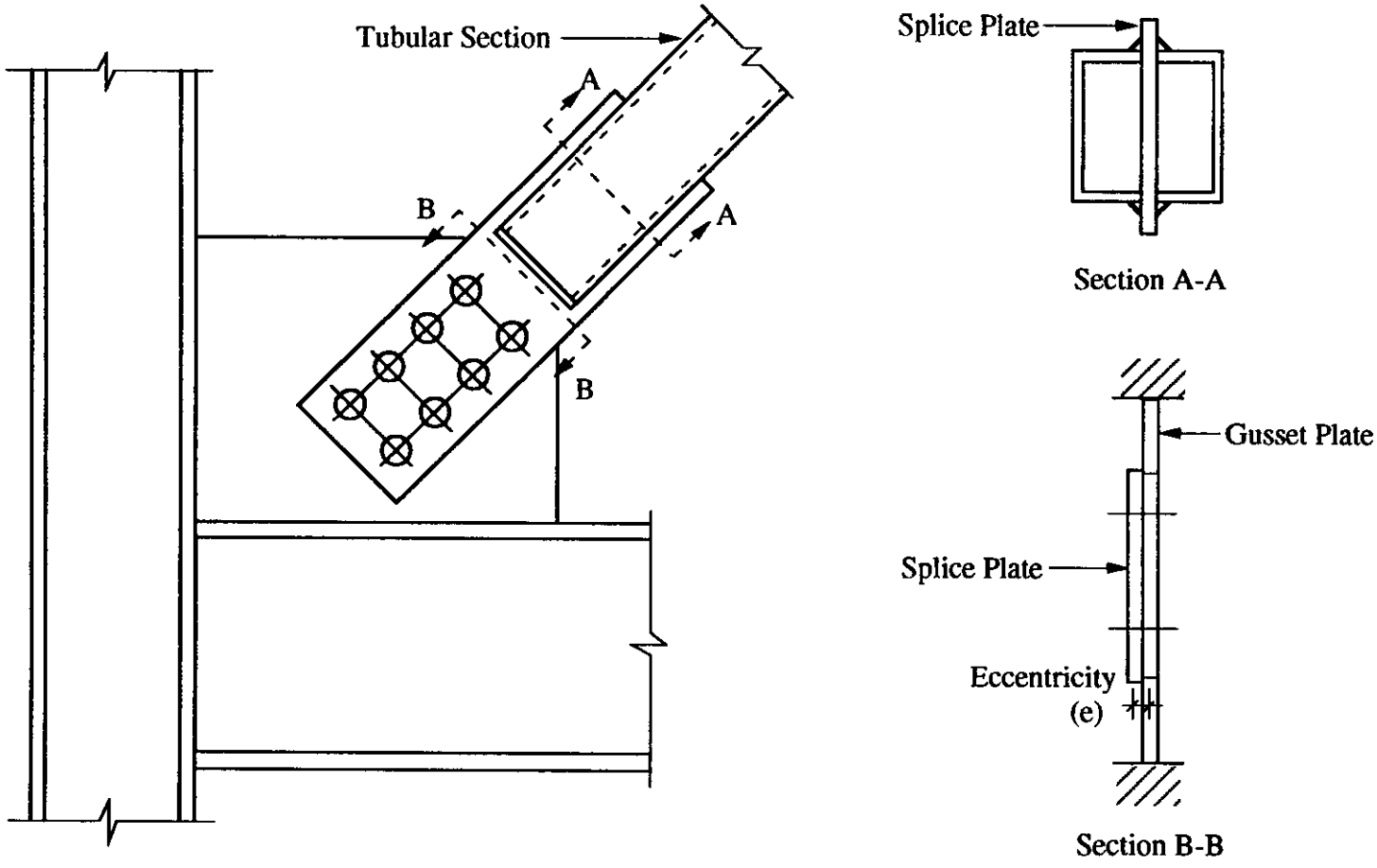

Fig. 2.2 Gusset Plate Connection of Tubular Section Bracing

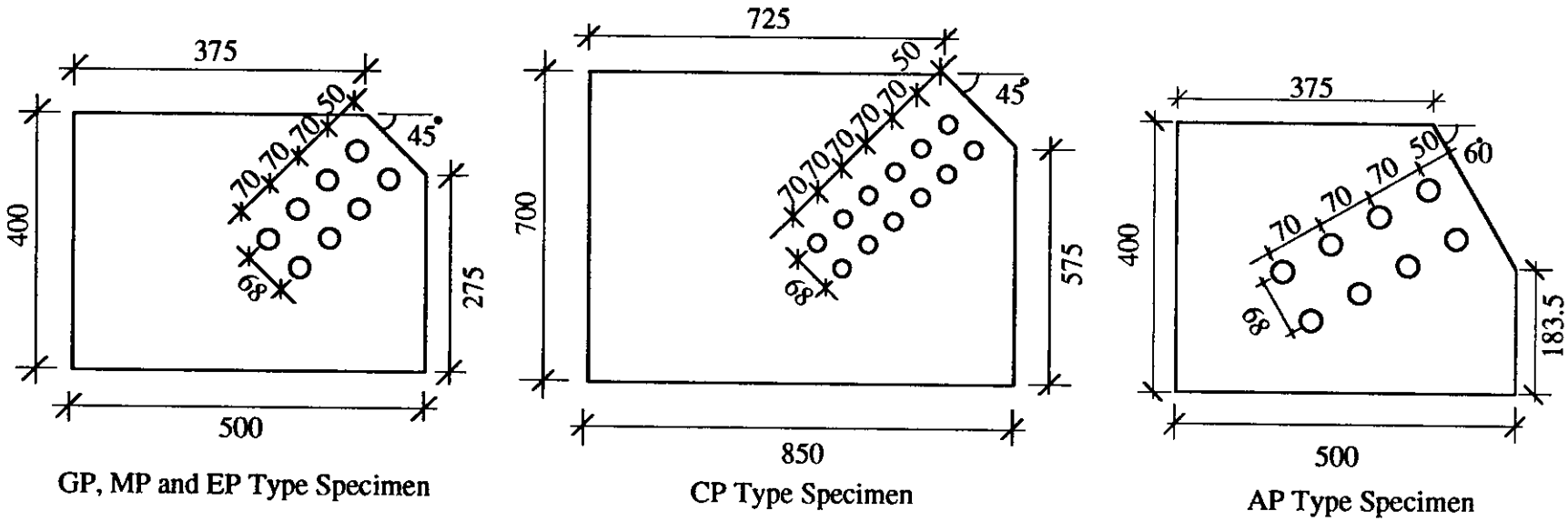

Fig. 2.3 Schematic of Test Specimens

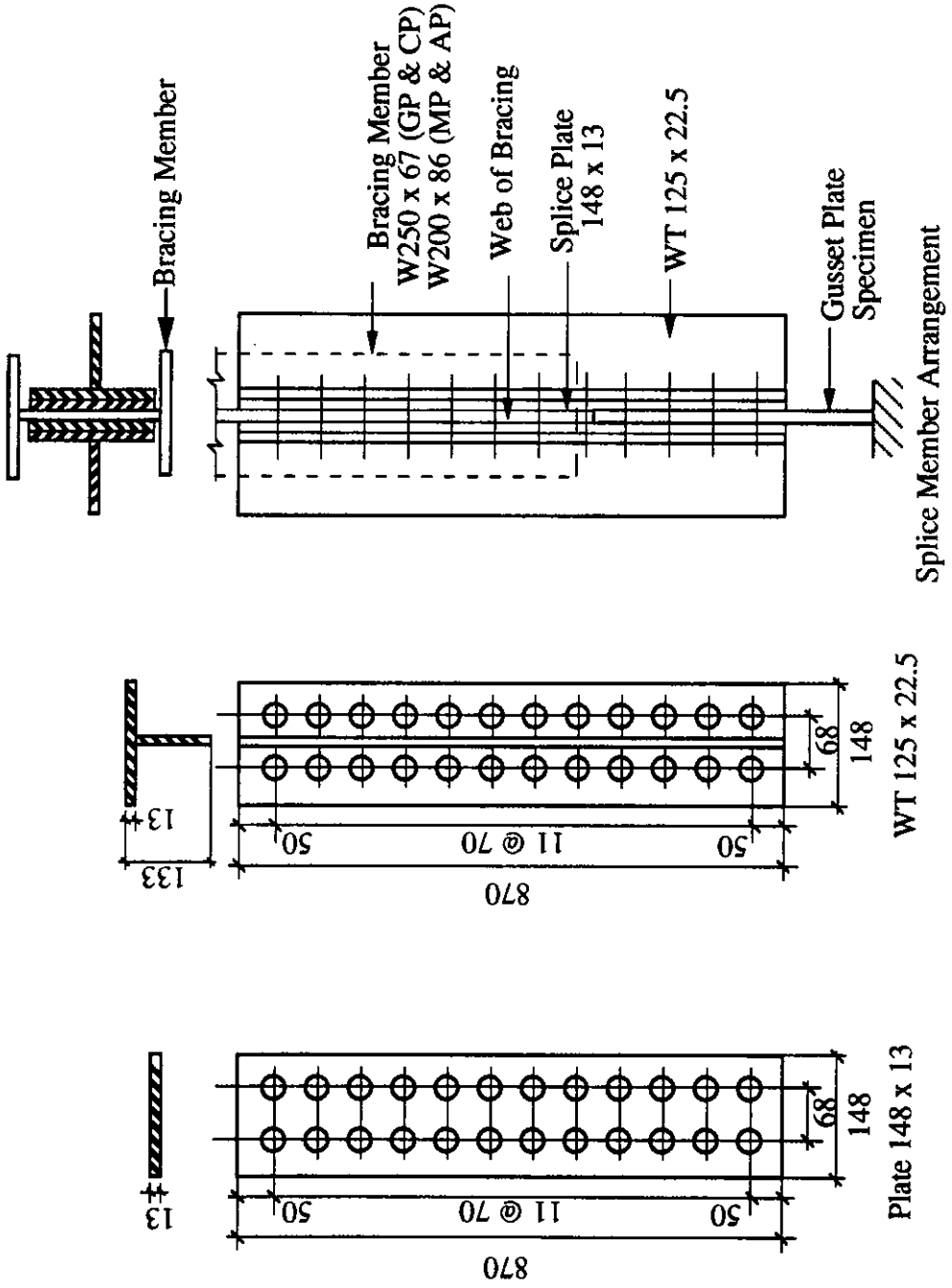

Fig. 2.4 Splice Members and Splicing Arrangement For GP, SP, MP and AP Type Specimens

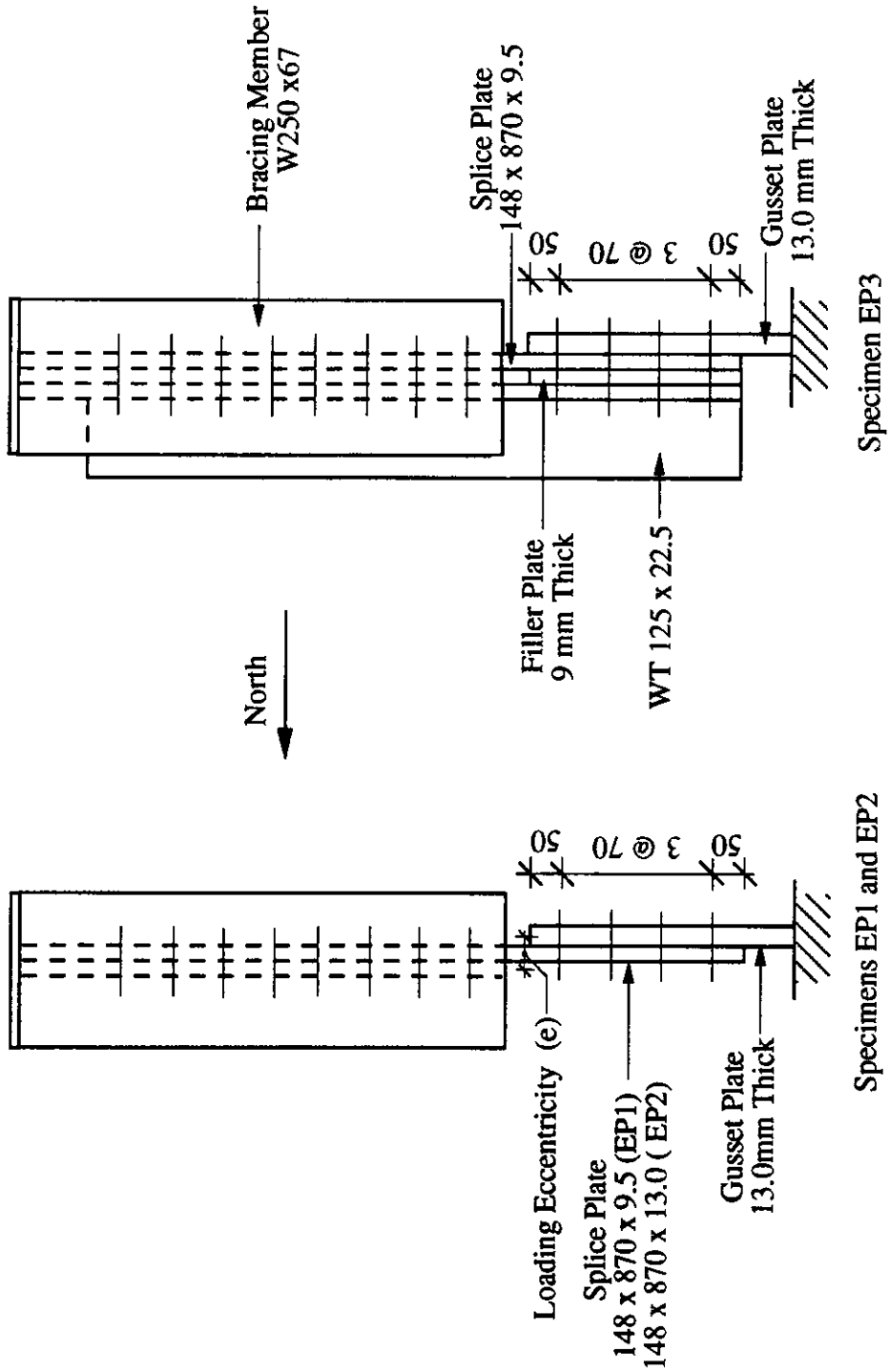

Fig. 2.5 Splice Member Arrangement for EP Type Specimens

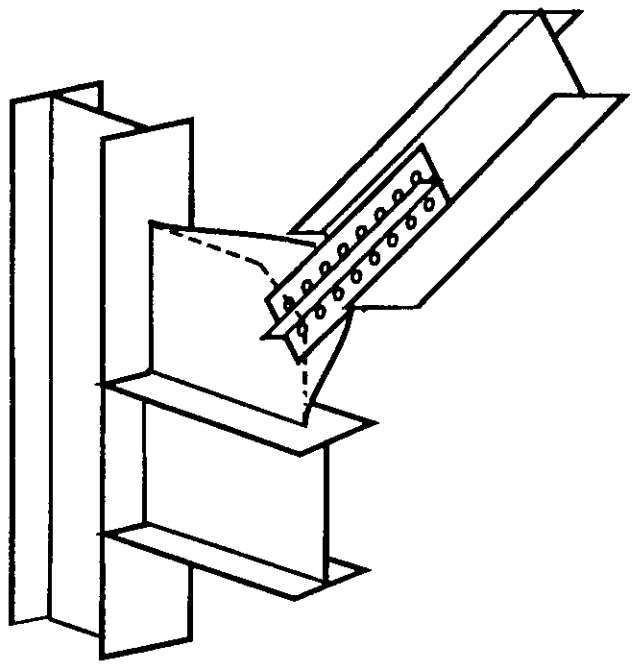

Fig. 2.6a Actual Braced Frame Behavior: Bracing Member and Gusset Plate Free Edges Deformed Out-of-Plane During Buckling

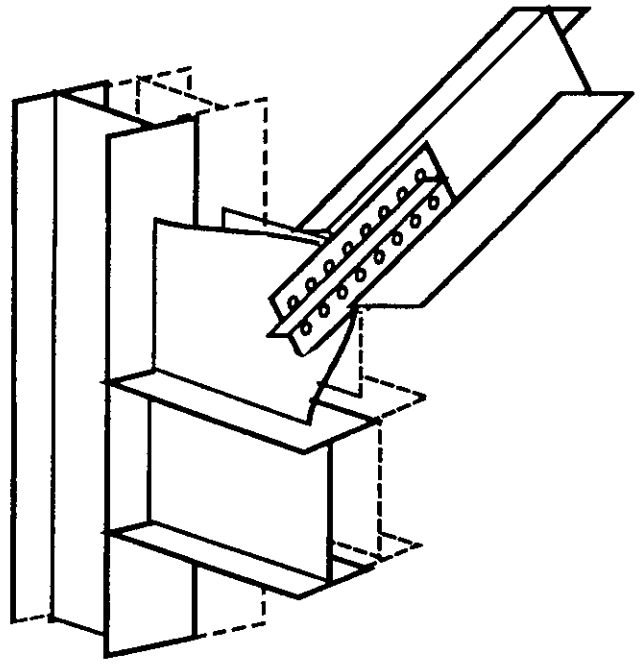

Fig. 2.6b Test Frame Behavior: The Beam and Column and Gusset Plate Fixed Edges Deformed Out-of-Plane During Buckling

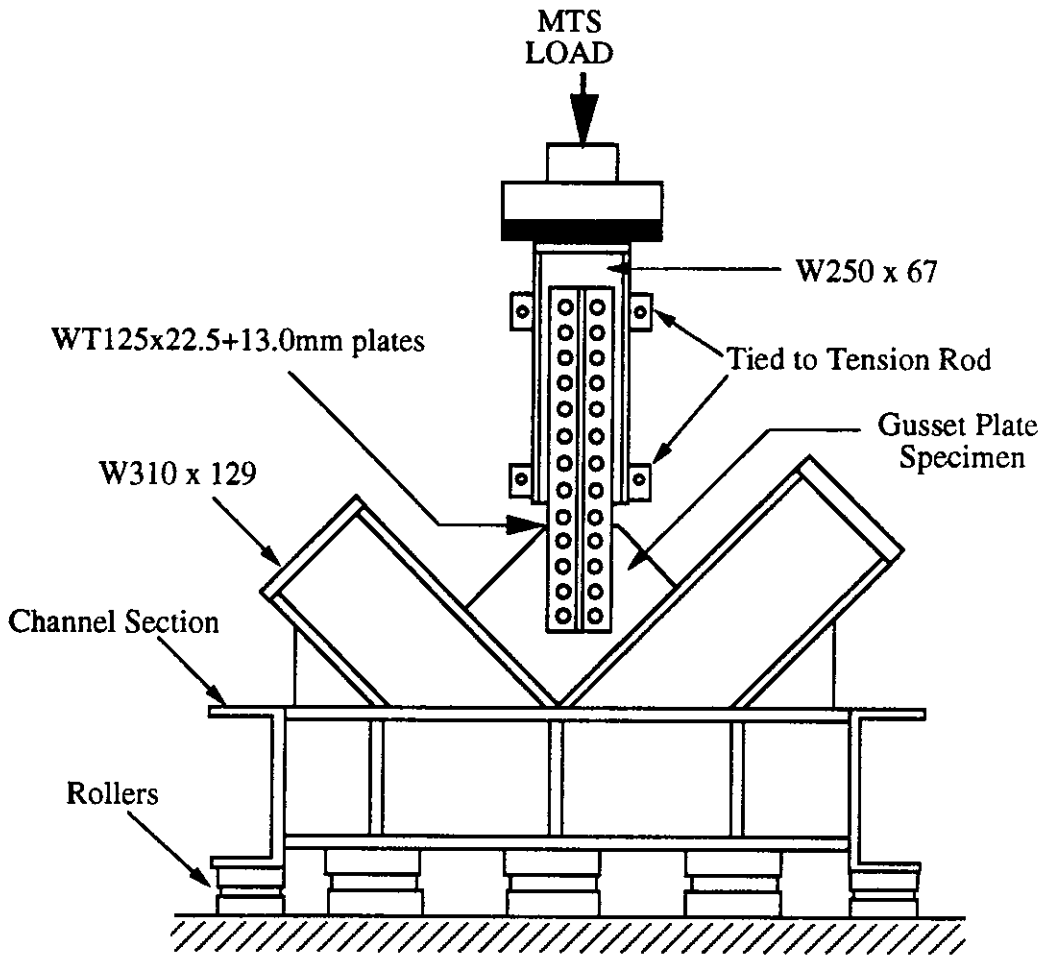

Fig. 2.7 Schematic of Test Setup for Phase I

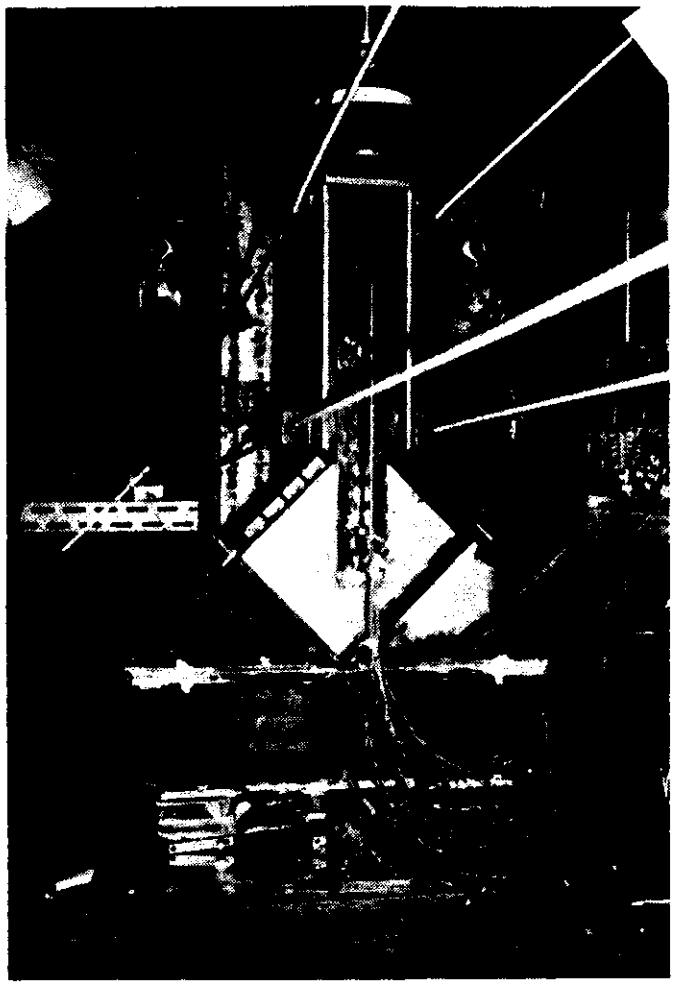

Fig. 2.8 Picture of Scheme I Test Setup

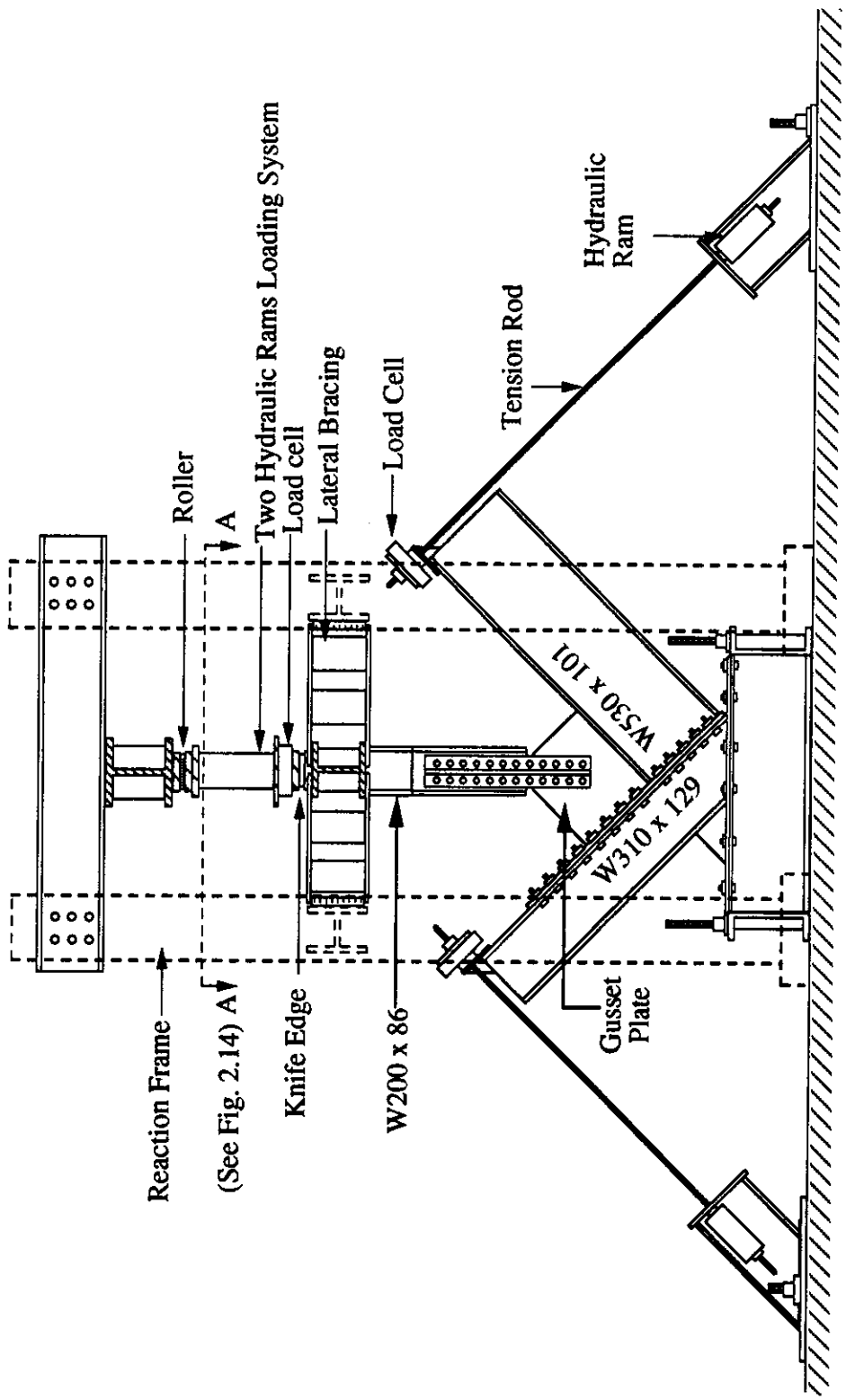

Fig. 2.9 Schematic of Test Setup for Phase II

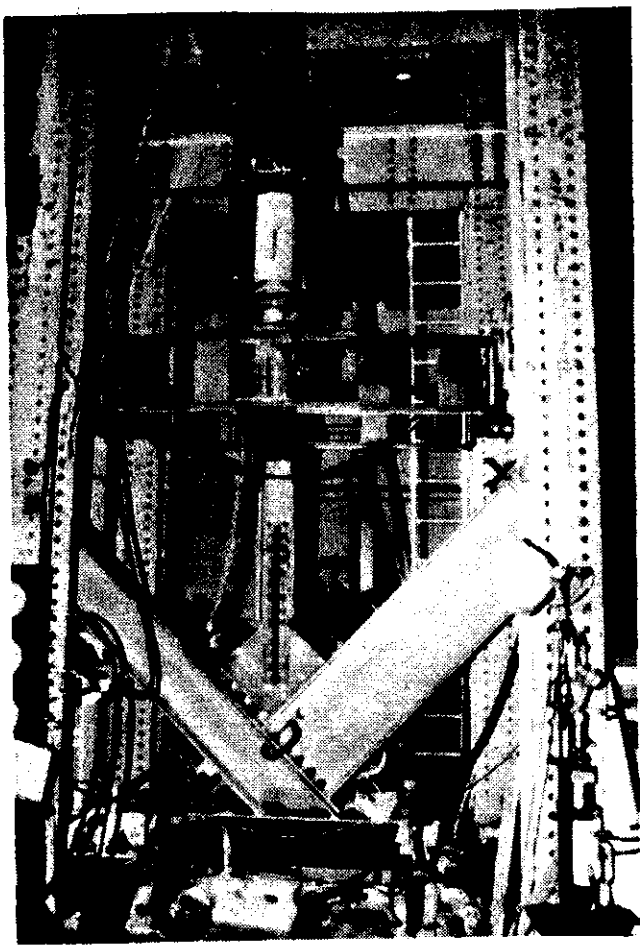

Fig. 2.10 Picture of Scheme II Test Setup

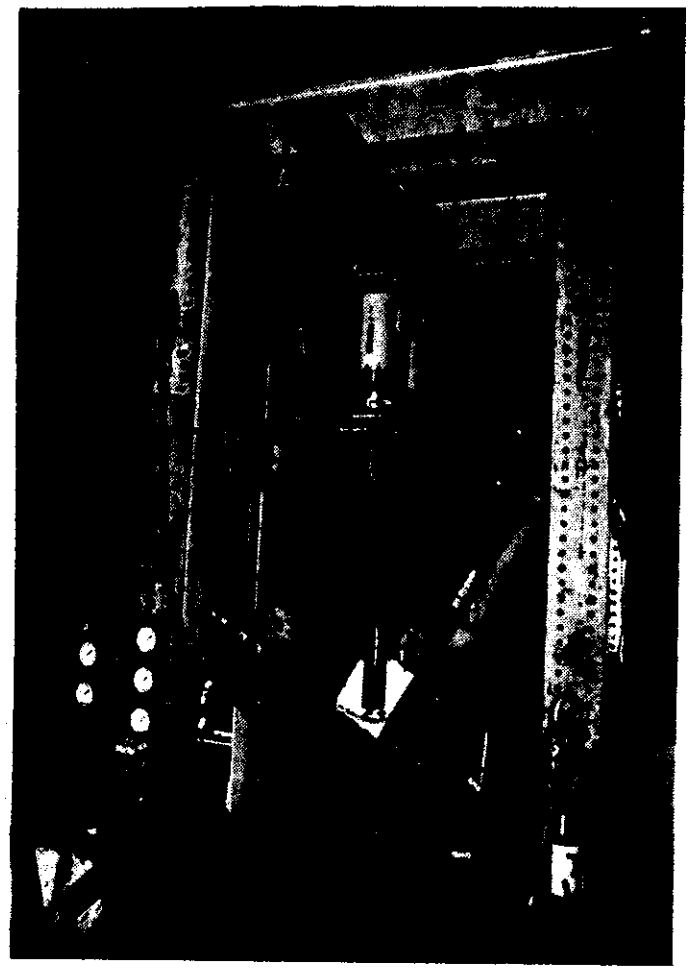

Fig. 2.11 Picture of Test Setup for AP Type Specimens

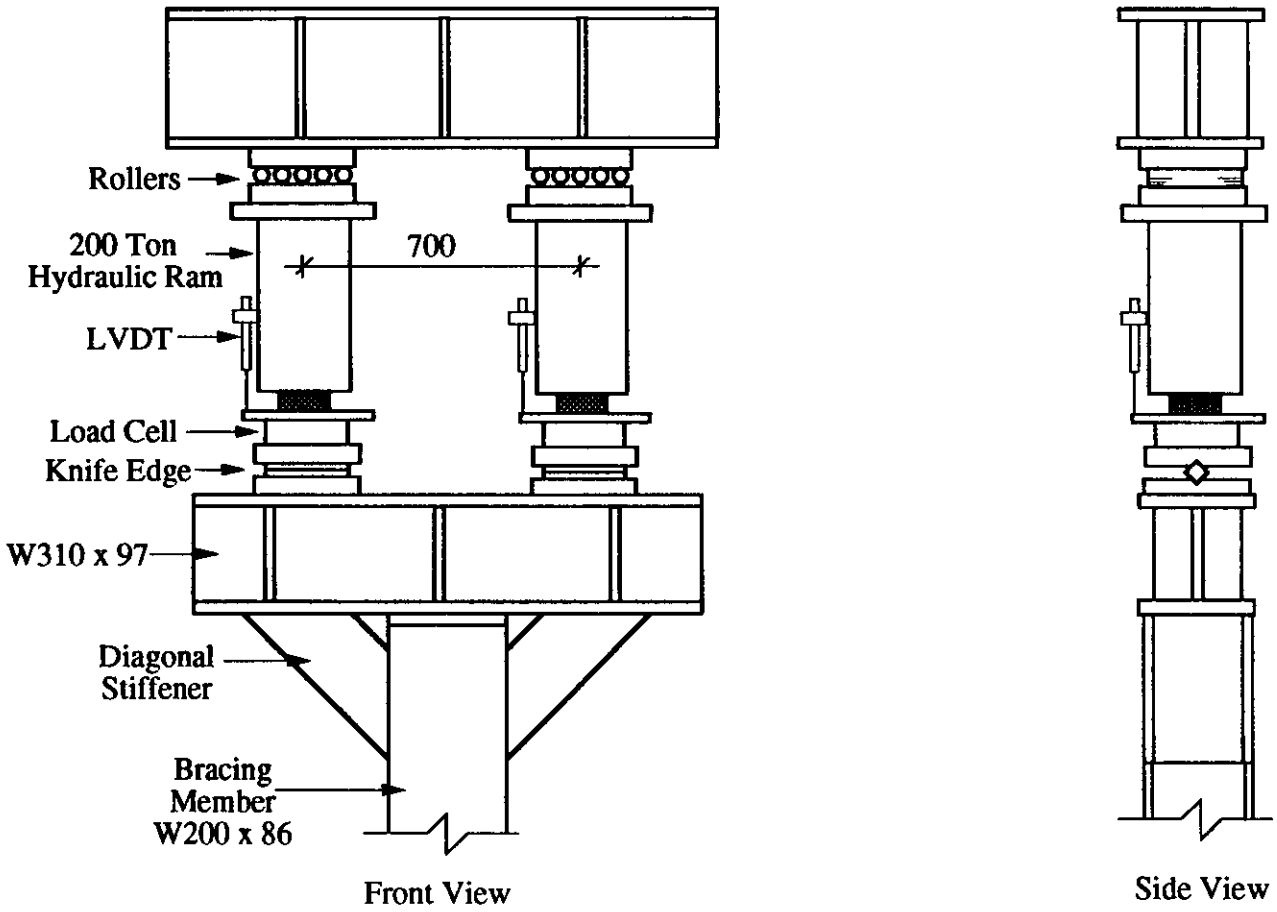

Fig.2.12 Schematic of Loading System

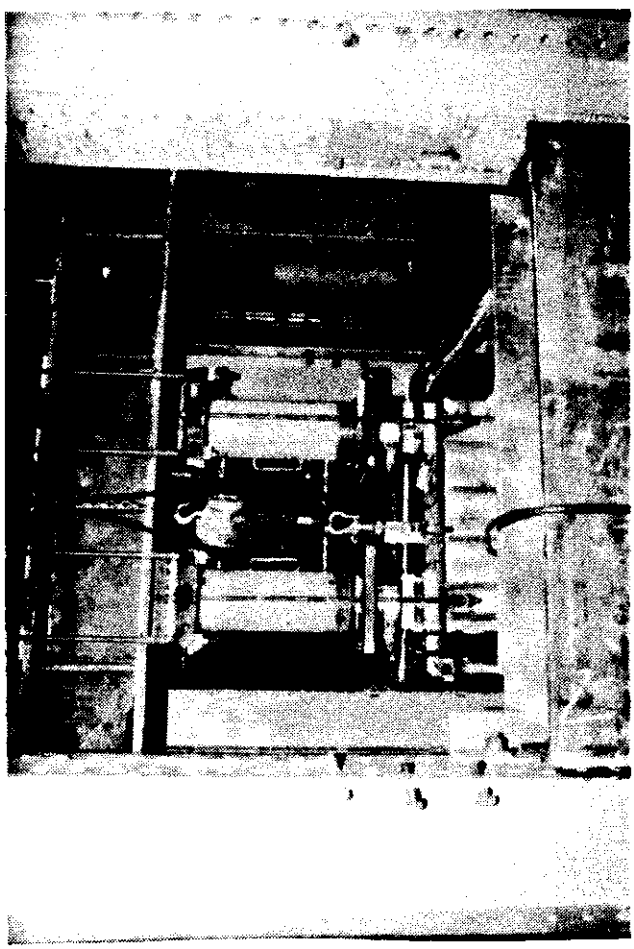

Fig. 2.13 Picture of Loading System

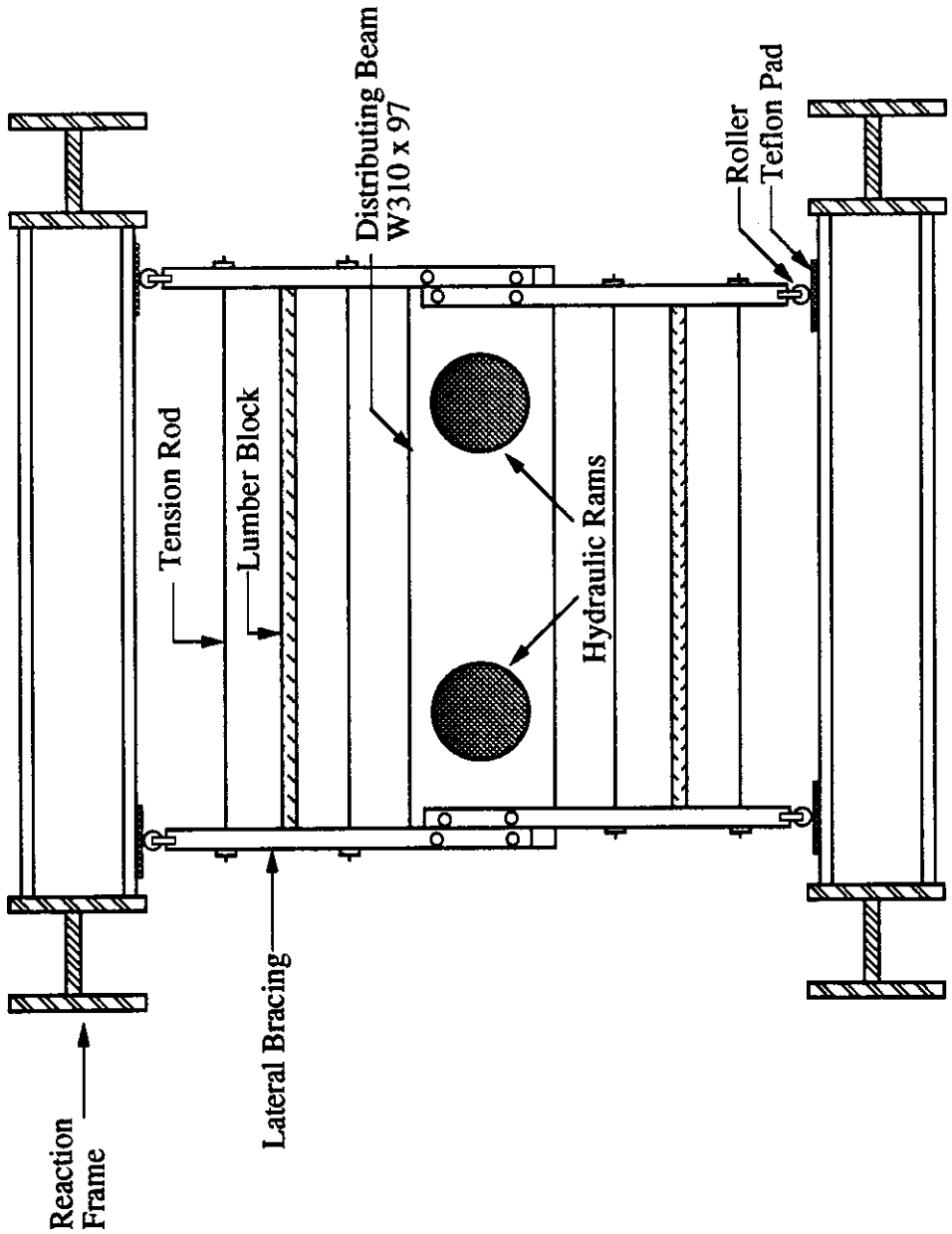

Fig. 2.14 Schematic of Lateral Bracing for the Loading Unit

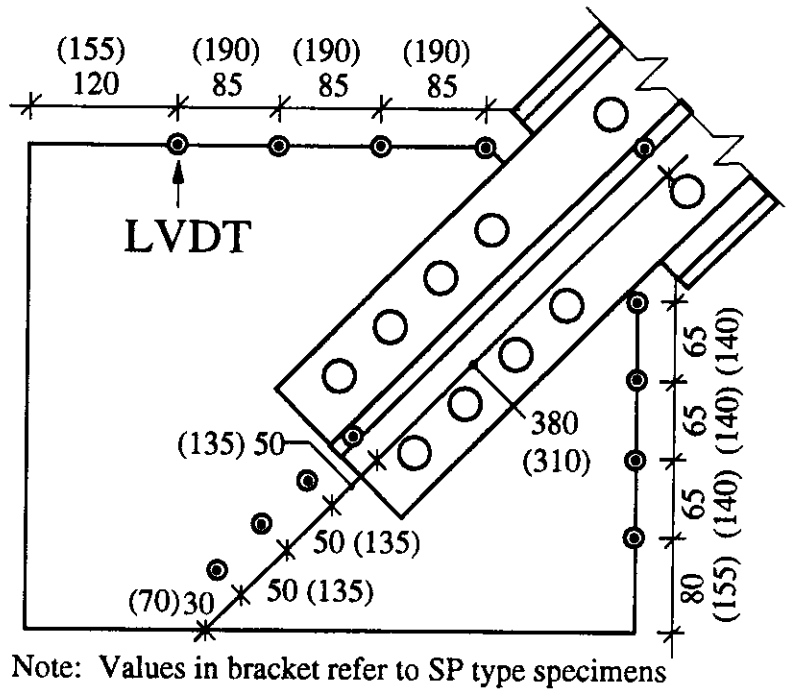

Note: Values in bracket refer to SP type specimens

Fig. 2.15 Schematic of LVDT Locations for GP, SP and MP Type Specimens

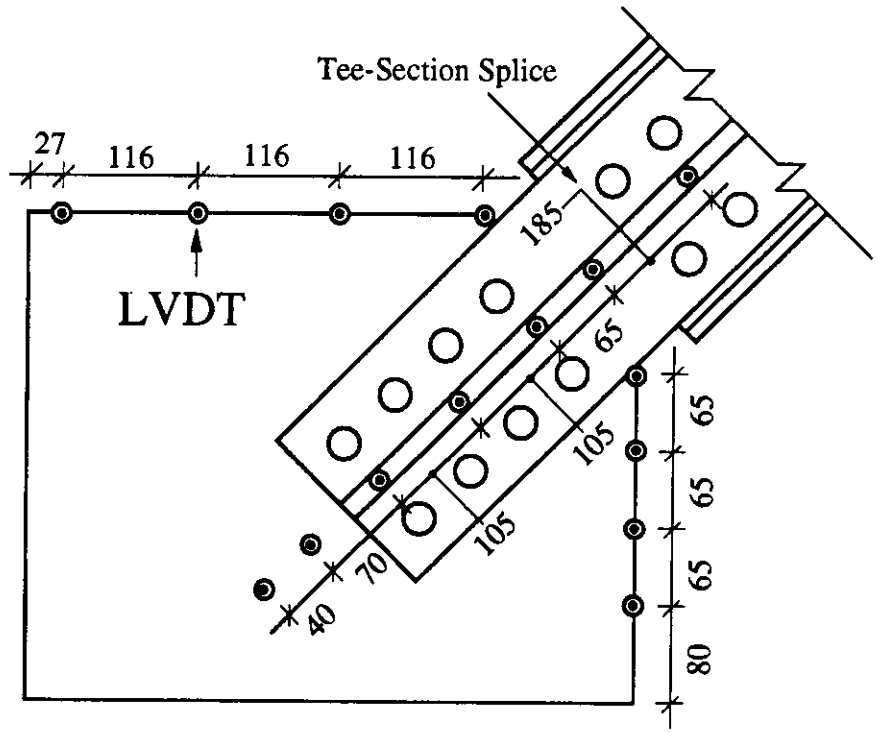

Fig. 2.16 Schematic of LVDT Location for EP Type Specimens

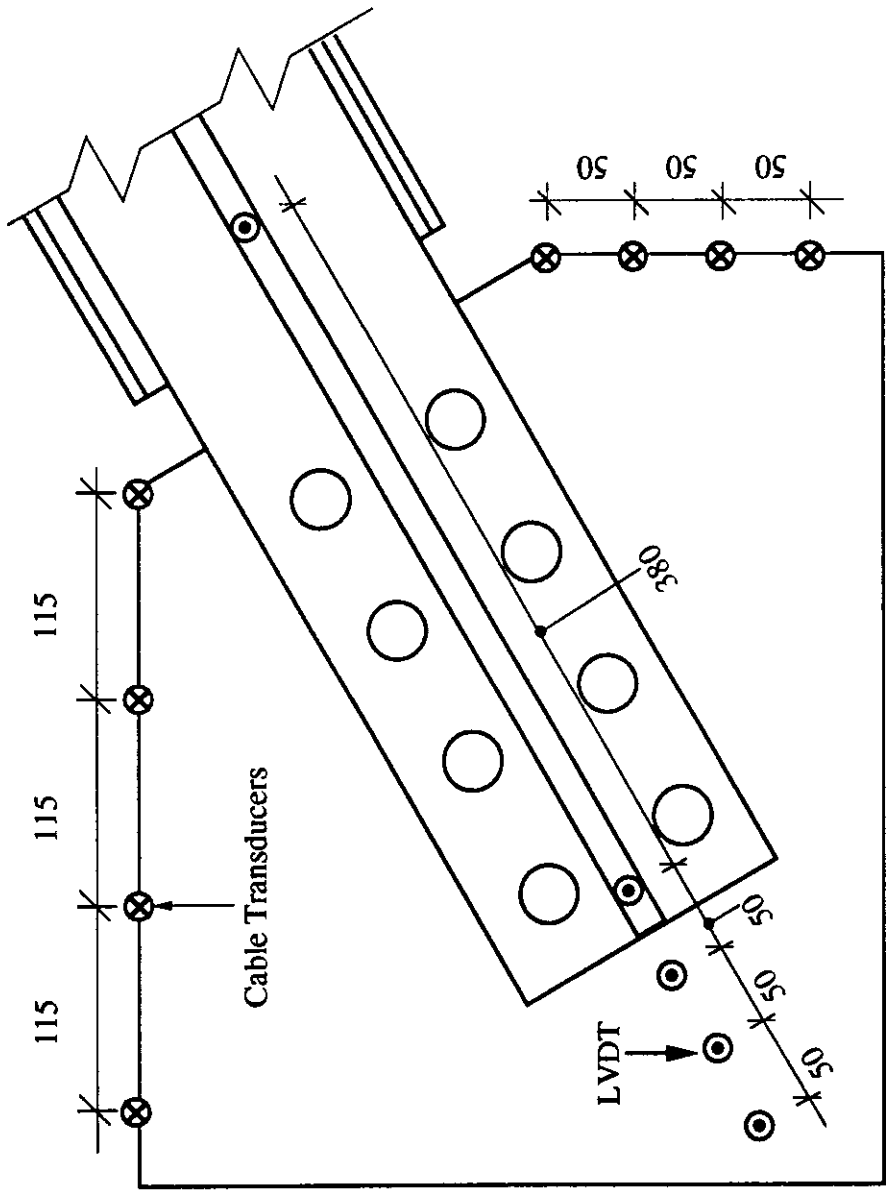

Fig. 2.17 Schematic of Cable Transducers and LVDTs Location for AP Type Specimens

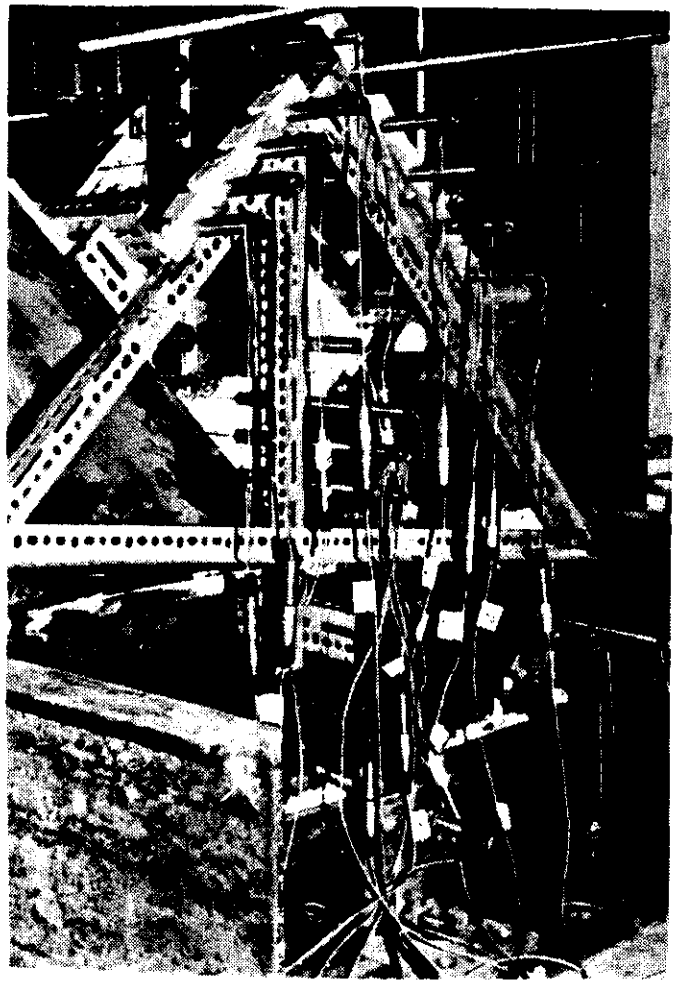

Fig. 2.18a LVDTs Arrangement on Supporting Frame

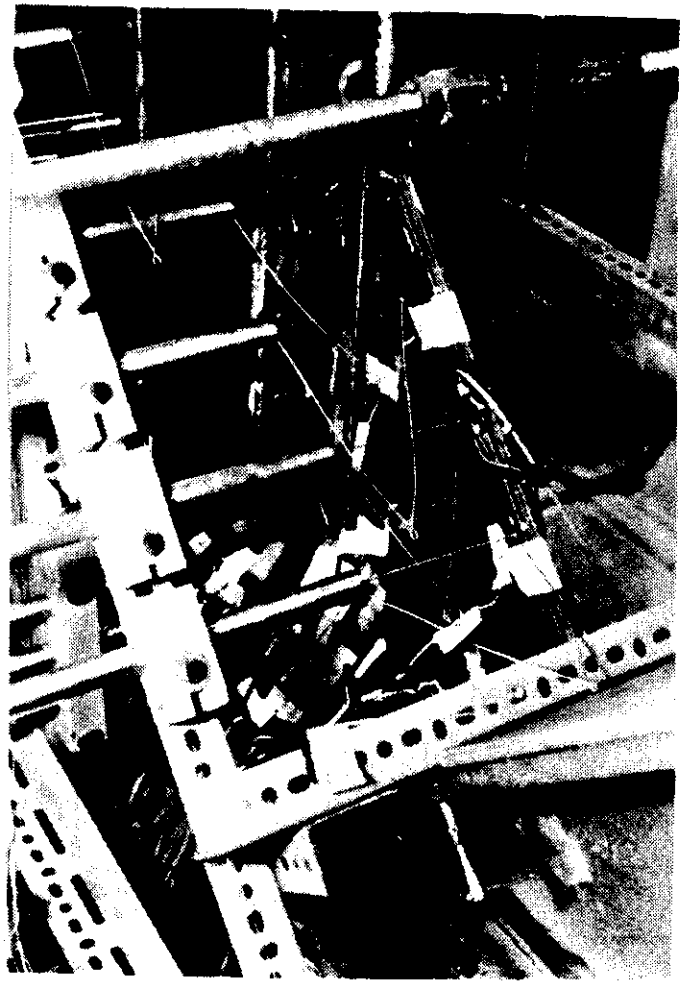

Fig. 2.18b Close-up of LVDTs on Short Free Edge of Specimen

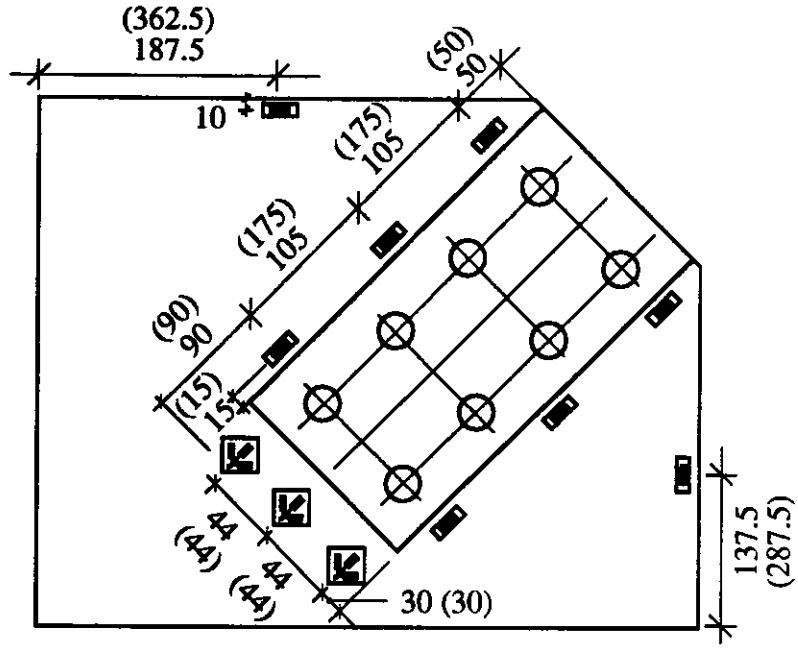

Note: Values in bracket refer to SP type specimens

Fig. 2.19 Strain Gauges Location for GP, SP and EP Types Specimens

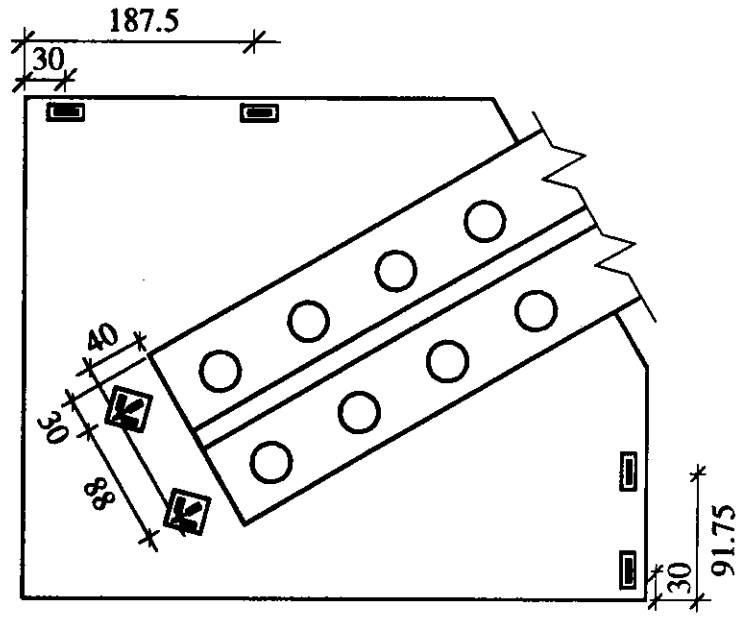

Fig. 2.20 Schematic of Strain Gauges Location for AP Type Specimens

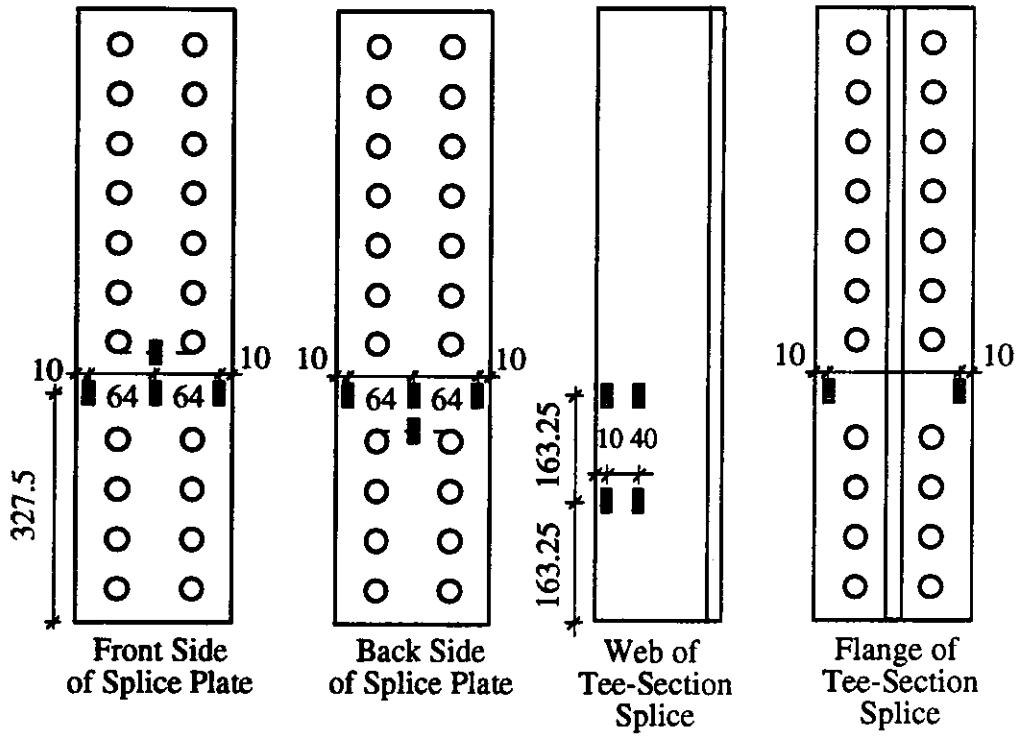

Fig. 2.21 Strain Gauges Location of Splice Member for EP Type Specimens

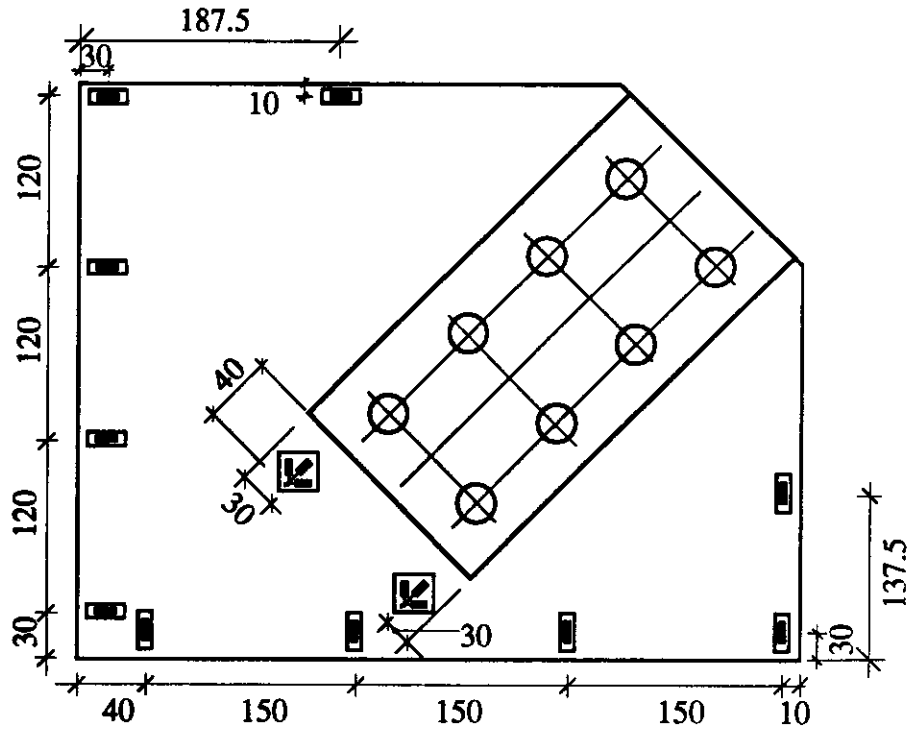

Fig. 2.22 Strain Gauges Location of MP Type Specimens

3. TEST RESULTS OF GP TYPE SPECIMENS

3.1 General

The GP type specimens were employed to examine the general behavior of gusset plate connection subject to compression in the inelastic range. Three plate thicknesses were tested and two out-of-plane restraint conditions at base of test frame were examined. The test results of the GP type specimens are summarized in Table 3.1. The Whitmore load based on the material static yield strength and the Thornton load based on an effective length factor, k, of 0.65 are also included in the table for comparison. In general, the test results show that the ultimate load of the specimens increased with increasing plate thickness. However, it can be seen from the table that providing out-of-plane restraint at the base of test frame did not affect the ultimate loads of the specimens significantly. In addition, both the Whitmore method and the Thornton method provided conservative estimate of the strength of specimens.

Since the same heats of steel plate thicknesses were used for all types of specimens (GP,SP,AP,MP and EP) with the same thickness, therefore, the material properties of the specimens will only be discussed once in this chapter. The material properties of the tested coupons are presented in Table 3.2 for each specimen plate thickness. The values shown in the table are averages of four coupons with two coupons tested in each orthogonal direction. The coupon tests results showed that similar material properties were recorded for coupons in both orthogonal directions. Complete stress-strain curves were also complied to provide the material models for later numerical analyses. However, it should be noted that average values were used to produce these curves. A typical stress-strain curve for plate thickness of 9.84 mm is shown Fig. 3.1.

3.2 Without Out-of-Plane Restraint at the Base of Test Frame

3.2.1 Behavior of Load vs. In-Plane Deformation

All the specimens were failed in sway buckling with the stub beam and column test frame deflected out-of-plane. The in-plane behavior of the specimens is best illustrated by examining the curves of load versus vertical displacement of the loading head as shown in Figs. 3.2 to 3.4. These curves show that linear behavior existed in the early loading stage for specimens GP1 and GP2 except in the initial stage when settling of the test fixtures took place. However, for specimen GP3 relatively linear behavior was observed from the beginning of loading until the ultimate load of the specimen was reached. This probably indicated that specimen GP3 did not experience a lot of yielding prior to failure occurred. The load level at which the curves of load versus vertical displacement turned nonlinear for specimens GP1 and GP2 correspond very well to the yield load predicted by the Whitmore method as shown in Figs. 3.2 and 3.3. Once the nonlinear behavior began, the curves turned gradually until the ultimate load of the specimen was reached. It should also be noted that the vertical displacement of the specimens only increased slightly after bifurcation occurred.

3.2.2 Behavior of Load vs. Out-of-Plane Displacement of Test Frame

The load versus out-of-plane displacement of the test frame curves for the specimens are shown in Figs 3.5 to 3.7. These curves indicate that initial imperfection existed in the specimens since out-of-plane displacement of the test frame was recorded from the beginning of loading. Figures 3.5 to 3.7 show that nonlinear load displacement behavior was observed for all the specimens prior to reaching the ultimate load. It can also be seen from the figures that lateral displacement of the test frame increased significantly after the ultimate load was reached. The final lateral displacement of the test frame ranges from 6 mm to 12 mm depending on the specimens. It was also observed that no significant

decrease in the load carrying capacity of the specimens was recorded after reaching the ultimate load.

3.2.3 Strain Gauges Results

The strain readings from the strain gauges mounted at the mid-length of the gusset plate long free edges were plotted against the applied load as shown in Figs 3.8 to 3.10. These plots show that the longitudinal strains at the mid-length of the long free edge increase linearly with respect to the applied load until strain bifurcation occurred at the ultimate load except specimen GP1 which showed slight strain reversal at about 75 percent of the ultimate load. In addition, that the strain readings from both sides of the gusset plate were only slightly different indicated small out-of-plane bending of the plate at the long free edge had occurred prior to reaching the ultimate load of the specimens. The curves of load versus longitudinal strains at mid-length of the short free edges of the specimens are shown in Figs. 3.11 to 3.13. It can be seen from the figures for specimens GP1 and GP2 that linear behavior was observed until at a load level (below the ultimate load) that strain reversal of the specimens at the short free edge occurred. For specimen GP2 the strain reversal process continued until strain bifurcation occurred, however, increase in longitudinal compressive strain was observed at the short free edge for specimen GP1 prior to strain bifurcation. The strain reversal process occurred at the free edges in these specimens may be attributed to the in-plane bending of the free edges caused by the extensive yielding of the gusset plate area underneath the splice member. Although linear load versus strain behavior was noticed for specimen GP3, different strain readings were recorded from both sides of the specimen from the beginning of loading indicated that bending at the short side free edge of the plate had occurred. It should be noted that all the longitudinal strain readings recorded from the free edges were within the elastic range prior to buckling. The rosette readings recorded from the plate area underneath the splice member were also examined. It was found that the rosette strain readings corresponded

very well to the prediction by the Whitmore method. The direction of principal strains occurred at an angle of approximately 40° from the horizontal. Since the brace angle for these specimens was 45°, therefore, it can be seen that the direction of principal strains at the rosettes almost aligned with the loading angle.

3.2.4 Yielding Behavior of Specimens

During the tests, extensive yielding was observed for specimens GP1 and GP2. However, specimens GP3 only showed moderate yielding at the gusset plate area underneath the splice member. To illustrate the load transfer mechanism from the splice member to the beam and column support boundary through the gusset plate specimen, yielding pattern and process of the specimens were recorded during tests. A schematic of the yielding pattern at various load levels for specimen GP1 is shown in Fig. 3.14 and photograph of the failed specimen are shown in Fig. 3.15. Yielding process similar to that of GP1 was observed for specimen GP2. As can be seen in Fig. 3.14, yield lines was first noticed at the gusset plate area underneath the splice member. These yield lines were oriented at an angle of approximately 45° to the horizontal. Subsequently, yielding at this region progressed towards the beam and column boundary and the yield lines developed were parallel to the boundary (Fig. 3.14b). As loading continued, horizontal yield lines were also observed in the area about the two sides of the splice member (Fig. 3.14d). Finally, as the applied load approached the ultimate load yield lines were developed at the free edges and extensive yielding was observed for the entire gusset plate area. The yield lines observed at the free edges were probably caused by plate out-of-plane bending when buckling occurred. It should also be noticed that the final yielding pattern of the specimens indicated a mechanism was formed for specimens GP1 and GP2. Yield line mechanism were observed at the mid-length of the free edges and underneath the splice member extending to the beam and column boundary as shown in Fig. 3.15.

Based on the above yielding pattern, it can be seen that the loading mechanism of these specimens can be described as follow. As predicted by the Whitmore method that the gusset plate area underneath the line passes through the last row of bolts was stressed significantly. Hence, at a load level close to the yield load, estimated by the Whitmore method, yield lines parallel to the beam and column boundary were observed at the area underneath the splice member. While the applied load increased, yielding at this area progressed. When extensive yielding at this area developed, load was redistributed to the gusset plate area about two sides of the splice member. Hence, compressive yield lines were also formed in this area as load increased. The yielding extended towards the remaining part of the gusset plate when applied load increased. The in-plane stiffness of the gusset plate deteriorated as yielding continued. Plastic bifurcation buckling of the gusset plate occurred when the in-plane stiffness decreased to a certain level.

3.2.5 Out-of-Plane Deflected Shapes of Free Edges and Along Centerline of Splicing Member

The out-of-plane deflected shapes of the specimens free edges and along the centerline of the splice member to the beam and column boundary are shown in Fig. 3.16 and a photograph of the deflected shape along the long free edge for specimen GP1 is shown in Fig. 3.17. These deflected shapes were normalized by the maximum displacement occurred in each specimen. In general, the deflected shapes resembled the buckled shape of a fixed-guided column. However, for specimen GP3 local deformation of the gusset plate was observed underneath the splice member as shown in Fig. 3.16. The figure also shows that small movement of the splice member at the tension rod restraint location was recorded. When the gusset plate deformed out-of-plane, the splice member would transfer a shear force induced by the secondary moment to the bracing member. Since the brace member was retrained by the tension rods which were attached to the supports mounted on the flanges of the brace member, therefore, the shear force caused local bending of the web

of the brace member about the tension rod supports. This slight bending of the web was also observed from the tests. Slight twisting of the splice member was also recorded when buckling occurred due to the unsymmetrical plate geometry.

3.3 With Out-of-Plane Restraint at the Base of Test Frame

3.3.1 Behavior of Load Versus In-Plane Deformation

The general failure mode of the specimens was plate local buckling. Depending on the specimens, plate local buckling could occur at the specimens free edges and the plate area underneath the splice member. Figures 3.18 to 3.20 illustrate the load versus vertical in-plane displacement of the loading head. Similar in-plane stiffnesses as without out-of-plane restraint (Figs. 3.2-3.4) were observed. Again, nonlinear behavior was observed for all the specimens at the beginning of loading due to settling of the test fixtures. Subsequently, linear behavior was observed until the specimens reached the yield load estimated by the Whitmore effective width method as shown in the figures. From then on, the curves gradually turned to the ultimate load and followed by moderate unloading. It should be noted that strain gauges were not used in these specimens since it was believed that the strain gauges results from the tests of the specimens without restraint would provide sufficient information on the stress and strain distribution for gusset plate subject to compression.

3.3.2 Behavior of Load Versus Out-of-Plane Displacement at Mid-Length of Long Free Edge

The load versus out-of-plane displacement at the mid-length of long free edge are shown in Figs. 3.21 to 3.23. It can be seen from the figures that relatively small lateral deflection at mid-length of the long free edge was recorded until the applied load approached the ultimate load. It was also observed that the load carrying capacity of the specimens did not decrease

significantly after reaching the ultimate load. The final lateral displacement of the specimens ranges from 9 mm to 20 mm.

3.3.3 Yielding Behavior of Specimens

During the tests, extensive yielding was observed for specimens GP1R and GP2R. For specimen GP3R, however, very slight yield lines were recorded when the plate almost reached the buckling load. These yielding progressed moderately at the plate area underneath the splice member as load increased to the ultimate load. In general, the yielding process for specimens GP1R and GP2R tested with restraint at the base of the test frame was similar to that of specimens tested without restraint. Initial yielding was observed at the plate area underneath the splice member at a load level close to the yield load predicted by the Whitmore method. Again, yielding continued to progress in this area as load increased. When applied load increased to a certain level, yield lines were observed in the area about both sides of the splice member. And finally, yield lines were also developed at the free edges when buckling occurred.

3.3.4 Out-of-Plane Deflected Shapes of Free Edges and Along Centerline of Splicing Member

The out-of-plane deflected shapes of the free edges and along the centerline of splice member for all the specimens are shown in Fig. 3.24. Again, these deflected shapes were normalized by the maximum displacement occurred in each specimen. It can be seen from these figures that considerable movement was recorded at the tension rod restraint location due to local bending of the web of bracing member about the tension rod support. In general, however, the deflected shapes of the free edges resembled the buckled shapes of a column fixed at one end and supported by lateral spring at the other end. The maximum displacement of the specimens occurred at about the mid-length of the long free edge.

Table 3.1 Test Results of GP Type Specimens

Specimen Designation	Plate Size (mm x mm x mm)	Ultimate Load (kN)	Whitmore Load P_w (kN)	Thornton Load P_t k = 0.65 (kN)
GP1	500 x 400 x 13.3	1956	1216	1142
GP2	500 x 400 x 9.8	1356	930	828
GP3	500 x 400 x 6.5	742	555	459
GP1R	500 x 400 x 13.3	2057	1216	1142
GP2R	500 x 400 x 9.8	1487	930	828
GP3R	500 x 400 x 6.5	790	555	459

Table 3.2 Material Properties

Material	Static Yield Strength (MPa)	Ultimate Strength (MPa)	Modulus of Elasticity (MPa)
13.3 mm Gusset Plate	295	501	207 600
9.8 mm Gusset Plate	305	500	210 200
6.5 mm Gusset Plate	275	467	196 000
13.0 mm Splice Plate	285	510	199 960
9.5 mm Splice Plate	435	540	201 500
13.0 mm Flange of Tee-Section Splice Member	284	503	197 800

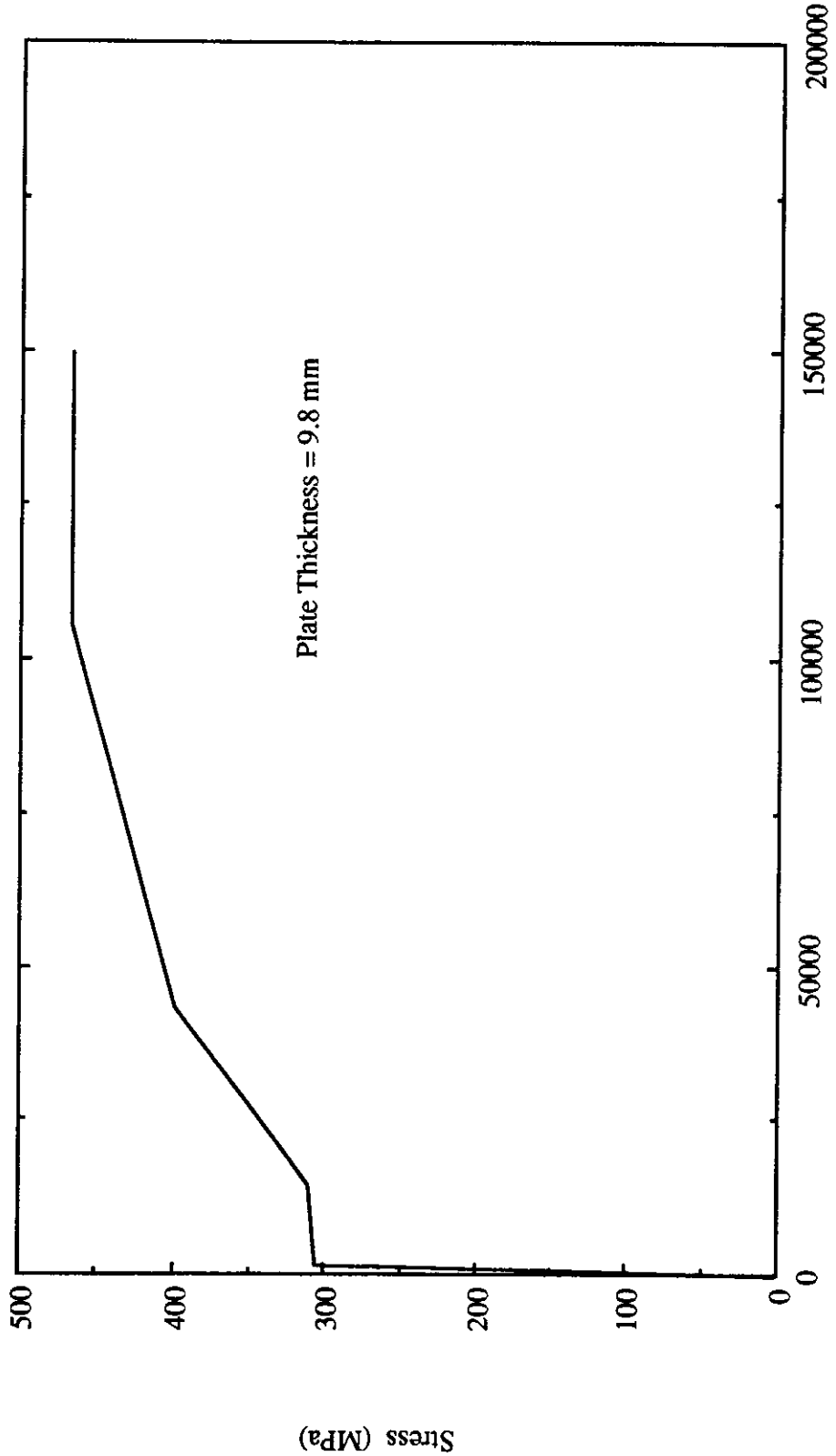

Fig. 3.1 Stress Strain Curve for 9.5 mm Thick Specimen

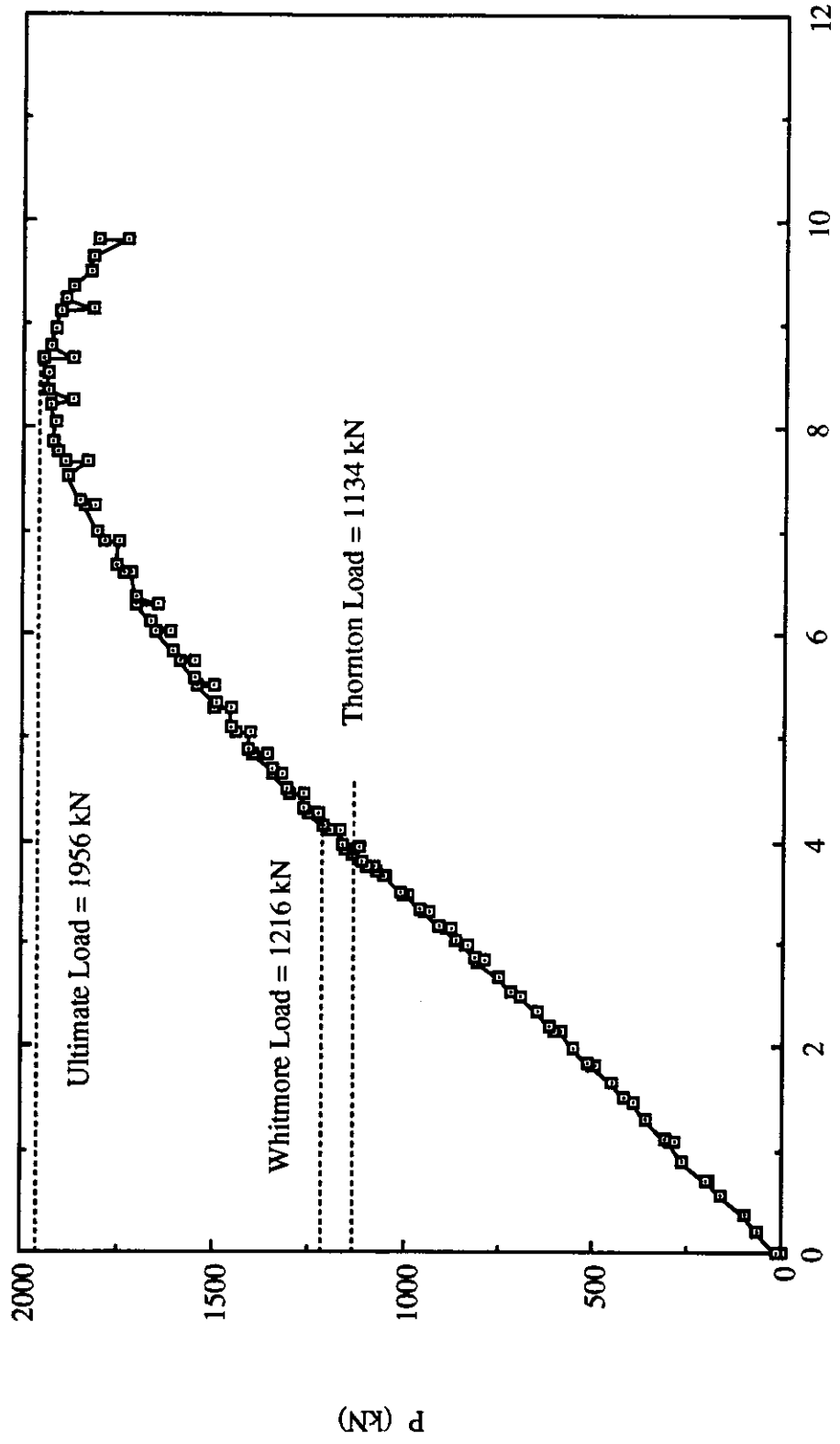

Fig. 3.2 Load vs. Vertical Displacement of Loading Head for Specimen GP1

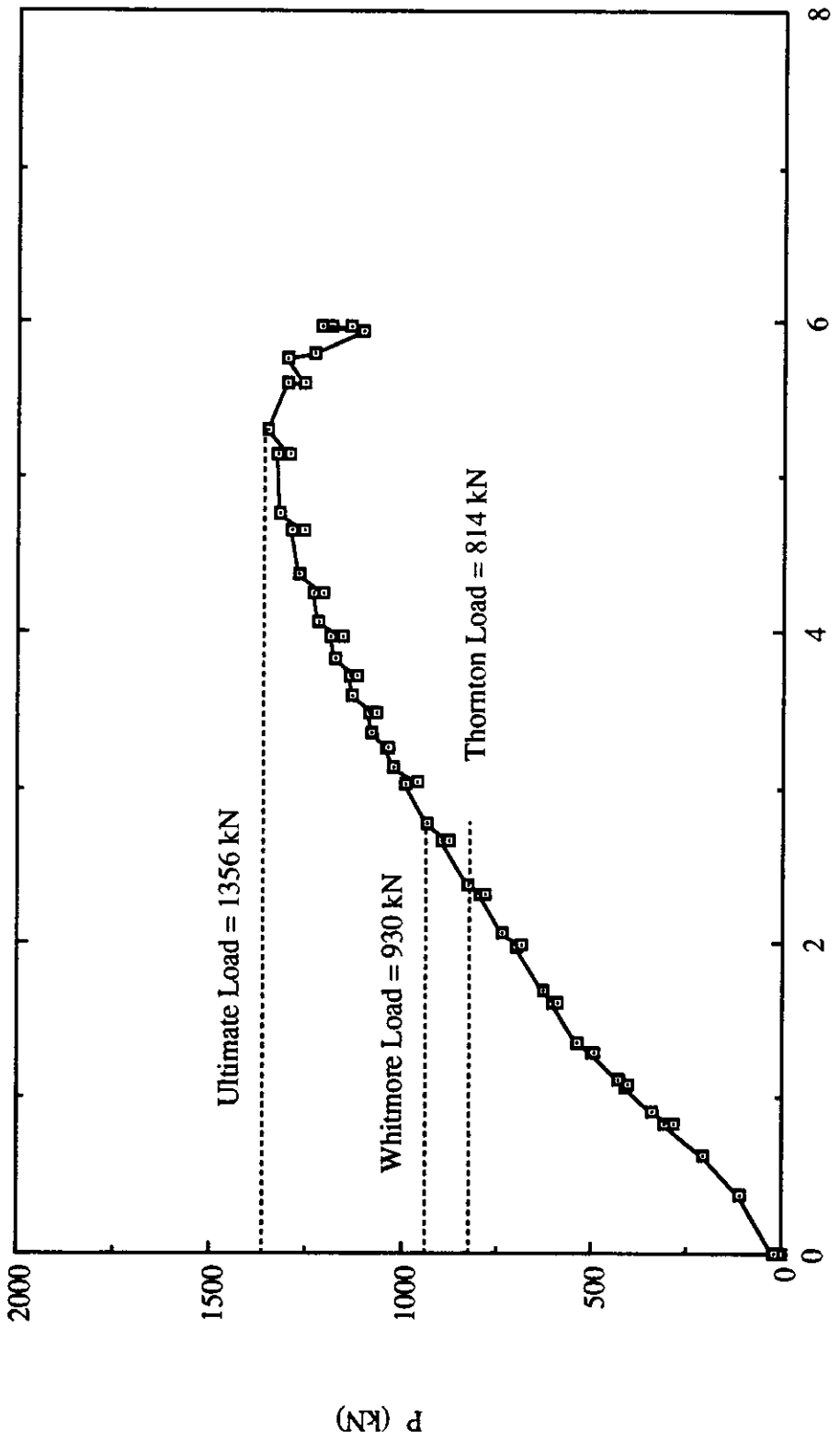

Fig. 3.3 Load vs. Vertical Displacement of Loading Head for Specimen GP2

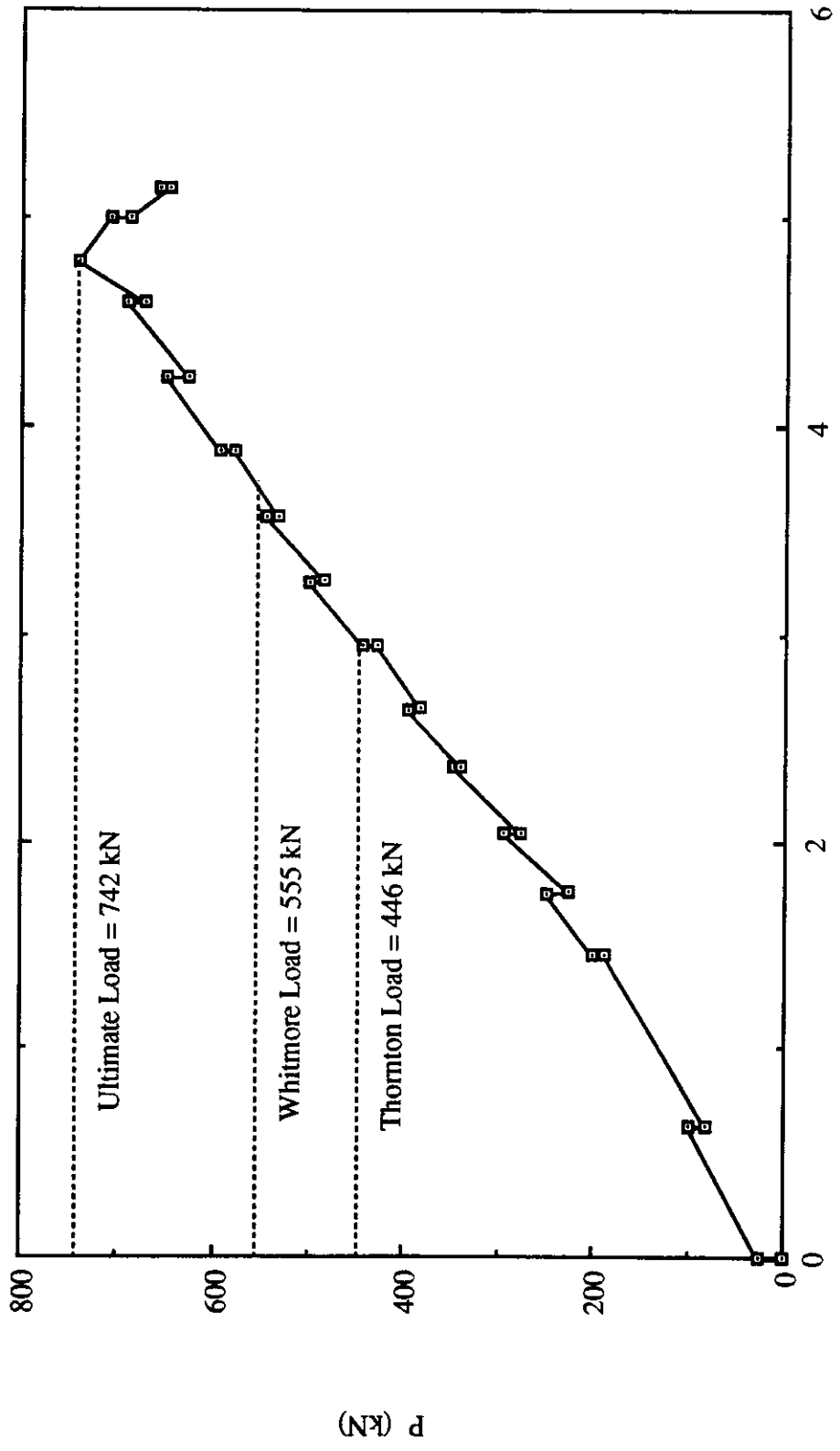

Fig. 3.4 Load vs. Vertical Displacement of Loading Head for Specimen GP3

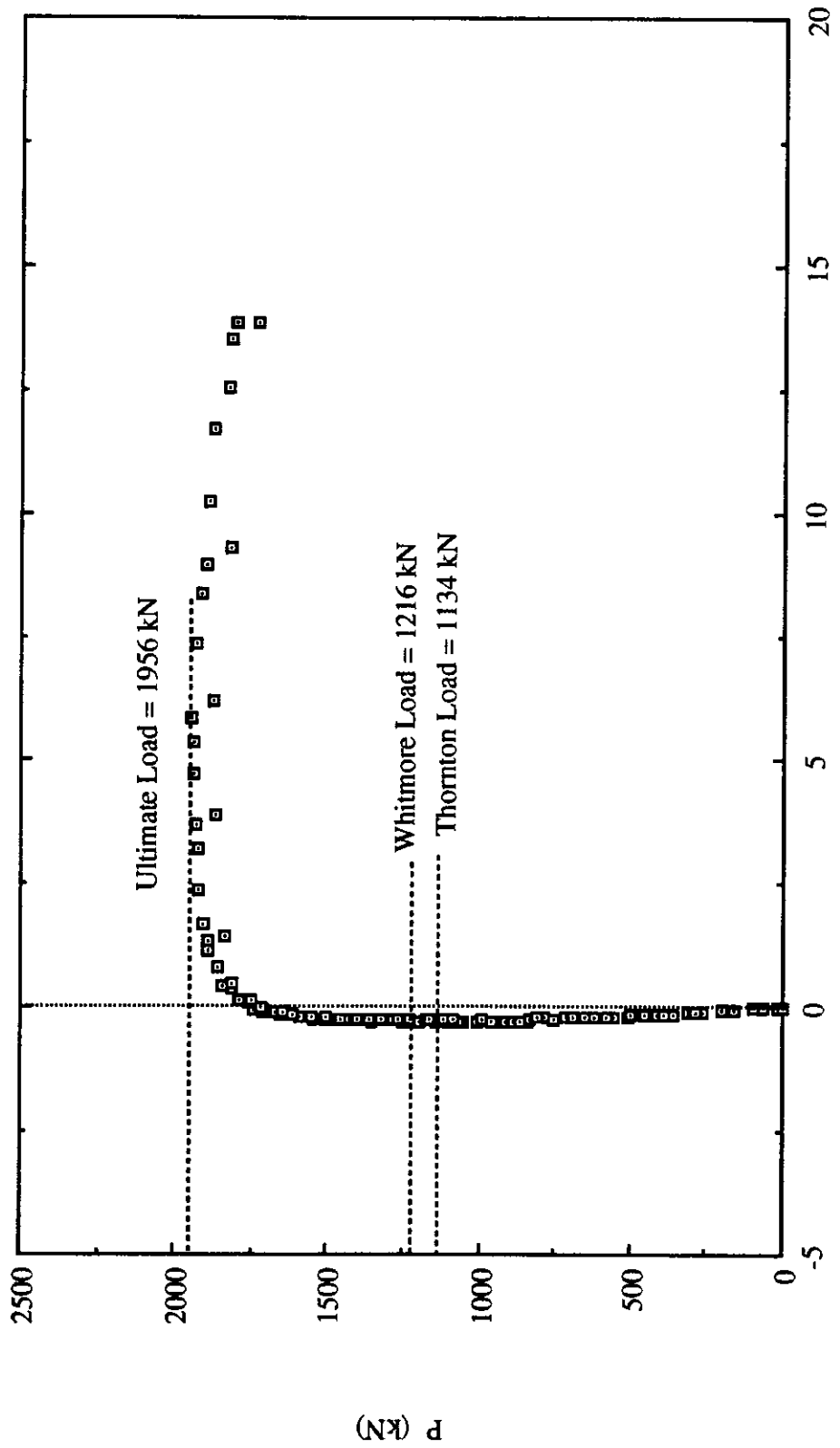

Fig. 3.5 Load vs. Out-of-Plane Displacement of Test Frame for Specimen GP1

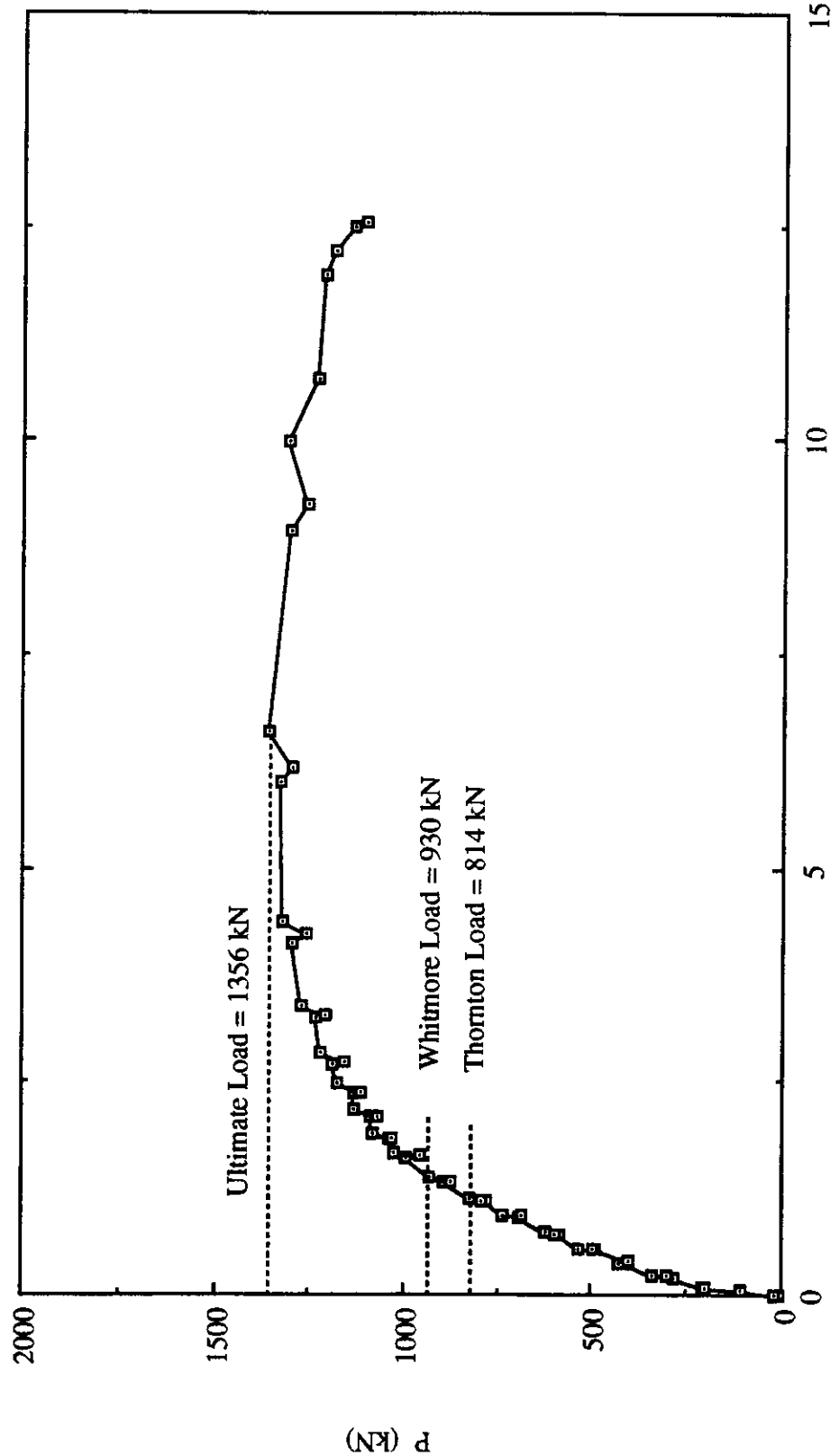

Fig. 3.6 Load vs. Out-of-Plane Displacement of Test Frame for Specimen GP2

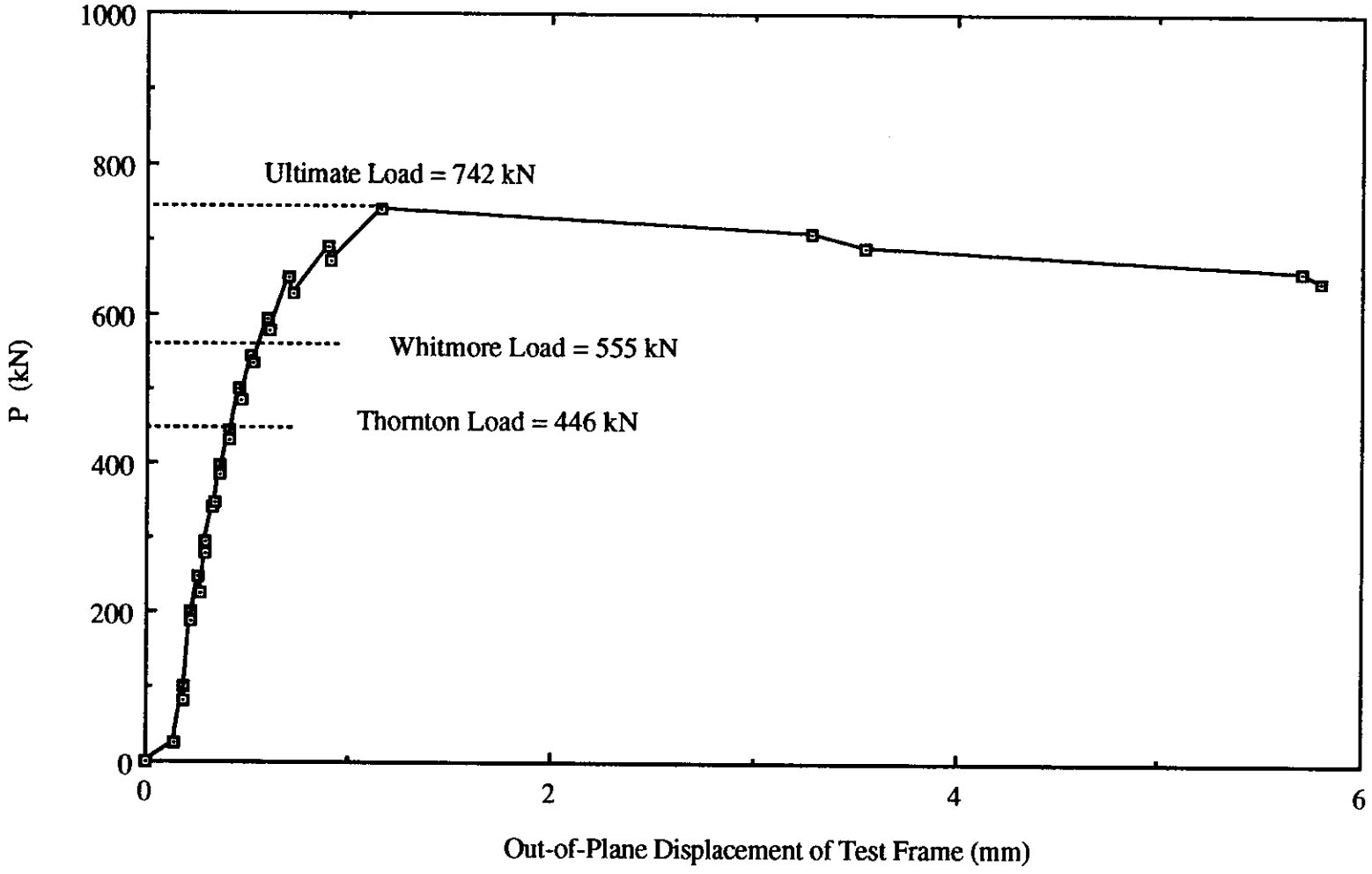

Fig. 3.7 Load vs. Out-of-Plane Displacement of Test Frame for Specimen GP3

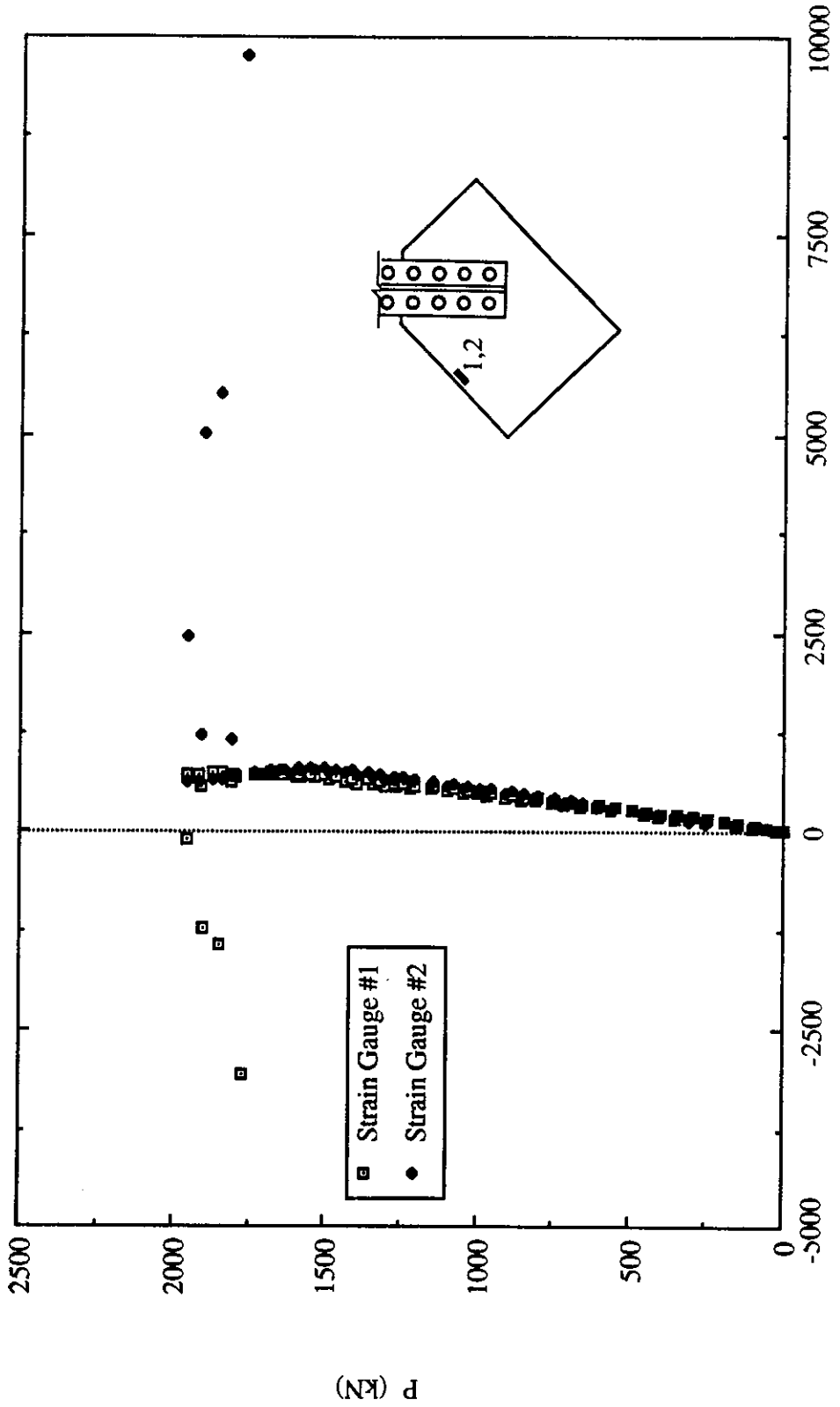

Fig. 3.8 Load vs. Strain Gauge Readings at Mid-Length of Long Free Edge for Specimen GP1

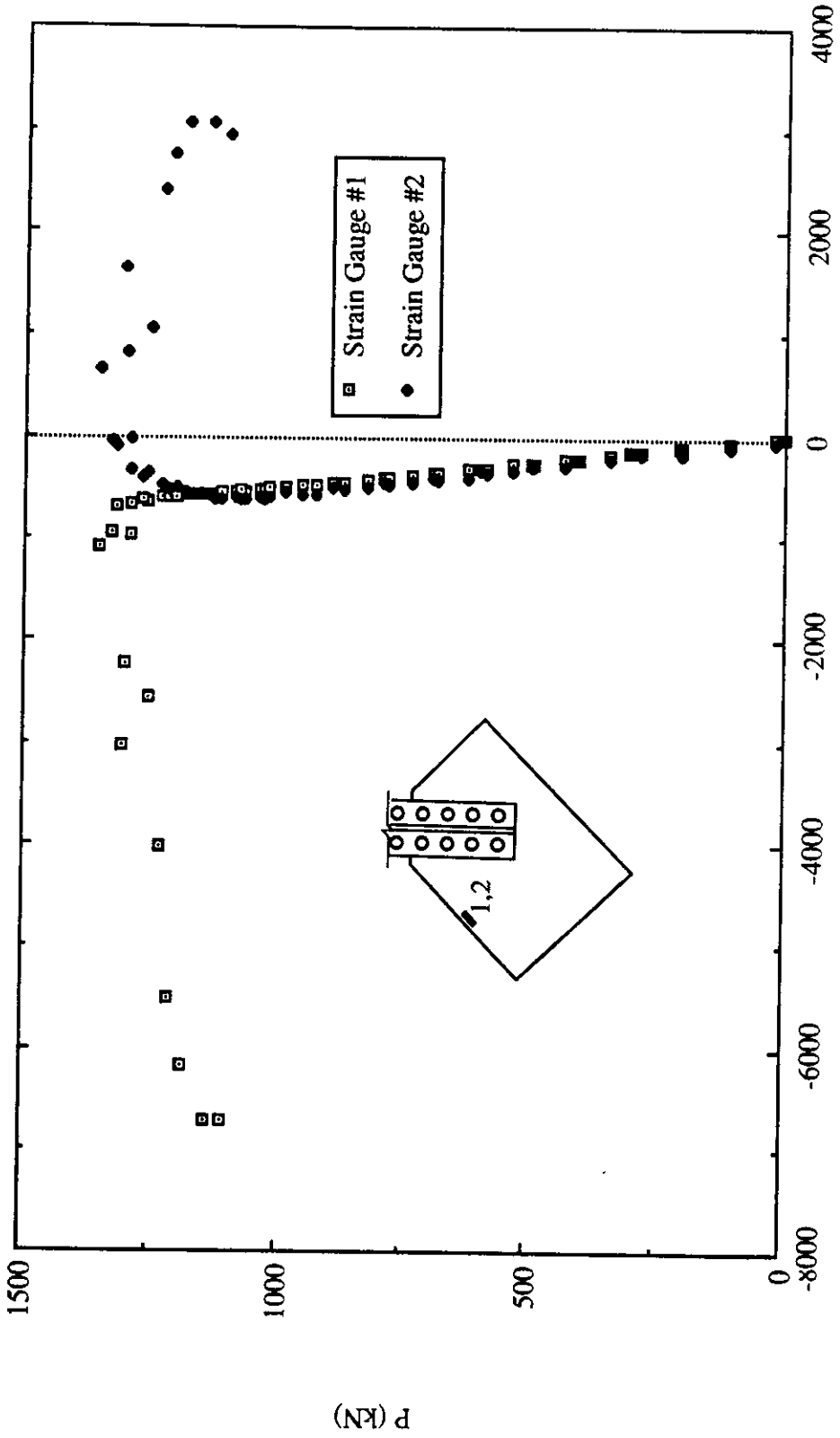

Fig. 3.9 Load vs. Strain Gauge Readings at Mid-Length of Long Free Edge for Specimen GP2

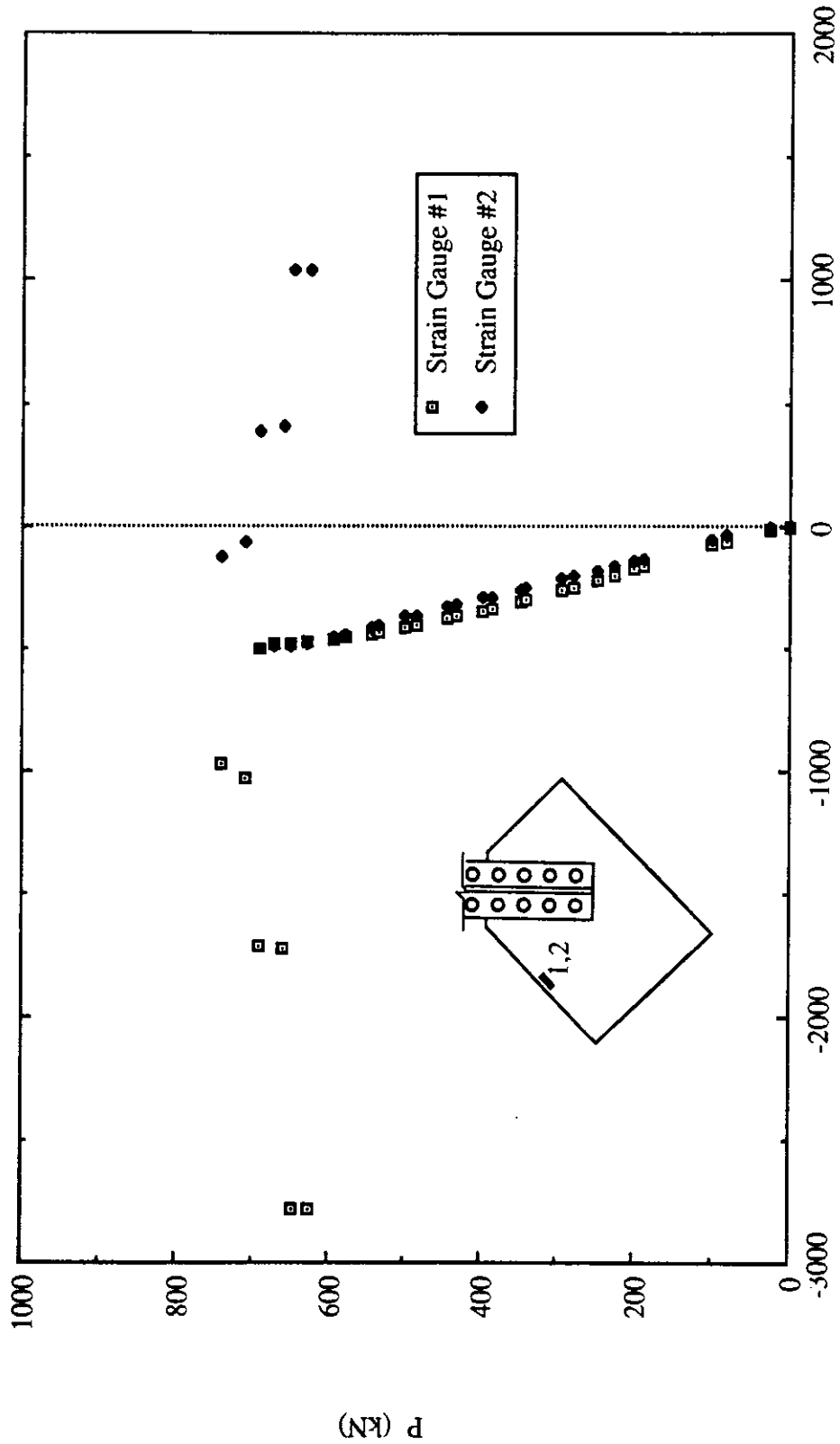

Fig. 3.10 Load vs. Strain Gauge Readings at Mid-Length of Long Free Edge for Specimen GP3

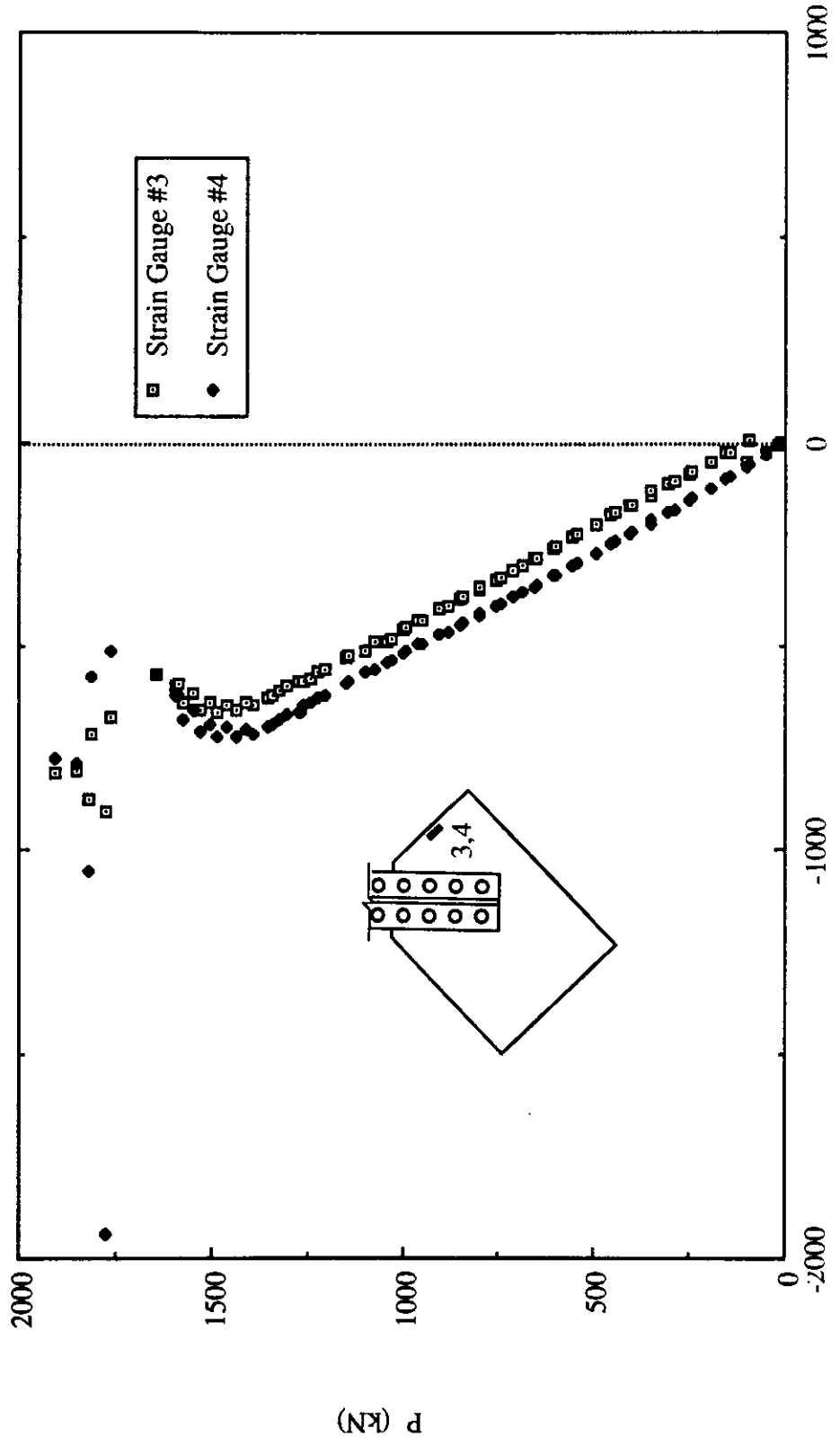

Fig. 3.11 Load vs. Strain Gauge Readings at Mid-Length of Short Free Edge for Specimen GP1

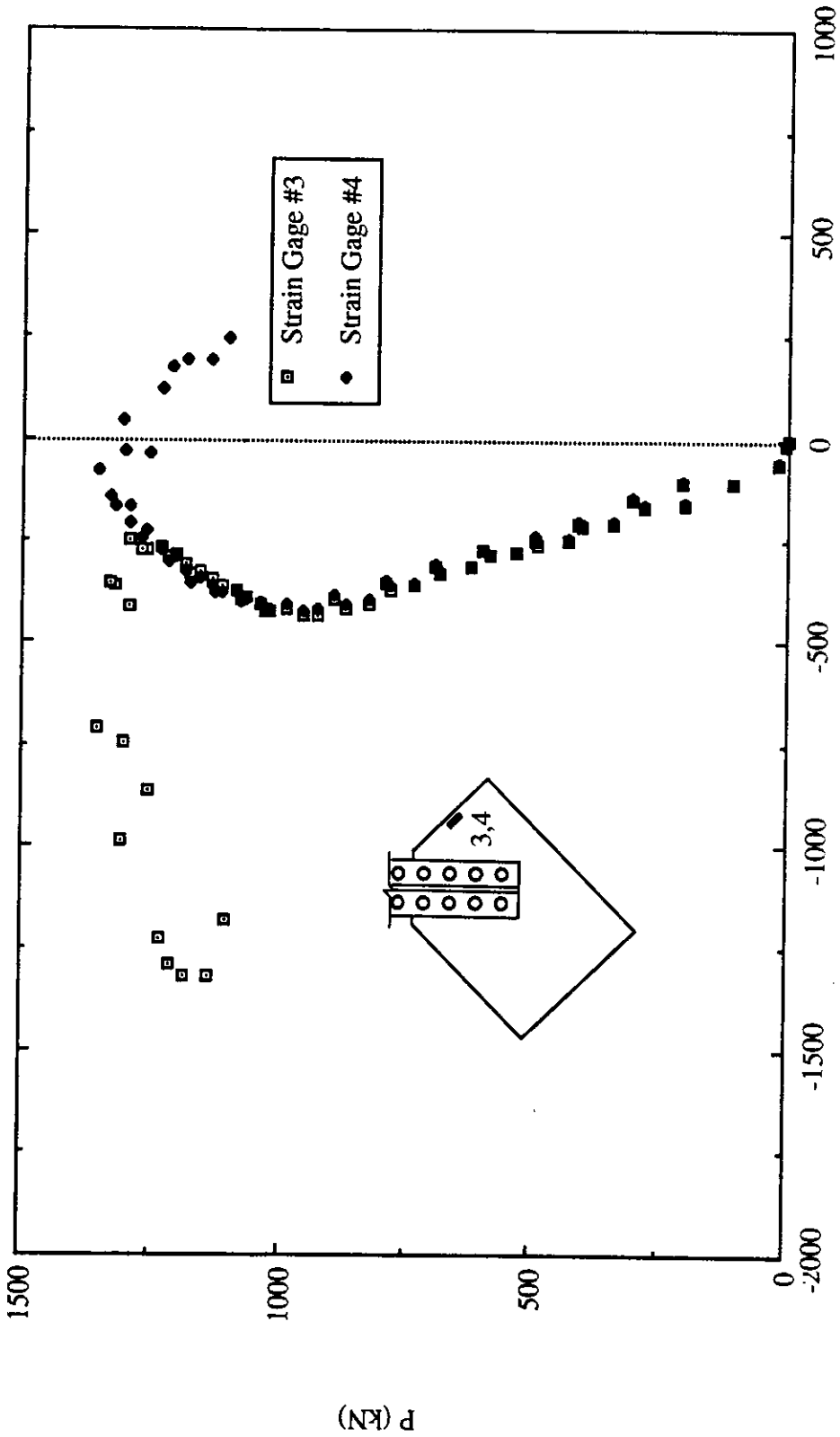

Fig. 3.12 Load vs. Strain Gauge Readings at Mid-Length of Short Free Edge for Specimen GP2

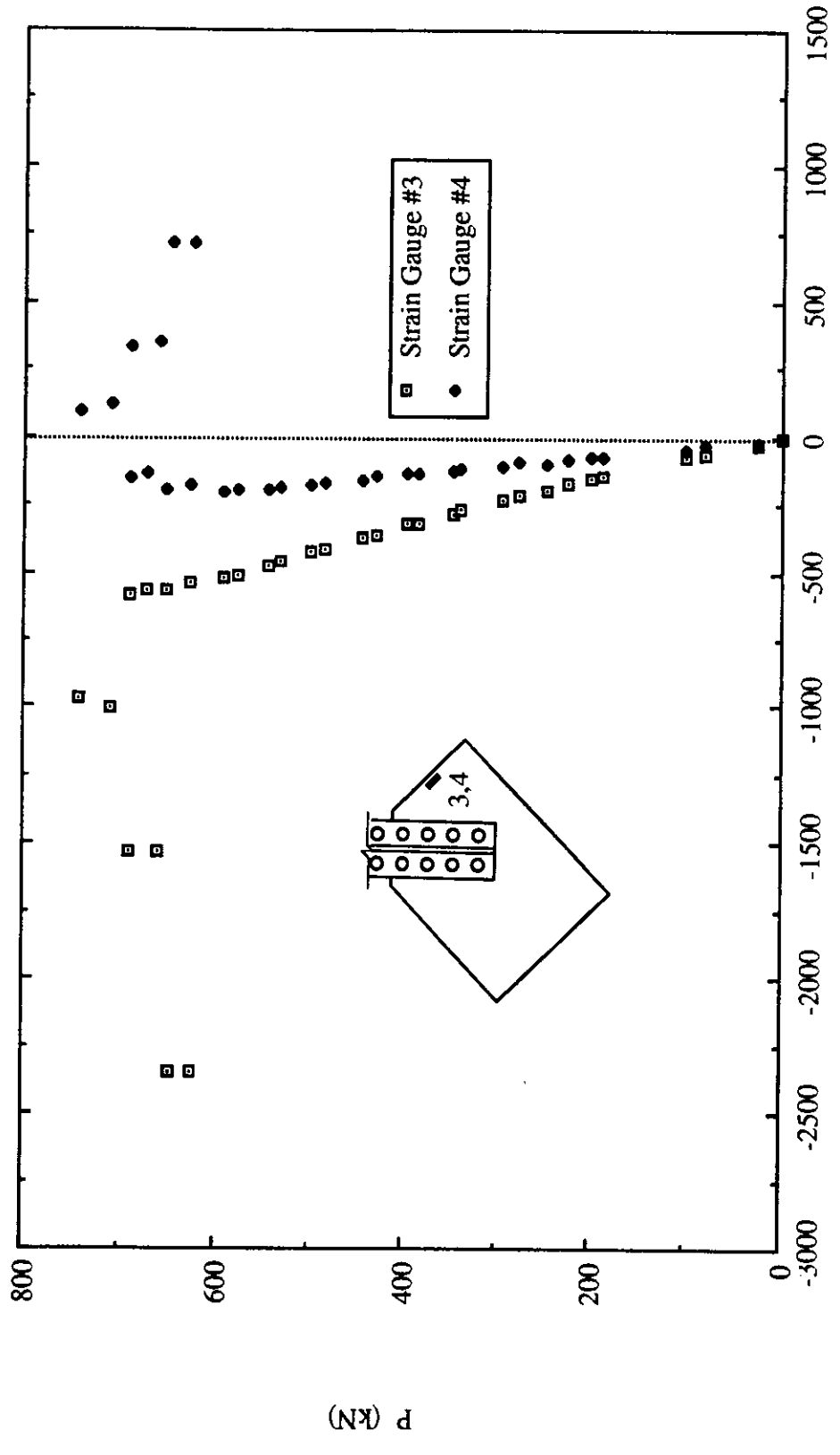

Fig. 3.13 Load vs. Strain Gauge Readings at Mid-Length of Short Free Edge for Specimen GP3

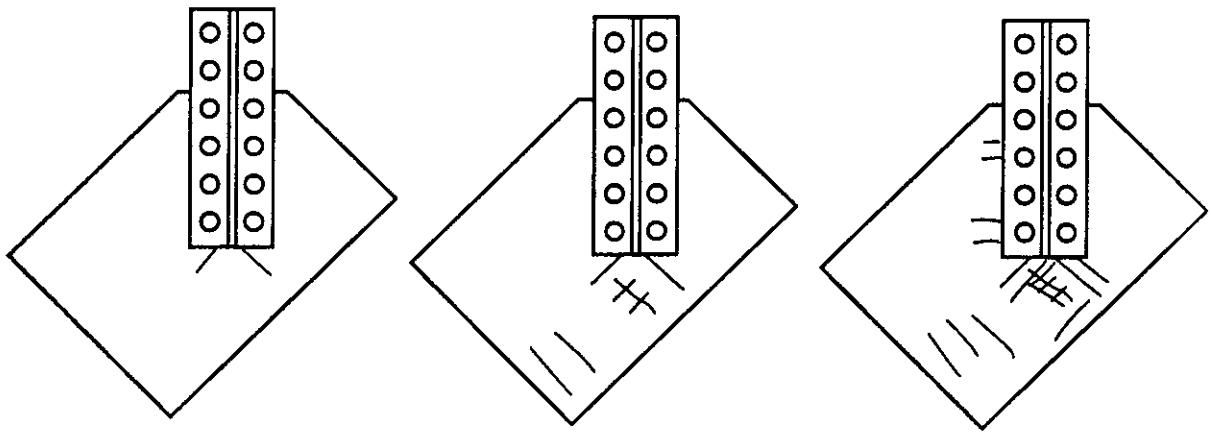

P = 1075 kN (a)

P = 1360 kN (b)

P = 1500 kN (c)

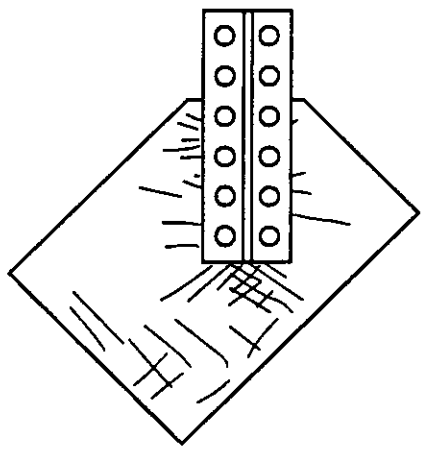

P = 1700 kN (d)

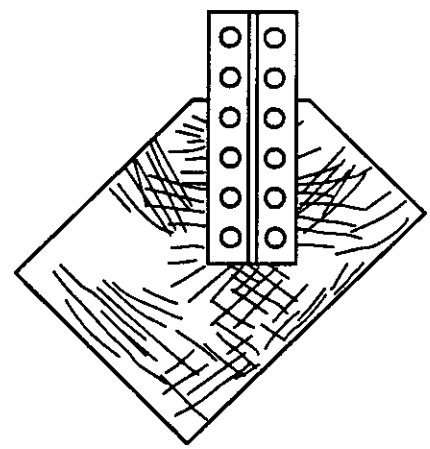

P = 1956 kN (e)

Fig. 3.14 Schematic of Yielding Process for Specimen GP1

Fig. 3.15 Picture of Failed Specimen GP1

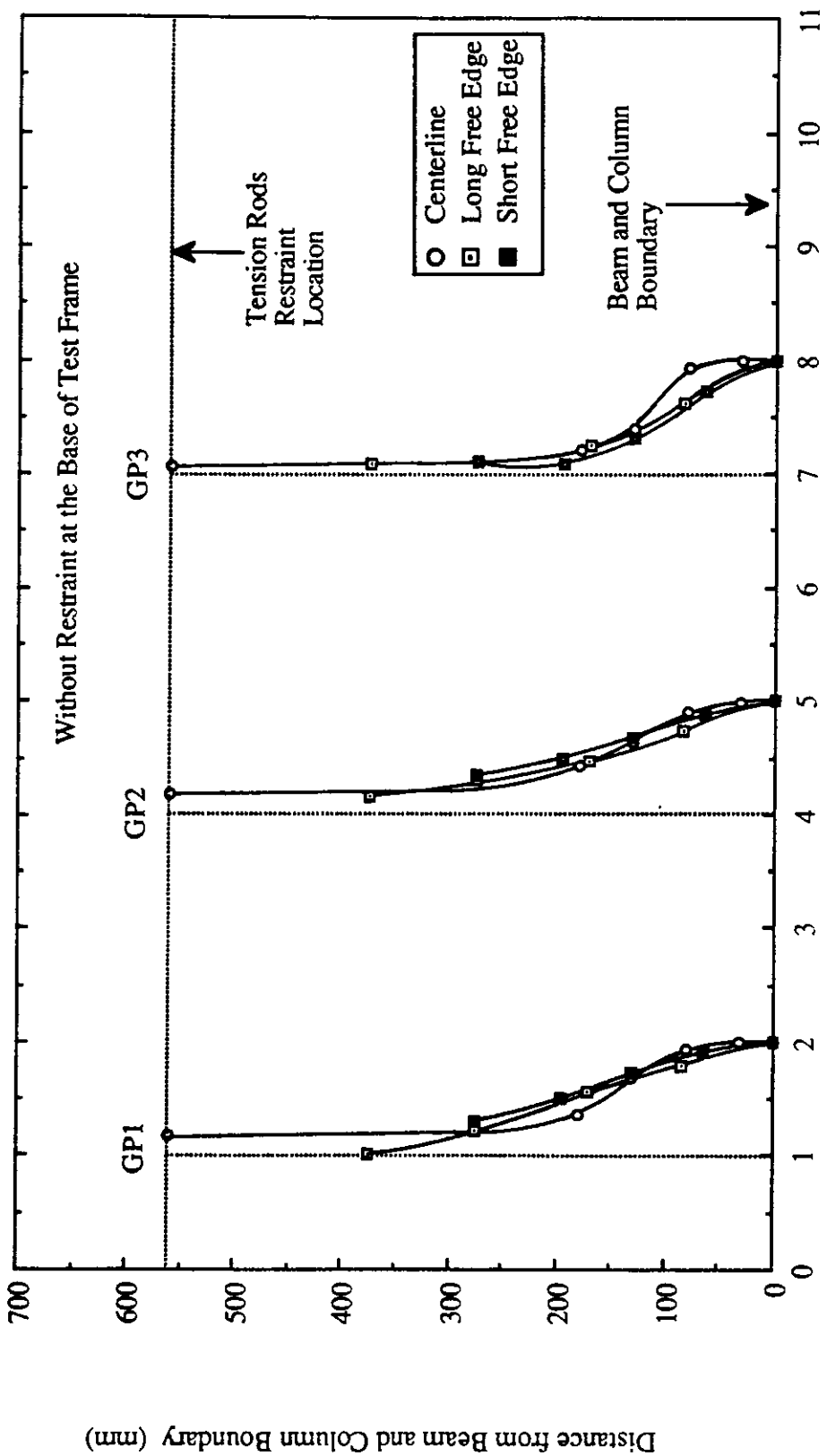

Fig. 3.16 Out-of-Plane Deflected Shapes at Free Edges and Along Centerline of Splice for GP Type Specimens

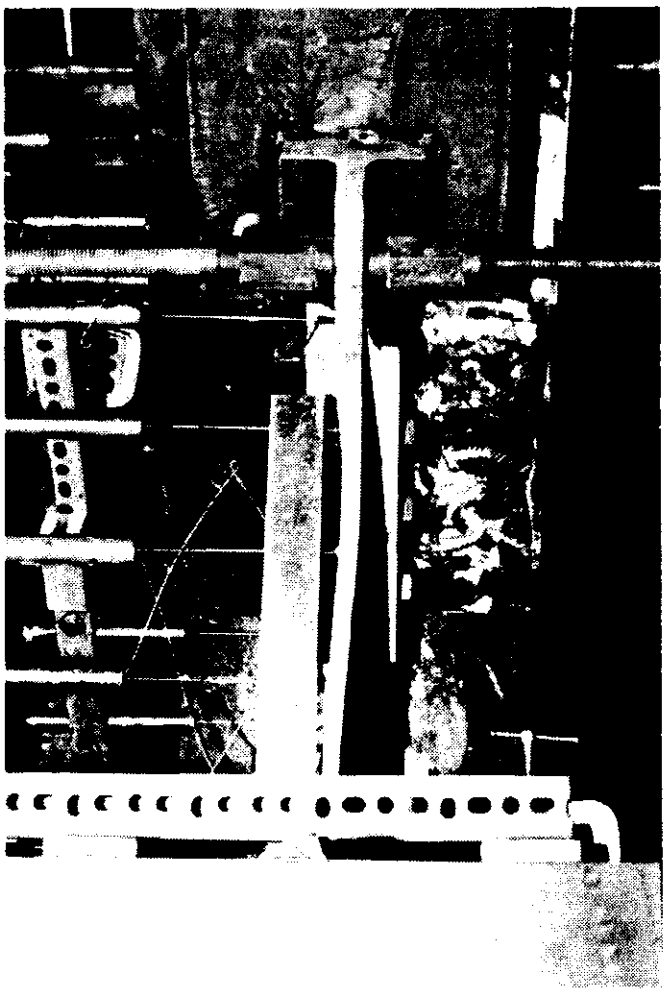

Fig. 3.17 Picture of Out-of-Plane Deflected Shapes at Long Free Edge for Specimen GP1

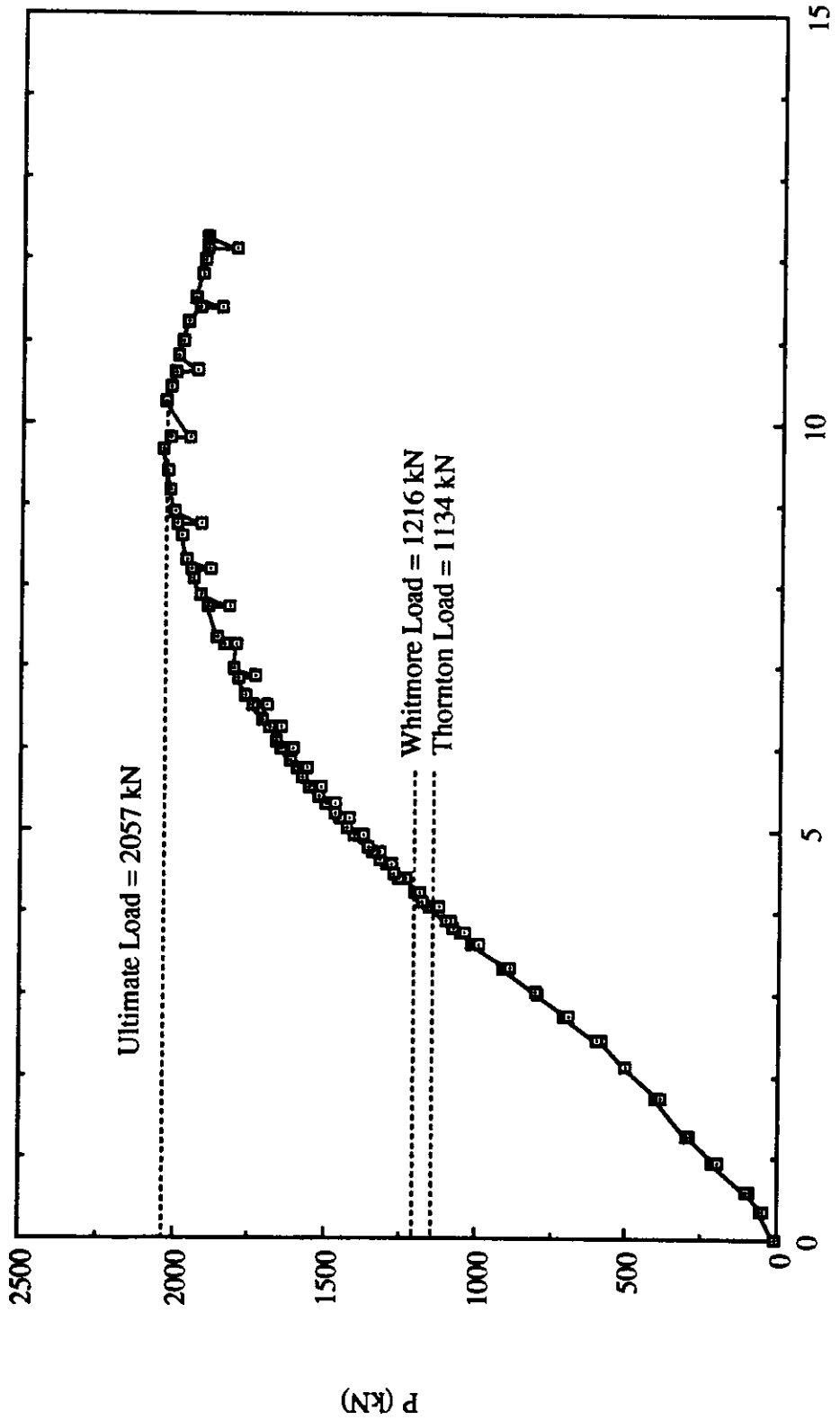

Fig. 3.18 Load vs. Vertical Displacement of Loading Head for Specimen GP1R

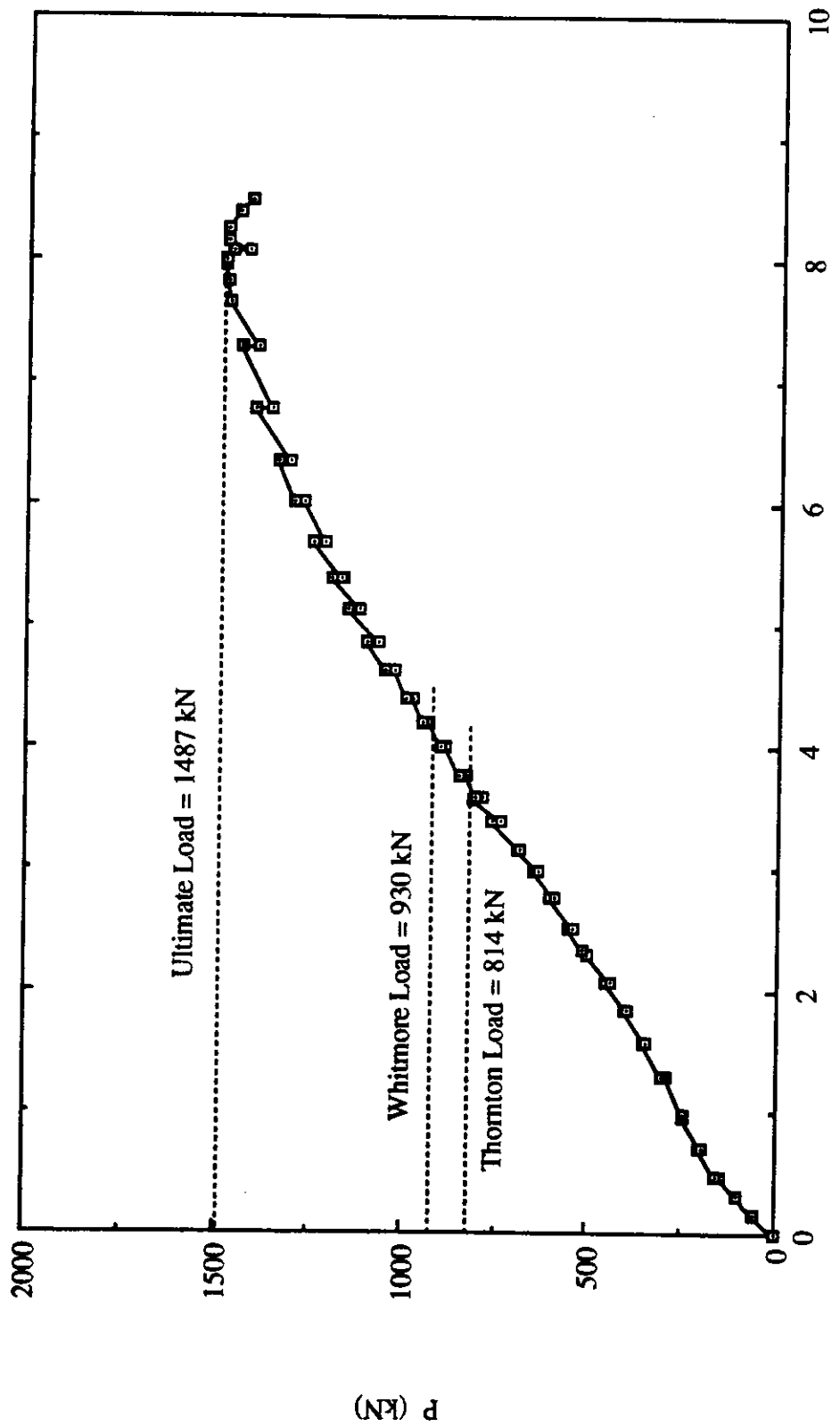

Fig. 3.19 Load vs. Vertical Displacement of Loading Head for Specimen GP2R

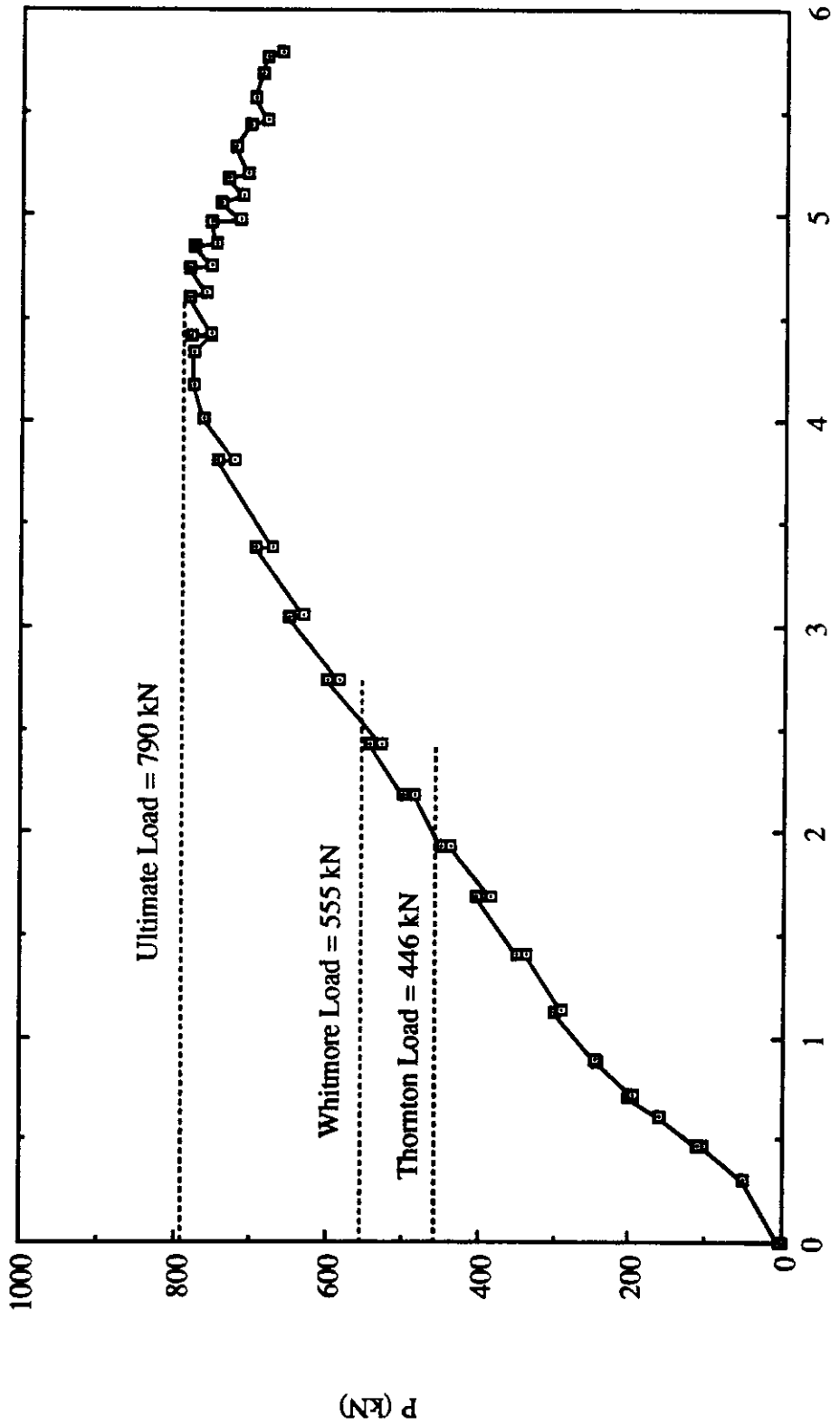

Fig. 3.20 Load vs. Vertical Displacement of Loading Head for Specimen GP3R

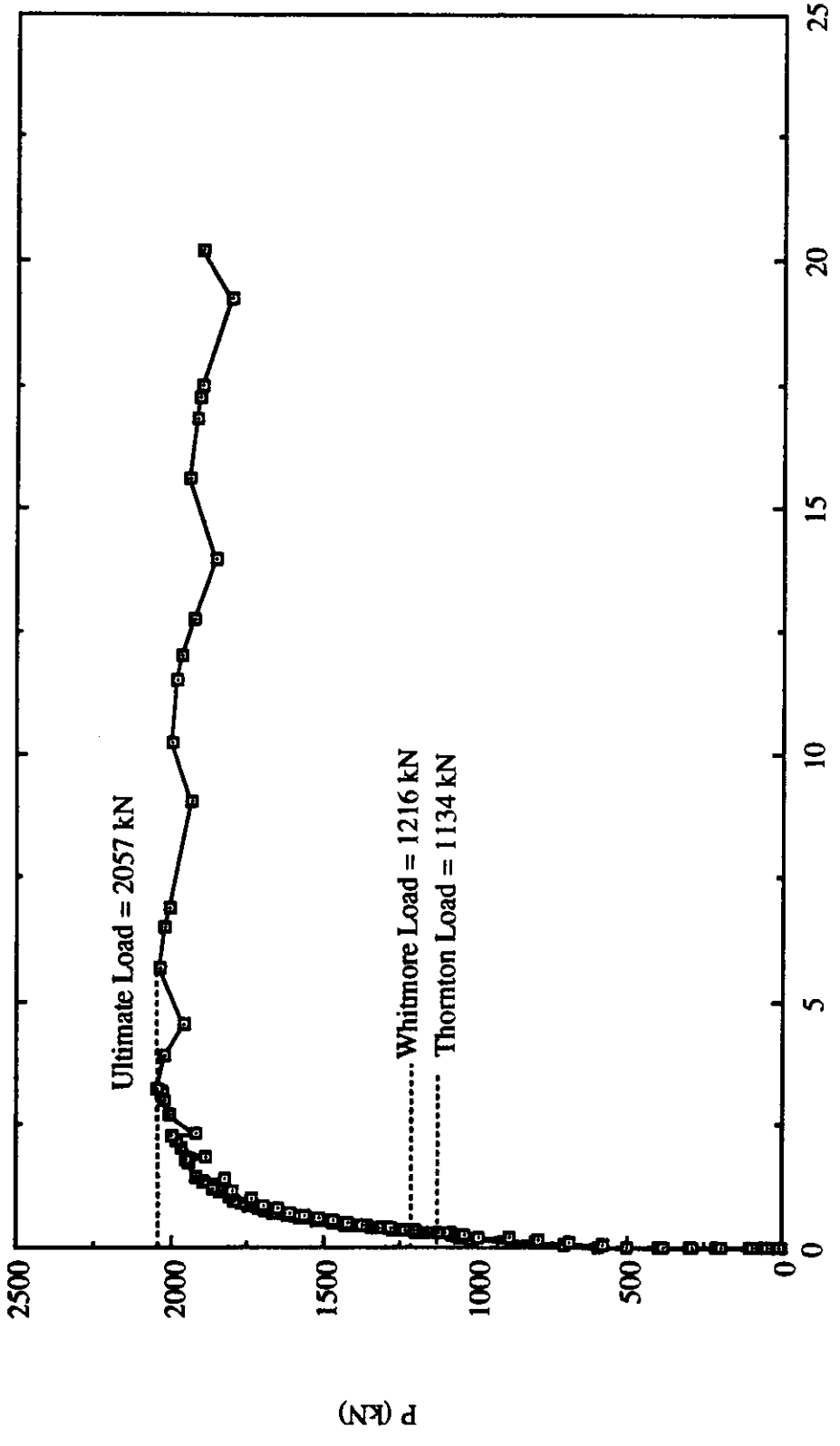

Fig. 3.21 Load vs. Out-of-Plane Displacement at Mid-Length of Long Free Edge for Specimen GP1R

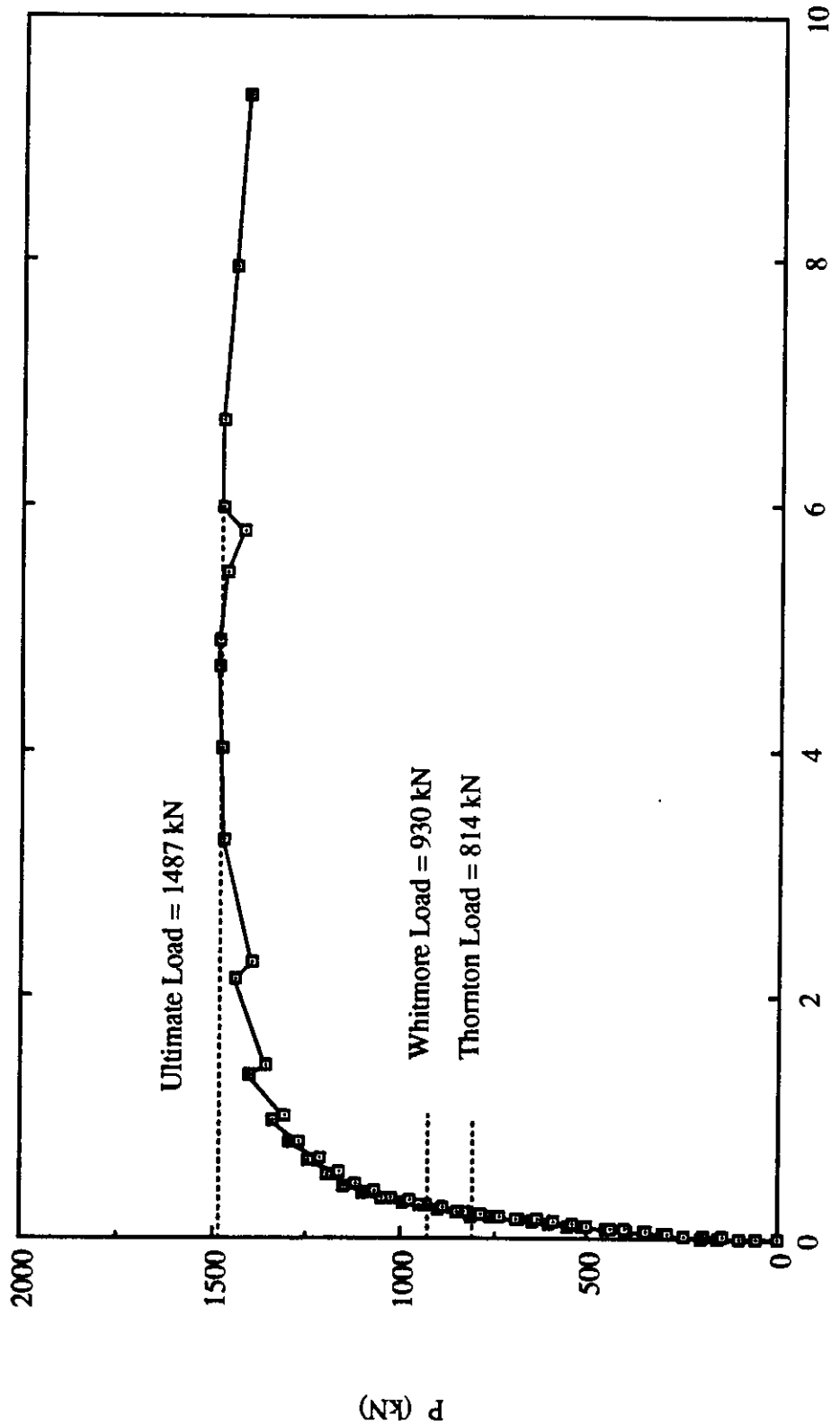

Fig. 3.22 Load vs. Out-of-Plane Displacement at Mid-Length of Long Free Edge for Specimen GP2R

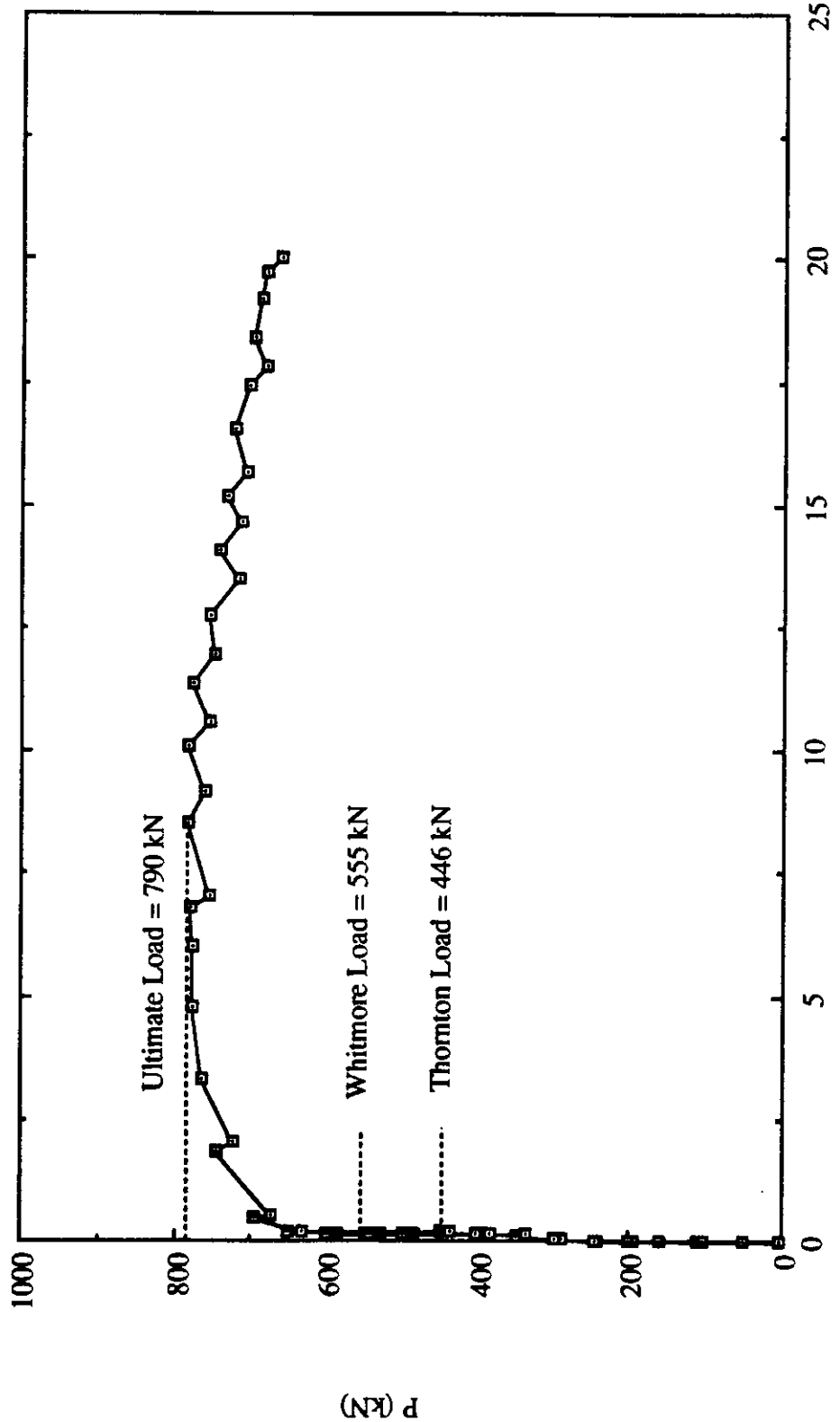

Fig. 3.23 Load vs. Out-of-Plane Displacement at Mid-Length of Long Free Edge for Specimen GP3R

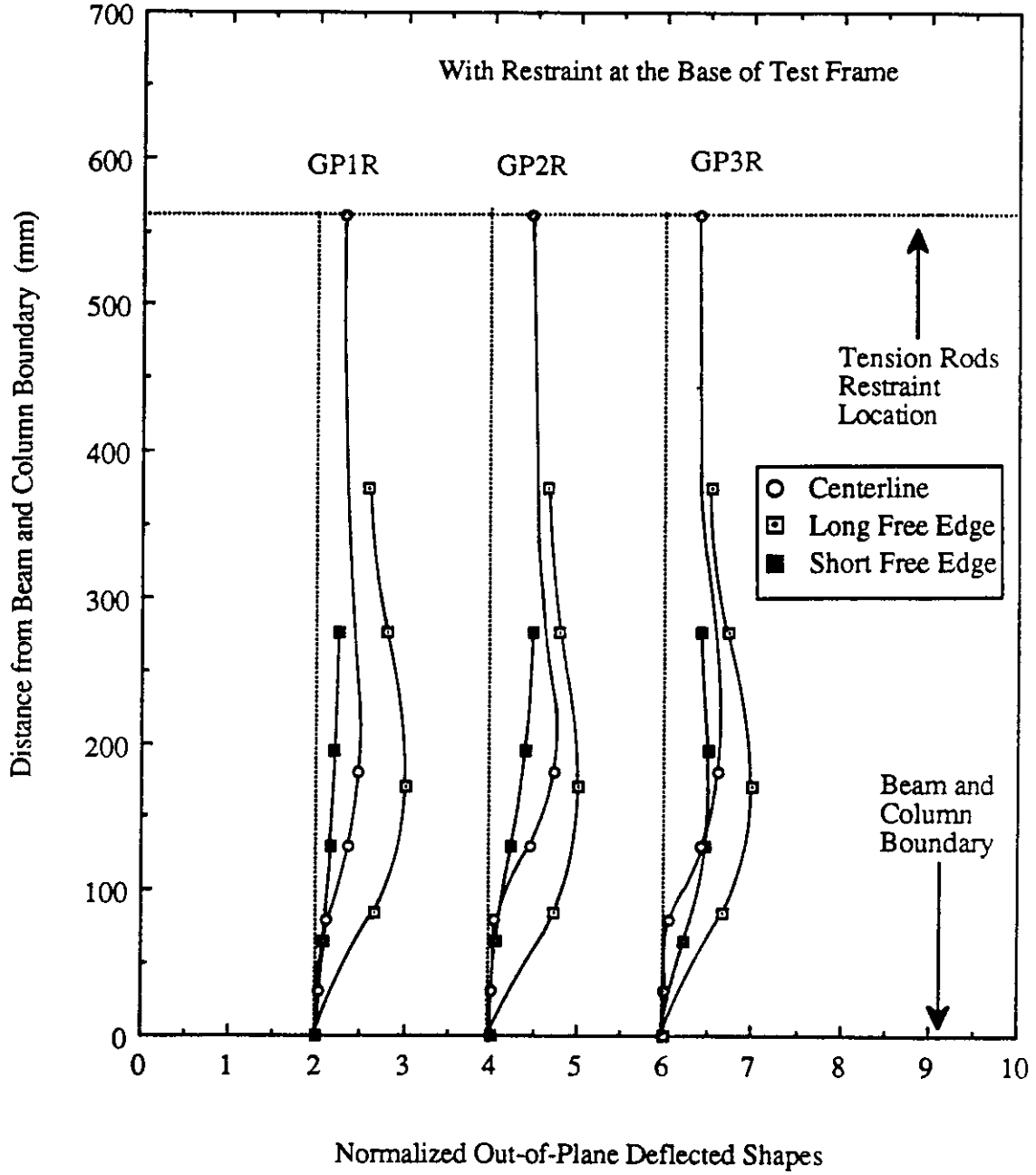

Fig. 3.24 Out-of-Plane Deflected Shapes at Free Edges and Along Centerline of Splice for GP Type Specimens - With Restraint

4. TEST RESULTS OF SP TYPE SPECIMENS

4.1 General

The SP type specimens were used to examine the effects of gusset plate size on the compressive behavior of the connection and two specimens were tested with plate thickness of 13.3 mm and 9.8 mm. Again, the out-of-plane restraint at the base of test frame was also included as a test variable in testing these specimens. The test results of the SP type specimens are summarized in Table 4.1. It can be seen from the table that the ultimate load of the specimens increased with increasing plate thickness. Test results also shows that appreciable increase in ultimate load was recorded for specimen SP1 when out-of-plane restraint was applied to the base of test frame. In addition, for specimen SP2 significant increase in ultimate load due to the out-of-plane restraint was observed as shown in Table 4.1. The predictions by both the Whitmore method and the Thornton method are also included in the table. In general, it can be seen that the Witmore method overestimated the strength of the specimens for both restraint conditions except for the case of specimen SP2 with restraint. On the other hand, the Thornton method provided conservative estimates of the strength of specimens.

4.2 Without Out-of-Plane Restraint at Base of Test Frame

4.2.1 Behavior of Load Versus In-Plane Deformation

The failure mode for both specimens SP1 and SP2 was sway buckling of the connection. The curves of load versus vertical displacement of the loading head are illustrated in Figs. 4.1 and 4.2. It can be seen from these figures that both specimens were not able to reach the yield load level estimated by the Whitmore's method. However, the ultimate load of the thick specimen (SP1-13.3 mm) reached about 87 percent of the corresponding Whitmore load. On the other hand, the thin specimen (SP2-9.8 mm) only reached about 71percent of the corresponding Whitmore load. Linear load deflection was observed until the applied

load was close to the ultimate load at which significant out-of-plane displacement had occurred. In particular, the load deflection curve for specimen SP2 was linear until it reached the ultimate load. The vertical displacement of the loading head only increased slightly after the specimens buckled.

4.2.2 Behavior of Load Versus Out-of-Plane Displacement of Test Frame

Out-of-plane displacement of the test frame was recorded for both specimens from the beginning of loading due to the presence of initial imperfections. These imperfections were caused by the initial out-of-straightness of the plate and the welding procedure. The curves of load versus out-of-plane displacement of the test frame are shown in Figs. 4.3 and 4.4. For specimen SP1 the load deflection curve gradually increased until the applied load reached approximately 1400 kN at which significant out-of-plane displacement was observed. The displacement continued to increase with slight increase in applied load. At a displacement of about 16 mm, a significant increase in stiffness of the connection was observed. This increase in stiffness was probably caused by local bending of the gusset plate underneath the splice member and this will be discussed later when examining the strain gauges readings. The ultimate load of the specimen was reached at 1606 kN and with a deflection of about 17.5 mm. For specimen SP2, the load versus out-of-plane displacement curve gradually increased until buckling of the specimen occurred. The ultimate load of the specimen was reached at 1010 kN with a displacement of about 17.5 mm. The final displacement of the test frame was approximately 24.5 mm and the applied load was maintained very close to the ultimate load of the specimen.

4.2.3 Strain Gauges Results

The curves of load versus strains are shown in Figs. 4.5 to 4.10. It can be seen from the plots for strain readings recorded at the mid-length of the free edges (Figs. 4.5, 4.6, 4.7, and 4.8) that bending of the plate occurred from the beginning of loading. Again, this was

mainly caused by the plate initial imperfections and hence the misalignment of loading head. Nonetheless, these plots indicated the occurrence of strain bifurcation when the specimens buckled. It should also be noted that the strain readings for the specimens were within the elastic range prior to reaching the ultimate load. As mentioned from above that a change of bending direction of the plate underneath the splice member was observed at a load level of about 1400 kN for specimen SP1. This phenomenon can be shown by the plot of load versus rosette strain readings at a load level close to ultimate for specimen SP1 as illustrated in Fig. 4.9. This figure illustrates that strain reversal existed at a load level of about 1380 kN at which a change of bending direction of the plate underneath the splice member had occurred. As out-of-plane displacement of test frame increased from this load level compressive strain at rosette gauge #22 decreased while increasing compressive strains were recorded at rosette gauge #21 as shown in Fig. 4.9. At a load level of about 1506 kN compressive strain at rosette gauge #22 increased due to local bending of the plate underneath the splice member and a significant increase in compressive strain at rosette gauge #21 was also observed. This local bending behavior of the plate might attribute to the increase in out-of-plane stiffness of the specimen at this load level. The applied load continued to increase with increasing compressive strain at rosette gauge #22 until ultimate load was reached.

4.2.4 Yielding Behavior of Specimens

In general, only moderate yielding was observed for the SP type specimens. For specimen SP1 yielding was first observed close to the corner of the beam and column boundary at a load level of about 1200 kN. As load increase to approximately 1550 kN, yield lines were observed in the area about the two sides of the splice member and also underneath the splice member. When the applied load approached the ultimate load, yielding at the corner of the beam and column boundary increased. Finally, at ultimate yield line mechanism was observed on the specimen along the beam and column boundary as shown in Fig. 4.11.

For specimen SP2 yield lines were first detected in the area about the two sides of the splice member when the applied load was approximately 900 kN. As load increased, yielding was also observed near the beam and column boundary. Again, yield line mechanism was formed along the beam and column boundary at ultimate.

4.2.5 Out-of-Plane Displacement of Free Edges and Along the Centerline of Splicing Member

The out-of-plane deflected shapes for the specimens are shown in Fig. 4.12. In general, it can be seen from this figure that the deflected shapes resembled the buckled shapes of a fixed-guided column except for the deflected shapes of the long free edge of specimen SP2. This different deflected shape was caused by the initial out-of-straightness of the free edge. In fact, significant warping of the specimen was observed after the plate was first welded to the beam and column. Hence, to correct the imperfection the specimen was cut from the beam and column and re-welded back on. However, noticeable imperfection still existed after re-welding. For specimen SP1, the LVDTs readings at early stage of loading indicated that the deflected shape along the centerline of the splice member was similar to that of the long free edge of specimen SP2. However, as the applied load increased close to the ultimate load the deflected shape shifted to the fixed-guided mode.

4.3 With Out-of-Plane Restraint at the Base of Test Frame

4.3.1 General

It was mentioned in the previous chapter that same SP type specimens were used in conducting tests of both out-of-plane restraint conditions at base of test frame. As expected, permanent deformation existed in the failed specimens after the tests of without restraint condition. Therefore, in order to correct the imperfection lateral force was applied to the beam and column to push the failed specimen back to its original position.

Unfortunately, appreciable imperfection still existed in the specimens after this remedial measure.

4.3.2 Behavior of Load Versus In-Plane Deformation

The curves of load versus vertical displacement of the loading head are illustrated in Figs. 4.13 and 4.14. Initial nonlinearity of load deflection curves existed due to settling of the test fixtures. Subsequently, linear behavior was observed until the applied load approached the ultimate load. In particular, the applied load increased gradually to the ultimate load for specimen SP1. On the other hand, a relatively rapid increase to the ultimate load was observed for specimen SP2. It can be seen from the figures that after reaching the ultimate load the applied load decreased with increasing vertical deflection.

4.3.3 Behavior of Load Versus Out-of-Plane Displacement at Mid-Length of Long Free Edge

The curves of load versus the out-of-plane displacement at mid-length of long free edge are shown in Figs. 4.15 and 4.16. For both specimens, nonlinear load deflection behavior was observed at the beginning of loading. This was mainly caused by the initial imperfection induced after the previous testing of the specimens as mentioned above. In addition, the curve for specimen SP2 indicated that the long free edge at mid-length originally deformed towards east. However, when loading continued the deformation gradually moved towards west until buckling occurred at which the plate deformed towards east again. This behavior was probably due to local bending of the specimen at the mid-length of long free edge caused by the imperfection. When the specimen reached the ultimate load, the connection buckled towards east which forced the long free edge to deform in the same direction.

4.3.4 Yielding Behavior of Specimens

Since these two specimens were tested previously, therefore, only additional yielding observed in the tests with restraint at conjunction of gusset-to-splice will be discussed. For both specimens yield lines were recorded at the gusset plate near the corner of the splice member as shown in Figs. 4.17 and 4.18. Local out-of-plane deflection of the specimens was also observed underneath the splice member. In addition, yield line mechanism was recorded at the mid-length of the free edges. This yield line mechanism was originated from the gusset plate area near the corner of the splice member and extended towards the mid-length of the free edges as shown in Fig. 4.19 .

4.3.5 Out-of-Plane Displacement of Free Edges and Along the Centerline of Splicing Member

The normalized out-of-plane displacement for the free edges and along the centerline of the splice member for both specimens are shown in Fig. 4.20. Again, it can be seen from the figure that out-of-plane movement at the conjunction of gusset-to-splice was recorded. Similar to GP type specimens, these displacement was caused by bending of the web of the bracing about the tension rod supports. Nonetheless, these figures show the effects of out-of-plane restraint on the buckled shapes of the specimens. It should also be noted that maximum out-of-plane displacement for both specimens occurred at the long free edge.

Table 4.1 Test Results of SP Type Specimens

Specimen Designation	Plate Size (mm x mm x mm)	Ultimate Load Without Restraint (kN)	Ultimate Load With Restraint (kN)	Whitmore Load P_w (kN)	Thornton Load P_t k=0.65 (kN)
SP1	850 x 700 x 13.3	1606	1760	1852	1228
SP2	850 x 700 x 9.8	1010	1477	1416	640

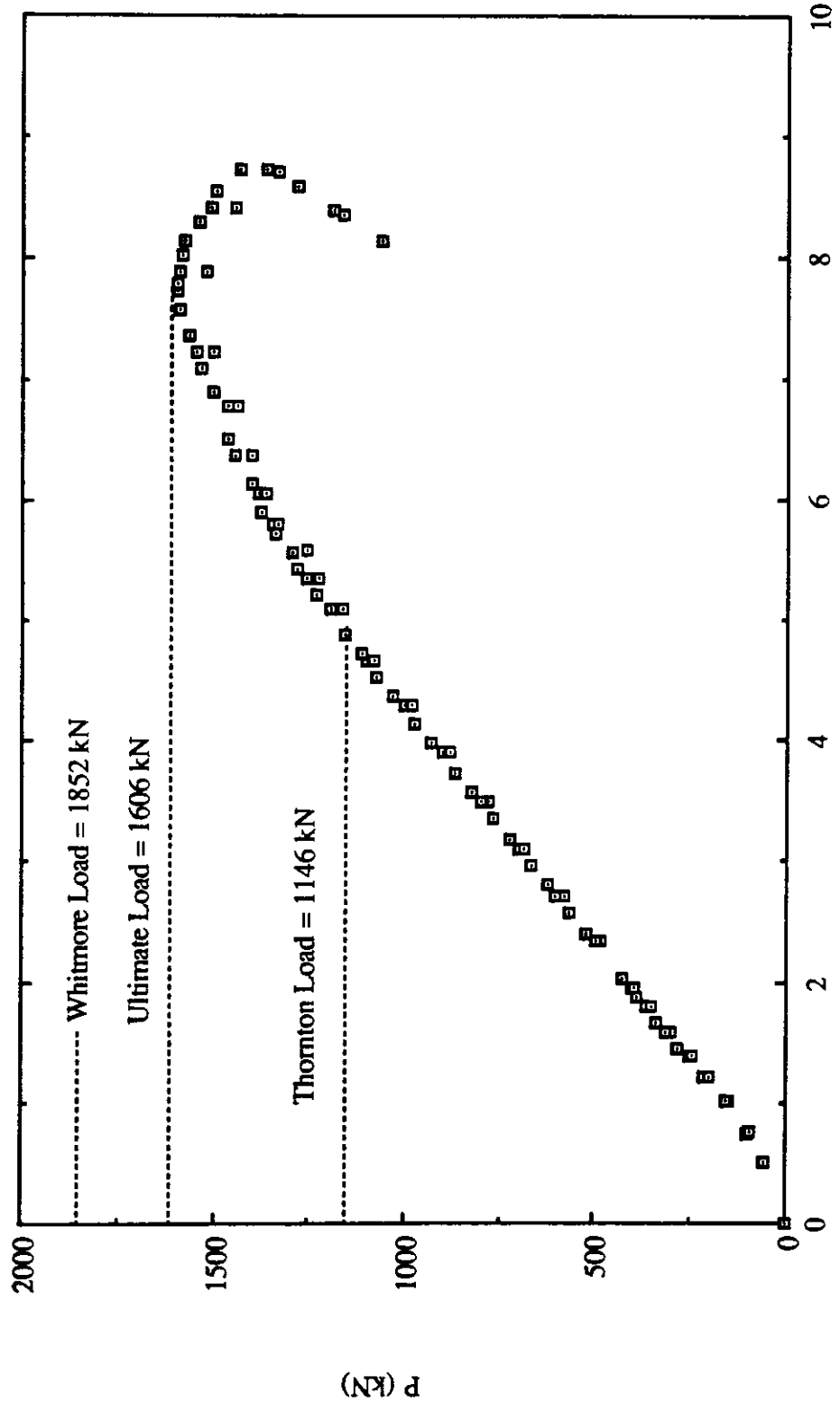

Fig. 4.1 Load vs. Vertical Displacement of Loading Head for Specimen SP1 - Without Restraint

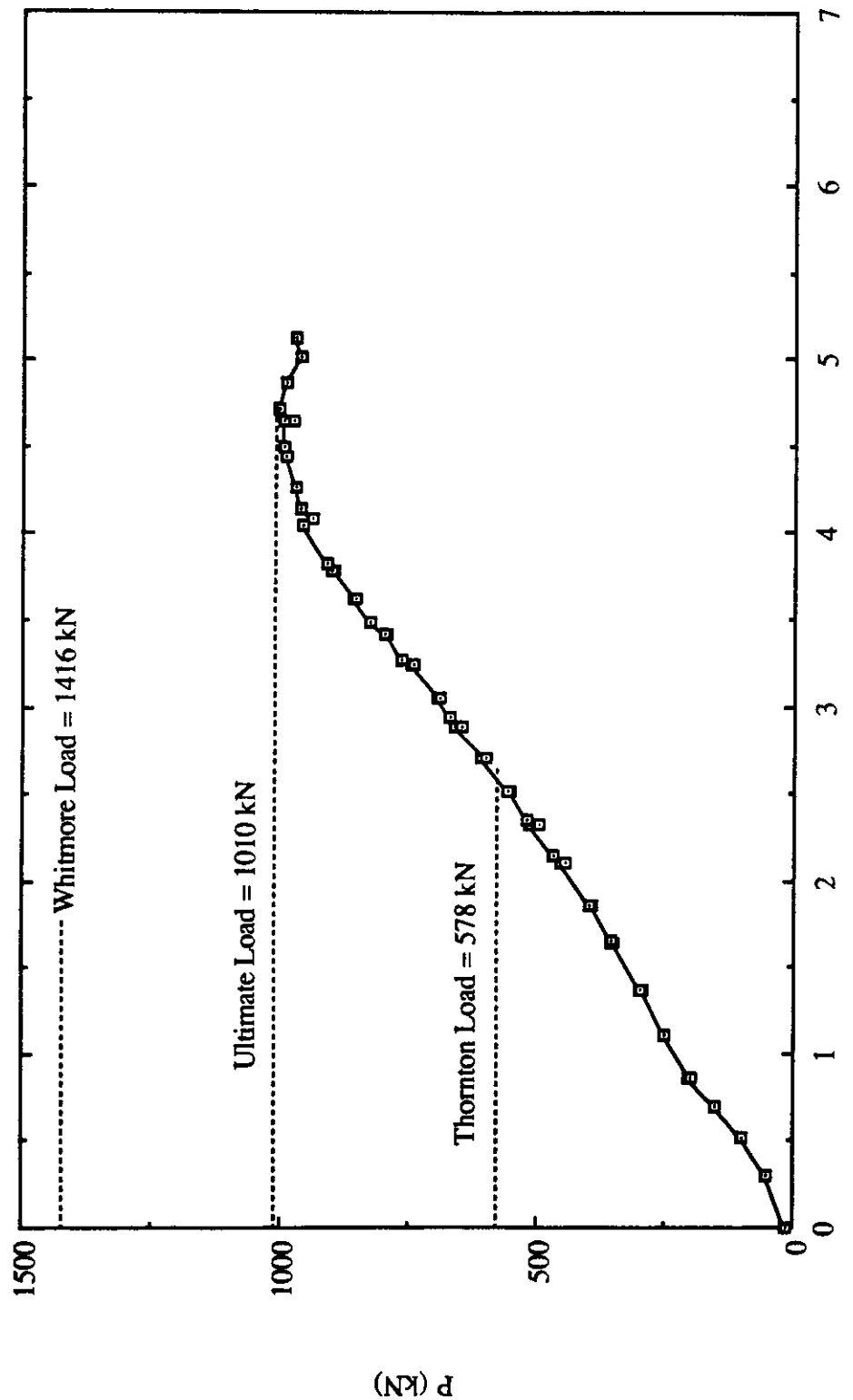

Fig. 4.2 Load vs. Vertical Displacement of Loading Head for Specimen SP2 - Without Restraint

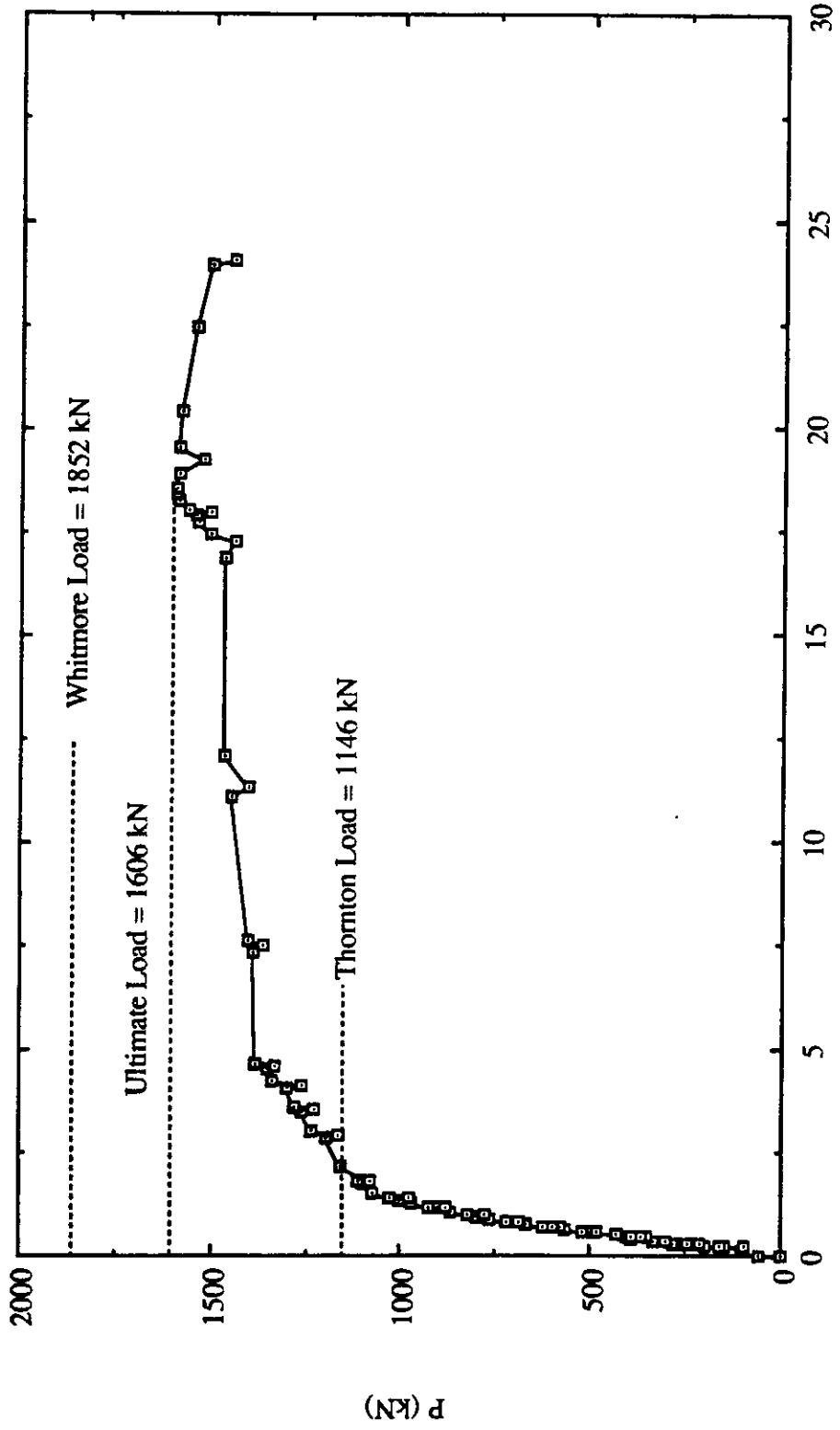

Fig. 4.3 Load vs. Out-of-Plane Displacement of Test Frame for Specimen SP1 - Without Restraint

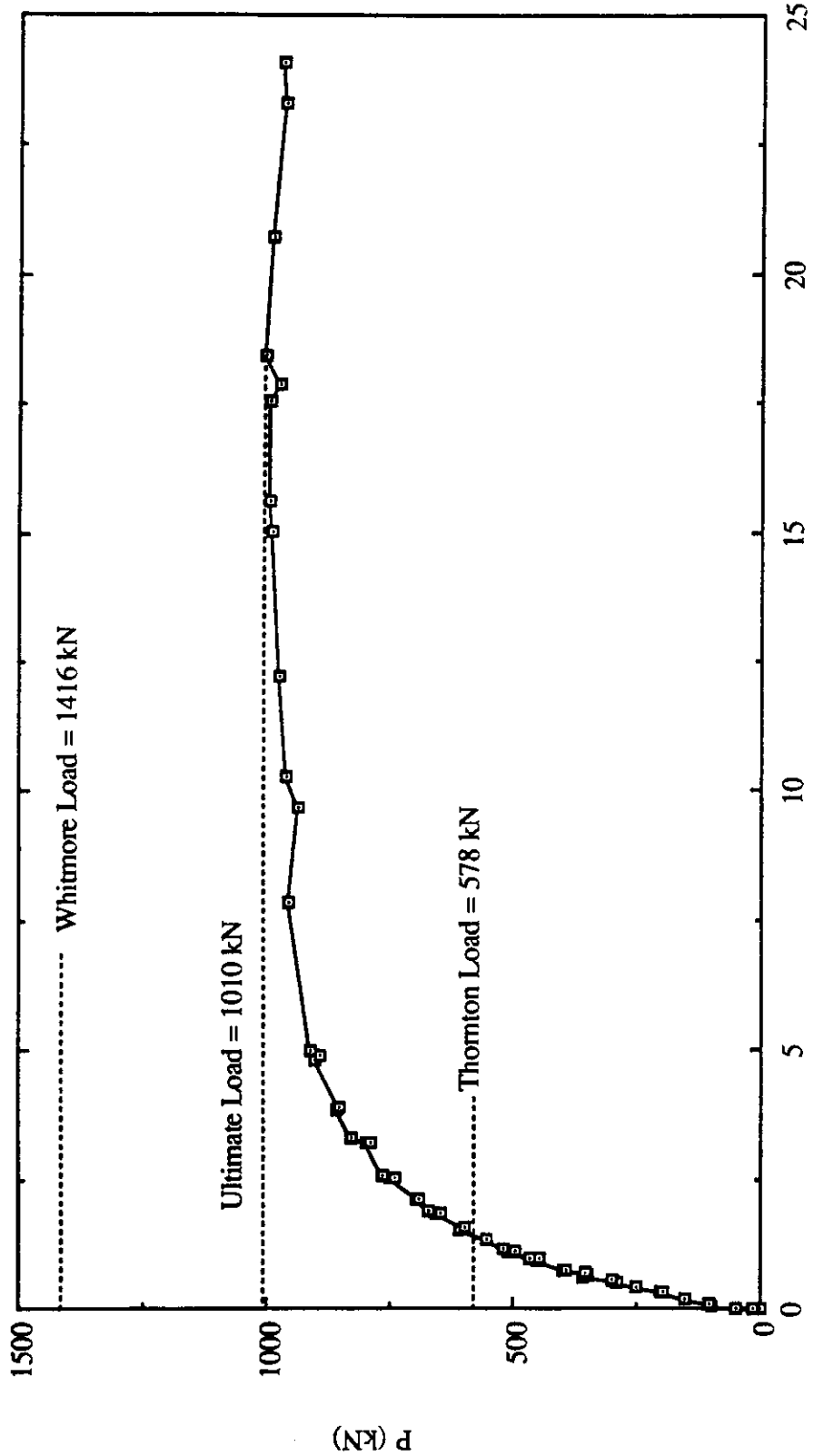

Fig. 4.4 Load vs. Out-of-Plane Displacement of Test Frame for Specimen SP2 - Without Restraint

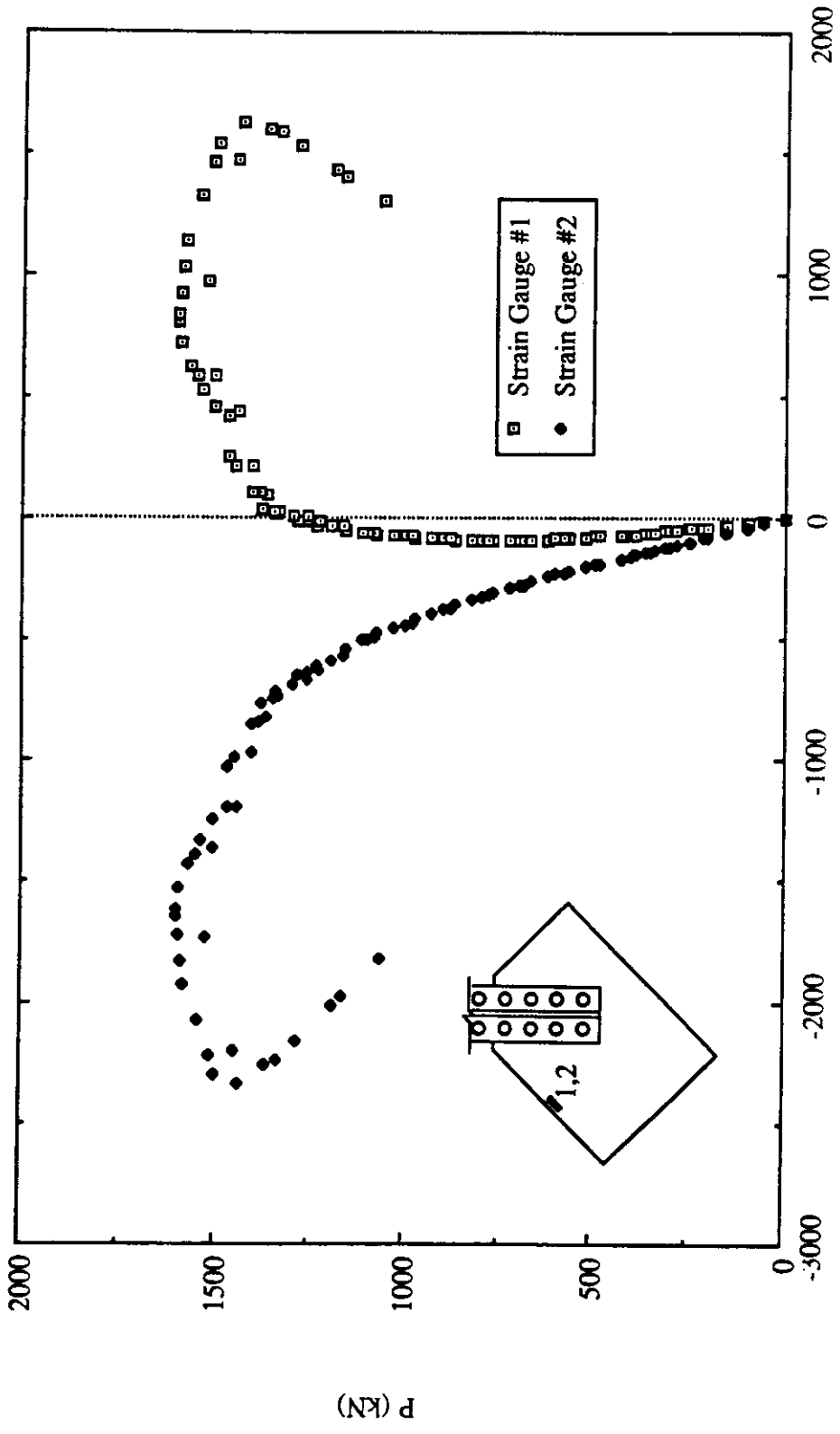

Fig. 4.5 Load vs. Strain Gauge Readings at Mid-Length of Long Free Edge for Specimen SP1 - Without Restraint

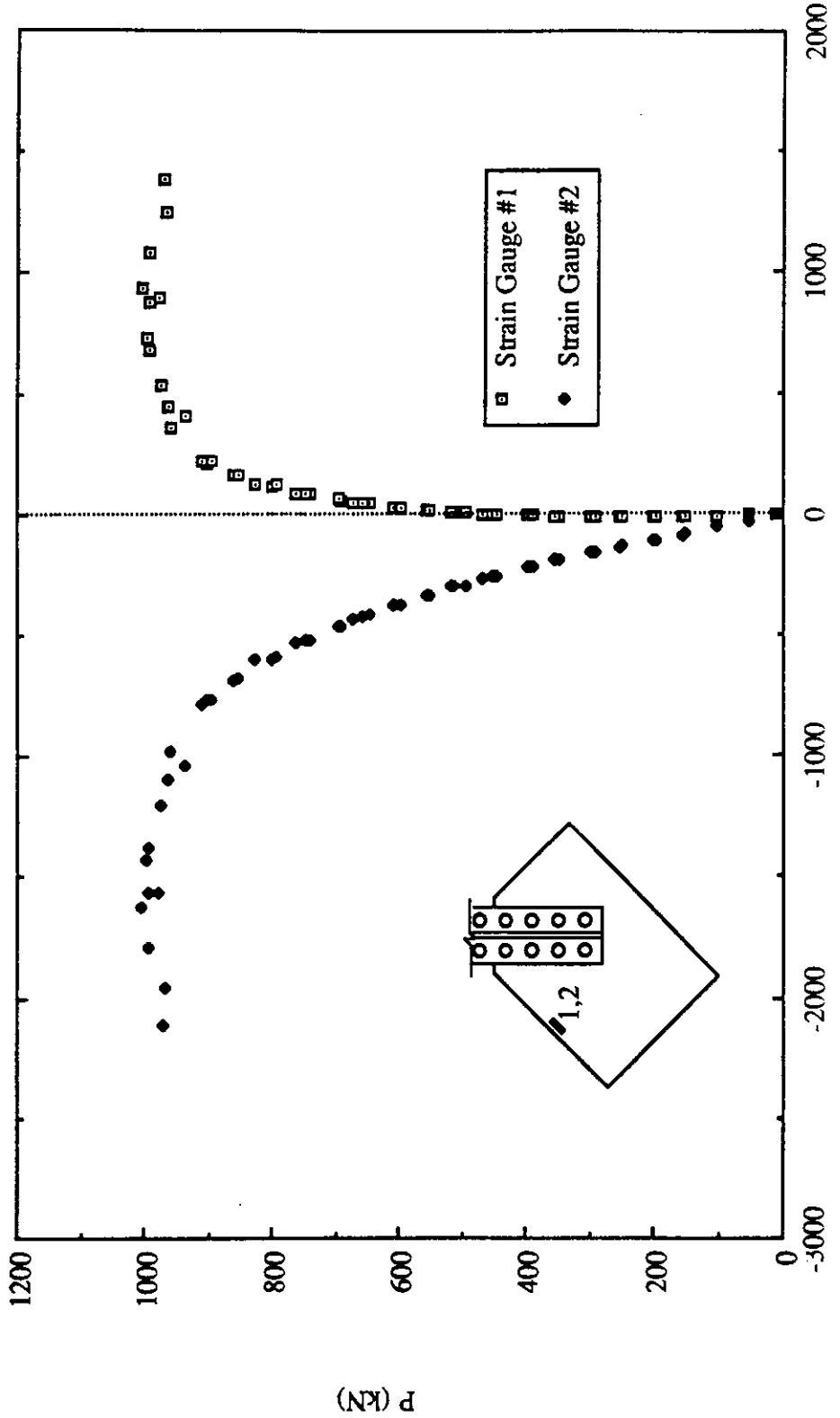

Fig. 4.6 Load vs. Strain Gauge Readings at Mid-Length of Long Free Edge for Specimen SP2 - Without Restraint

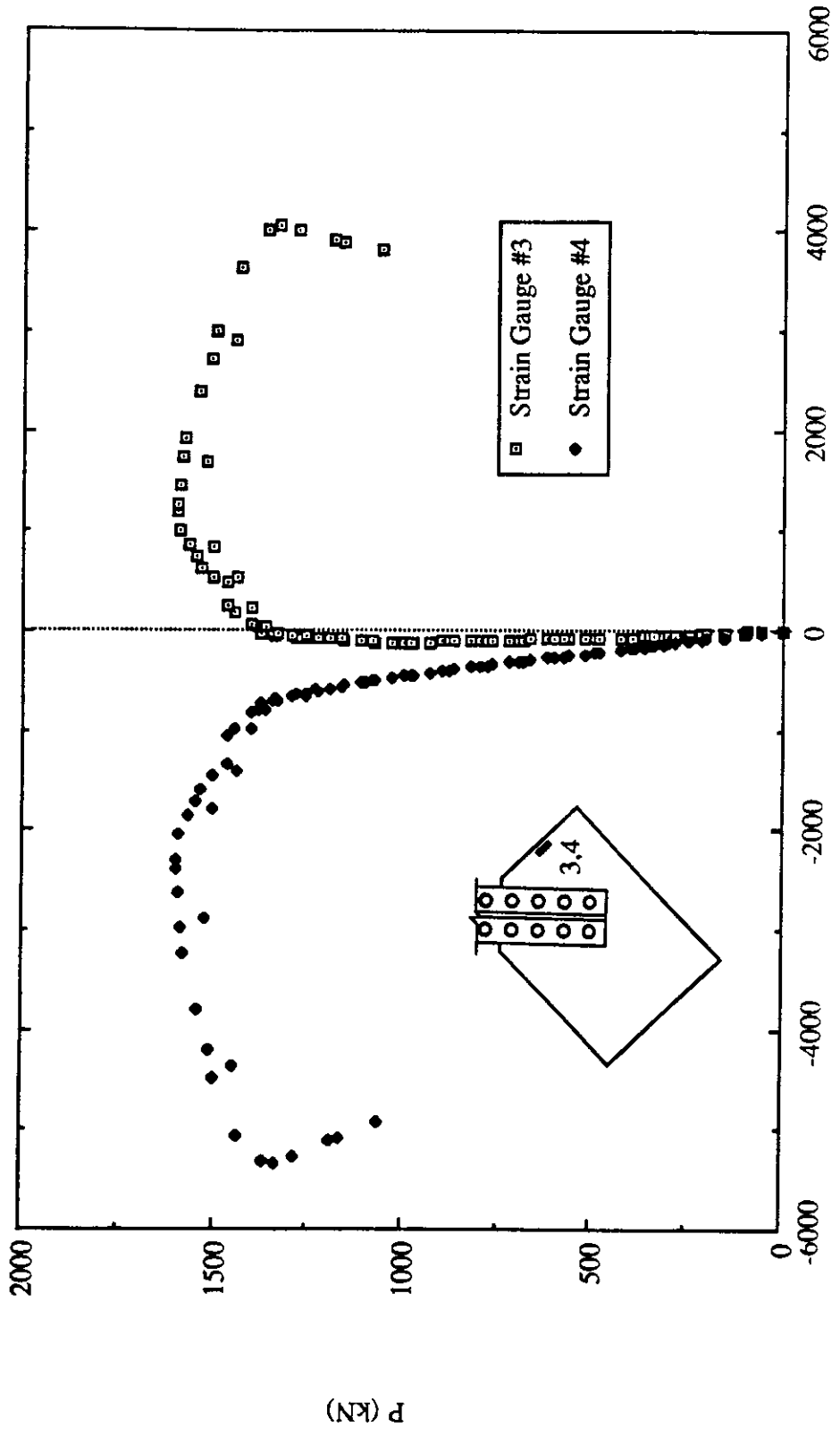

Fig. 4.7 Load vs. Strain Gauge Readings at Mid-Length of Short Free Edge for Specimen SP1 - Without Restraint

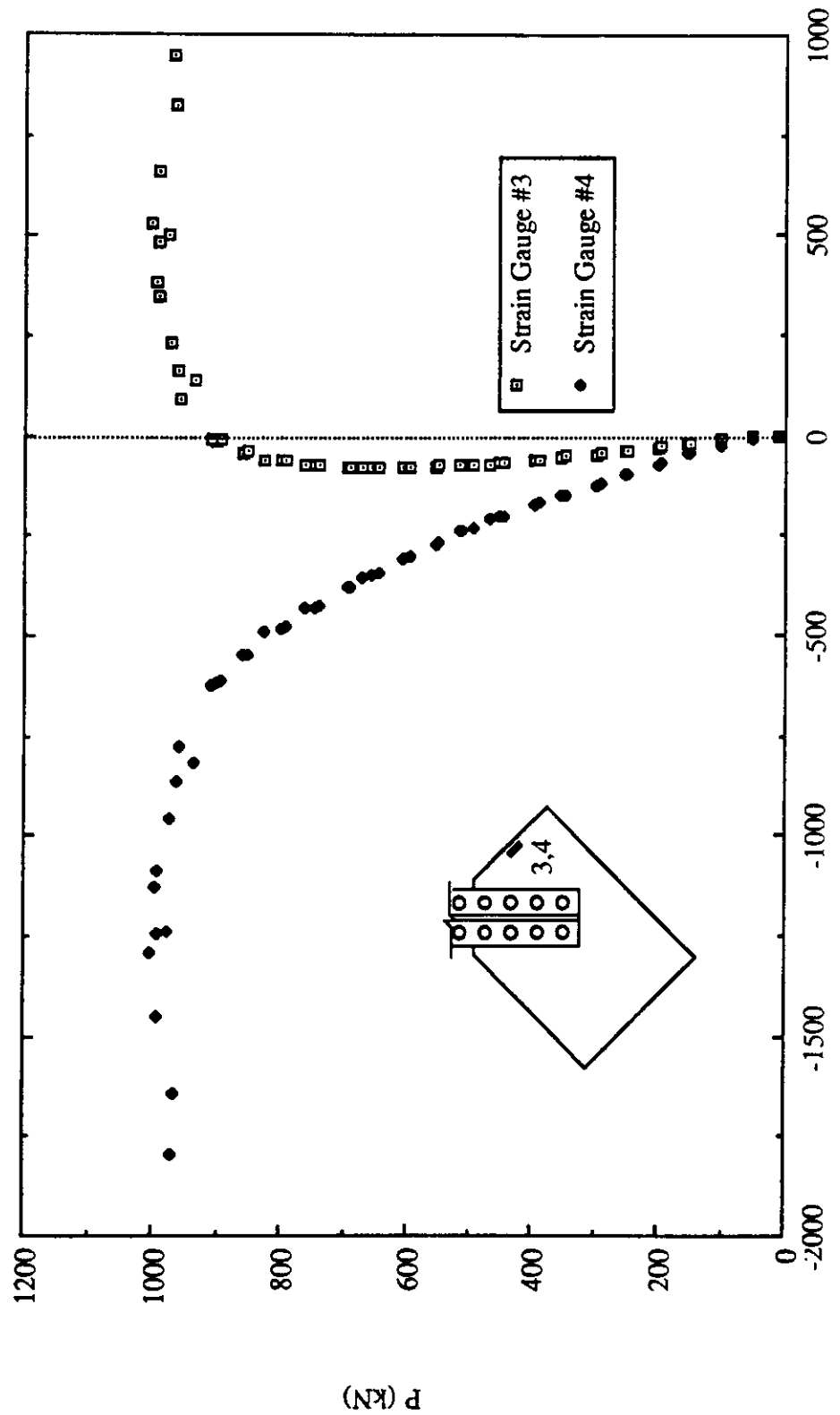

Fig. 4.8 Load vs. Strain Gauge Readings at Mid-Length of Short Free Edge for Specimen SP2 - Without Restraint

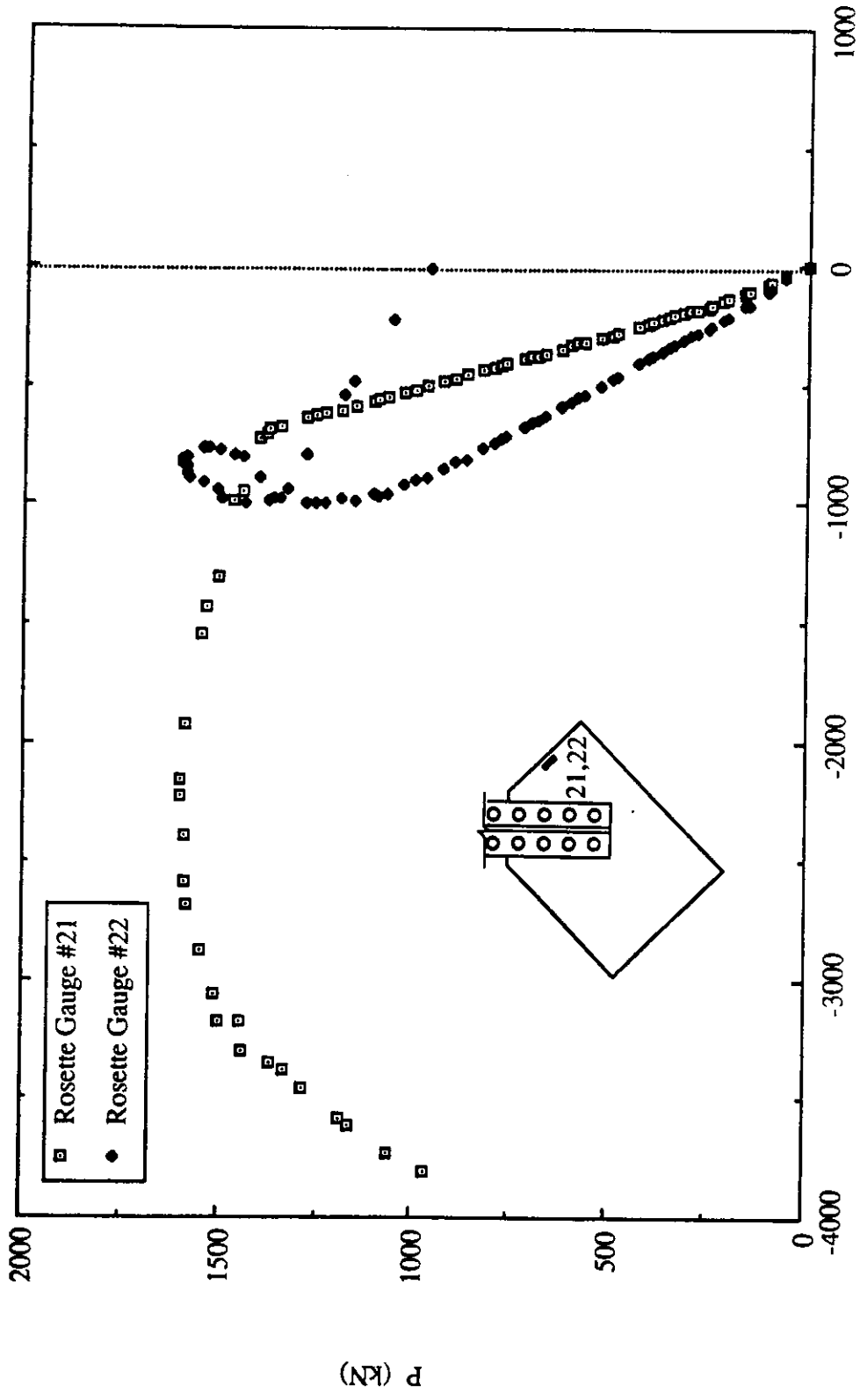

Fig. 4.9 Load vs. Strain Readings at Rosette Location for Specimen SP1 - Without Restraint

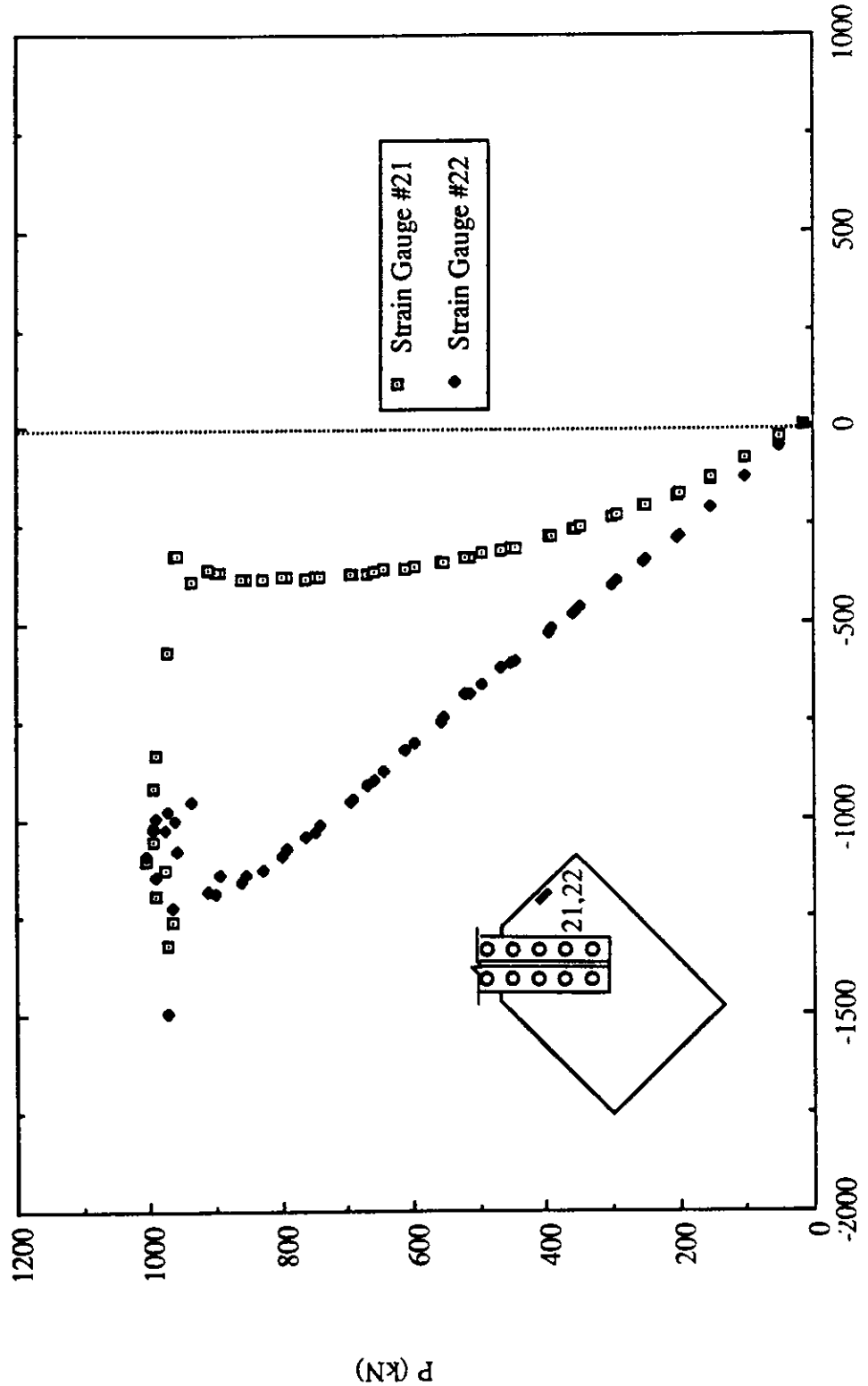

Fig. 4.10 Load vs. Strain Readings at Rosette Location for Specimen SP2 - Without Restraint

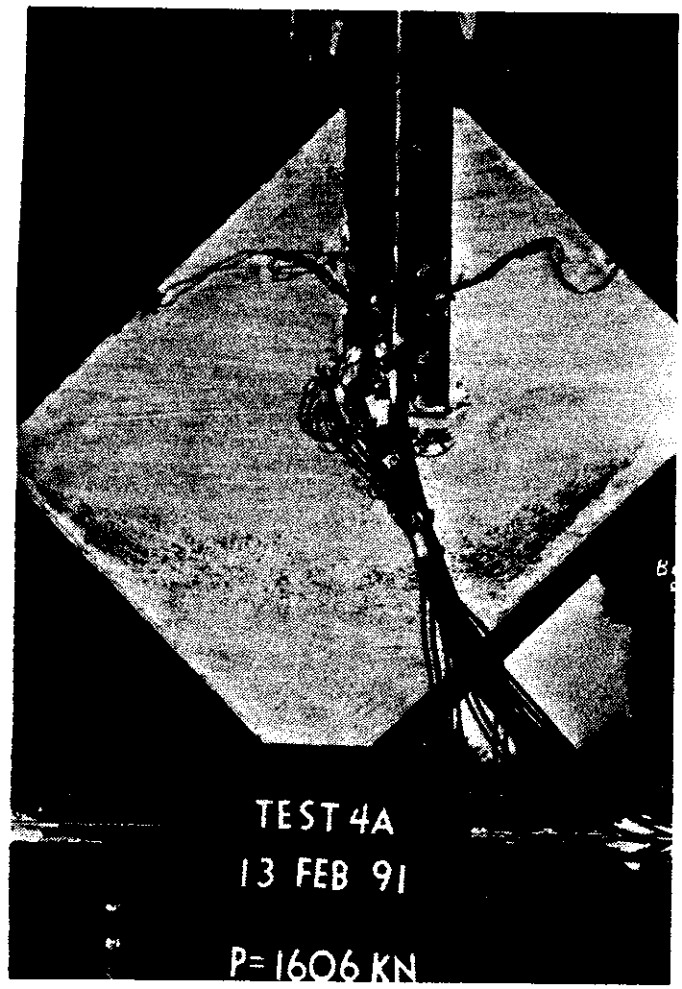

Fig. 4.11 Picture of Failed Specimen SP1

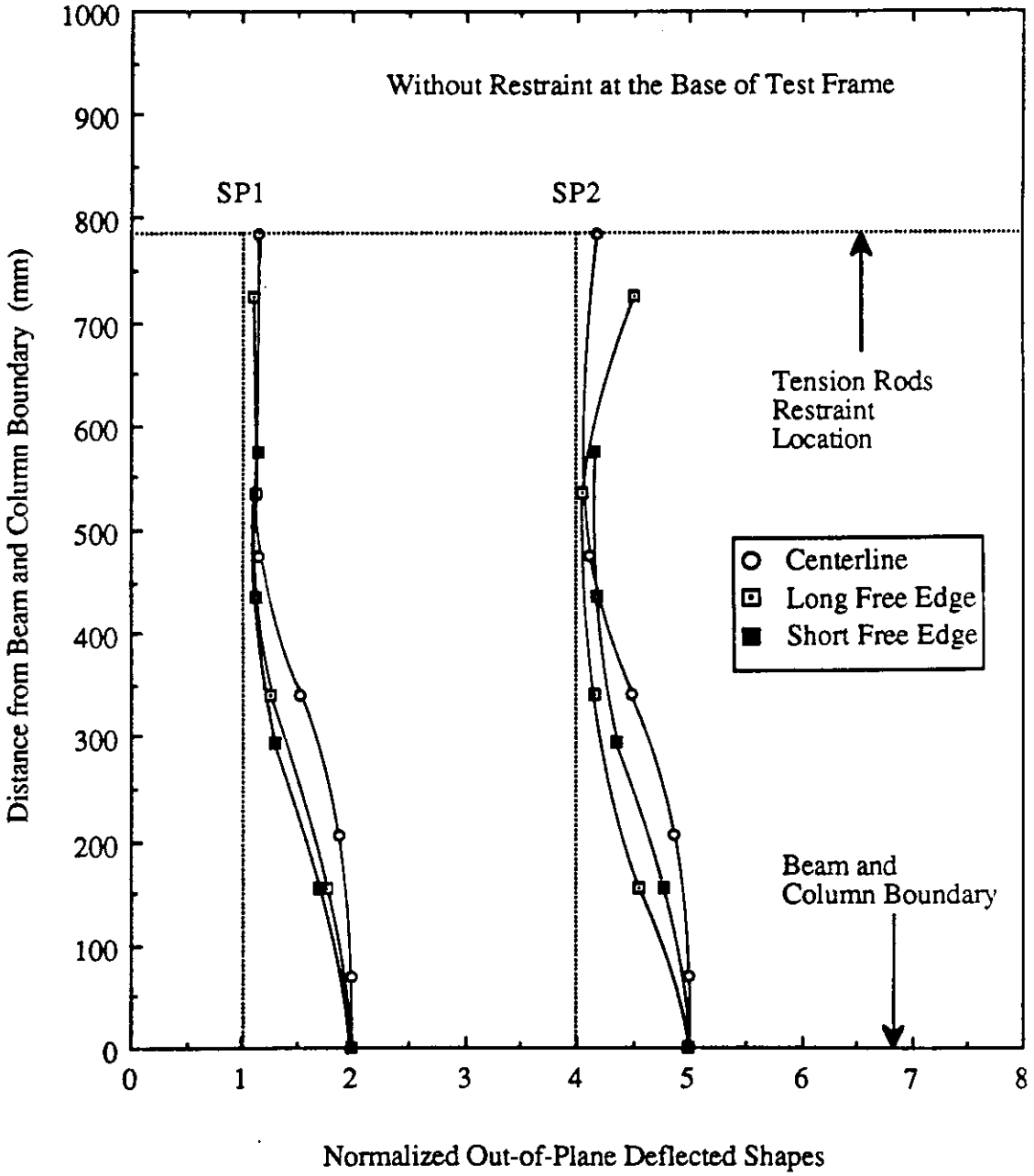

Fig. 4.12 Out-of-Plane Deflected Shapes at Free Edges and Along the Centerline of Splice for SP Type Specimens - Without Restraint

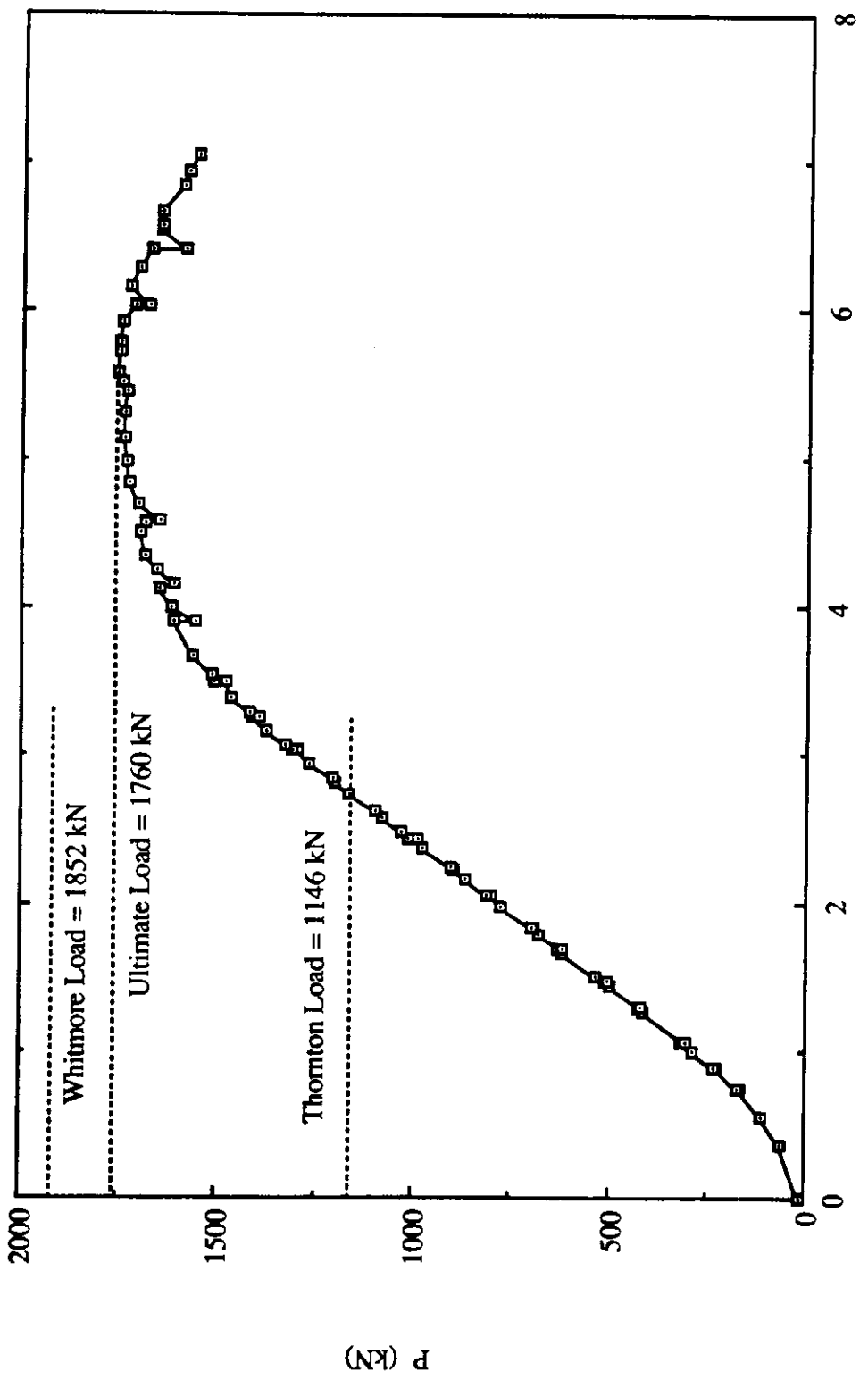

Fig. 4.13 Load vs. Vertical Displacement of Loading Head for Specimen SP1 - With Restraint

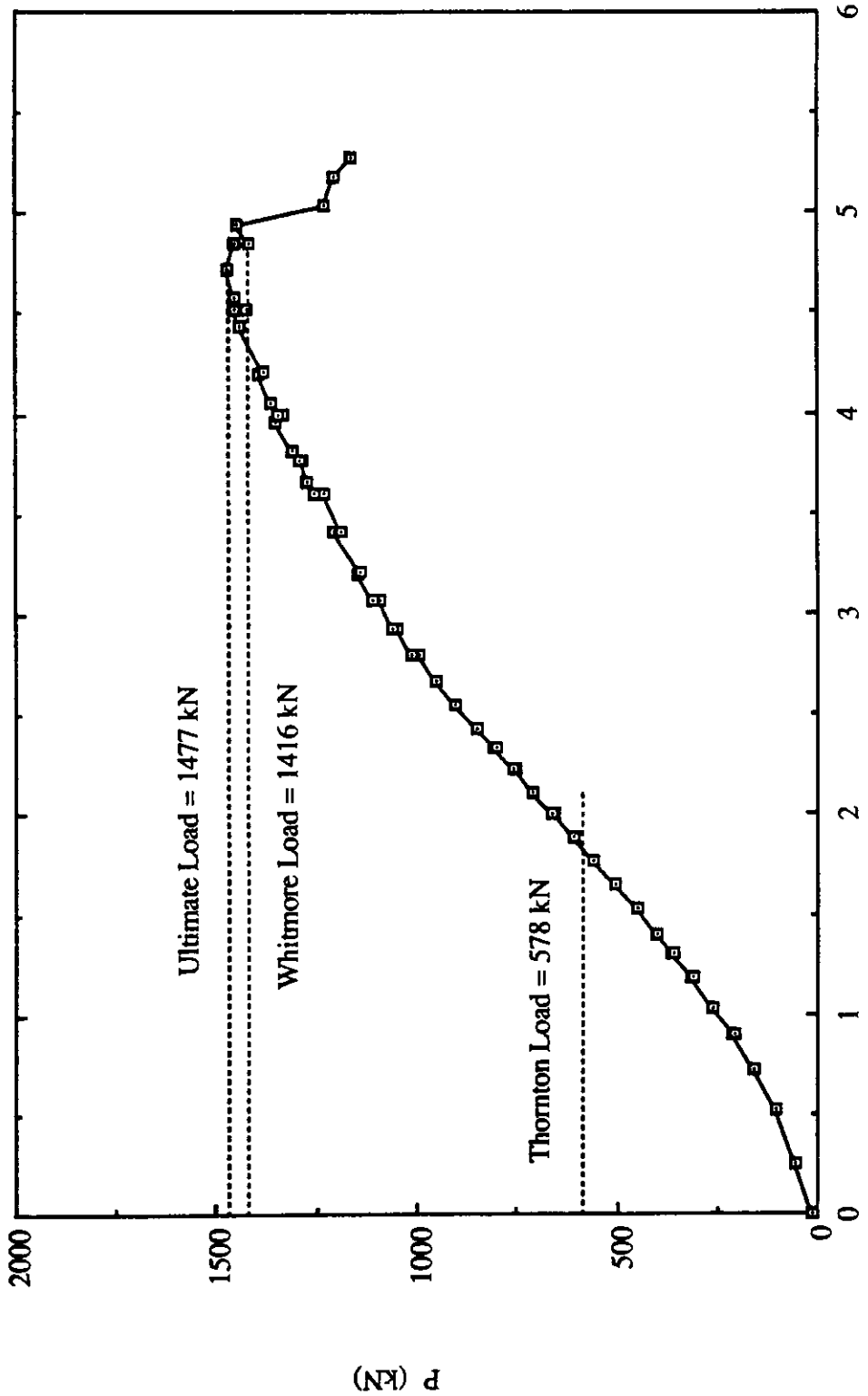

Fig. 4.14 Load vs. Vertical Displacement of Loading Head for Specimen SP2 - With Restraint

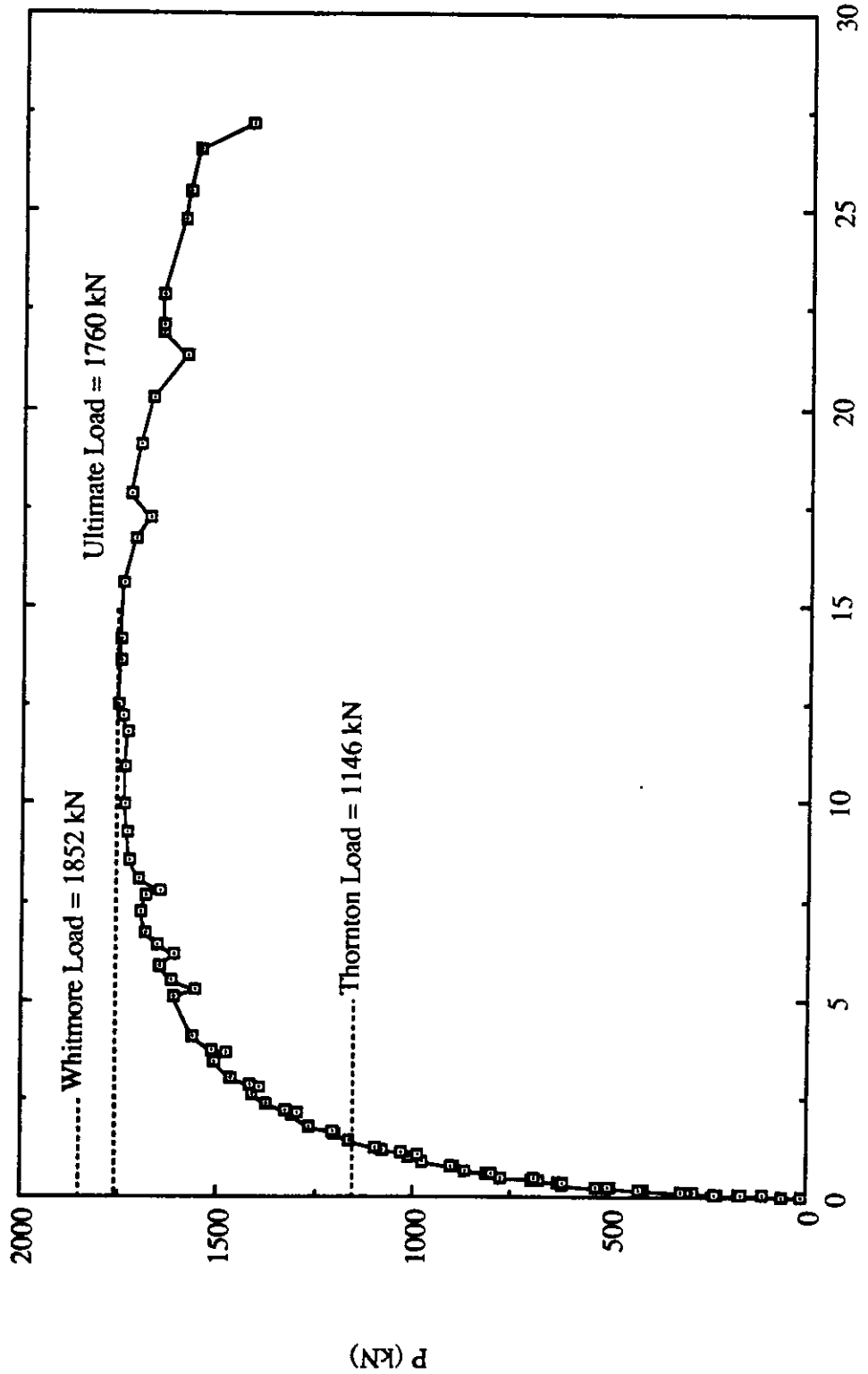

Fig. 4.15 Load vs. Out-of-Plane Displacement at Mid-Length of Long Free Edge for Specimen SP1 - With Restraint

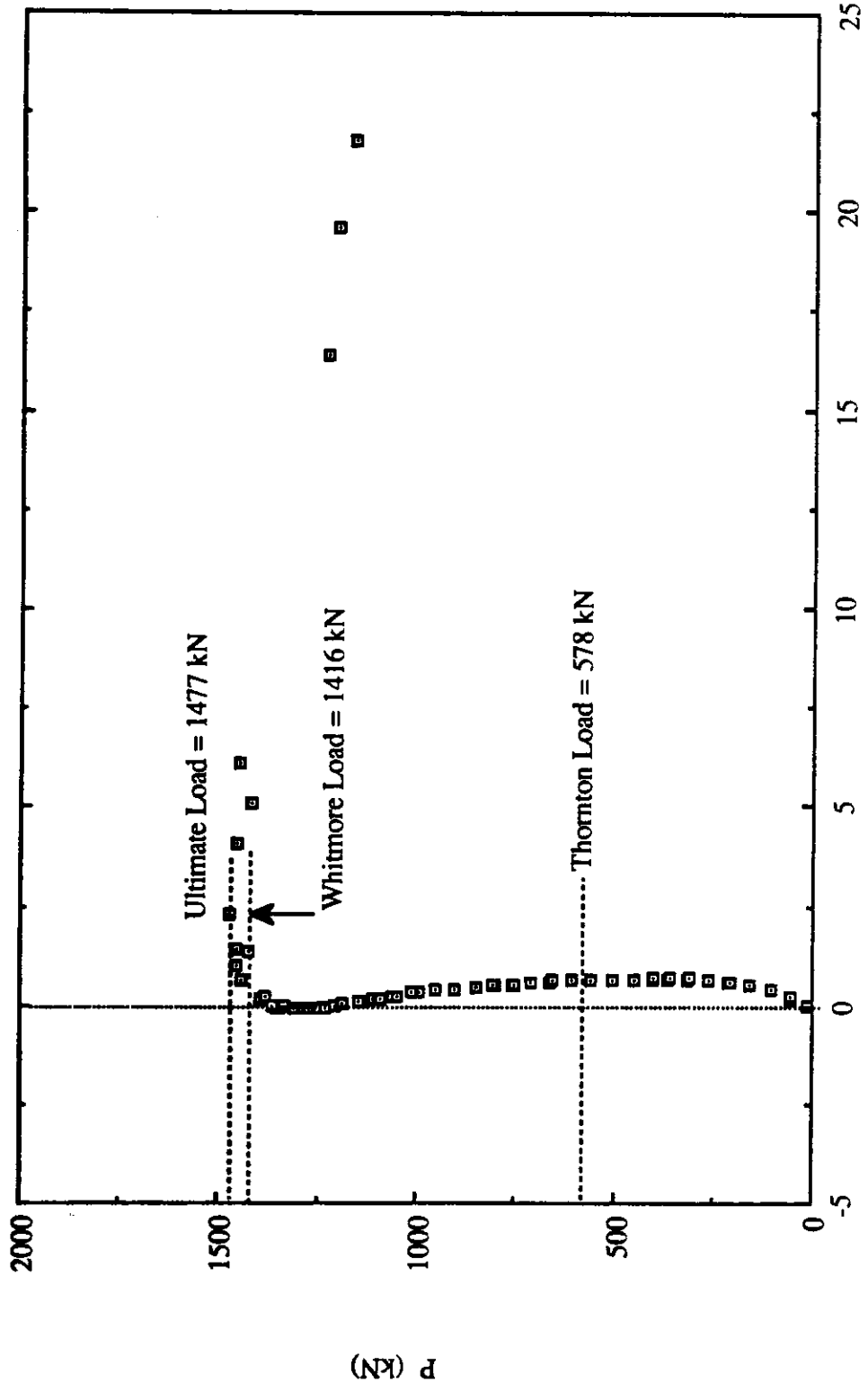

Fig. 4.16 Load vs. Out-of-Plane Displacement at Mid-Length of Long Free Edge for Specimen SP2 - With Restraint

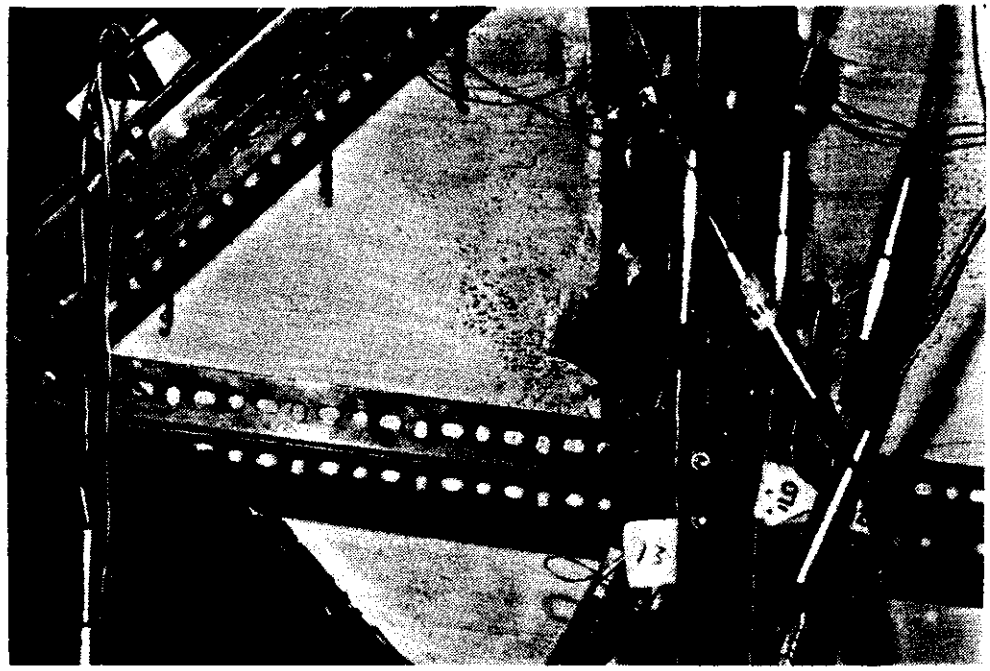

Fig. 4.17 Yield Lines Observed Near South Corner of Splice for Specimen SP1 - With Restraint

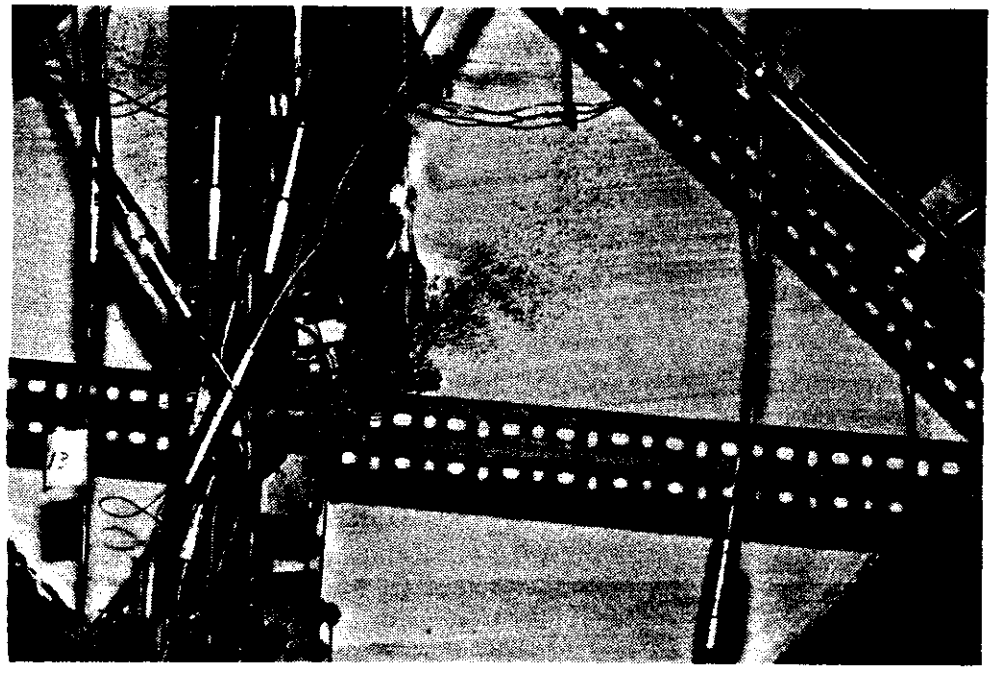

Fig. 4.18 Yield Lines Observed Near North Corner of Splice for Specimen SP1 - With Restraint

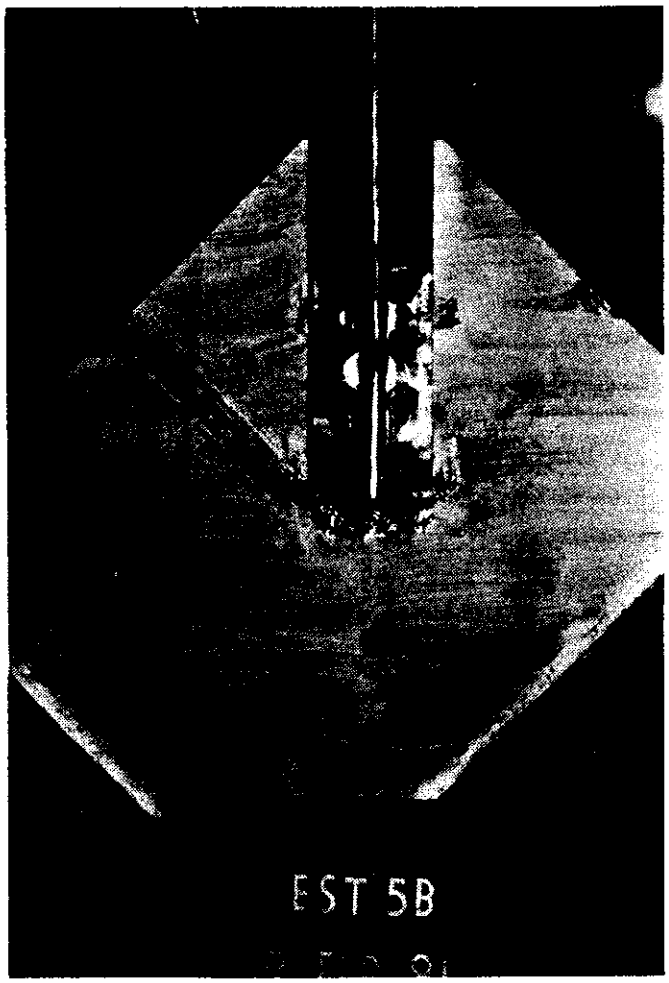

Fig. 4.19 Yield Line Mechanism for Specimen SP1 - With Restraint

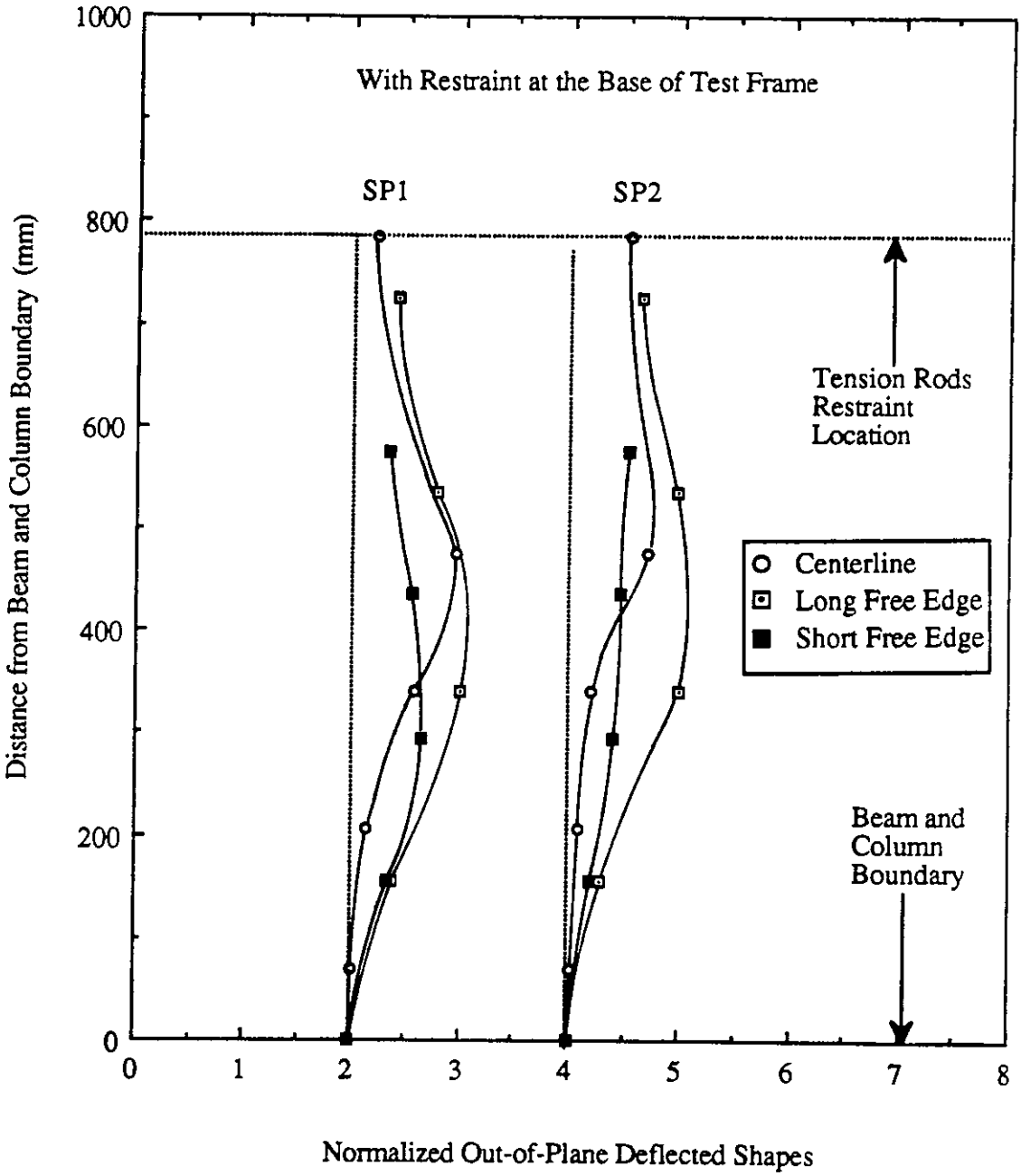

Fig. 4.20 Out-of-Plane Deflected Shapes at Free Edges and Along Centerline of Splice SP Type Specimens- With Restraint

5. TEST RESULTS OF AP TYPE SPECIMENS

5.1 General

This particular set of specimens were employed to study the effects of brace angle on the behavior and ultimate load of the gusset plate connections. The same plate geometry as that of the GP type specimens were used for the AP type specimens. It should be noted that scheme II test setup was employed to perform the tests. A 30^c brace angle was chosen for the AP type specimens such that comparsion can be made with the GP type specimen which has a 45^c brace angle. Three gusset plate thicknesses were tested with similar splice member as that of the GP specimens. The test results of the AP type specimens are shown in Table 5.1. The failure mode of the specimens was sway buckling with the bracing member deflected out-of-plane.

5.2 Behavior of Load Versus In-Plane Deformation

As described in the previous chapter, a LVDT was attached to the bottom of the splice member to record the vertical deformation of the specimen. However, for specimens AP1 and AP3 this particular LVDT did not function probably during testing. Nonetheless, testing for these two specimens were continued since the applied load was significantly high when the LVDT became malfunction. On the other, the LVDT performed normally during testing of specimen AP2. Therefore, for specimens AP1 and AP3 readings recorded from the LVDTs attached to the hydraulic rams to measure the vertical stroke were used to examine the behavior of load versus vertical deformation of the specimen. However, it should be noted that the LVDTs measurements also included the elastic deflections of the reaction beam and channels.

The curves of load versus vertical stroke of the hydraulic rams are illustrated in Figs. 5.1 to 5.3. As can be seen from the figures that the strokes from both hydraulic rams were maintained quite close to each other except at the final stage of loading. Fig. 5.1 shows

that bolt slip occurred at load levels of about 1000 kN and 1350 kN. However, no bolt slip was recorded for specimens AP2 and AP3. In general, nonlinear load deflection behavior was observed for the specimens at initial loading stage due to the settling of test fixtures. Subsequently, linear load deflection was observed for the specimens until the applied load reached the corresponding Whitmore load level at which nonlinear behavior began as shown in the figures. After reaching the ultimate load, a drop in applied load without significant increase in strokes was observed. For specimens AP2 and AP3, the rate of unloading decreased as strokes increased. The curve of load versus in plane deformation measured at the end of splice by a LVDT for specimen AP2 is shown in Fig. 5.4. The curve shows that except in early loading stage the load deflection behavior was linear until the applied load reached the Whitmore load level at 930 kN. From then on nonlinear behavior was observed until ultimate load was reached. When comparing Figs. 5.2 to 5.4, it can be seen that about 7 mm of elastic deflection of the reaction beams was recorded. However, the general behavior of these two curves were quite similar

5.3 Behavior of Load Versus Out-of-Plane Displacement

The curves of load versus out-of-plane displacement of the gusset plate at the conjunction of gusset-to-splice are shown in Figs. 5.5 to 5.7. As can be seen from Fig. 5.5, a discontinuity of the load deflection curve was observed for specimen AP1. This discontinuity was caused by a sudden vibration occurred during bolts slip. The recorded bolts slip has been discussed in the pevious section. In general, linear load deflection behavior was observed for the specimens until the applied load was close to the ultimate load. Both specmiens AP1 and AP2 were able to maintain the load level close to the ultimate load after buckling occurred except specimen AP3 which showed an appreciate decrease in ultimate load. This may be due to the fact that specimen AP3 had relatively low bending rigidity comparing to specimens AP1 and AP2. Hence, when buckling occurred yielding of specimen AP3 progressed rapidly and therefore the applied load dropped

quickly after the specimen reached the ultimate load. The final out-of-plane displacement for all the specimens was approximately 25mm which is the physical limit of the measuring LVDT.

5.4 Strain Gauges Results

The strain readings at mid-length of the free edges and the area underneath the splice member were examined. Again, strain readings at free edges indicated that elasic strain distribution occurred in the vicinity of the free edges prior to reaching the ultimate load. The curves of load versus strain at the mid-length of long free edge are shown in Figs. 5.8 to 5.10. These figures show that linear behavior was observed until the applied load was close to the ultimate load. As can be seen from the figures that strain readings from both sides of the specimen showed similar at the early loading stage. However, as load increased these strain readings deviated from each other. When load increased to the ultimate load level, strain bifurcation occurred as illustrated by the figures. Strain readings at the short free edge show that compressive strains were recorded in the initial stage of loading. However, as loading progressed unloading was observed in the vicinity of the short free edge and eventually tensile strains were recorded as illustrated typically in Fig. 5.11 for specimen AP3. This unloading behavior was probably caused by the in-plane bending of the plate. Since these specimens were tested with a brace angle of 30°, therefore, the horizontal component of the applied load might be significant to cause this in-plane bending behavior. The curves of load versus strain recorded at the center gauges of the rosette are shown in Figs. 5.12 to 5.14. These two gauges recorded the strain readings from both sides of the plate. It can be seen from these figures that out-of-plane bending of the plate, which was probably due to the initial imperfection, occurred at early stage of loading. In particular, specimen AP3 showed nonlinear behavior from the beginning of loading.

5.5 Yielding Behavior of Specimens

The general yield pattern of the AP type specimens was similar to that of the GP type specimens. However, for the AP type specimens yield lines were first observed close to the beam and column boundary. For specimen AP1, yield lines underneath the splice member were recorded at about 58 percent of the ultimate load. Again, as loading progressed yielding was spread about the two sides of the splice member. However, only moderate yielding was observed about the side of the splice member close to the long free edge. On the other hand, significant yielding was recorded about the other side of the splice member near the short side free edge. Extensive yielding was observed underneath the splice member and yielding about the side of the splice member close to the short free edge progressed significantly at a load level of approximately 85 percent of the ultimate load. The failed specimen AP1 which indicated severe yielding occurred in the area of the short side free edge is shown in Fig. 5.15. Figure 5.16 illustrates the other side of the failed specimen AP1 which showed the severity of the yielding. Yield line mechanism, which was similar to that of GP type specimens, were also observed along the beam and column boundary and at the mid-length of the long free edge of the failed specimens as shown typically in Figs. 5.15 and 5.16. The yielding process and pattern for specimen AP2 were similar to that of specimen AP1. However, yielding underneath the splice member was detected at about 45 percent of the ultimate load. Again, extensive yielding was recorded in the area of the short side free edge. The failed specimen AP2 also indicated that severe yielding occurred in the area underneath the splice member. Figures 5.17 and 5.18 illustrate the failed specimen of AP2 with the presence of the yield line mechanism along the beam and column boundary and at the mid-length of the long free edge. For specimen AP3, flaking of whitewash underneath the splice member was observed at a load level of about 80 percent of the ultimate load. Again, as load increased yielding occurred about the two sides of the splice member. The failed specimen indicated that only moderate yielding existed underneath the splice member when comparing to that

of specimens AP1 and AP2. However, extensive yielding similar to that of specimens AP1 and AP2 in the area of the short free edge was recorded for specimen AP3. Again, yield line mechanism formed along the beam and column boundary and at the mid-length of the long free edge.

5.6 Out-of-Plane Deflected Shapes of Free Edges and Along Centerline of Splicing Member

The normalized out-of-plane deflected shapes of the specimens are shown in Fig. 5.19. It can be seen from the figure that the maximum deflection occurred at the long free edge. In general, the deflected shapes resembled the buckled shape of a fixed-guided column. The deflected shapes for specimens AP1 and AP2 indicated that significant rotation occurred at the beam and column boundary due to severe yielding. The long free edge deflected shape for specimen AP3 also showed slight local bending near the mid-length. A picture of the out-of-plane deflected shape along the long free edge of specimen AP2 is shown in Fig. 5.20.

Table 5.1 Test Results of AP Type Specimens

Specimen Designation	Plate Size (mm x mm x mm)	Ultimate Load (kN)	Whitmore Load P_w (kN)	Thornton Load P_t k = 0.65 (kN)
AP1	500 x 400 x 13.3	1720	1216	1147
AP2	500 x 400 x 9.8	1210	930	833
AP3	500 x 400 x 6.5	728	555	469

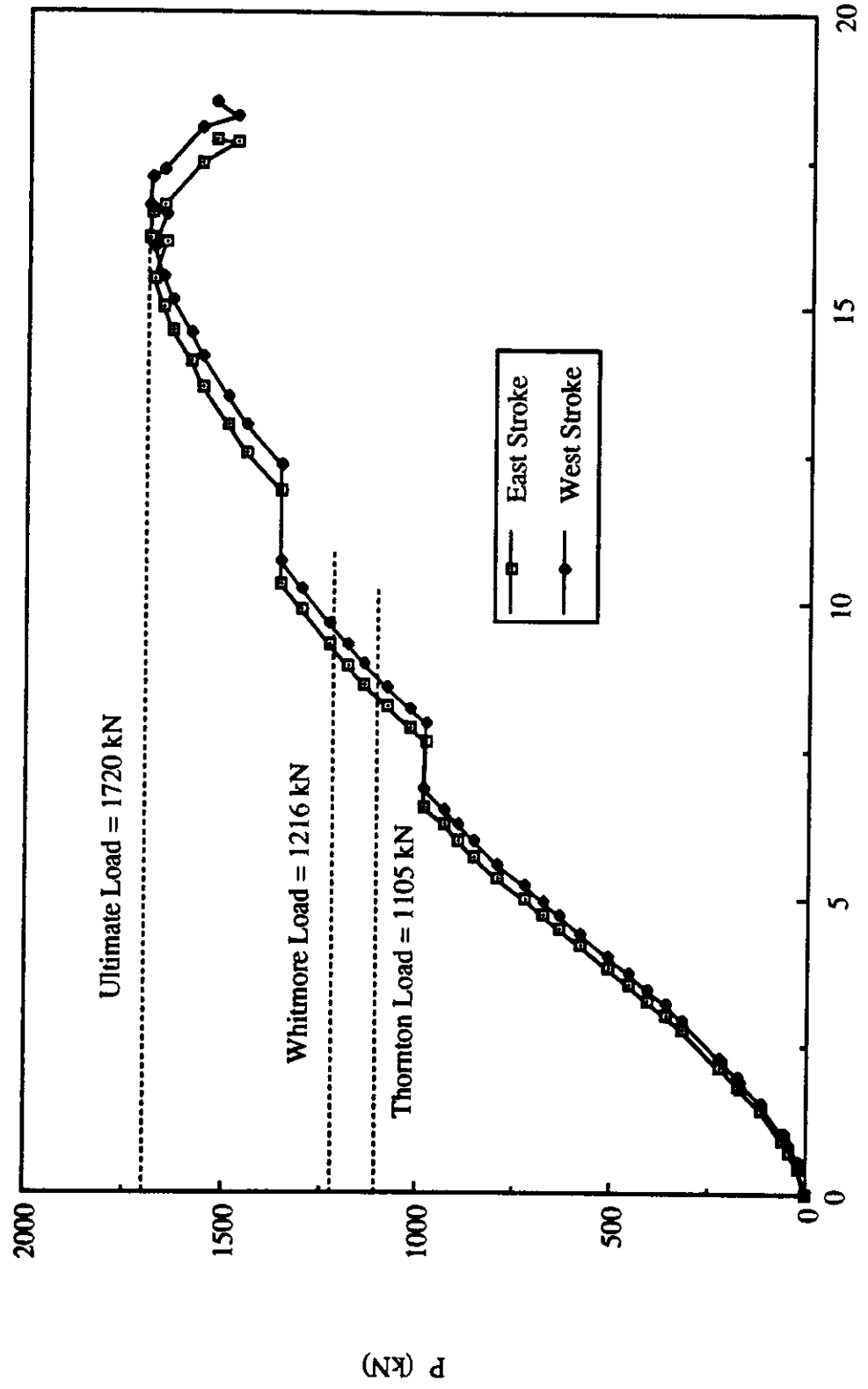

Fig. 5.1 Load vs. Vertical Strokes of Hydraulic Rams for Specimen AP1

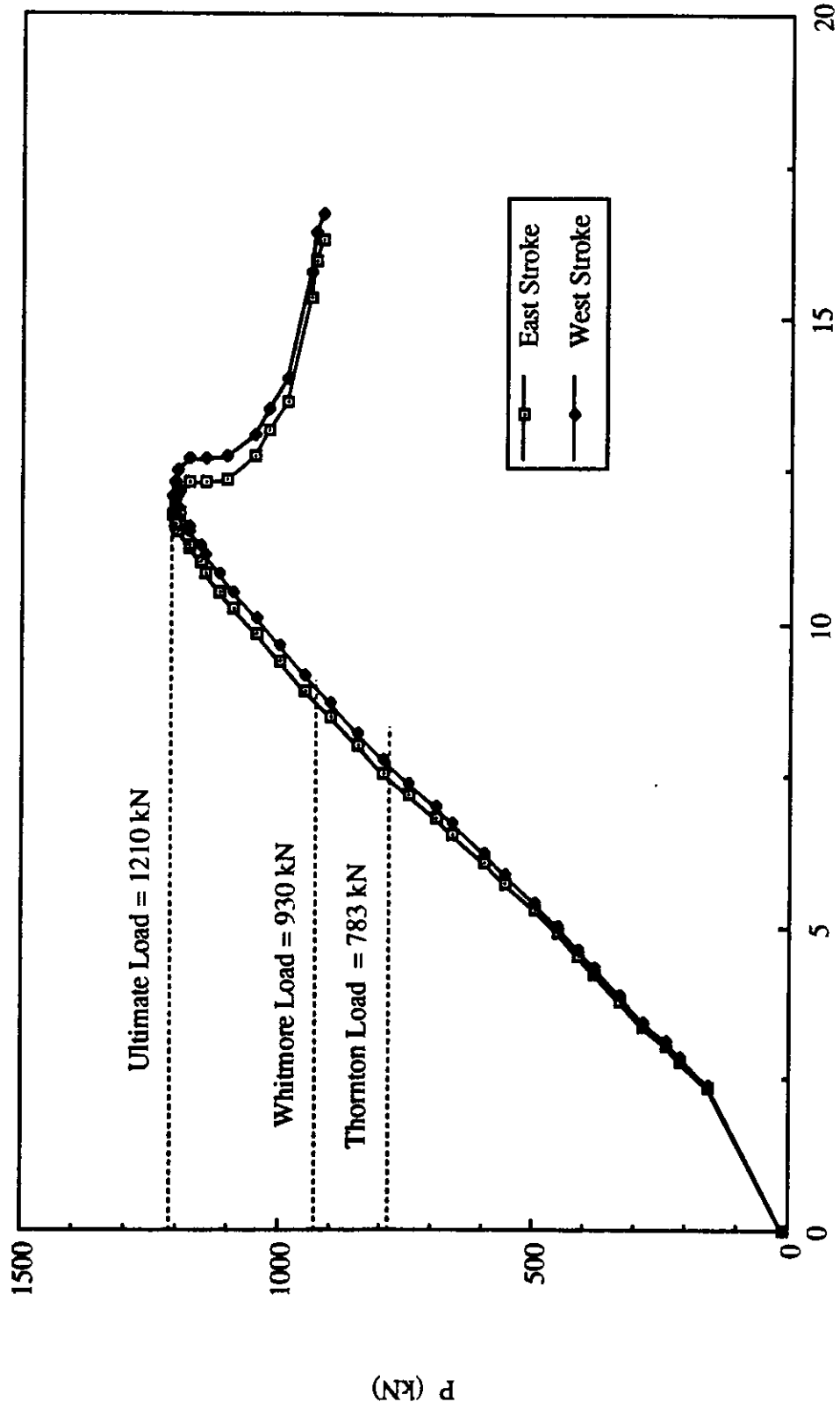

Fig. 5.2 Load vs. Vertical Strokes of Hydraulic Rams for Specimen AP2

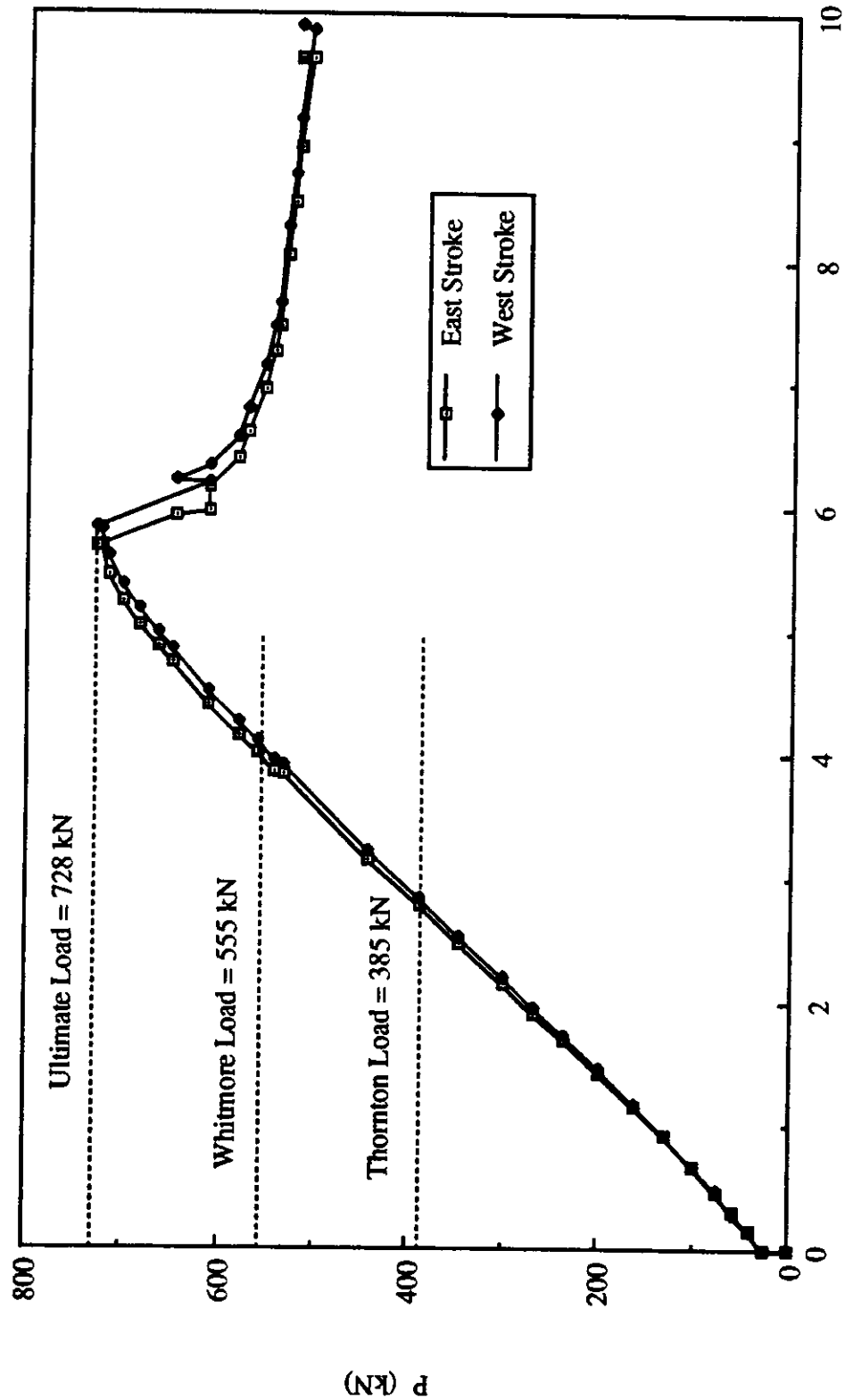

Fig. 5.3 Load vs. Vertical Stroke of Hydraulic Rams for Specimen AP3

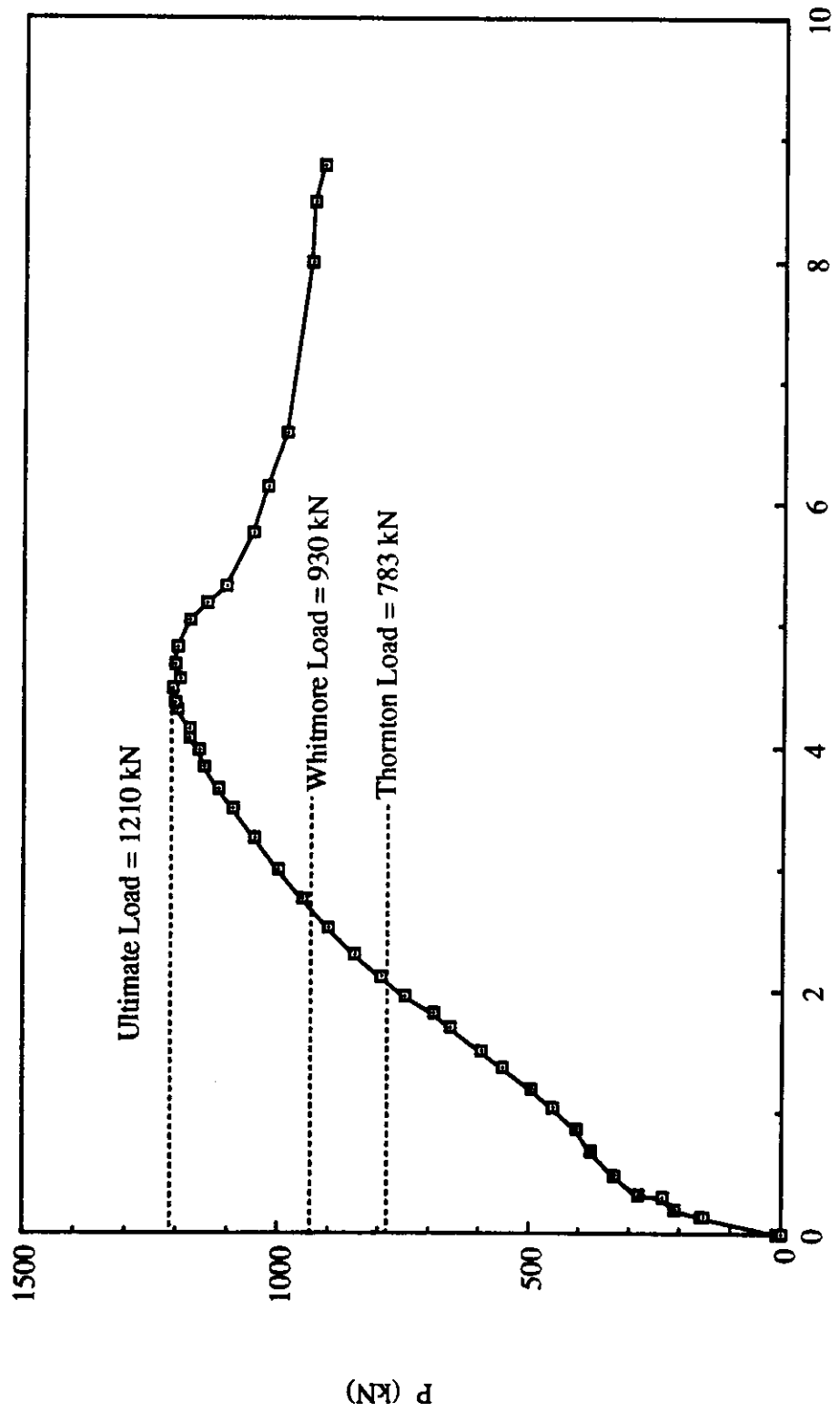

Fig. 5.4 Load vs. In-Plane Deformation Measured at End of Splice for Specimen AP2

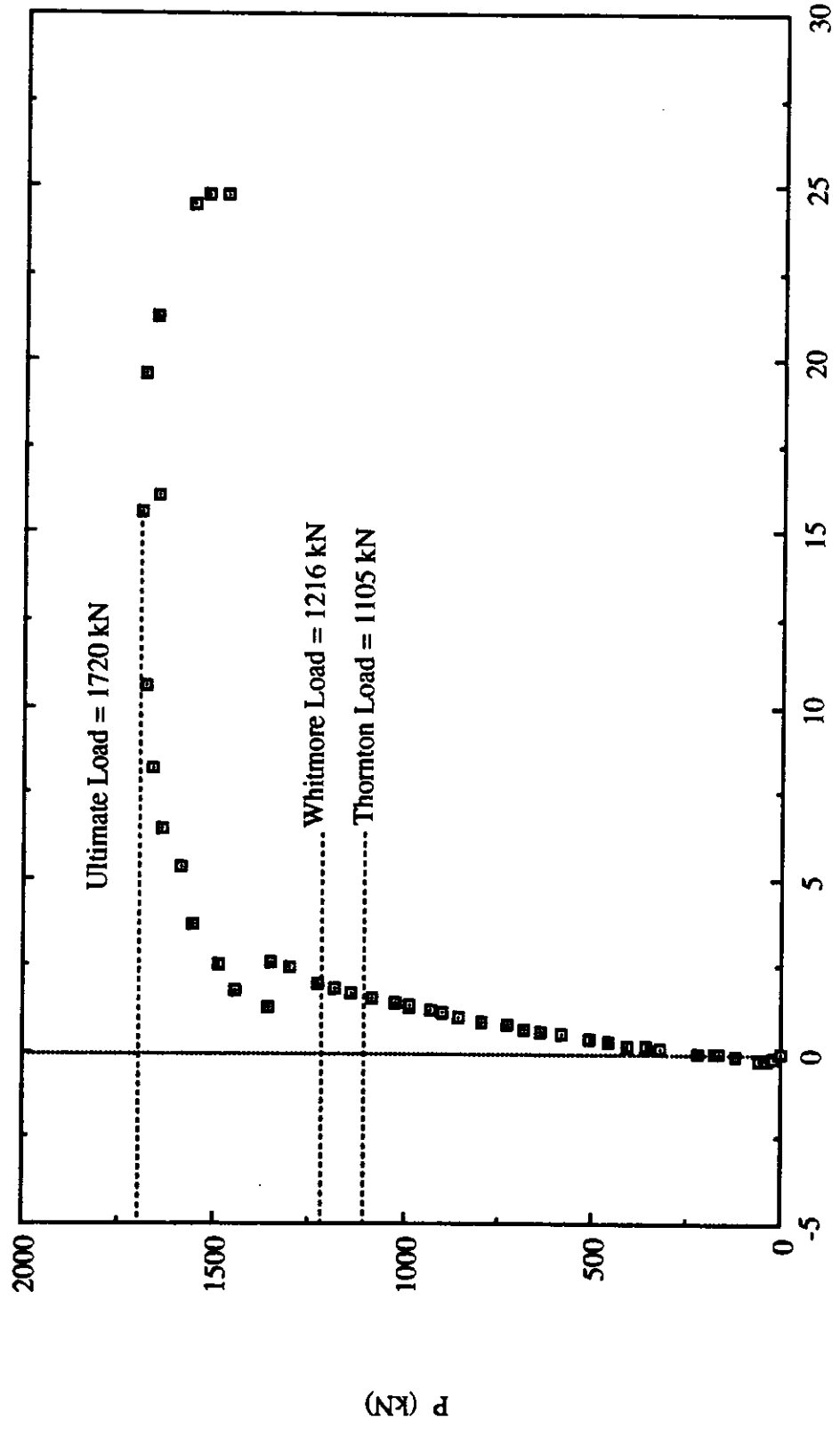

Fig. 5.5 Load vs. Out-of-Plane Displacement at Conjunction of Gusset-to-Splice for Specimen AP1

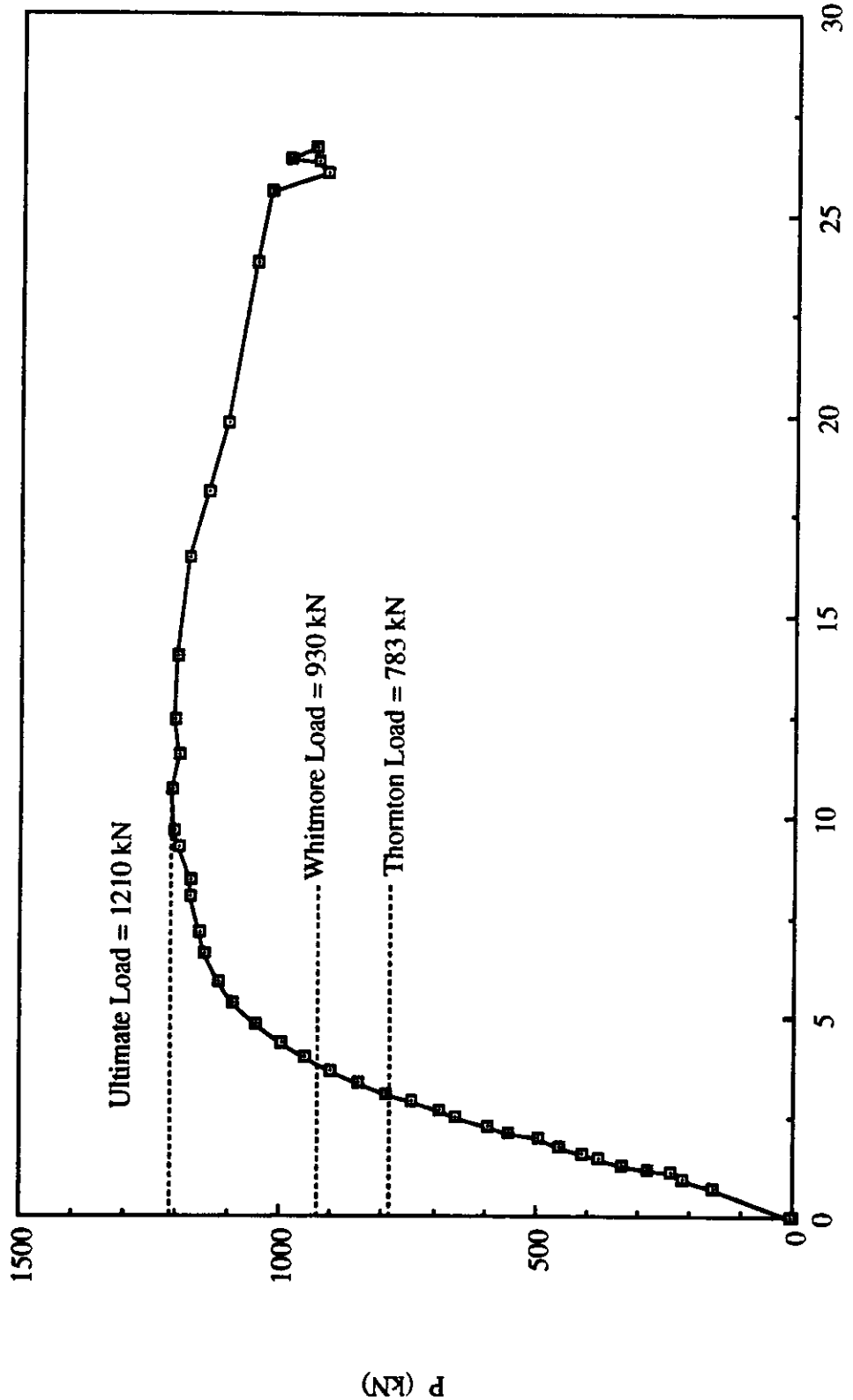

Fig. 5.6 Load vs. Out-of-Plane Displacement at Conjunction of Gusset-to-Splice for Specimen AP2

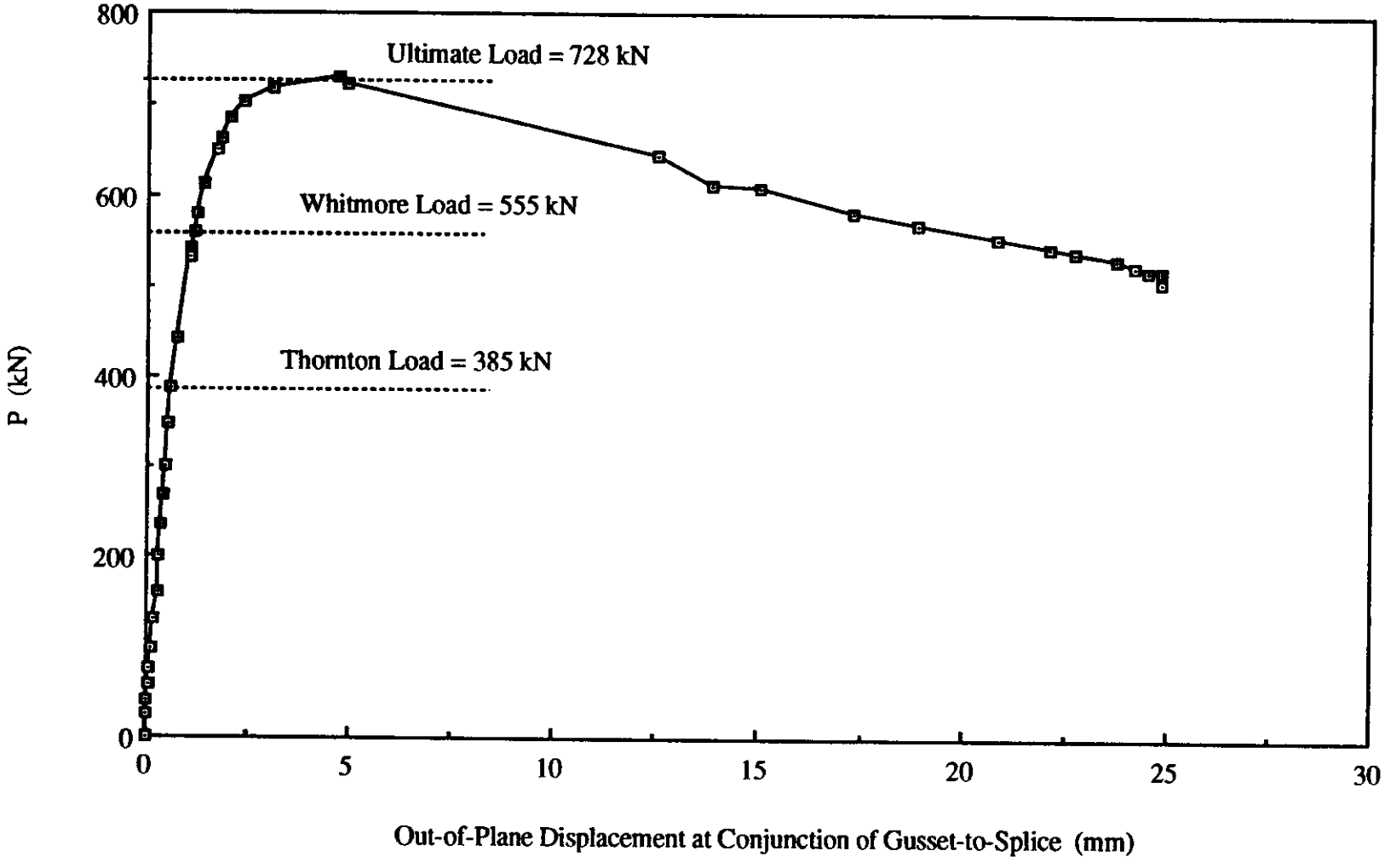

Fig. 5.7 Load vs. Out-of-Plane Displacement at Conjunction of Gusset-to-Splice for Specimen AP3

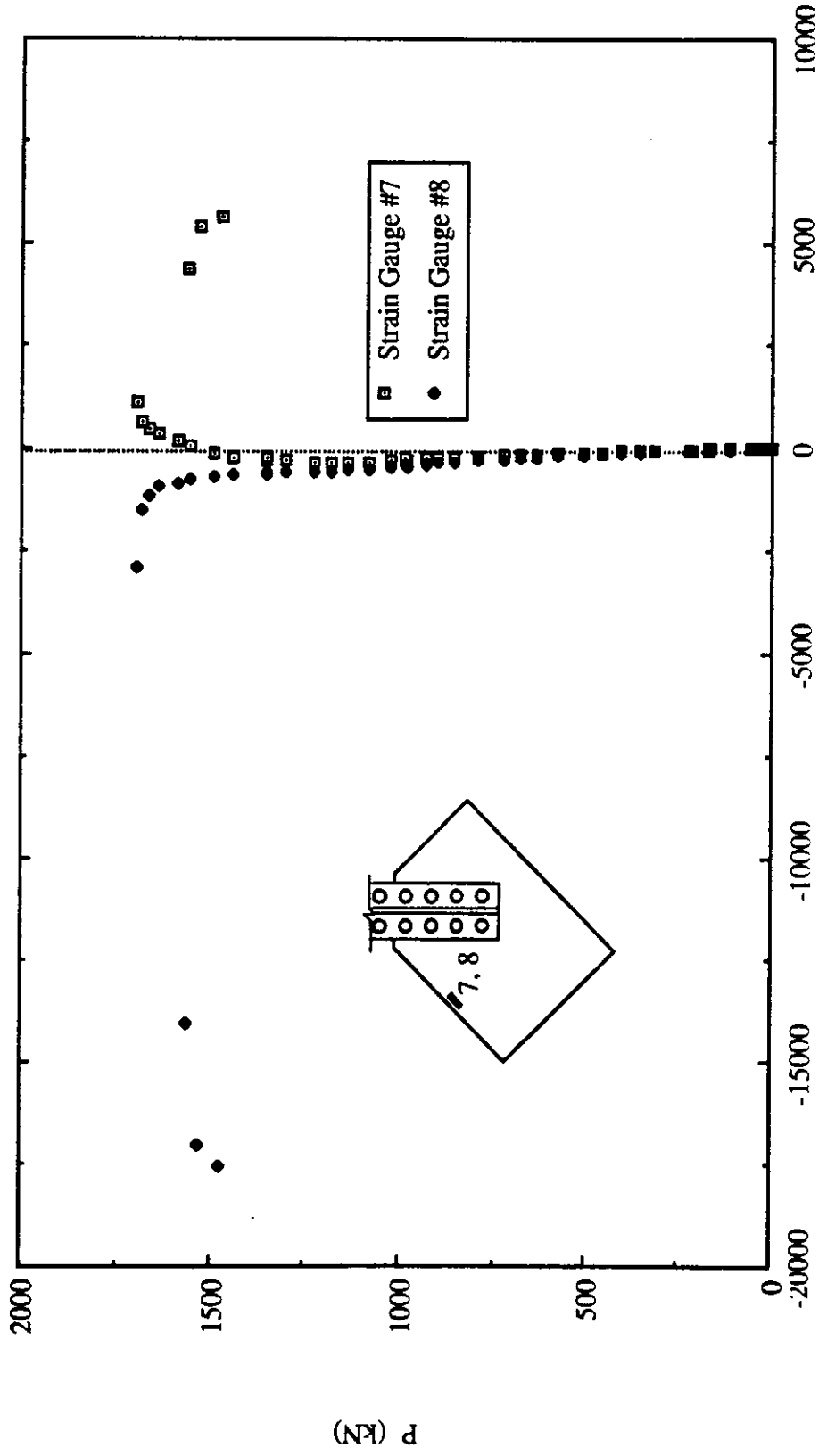

Fig. 5.8 Load vs. Strain Gauge Readings at Mid-Length of Long Free Edge for Specimen AP1

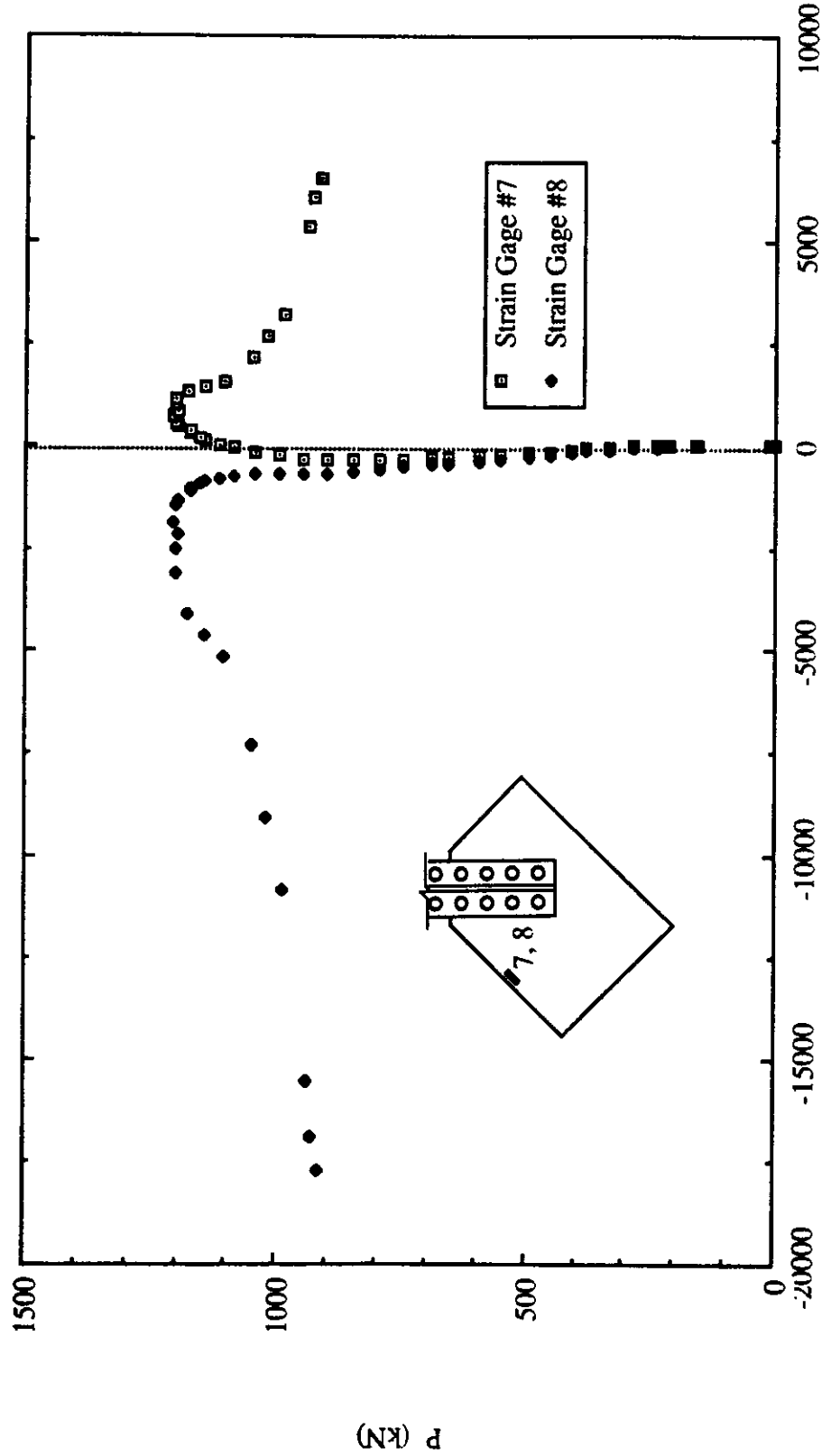

Fig. 5.9 Load vs. Strain Gauge Readings at Mid-length of Long Free Edge for Specimen AP2

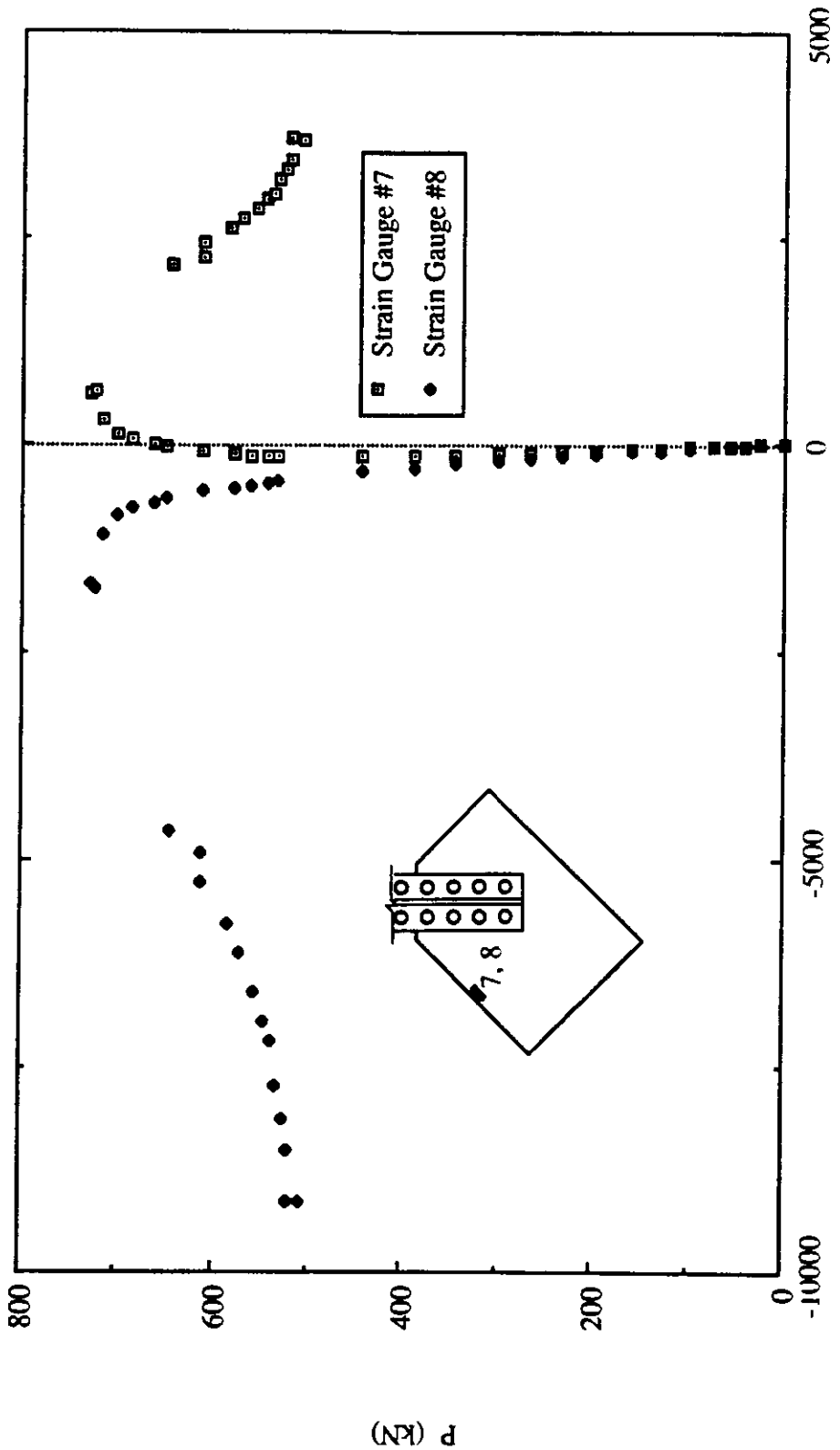

Fig. 5.10 Load vs. Strain Gauge Readings at Mid-Length of Long Free Edge for Specimen AP3

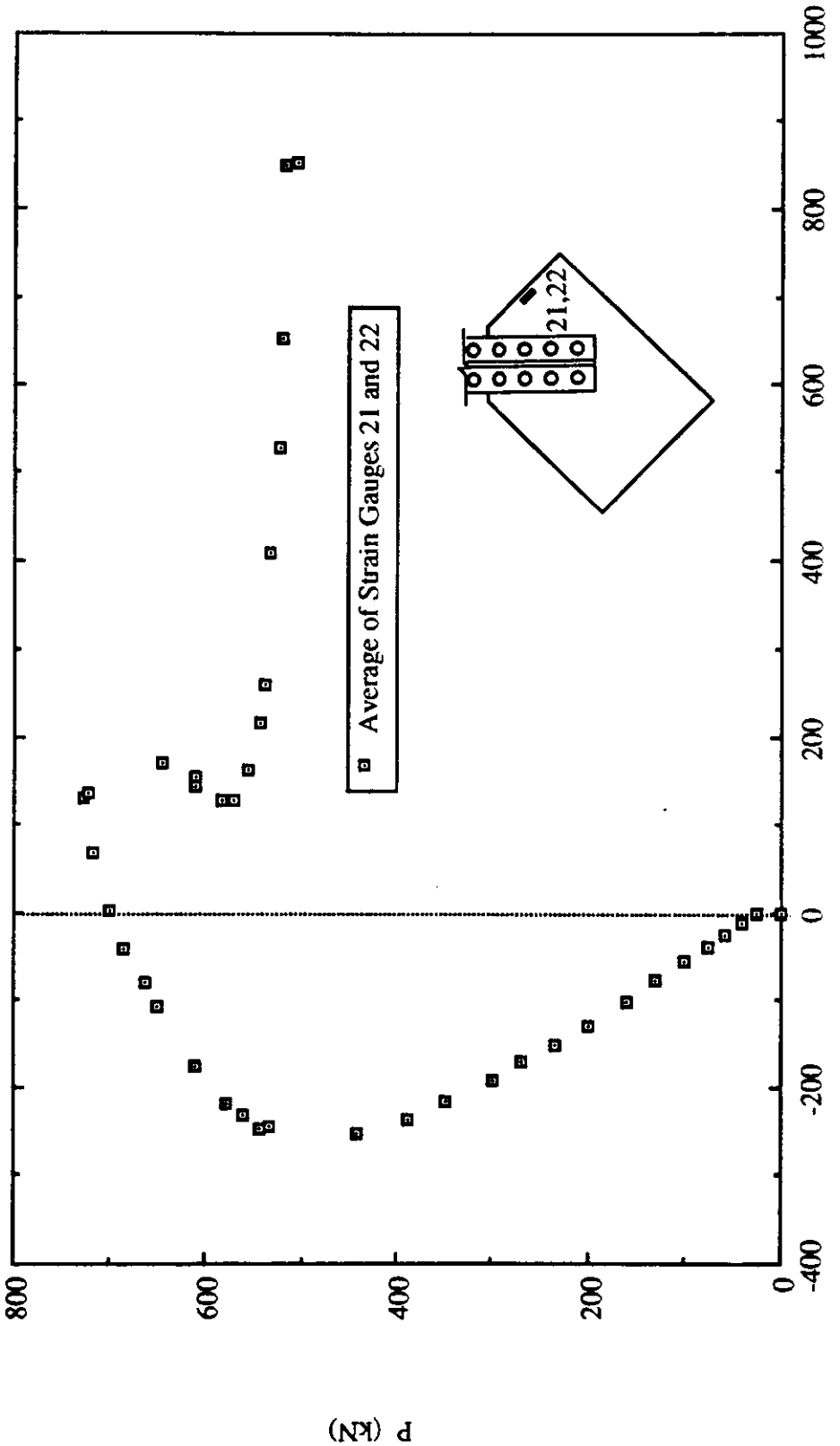

Fig. 5.11 Load vs. Average Strain Gauge Readings at Mid-Length of Short Free Edge for Specimen AP3

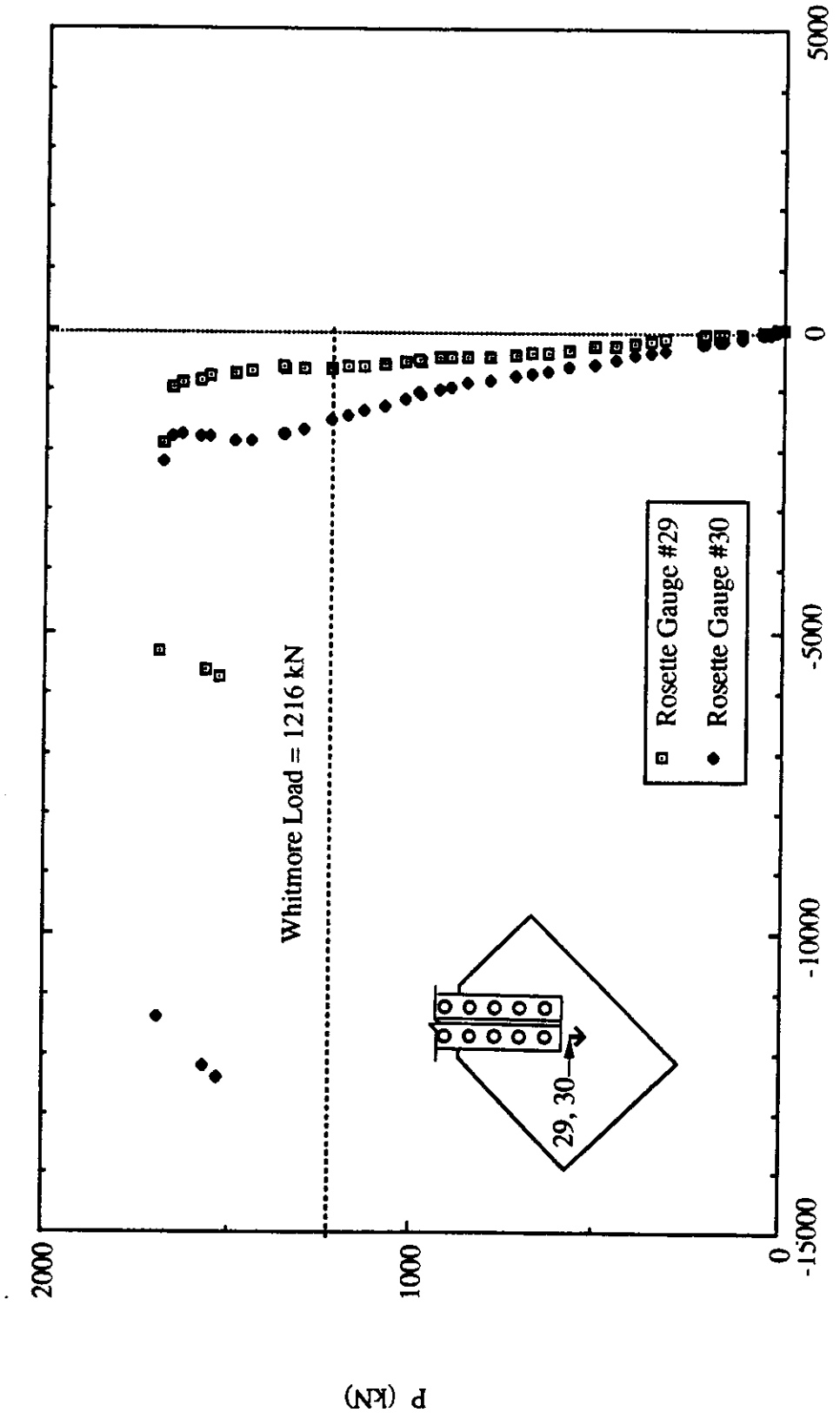

Fig. 5.12 Load vs. Rosette Gauge Readings for Specimen AP1

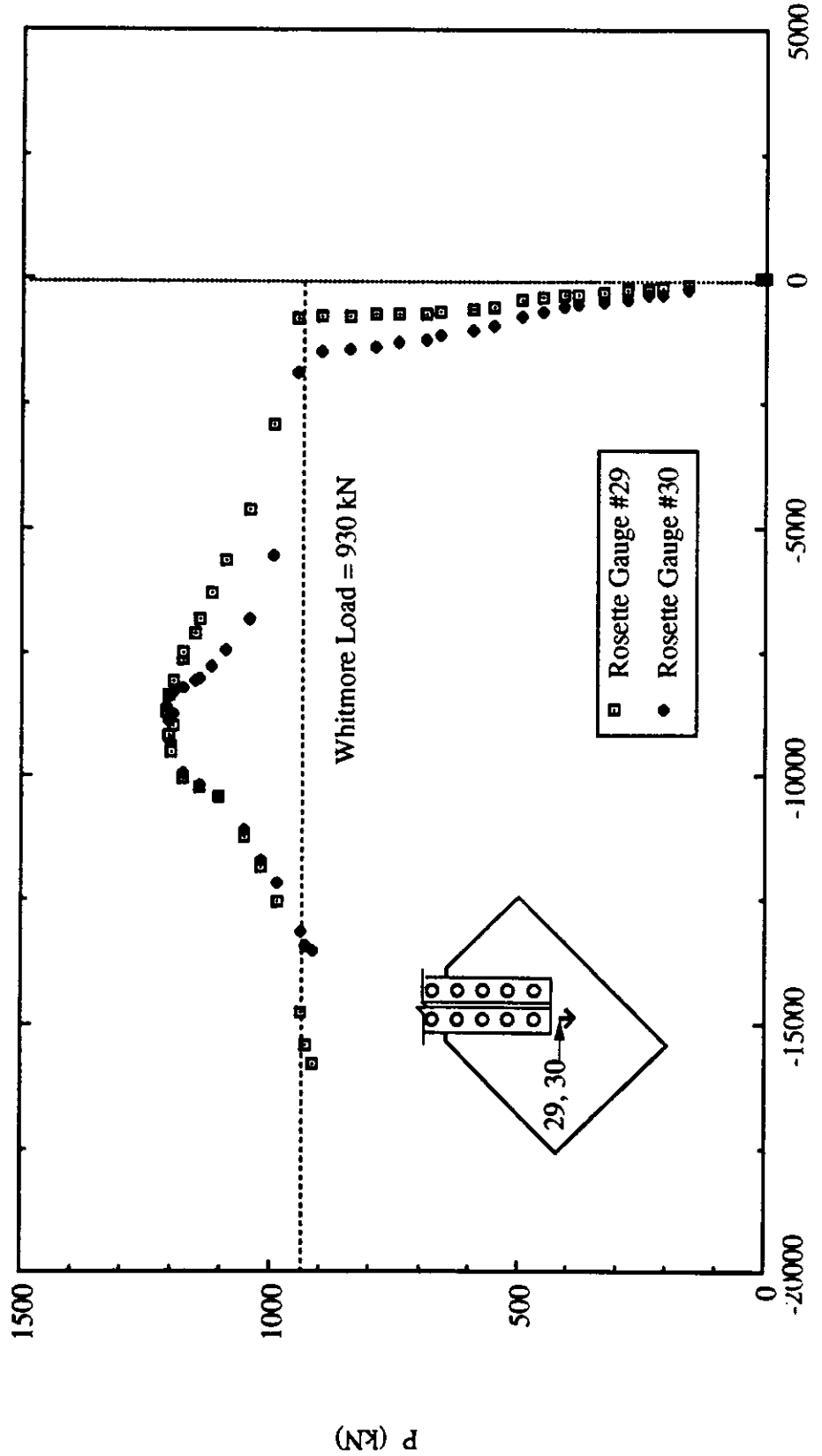

Fig. 5.13 Load vs. Rosette Gauge Readings for Specimen AP2

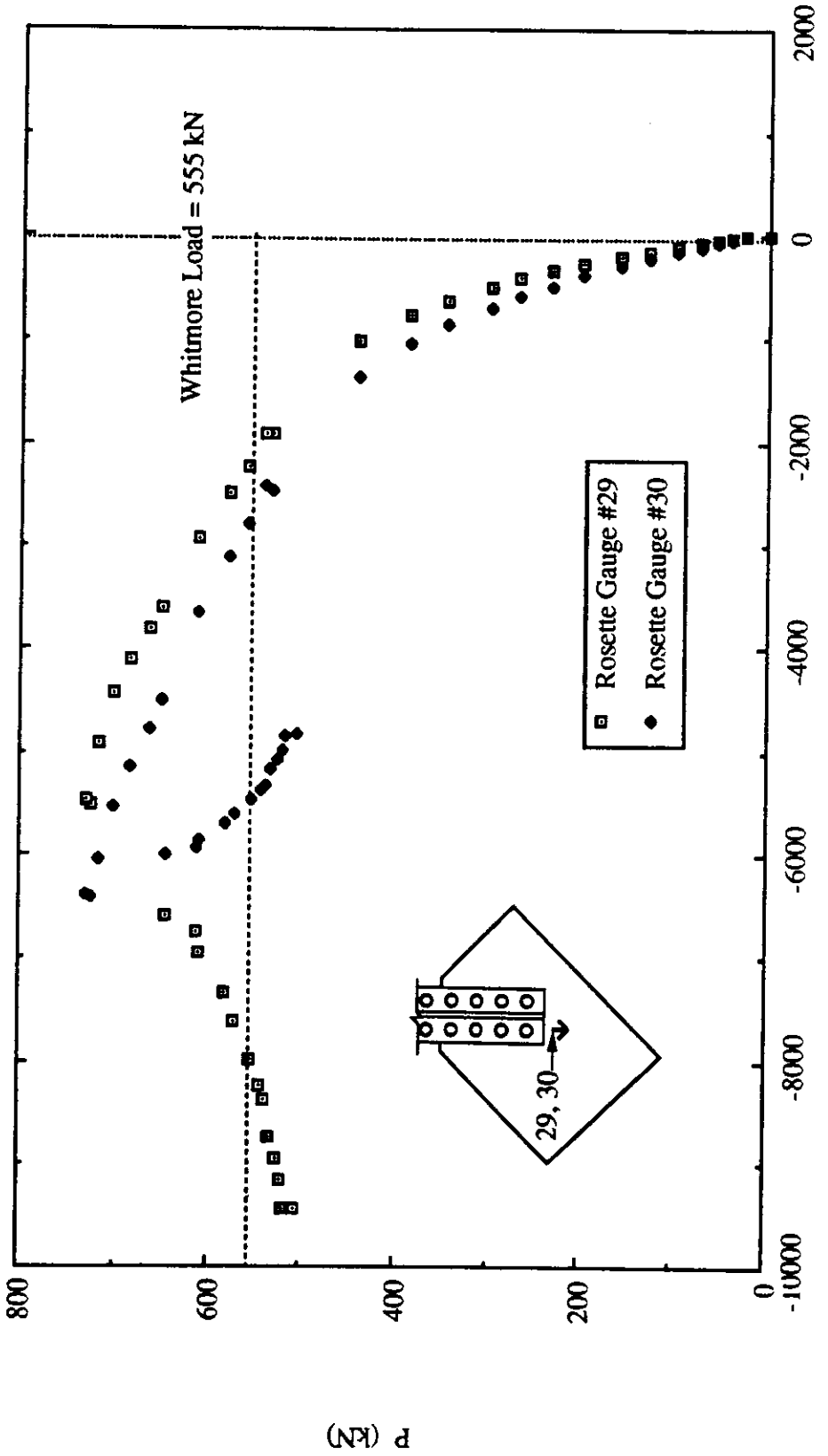

Fig. 5.14 Load vs. Rosette Gauge Readings for Specimen AP3

Fig. 5.15 Yielding at West Side of Failed Specimen AP1

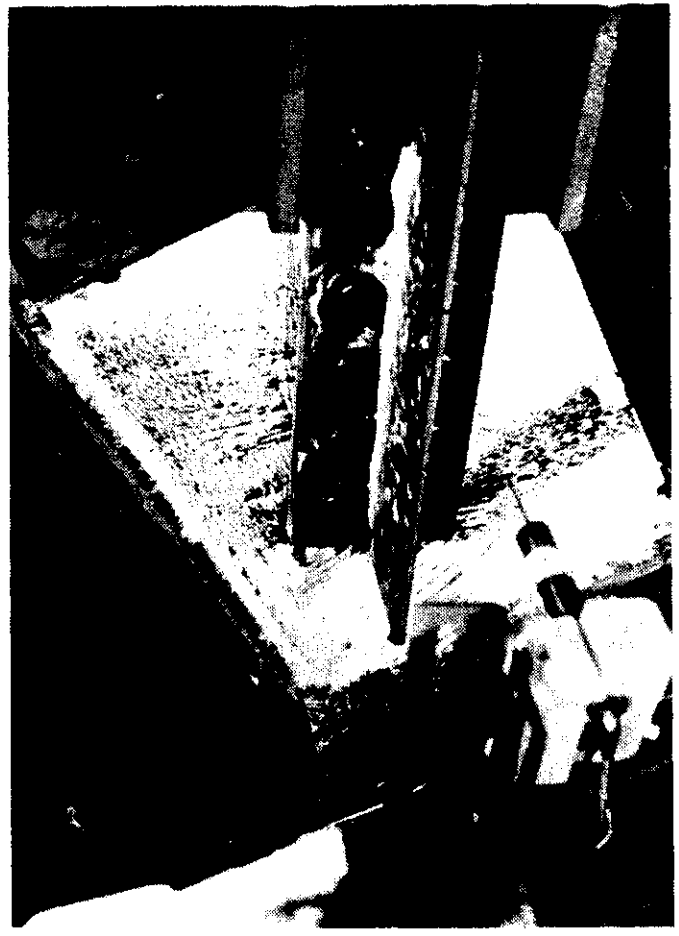

Fig. 5.16 Yielding at East Side of Failed Specimen AP1

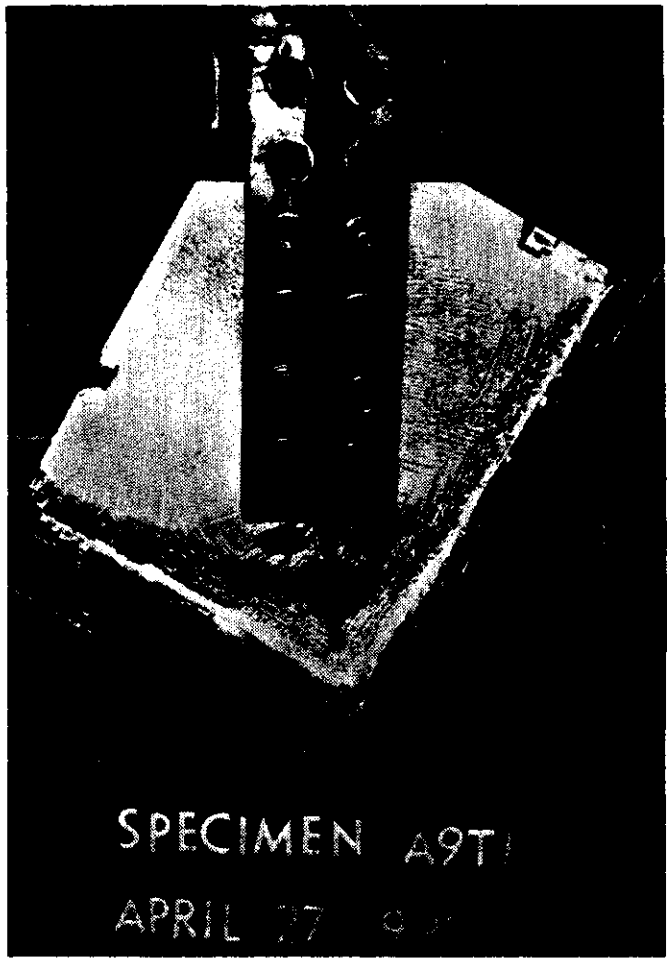

Fig. 5.17 Yielding at West Side of Failed Specimen AP2

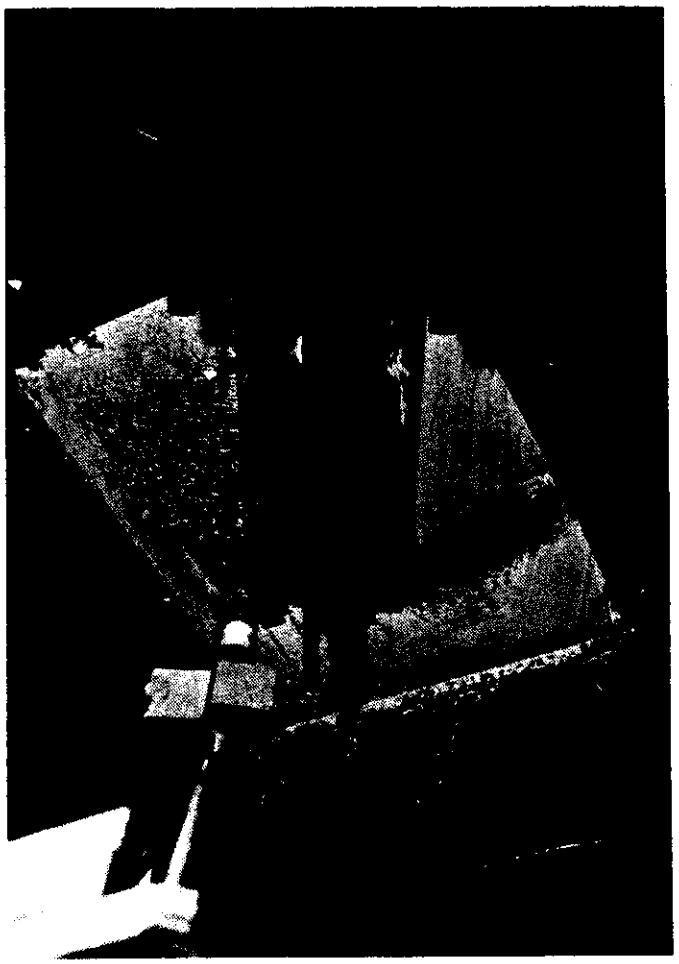

Fig. 5.18 Yielding at East Side of Failed Specimen AP2

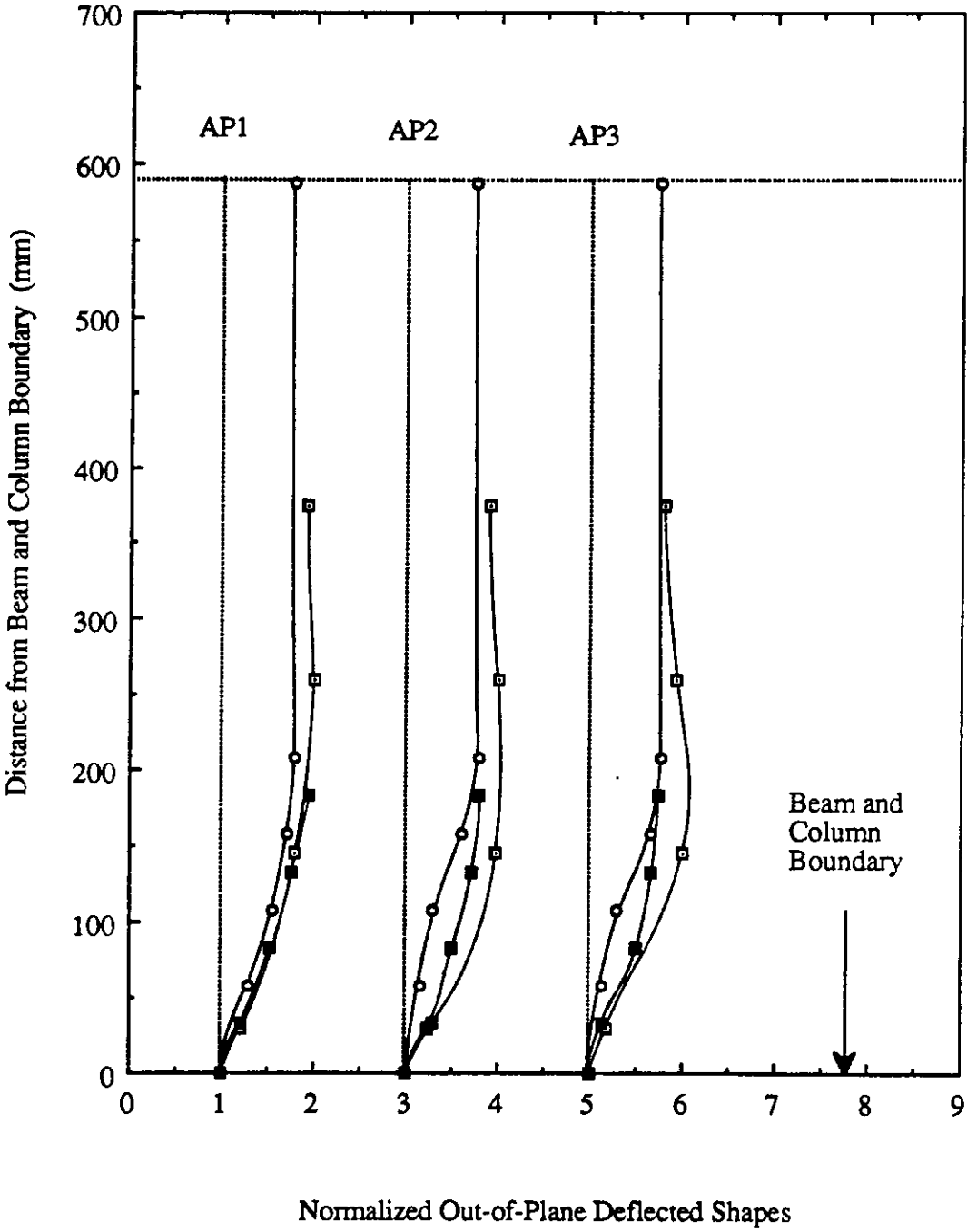

Fig. 5.19 Out-of-Deflected Shapes at Free Edges and Along Centerline of Splice for AP Type Specimens

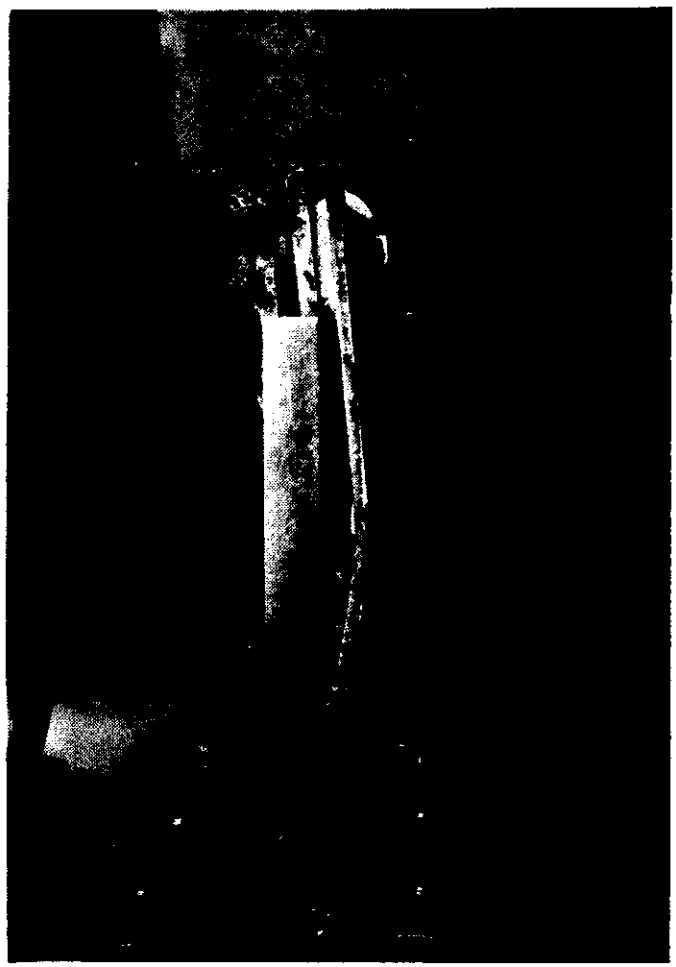

Fig. 5.20 Picture of Out-of-Plane Deflected Shapes at Long Free Edge for Specimen AP2

6. TEST RESULTS OF MP TYPE SPECIMENS

6.1 General

The test results of the GP, SP and AP types specimens described previously only concerned the compressive behavior of gusset plate connection without the effects of beam and column moments. However, the delivery of compression to the gusset plate must involve the beam and column moments, shears and axial force. It is the intent of the MP type specimens to investigate the effects of the beam and column moments on the compressive behavior and ultimate strength of the gusset plate specimens. To study the effects of the beam and column moments, specimen size and geometry similar to that of the GP type specimens were used for the MP type specimens. As a reminder, the beam and column moments used for specimens MP1, MP2 and MP3 were 250 kN·m and 125.5 kN·m, respectively. For specimen MP3A, a higher beam and column moments of 375 kN·m and 186.5 kN·m was applied. Finally, specimen MP3B was tested without beam and column moment. The test results of the MP type specimens are summarized in Table 6.1. Again, the failure mode of specimens was sway buckling of the connection.

6.2 Behavior of Load Versus In-Plane Deformation

The curves of load versus in-plane vertical deformation of the specimen and load versus vertical displacement of the hydraulic rams are shown in Figs. 6.1 to 6.10. It should be noted that the vertical deformation of the specimen was recorded by a LVDT attached to the end of the splice member. For specimen MP1, the curve of in-plane deformation illustrated the occurrence of bolt slips during testing. The first bolt slip was recorded at a load level of about 700 kN at which a drop in applied load accompanied with an increase in vertical displacement was observed. However, for the curve of vertical displacement of the hydraulic rams bolt slip occurred without significant increase in vertical displacement. This was due to the fact that since there was a decrease in applied load during bolt slip therefore

the elastic deflection of the reaction beam was also decreased. Hence, the LVDTs attached to the hydraulic rams (supported by the reaction beam) moved downward during bolt slip while the core of the LVDTs would still record the vertical displacement caused by the bolt slip and thus these two movements counteracted each other. Therefore, the LVDTs readings did not show a significant vertical displacement during this particular bolt slip. Bolts slips were again recorded as loading continued, however, both curves showed similar vertical movement during these slips since there was negligible decrease in applied load when bolt slips occurred. The curve of in-plane deformation of the specimen also shows that the specimen started to behave nonlinear at an applied load of about 1000 kN. When the applied load reached about 1600 kN, another bolt slip with decrease in applied load level was observed. As loading continued, the curve gradually turned to the ultimate load level. The unloading path of the specimen was not recorded since the out-of-plane displacement already reached the physical limit of the measuring device. The curve for the vertical displacement of the hydraulic rams shows that almost identical vertical movement was recorded for both rams during testing and this was the objective of the loading system as mentioned in Chapter 2. It was also observed that the vertical displacement of the hydraulic rams was higher than the in-plane deformation of the specimen due to the elastic deflection of reaction beam.

For specimen MP2, nonlinear load deflection behavior of load versus vertical displacement of hydraulic ram and in-plane vertical deformation of the specimen was observed at a load level of about 500 kN as shown in Figs 6.3 and 6.4. Figure 6.4 shows that the in-plane stiffness of specimen MP2 decreased rapidly followed by the initial stage of nonlinearity. However, the in-plane stiffness was maintained once the applied load was increased to about 750 kN at which an almost constant in-plane stiffness was observed until the specimen reached the ultimate load. Subsequently, a gradual unloading path was observed and the specimen appeared to stabilize at lower load level of about 900 kN. Similar behavior was observed for the curve of load versus vertical displacement of hydraulic

rams, however, the degree of nonlinearity of the load deflection curve was less than that of the vertical displacement of the specimen due to the presence of the elastic deflection of the reaction beam.

In general, the behavior of load versus vertical displacement of hydraulic ram and in-plane deformation of the specimen was similar for specimens MP3, MP3A and MP3B. However, the in-plane stiffness for specimen MP3B prior to reaching the ultimate was relatively higher than that of specimens MP3 and MP3A. It was also observed that the in-plane stiffness for specimen MP3 was higher than that of specimen MP3A. This behavior was probably due to the effects of beam and column moments and will be discussed in Chapter 8. The curves of load versus in-plane vertical deformation of the specimens show that nonlinear load deflection behavior for specimens MP3 and MP3A occurred at about 50 percent of the corresponding ultimate loads as shown in Figs. 6.6 and 6.8. For specimen MP3B nonlinear behavior was observed at about 70 percent of the ultimate load as illustrated in Fig.6.10. Again, as loading continued the curves gradually turned to the corresponding ultimate load levels. However, for specimen MP3A, bolt slip was recorded at a load level of about 760 kN and the applied dropped to approximately 710 kN before reaching the ultimate load level. Gradual unloading path was observed for the specimens and these curves show that the specimens appeared to stabilize at a load level of about 450 kN.

6.3 Behavior of Load Versus Out-of-Plane Displacement

The curves of load versus out-of-plane displacement at the conjunction of gusset-to-splice for the specimens are shown in Figs. 6.11 to 6.15. For specimen MP1, relatively linear load deflection behavior was observed until the applied load reached approximately 1000 kN. It should also be noted that the displacement at the early loading stage was relatively small probably due to the effects of the beam and column moment. When the applied load reached to about 1650 kN a sudden drop in load to approximately 1450 kN was recorded.

Subsequently, the applied load increased again back to the a load level of about 1600 kN without significant increase in out-of-plane displacement. From then on, the applied load increased with increasing displacement until the load reached an ultimate load of 1933 kN with a displacement of about 11mm. After reaching the ultimate load, the specimen unloaded gradually without significant decrease in applied load as shown in Fig. 6.11. When examined closely the load deflection curve in the early loading stage, it can be seen that drops in applied load due to bolt slips were recorded as already been discussed in the previous section.

For specimens MP2 and MP3, the load deflection behavior were quite similar as shown in Figs. 6.12 and 6.13. Linear load deflection behavior was observed until the applied load reached approximately 40 percent and 50 percent of the ultimate loads for specimens MP2 and MP3 respectively. However, the out-of-plane stiffness of both specimens only reduced slightly as loading continued until the specimens reached the ultimate loads. It should also be noted that the out-of-plane displacement of the specimens recorded prior to buckling was relatively small as shown in the figures. The recorded displacement at ultimate for both specimens was about 3 mm. A gradual unloading behavior was also observed for both specimens. However, for specimen MP2 the rate of unloading was lesser than that of specimen MP3.

The curve of load versus out-of-plane displacement for specimen MP3A shows a slightly different behavior than that of specimen MP3 as shown in Fig. 6.14. In general, negligible out-of-plane displacement was recorded for this specimen prior to reaching the ultimate load. As can be seen from the figure, the specimen originally deformed towards east, however, a sudden change in displacement direction at load step #7 was observed. This opposite movement of the specimen was due to the application of the full values of beam and column moment (375 kN·m and 186.5 kN·m, respectively) at that particular load step. As loading continued, only very slight increase in out-of-plane displacement towards west

was observed. When the applied load reached the ultimate load of 819 kN bifurcation occurred with the specimen deformed towards west. Since the buckling phenomenon occurred rapidly, therefore, it was unable to record readings between the ultimate load and the next load level which had a displacement of 15 mm. However, it can still be seen that the unloading process for the specimen was quite gradual.

For specimen MP3B, which excluded the beam and column moments, the curve of load versus out-of-plane displacement was similar to that of specimen MP3 as shown in Fig. 6.15. The curve was relatively linear up to 700 kN. Then the curve slowly turned to the ultimate load of 821 kN. Again, it was unable to record successive readings after the ultimate load until the applied load reached a lower load level. However, gradual unloading process was observed for the specimen. It should be noted that all the MP type specimens with plate thickness of 6.5 mm reached approximately the same load level of 450 kN at the final load step regardless of the level of the applied beam and column moments.

6.4 Strain Gauges Results

The in-plane stress distribution of the specimen was affected by the beam and column moments as observed from the strain gauges readings. For specimen MP1, yielding was first observed at the rosette close to the beam boundary at an applied load of about 770 kN. However, the yield load predicted by the Whitmore method was approximately 1200 kN. This early yielding of the specimen may be attributed to the effects of the beam and column moment. Similar behavior was also observed for the other MP type specimens. In particular, for specimen MP2 and MP3 yielding at rosette occurred at an applied load of about 35 and 30 percent of the corresponding yield loads predicted by the Whitmore method. It should be noted that for specimens MP1, MP2, and MP3 full values of the beam and column moments had already been applied to the specimens when the test yield loads were recorded. However, specimen MP3A, which was subject to higher beam and column moment (Mb=375 kN·m, Mc=186.5 kN·m), showed yielding at rosette when the

applied load was maintained at about 100 kN and the applied beam and column moments were increased from 50 percent to the full values.

The curves of load versus strains recorded at mid-length and fixed end of the free edges are shown in Figs.6.16 to 6.31. In general, the plots of load versus longitudinal strains at mid-length of free edges show that strain readings in the elastic range were recorded prior to reaching the ultimate load of the specimens. Furthermore, similar strain readings were recorded from both sides of the specimens before strain bifurcation occurred at ultimate load levels except specimen MP1. For specimen MP1, strain reversal was observed at the long free edge as shown in Fig. 6.16 and the strain readings from both sides of the specimen at the short free edge deviated at early loading stage as illustrated in Fig. 6.24. The strain readings recorded at the fixed ends of the free edges showed that tension existed in that vicinity. In particular, specimens MP3 and MP3A showed tensile yielding at the fixed ends of free edges when the full values of the beam and column moments were applied as shown in Figs. 6.29 and 6.31, respectively. As loading continued, tensile strain recorded at the fixed ends of free edges increased slightly until strain bifurcation occurred at ultimate loads. It should also be noted that strain gauges located at the fixed end of the free edges were mounted 30 mm away from the boundary. Hence, it is believed that tensile yielding should have occurred right at the fixed end of free edges before even detected by the strain gauges. In addition, the vicinity of the fixed end of the free edges was also a stress concentration area due to abrupt change of geometry.

To investigate the effects of beam and column moments on the in-plane stress distribution of the specimen, strain readings along the beam and column boundary were examined. A plot of strain readings along the beam and column boundary at three levels (1/3, 2/3, and full values) of applied beam and column moments for specimen MP1 is shown in Fig. 6.32. The strain readings shown in the figure had already excluded the effects of the axial load. It can be seen from the figure that high stress gradient existed along the beam

and column boundary especially along the beam boundary in the vicinity of the short free edge. In general, tensile strains were observed along the column boundary. However, compressive strains were recorded near the mid-length of the beam boundary as shown in the figure. The reduced strain readings at rosettes indicated that the applied beam and column moments induced compressive strains in the plate area underneath the splice member. Hence, early yielding at that particular region was recorded for the MP type specimens.

6.5 Yielding Behavior of Specimens

The yielding process and pattern for the MP type specimens were only slightly different than that of the GP type specimens except specimen MP3B which behaved similar to specimen GP3. In general, yield lines were first observed near the beam boundary. These yield lines were almost parallel to the boundary . Then, yielding underneath the splice member was recorded. As loading continued, yielding underneath the splice member progressed and yield lines were also recorded about the two sides of the splice member. In particular, for specimens MP1, MP2 and MP3B extensive yielding of the specimens were observed prior to buckling. However, for specimen MP3 moderate yielding was observed underneath the splice member. After buckling occurred, yield line mechanism were also formed at the mid-length of the long free edge and along the beam and column boundary. A picture of failed specimen MP1 is shown in Fig. 6.33. This picture illustrates the extent of the yielding and also the location of the yield line mechanism. When examined the failed specimen MP3, fracture from the weld at the fixed end of short free edge was observed. Hence, for specimens MP3A and MP3B larger weld size was used to prevent fracture at that location.

6.6 Out-of-Plane Deflected Shapes of Free Edges and Along Centerline of Splicing Member

The normalized out-of-plane deflected shapes of the MP type specimens are shown in Fig. 6.34. In general, the out-of-plane deflected shapes of the specimens resembled the buckled shape of a fixed-pinned column. The figure shows that the end of the free edges attached to the beam and column boundary exhibited quite significant rotation. This is probably due to the tensile yielding caused by the beam and column moments. Pictures of the free edges deflected shapes for specimen MP3A are shown in Fig.6.35 to illustrate the amount of rotation existed at the ends. It can be seen from these pictures that the lower end of the free edges was almost in a straight position indicating that the lower end rotated as a rigid body.

Table 6.1 Test Results of MP Type Specimens

Specimen Designation	Plate Size (mm x mm x mm)	Beam Moment Mb (kN·m)	Column Moment Mc (kN·m)	Ultimate Load (kN)	Whitmore Load P_w (kN)	Thornton Load P_t k = 0.65 (kN)
MP1	500 x 400 x 13.3	250	125	1933	1216	1142
MP2	500 x 400 x 9.8	250	125	1316	930	828
MP3	500 x 400 x 6.5	250	125	721	555	459
MP3A	500 x 400 x6.5	375	187.5	819	555	459
MP3B	500 x 400 x 6.5	0	0	821	555	459

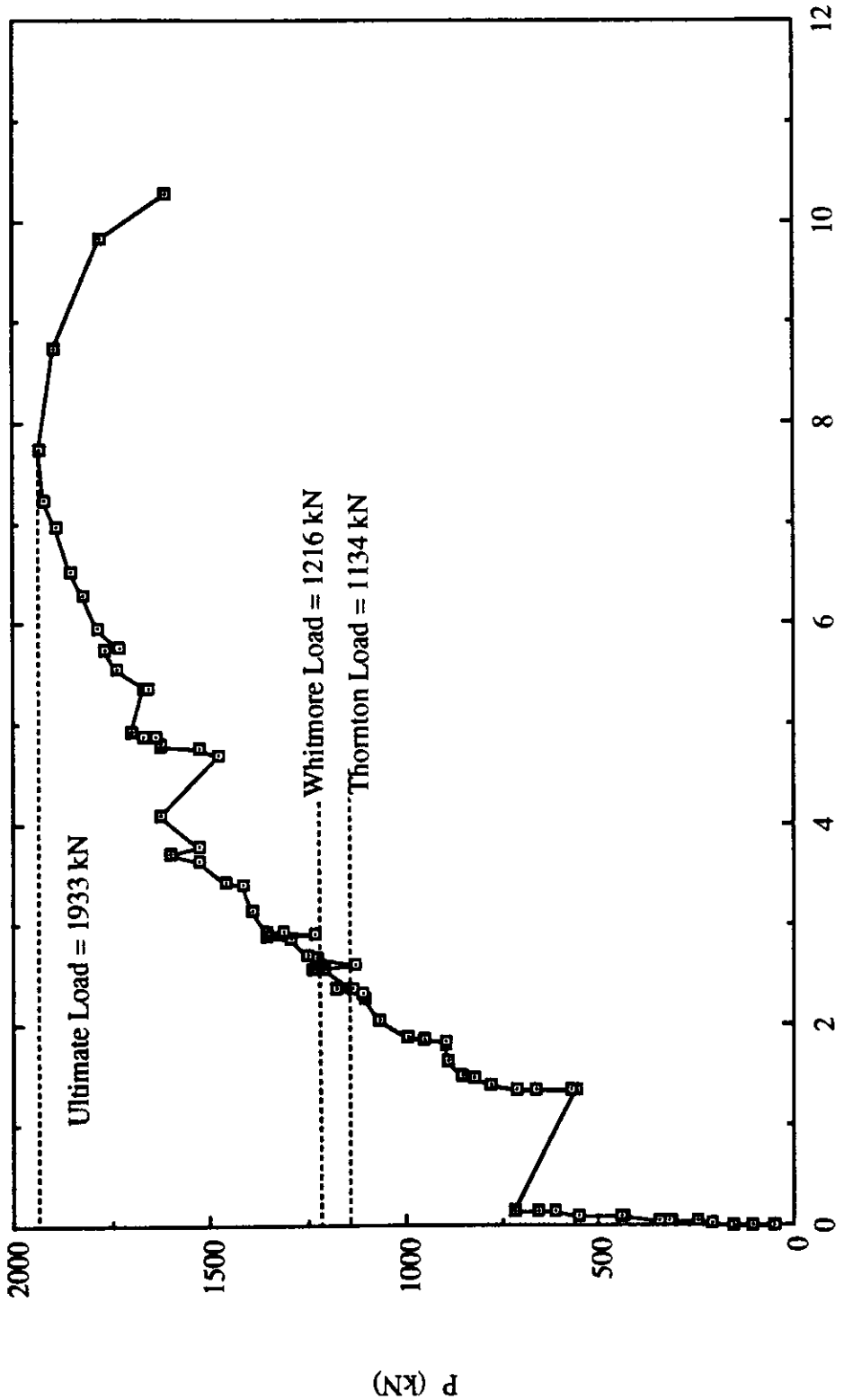

Fig. 6.1 Load vs. In-Plane Deformation Measured at End of Splice for Specimen MP1

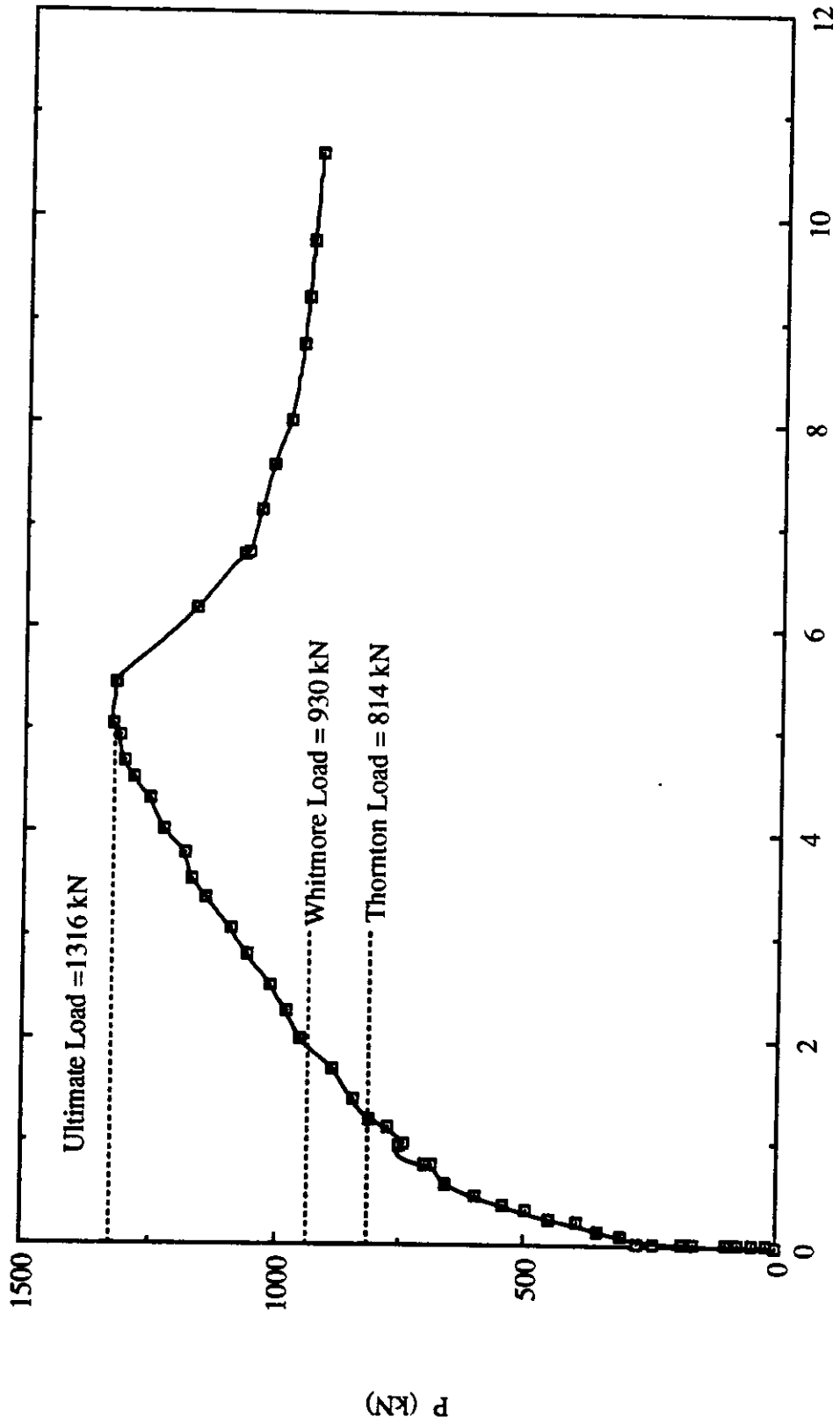

Fig. 6.2 Load vs. In-Plane Deformation Measured at End of Splice for Specimen MP2

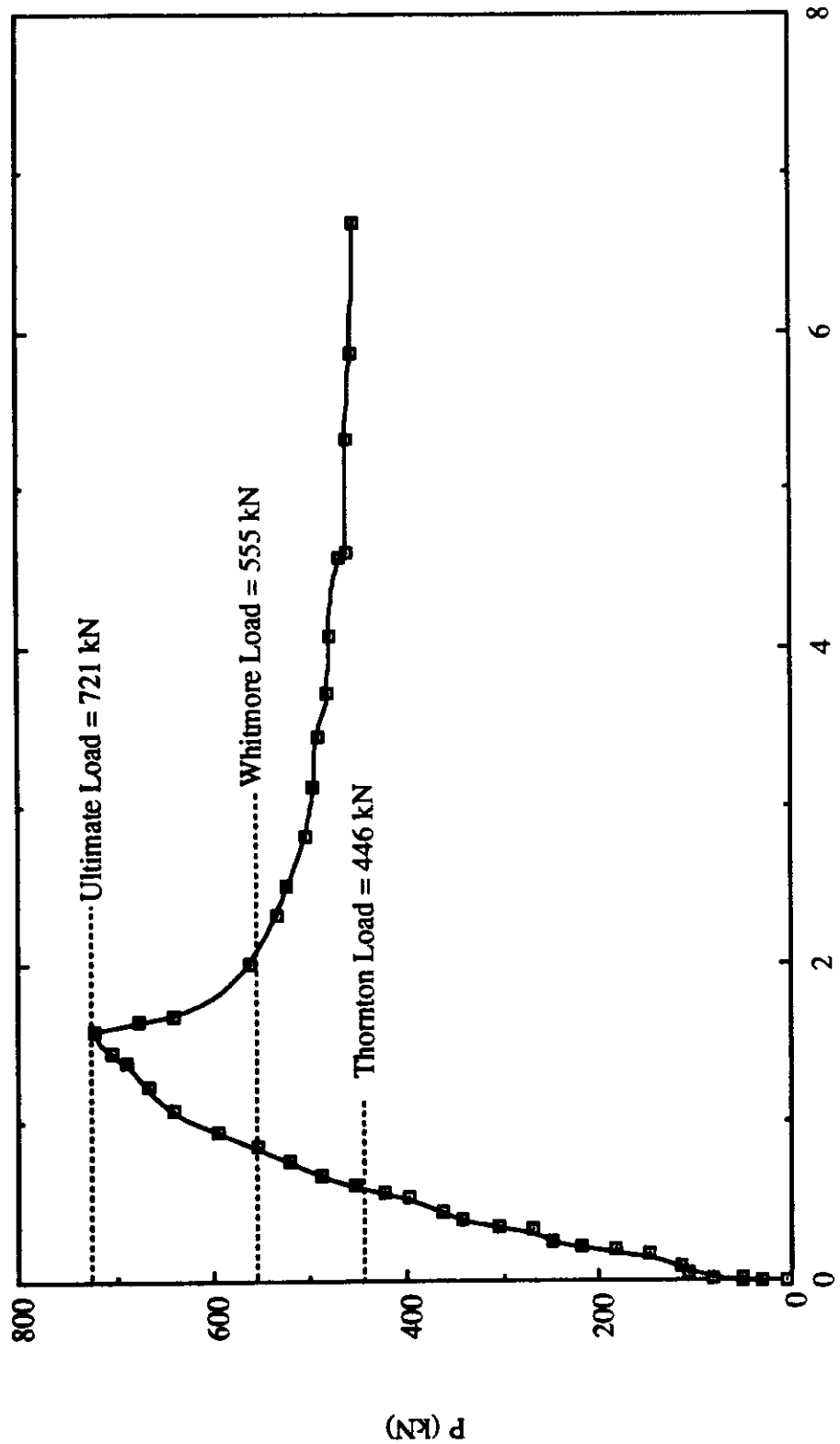

Fig. 6.3 Load vs. In-Plane Deformation Measured at End of Splice for Specimen MP3

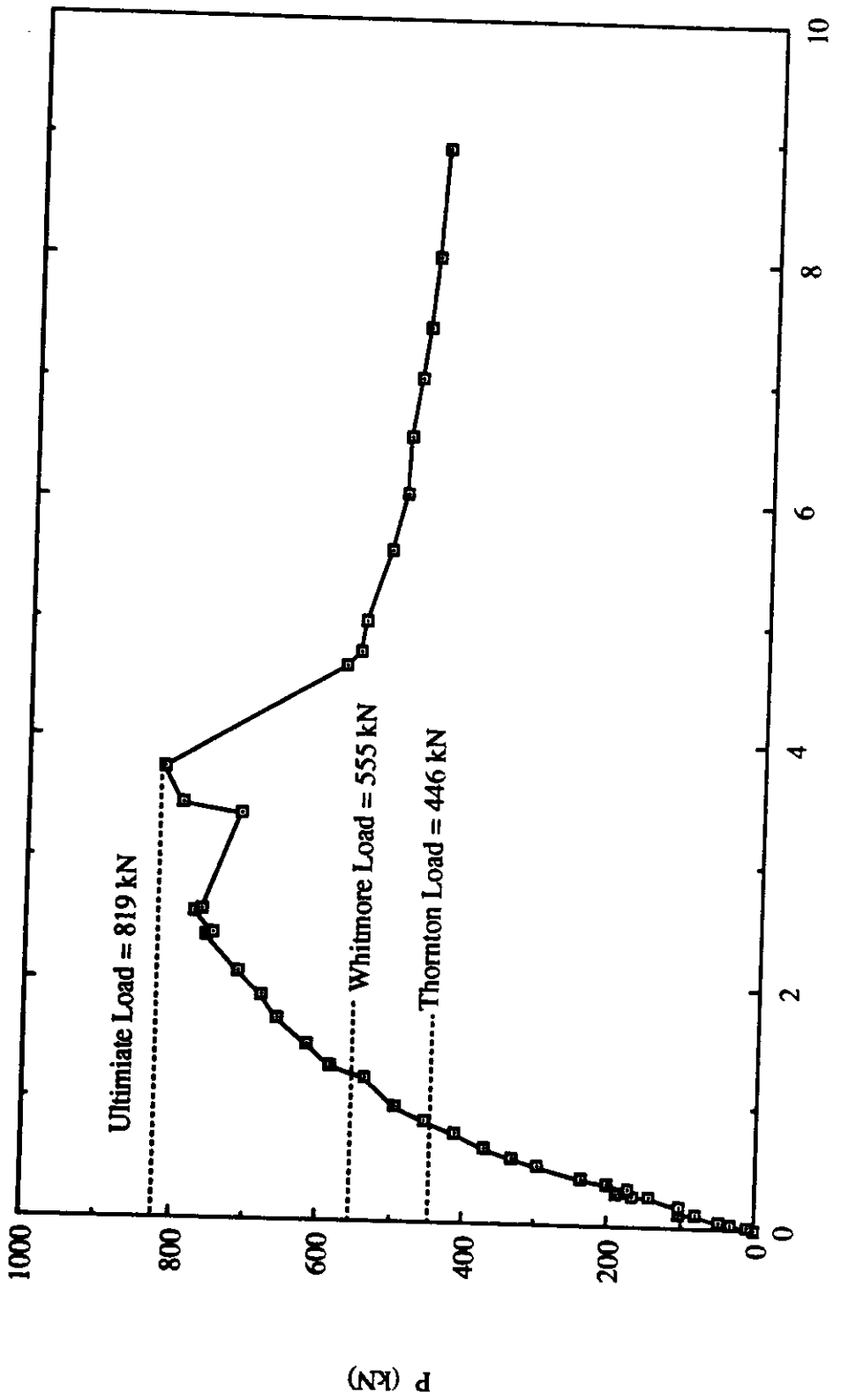

Fig. 6.4 Load vs. In-Plane Deformation Measured at End of Splice for Specimen MP3A

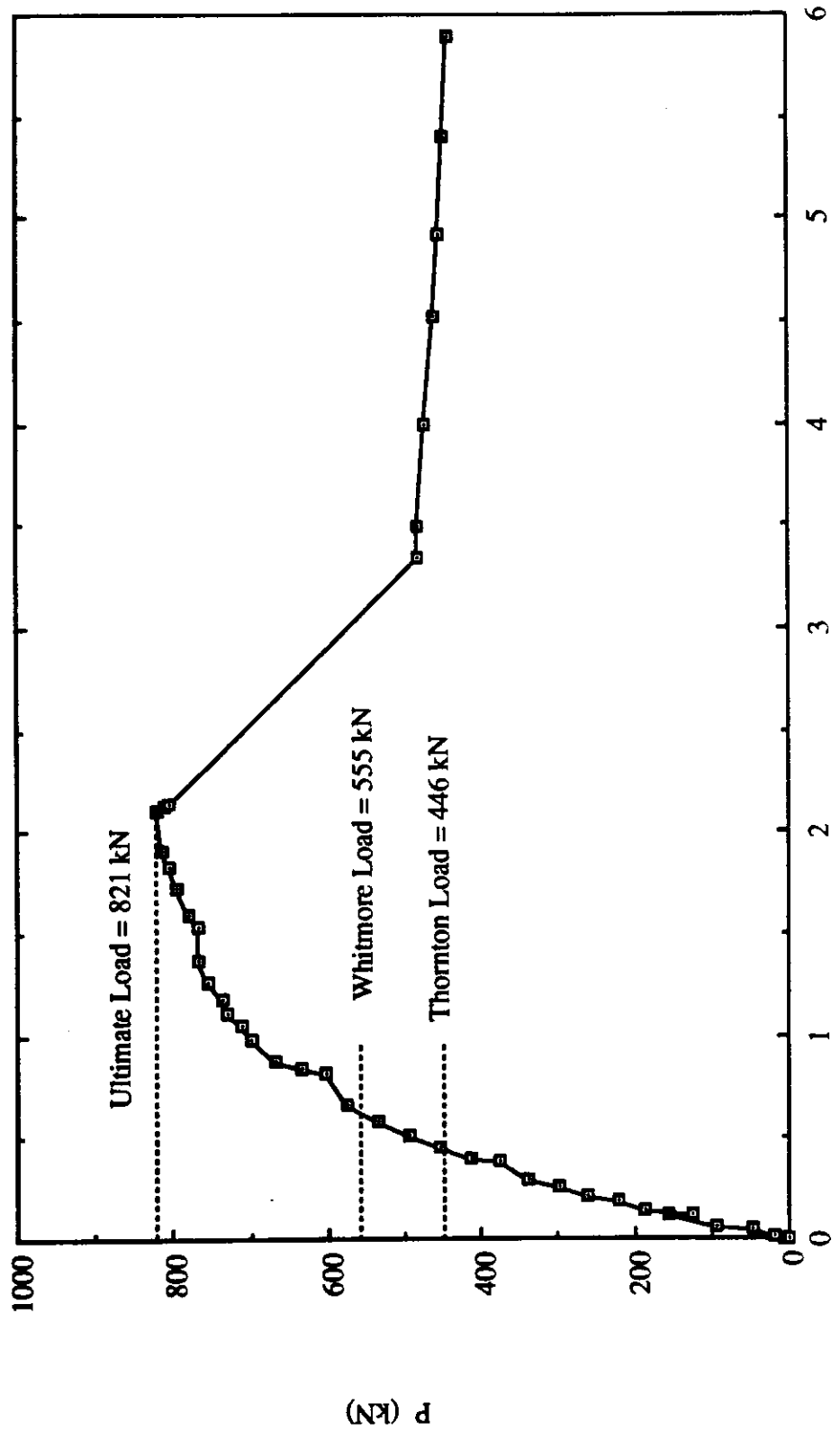

Fig. 6.5 Load vs. In-Plane Deformation Measured at End of Splice for Specimen MP3B

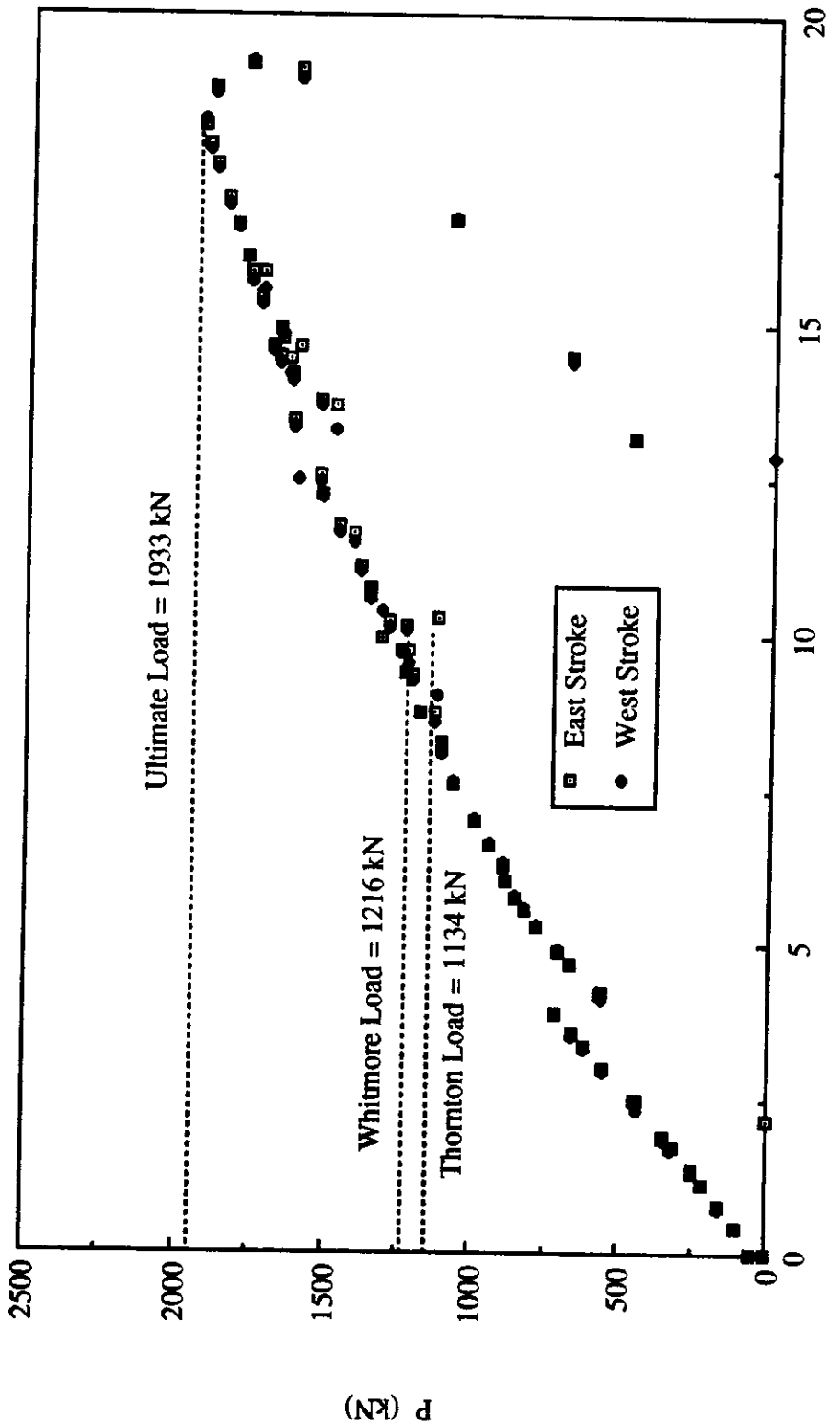

Fig. 6.6 Load vs. Vertical Strokes of Hydraulic Rams for Specimen MP1

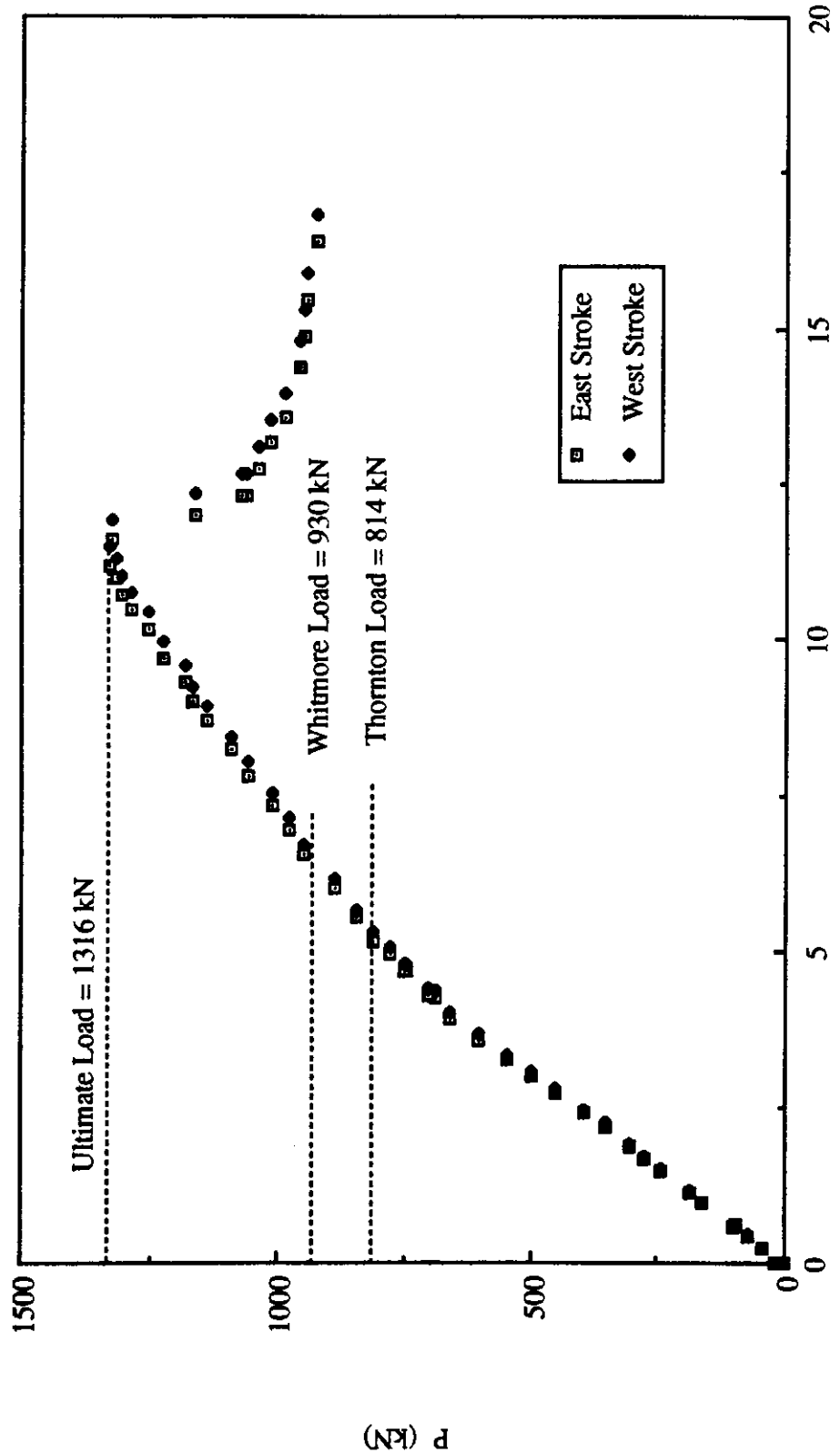

Fig. 6.7 Load vs. Vertical Strokes of Hydraulic Rams for Specimen MP2

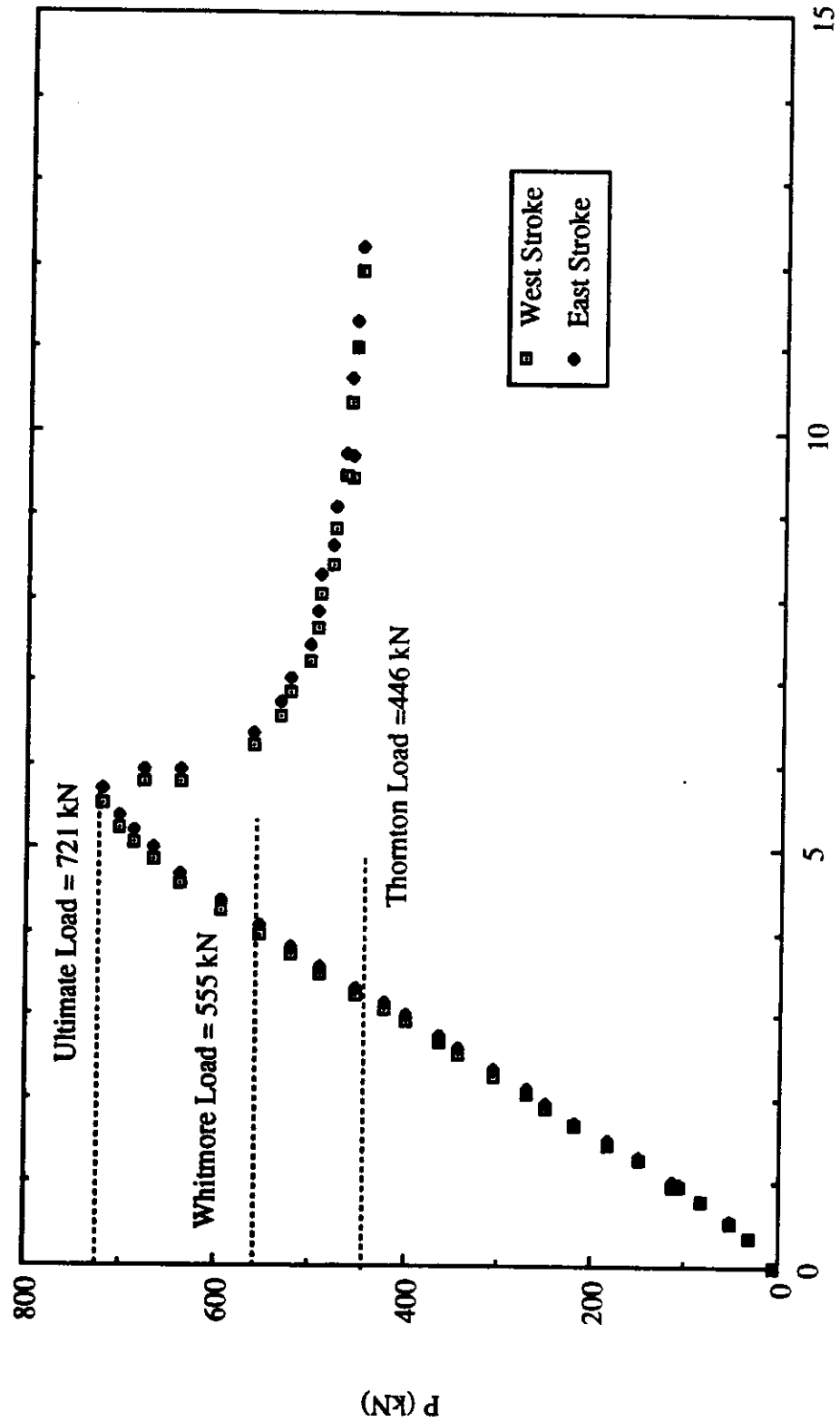

Fig. 6.8 Load vs. Vertical Strokes of Hydraulic Rams for Specimen MP3

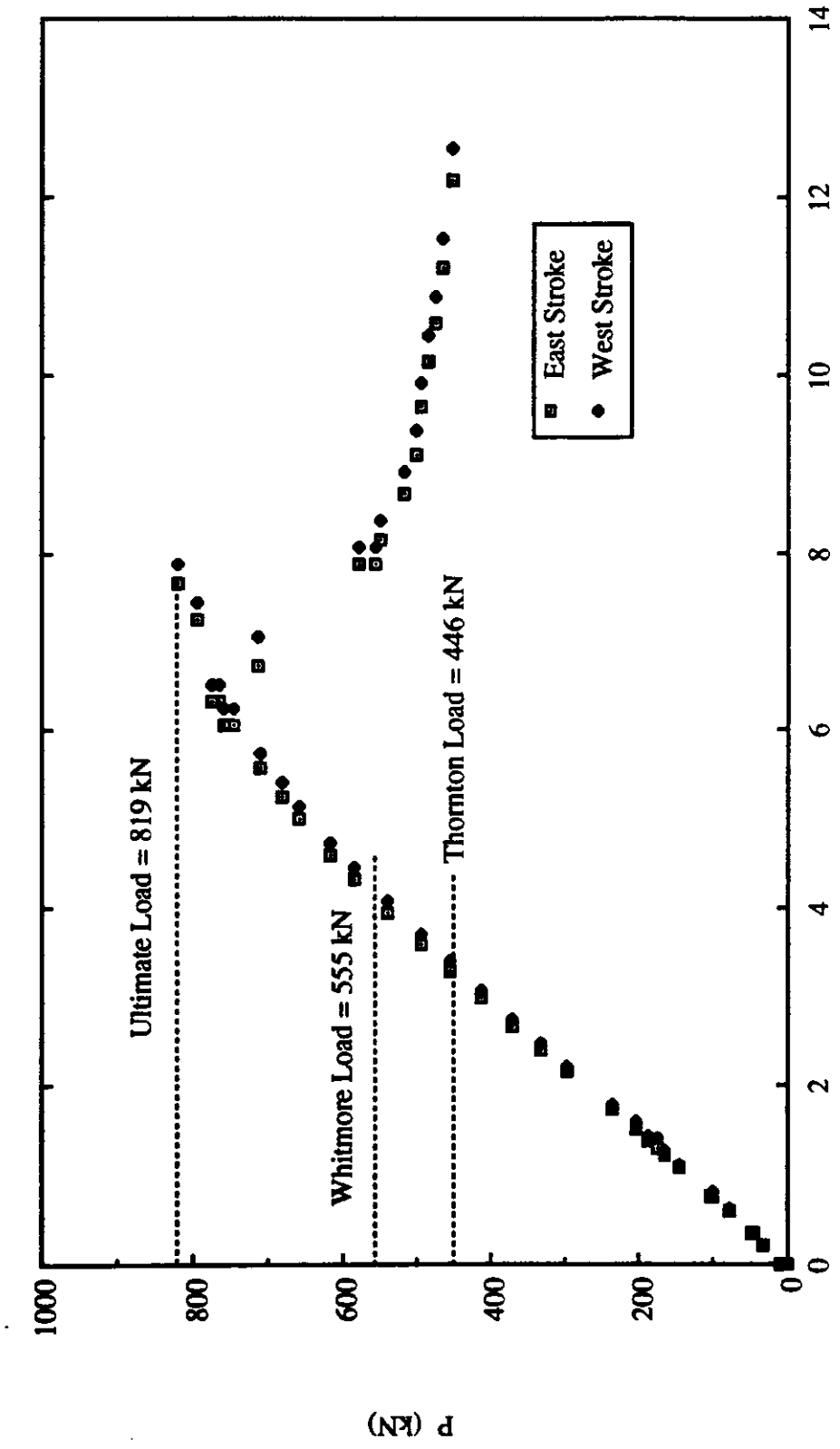

Fig. 6.9 Load vs. Vertical Strokes of Hydraulic Rams for Specimen MP3A

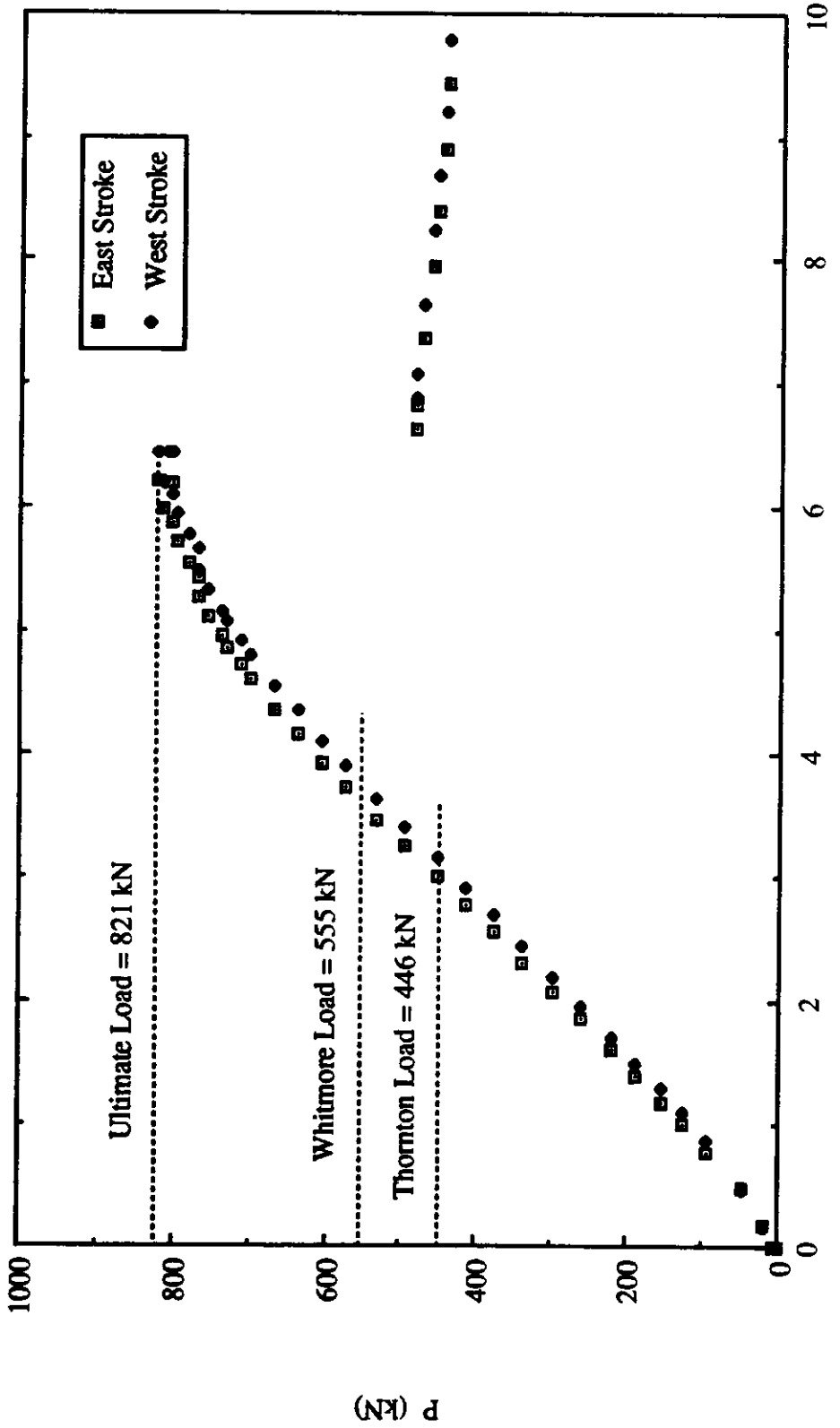

Fig. 6.10 Load vs. Vertical Strokes of Hydraulic Rams for Specimen MP3B

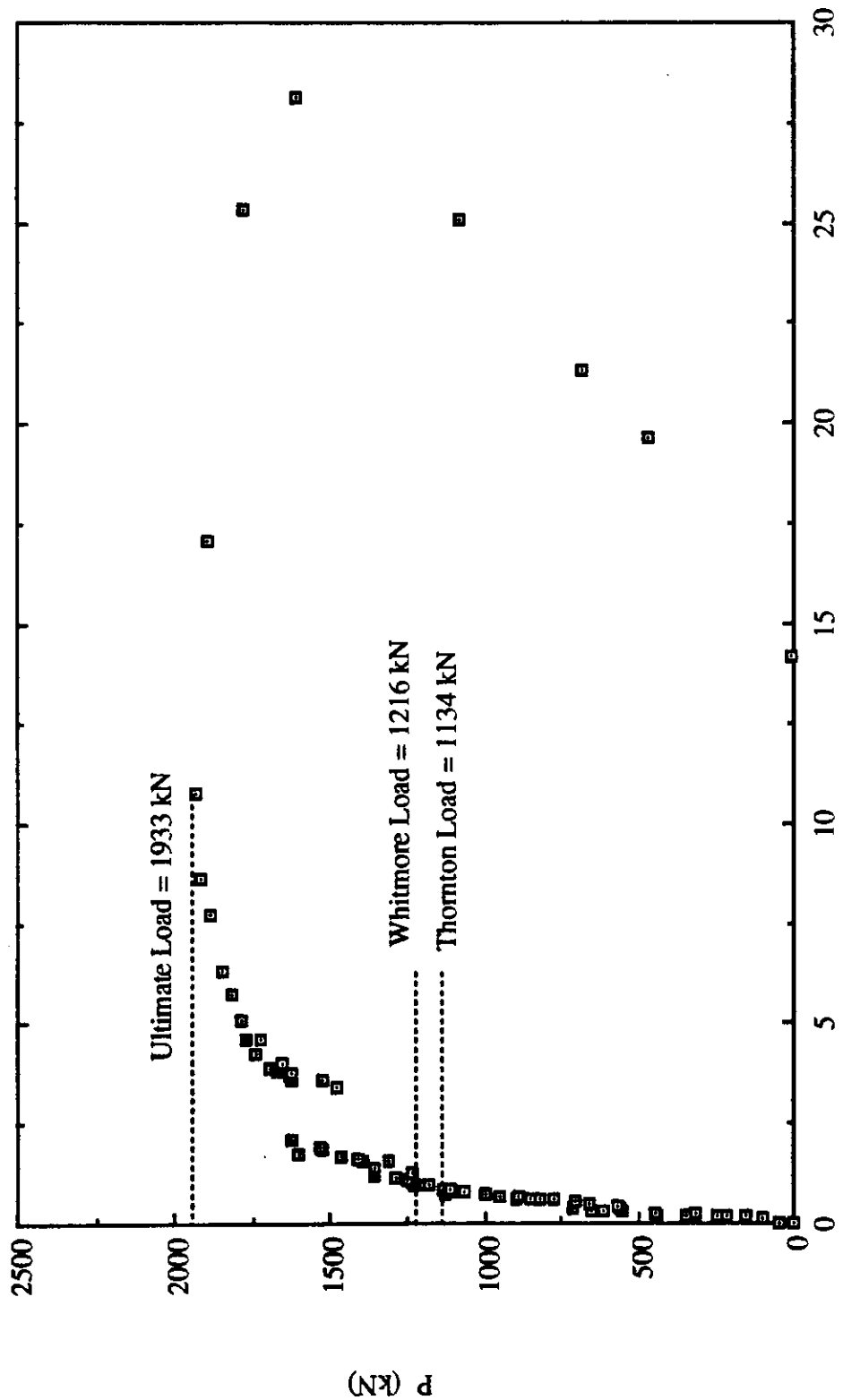

Fig. 6.11 Load vs. Out-of-Plane Displacement at Conjunction of Gusset-to-Splice for Specimen MP1

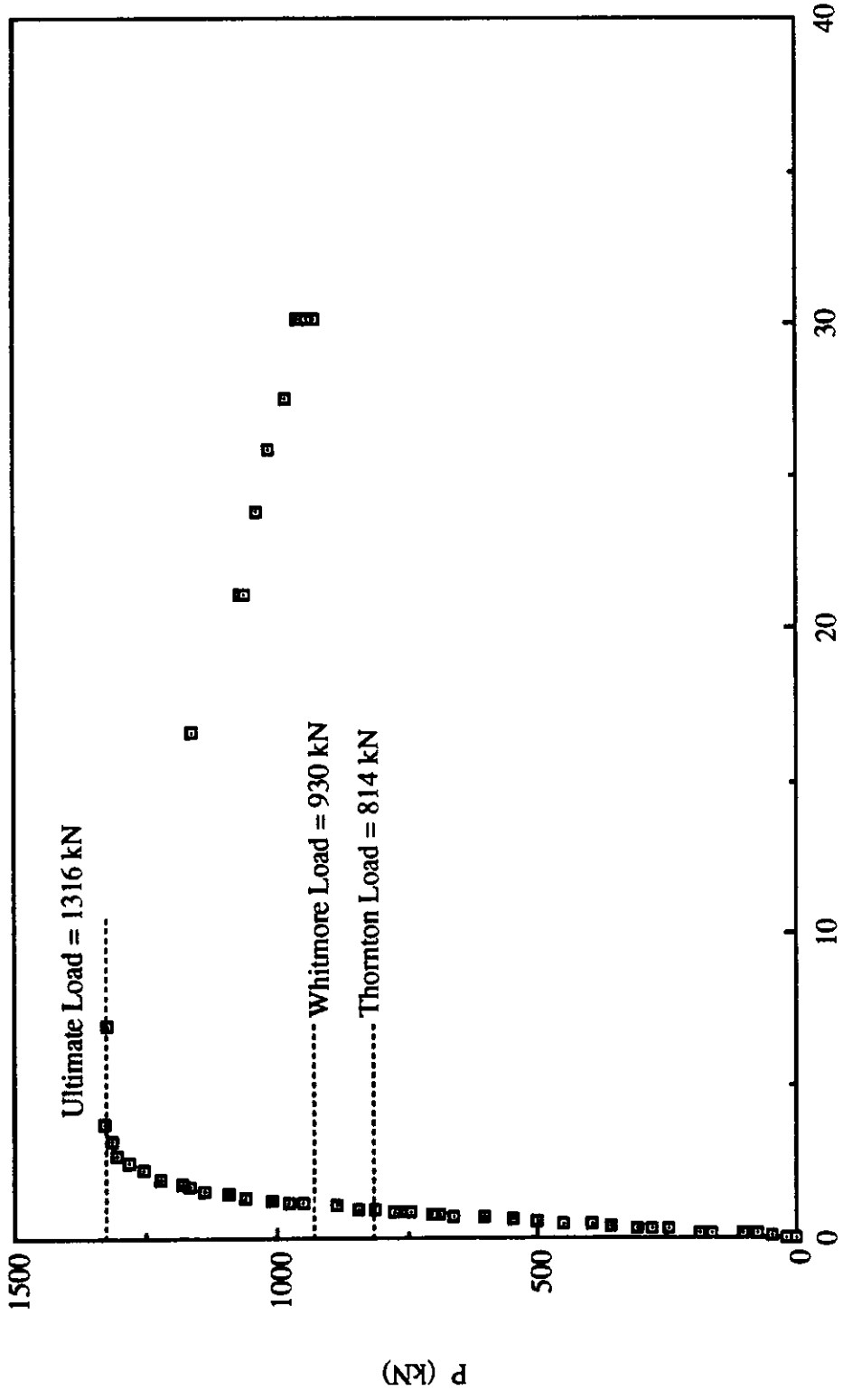

Fig. 6.12 Load vs. Out-of-Plane Displacement at Conjunction of Gusset-to-Splice for Specimen MP2

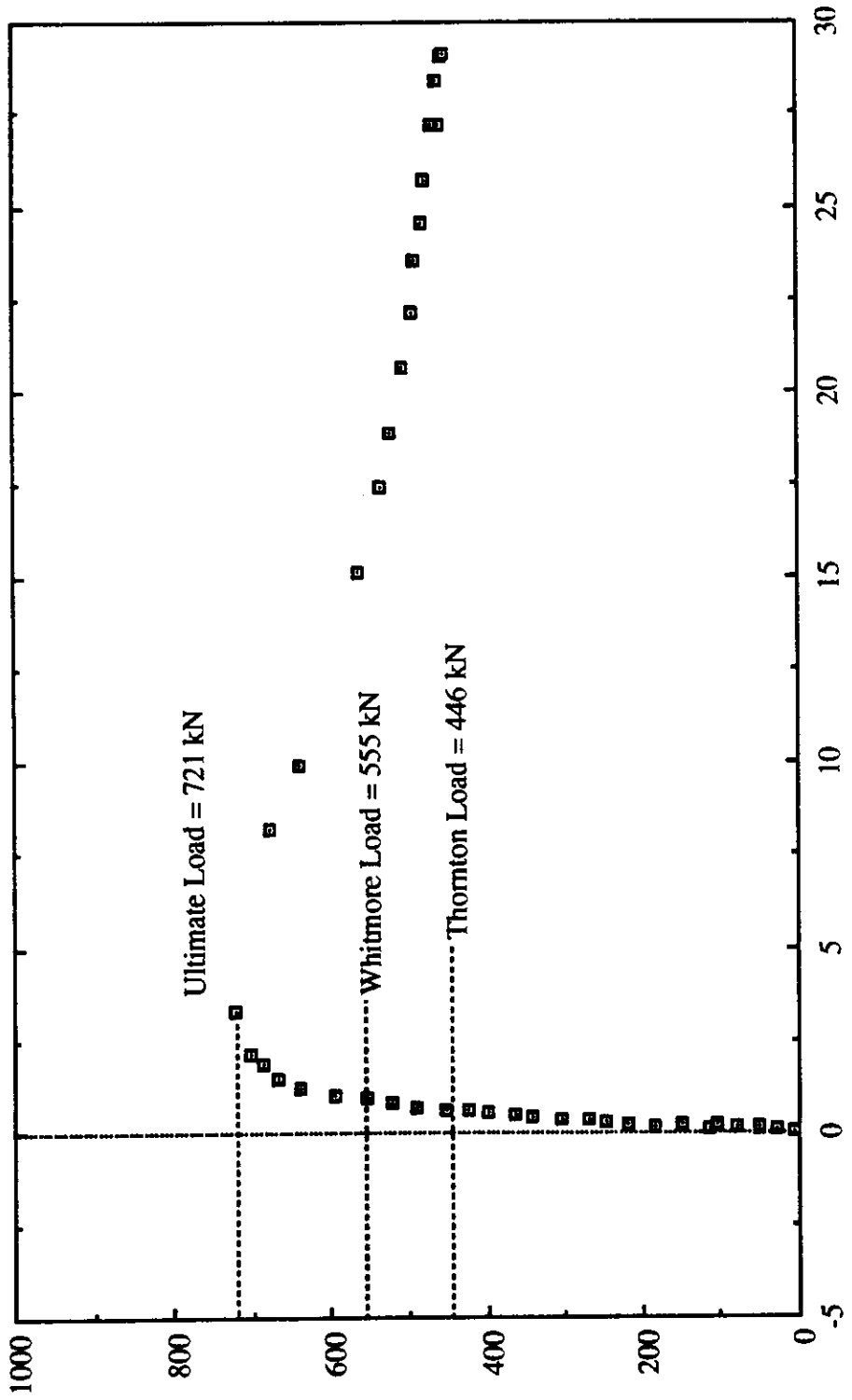

Fig. 6.13 Load vs. Out-of-Plane Displacement at Conjunction of Gusset-to-Splice for Specimen MP3

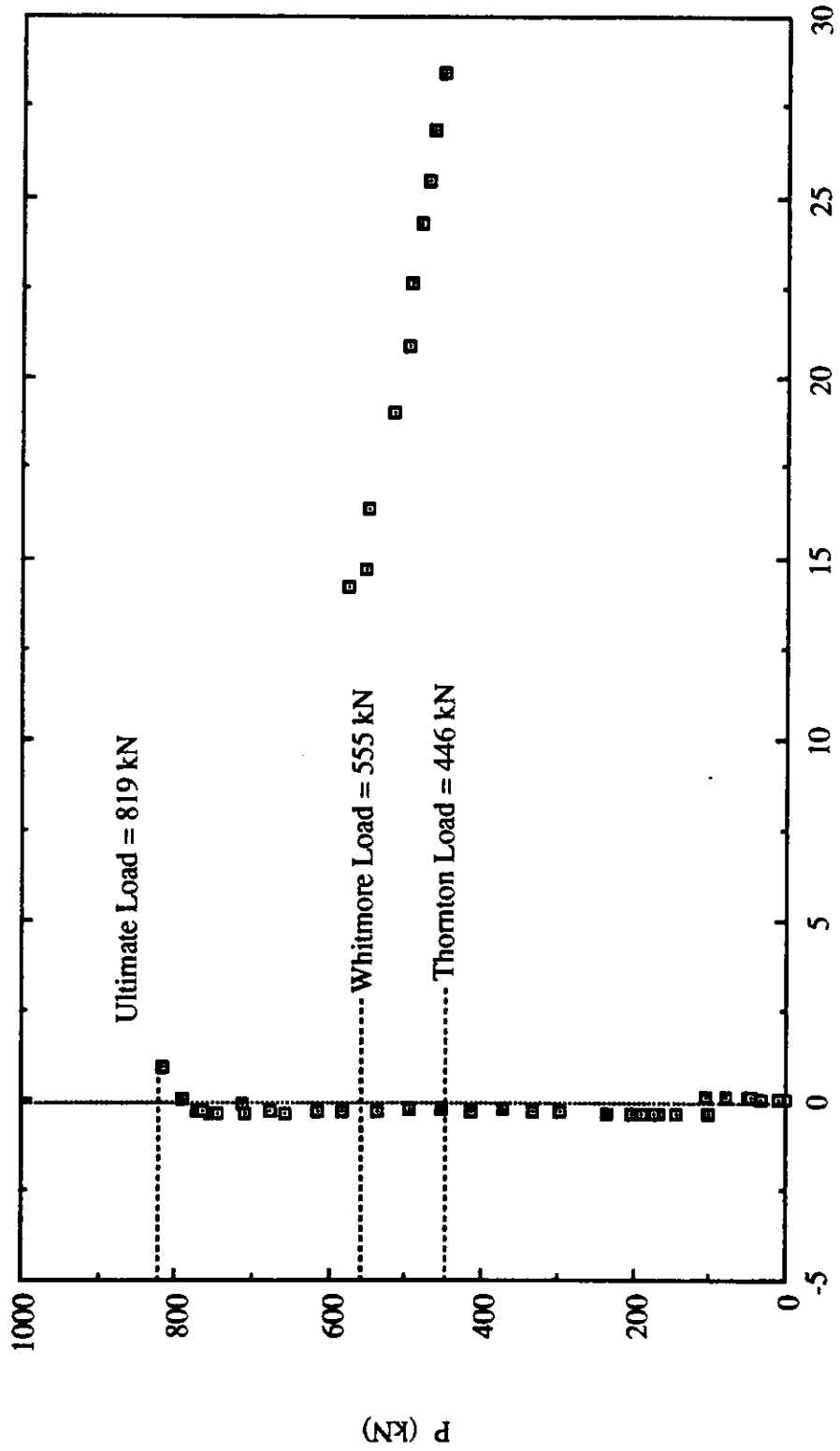

Fig. 6.14 Load vs. Out-of-Plane Displacement at Conjunction of Gusset-to-Splice for Specimen MP3A

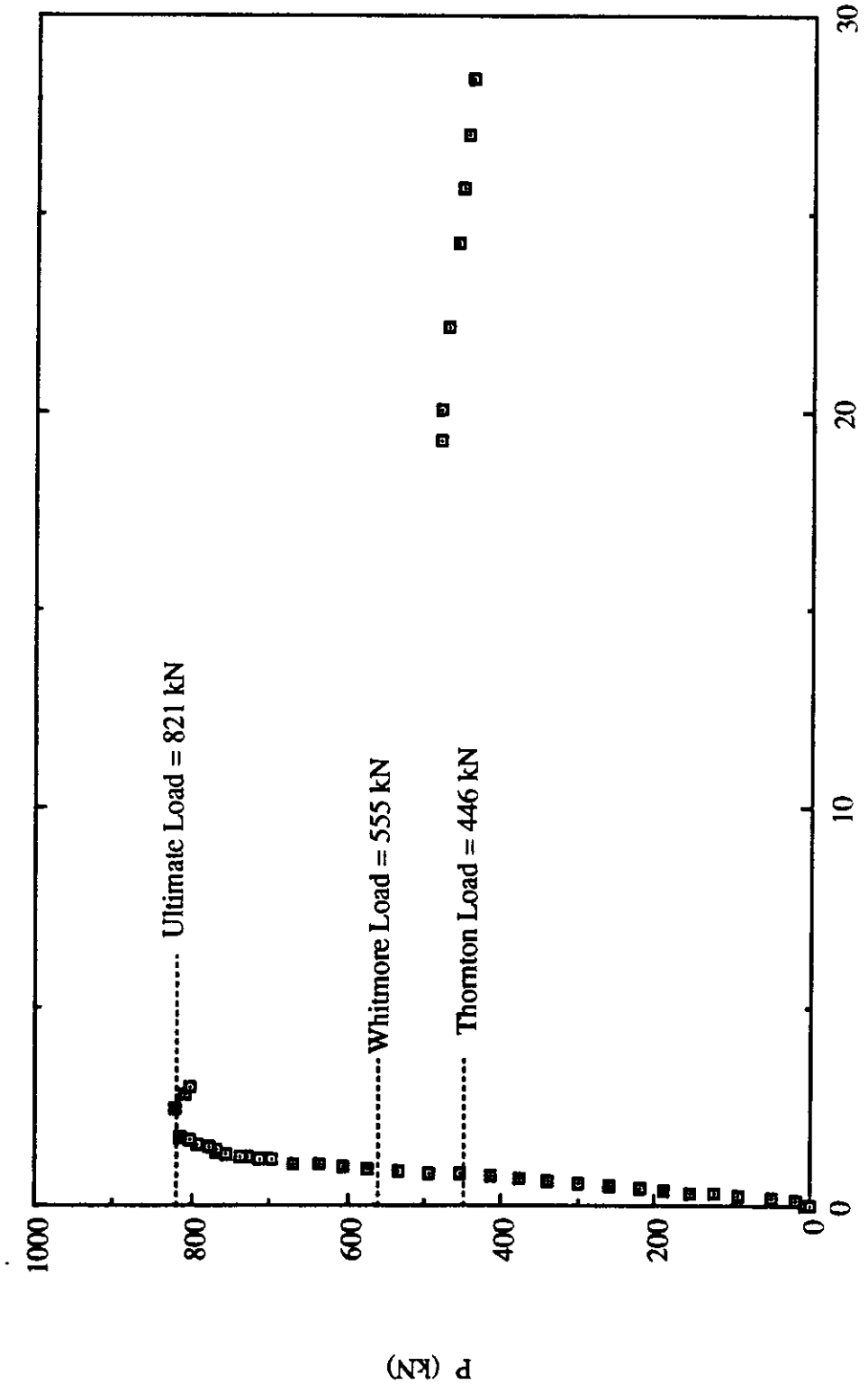

Fig. 6.15 Load vs. Out-of-Plane Displacement at Conjunction of Gusset-to-Splice for Specimen MP3B

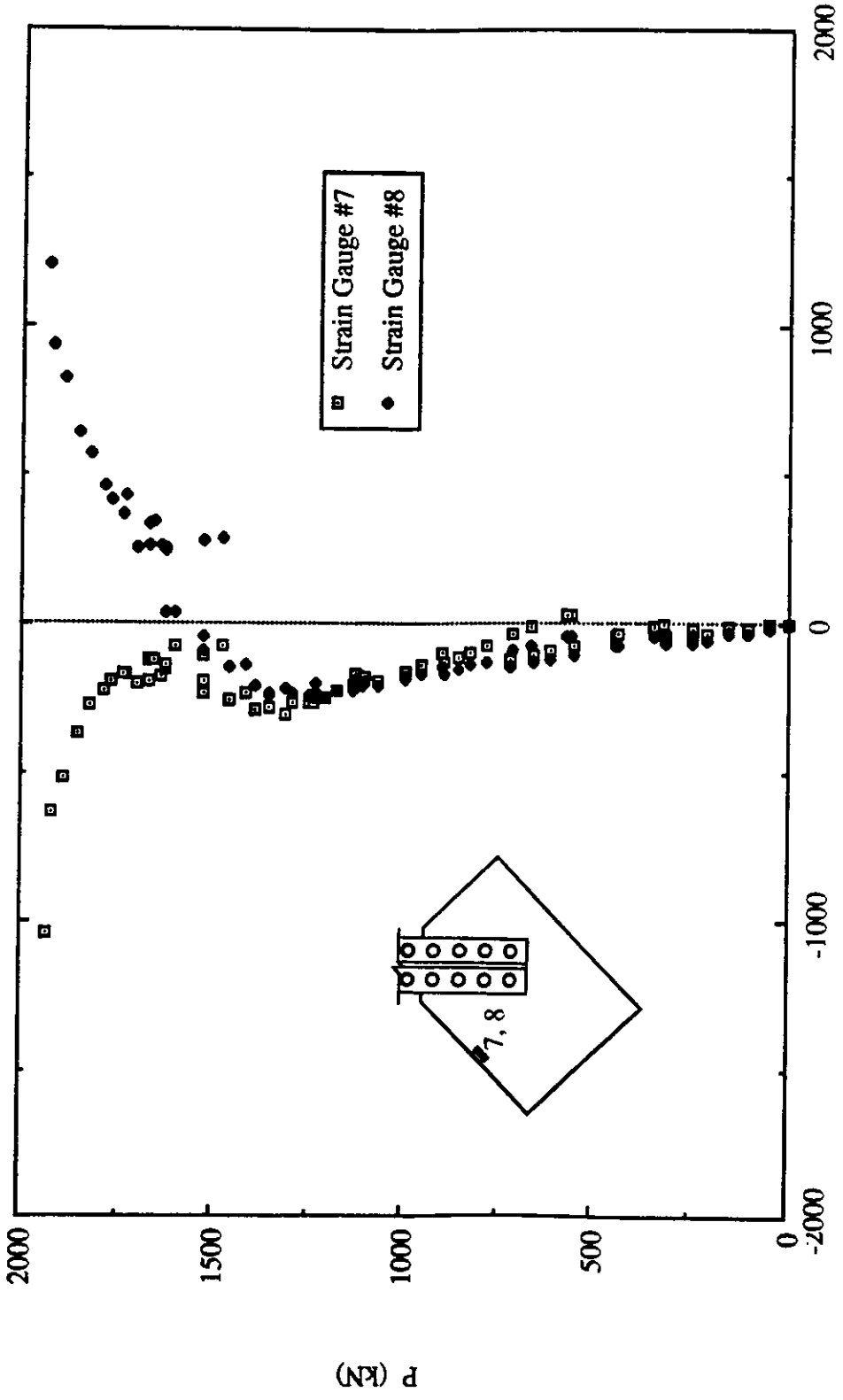

Fig. 6.16 Load vs. Strain Gauge Readings at Mid-Length of Long Free Edge for Specimen MP1

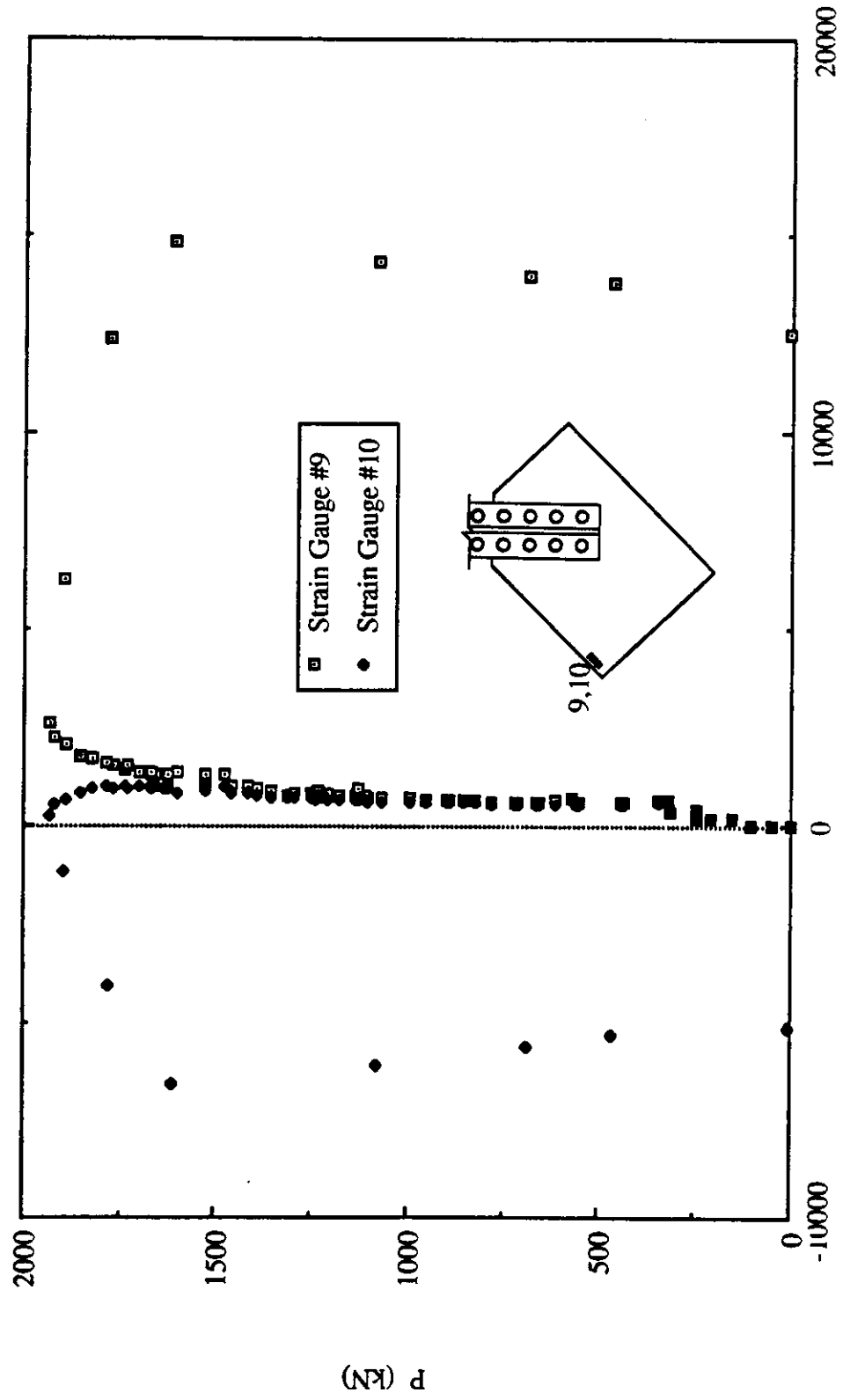

Fig. 6.17 Load vs. Strain Gauge Readings at End of Long Free Edge for Specimen MP1

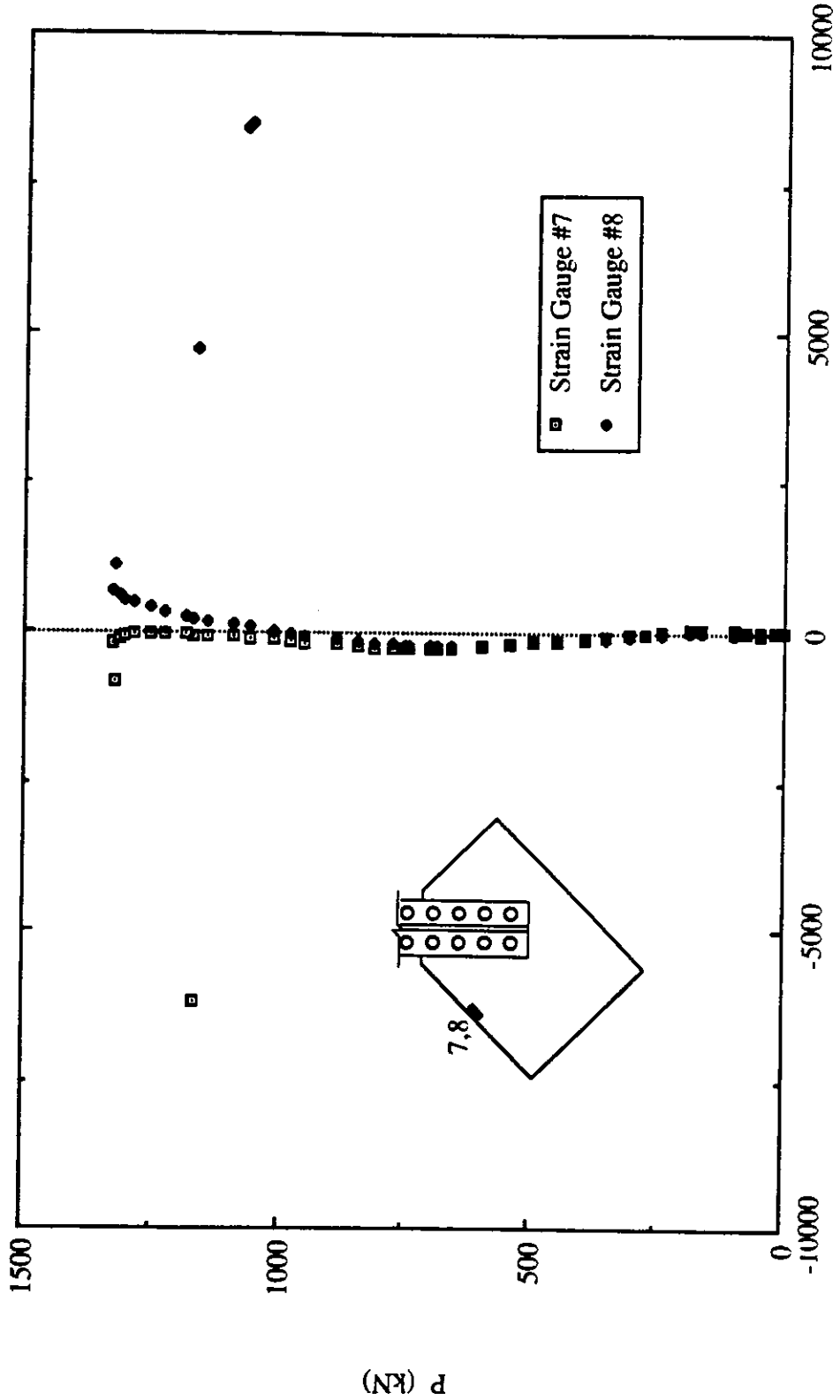

Fig. 6.18 Load vs. Strain Gauge Readings at Mid-Length of Long Free Edge for Specimen MP2

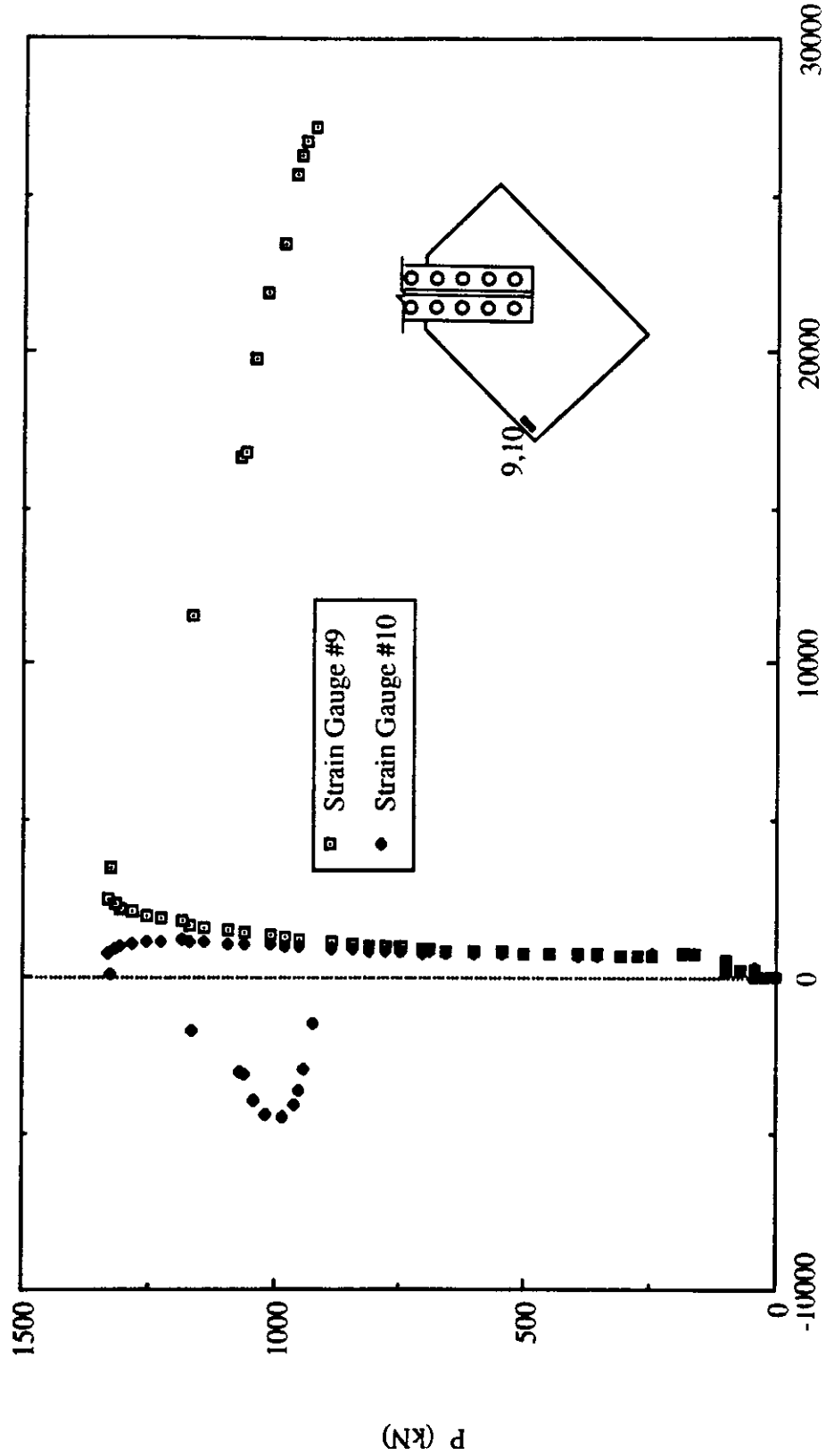

Fig. 6.19 Load vs. Strain Gauge Readings at End of Long Free Edge for Specimen MP2

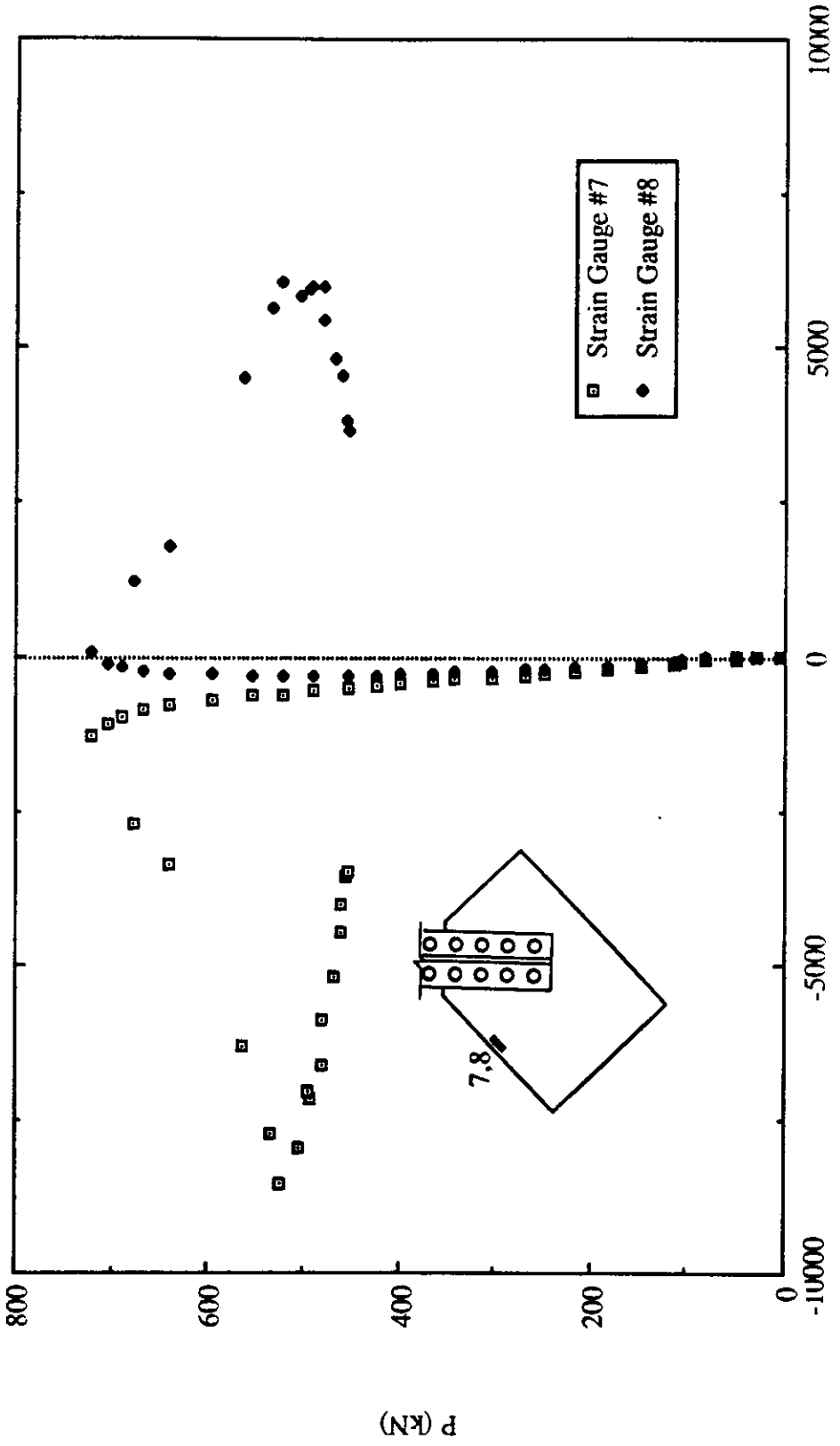

Fig. 6.20 Load vs. Strain Gauge Readings at Mid-Length of Long Free Edge for Specimen MP3

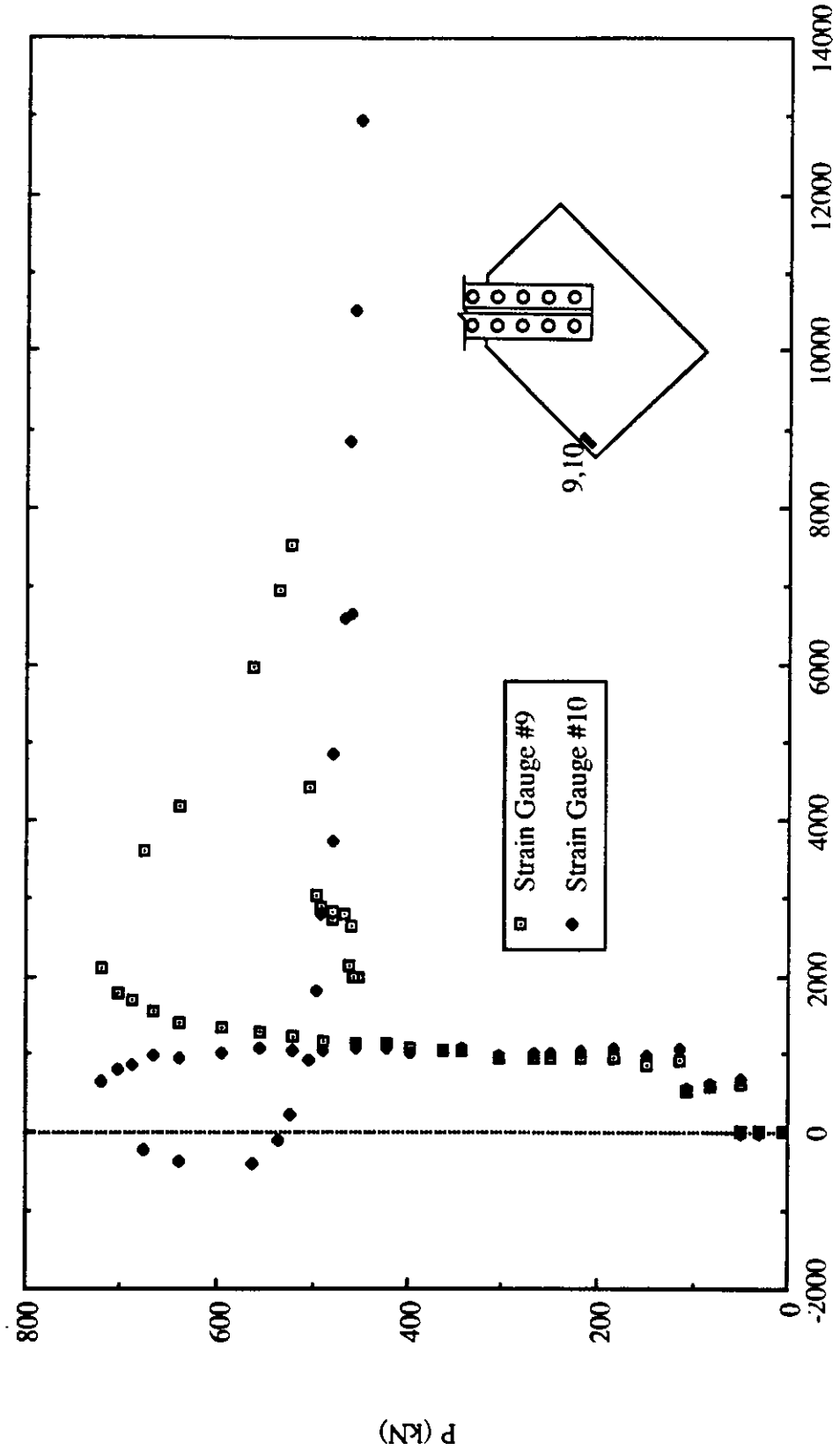

Fig. 6.21 Load vs. Strain Gauge Readings at End of Long Free Edge for Specimen MP3

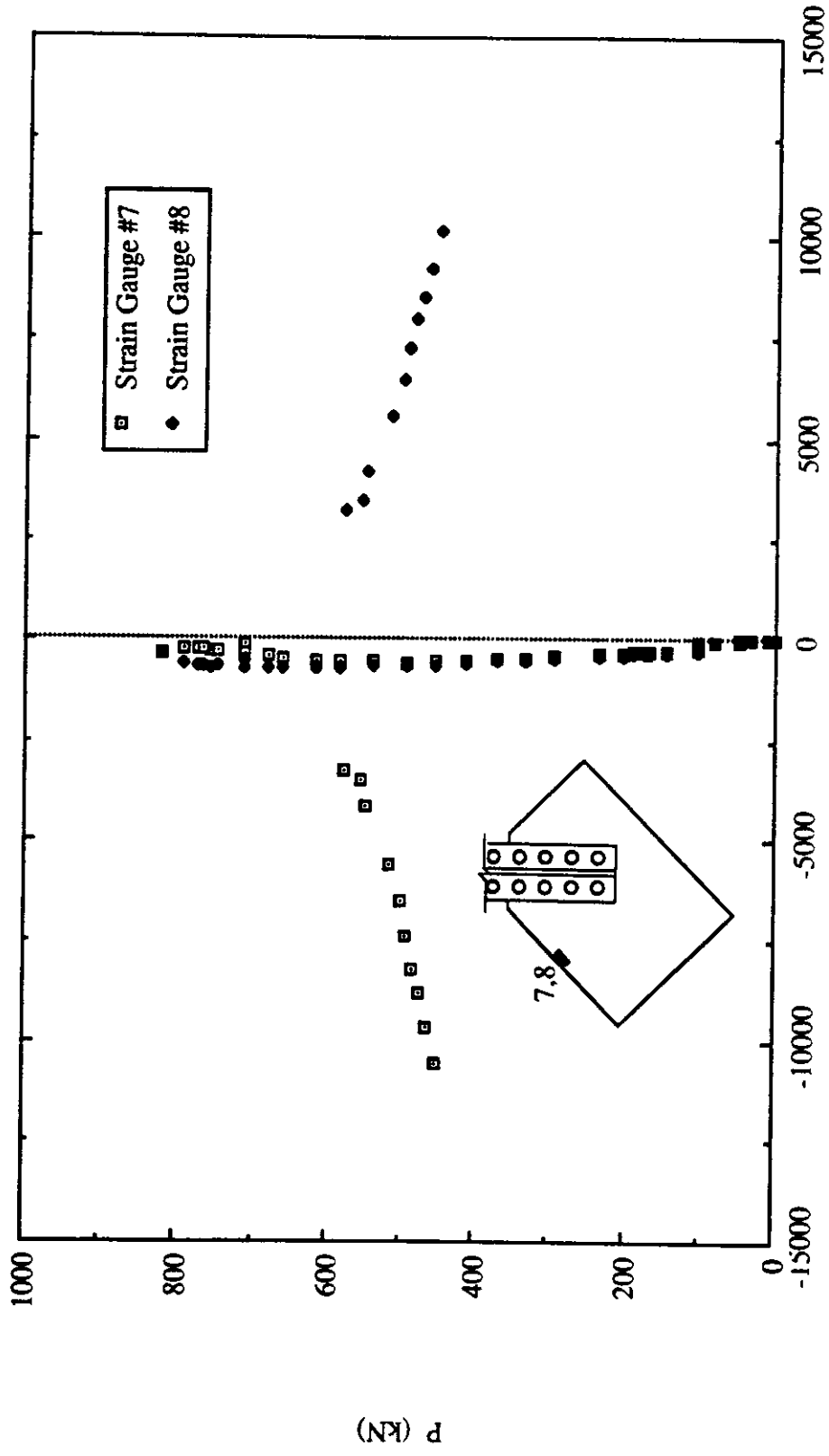

Fig. 6.22 Load vs. Strain Gauge Readings at Mid-Length of Long Free Edge for Specimen MP3A

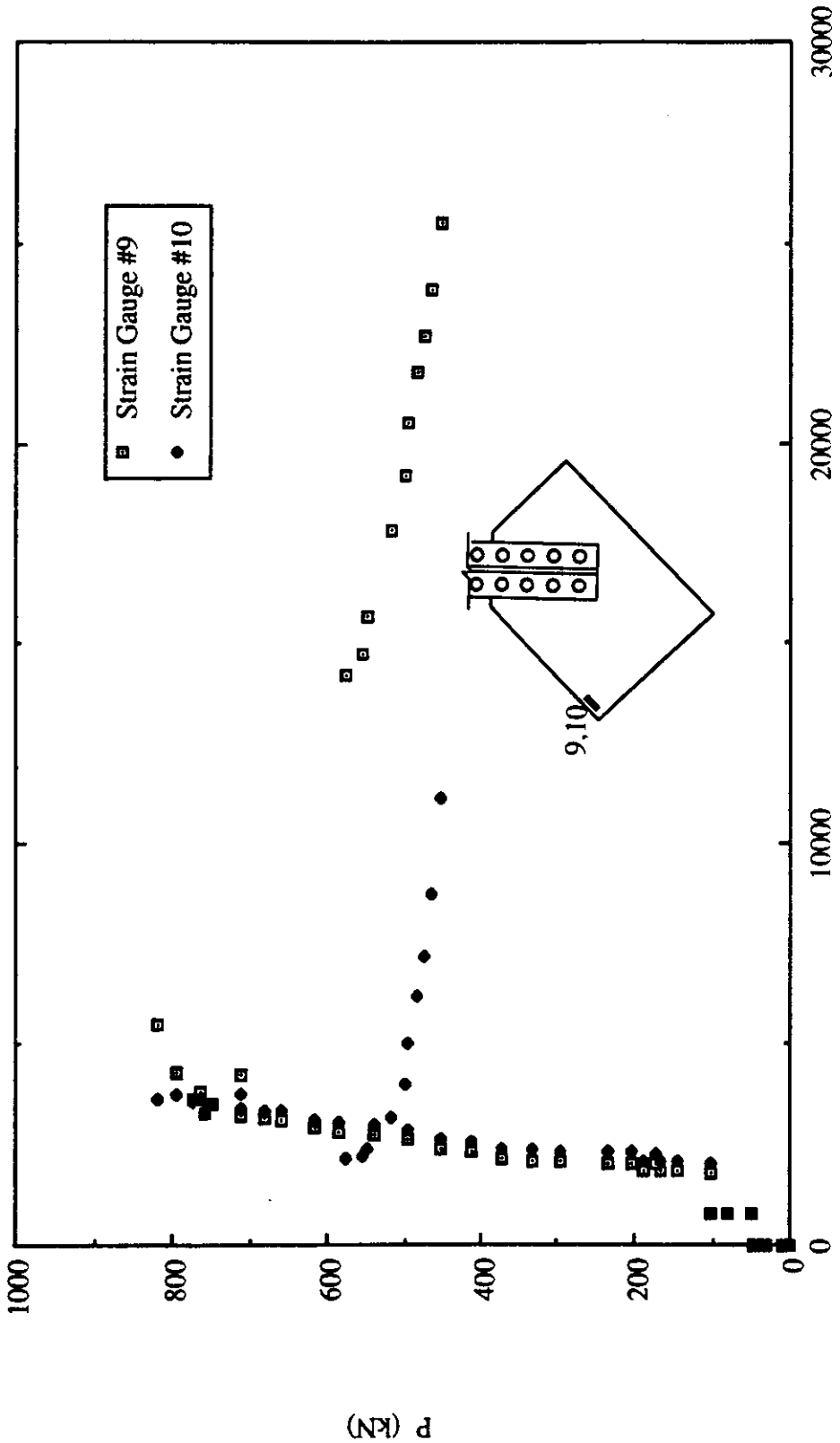

Fig. 6.23 Load vs. Strain Gauge Readings at End of Long Free Edge for Specimen MP3A

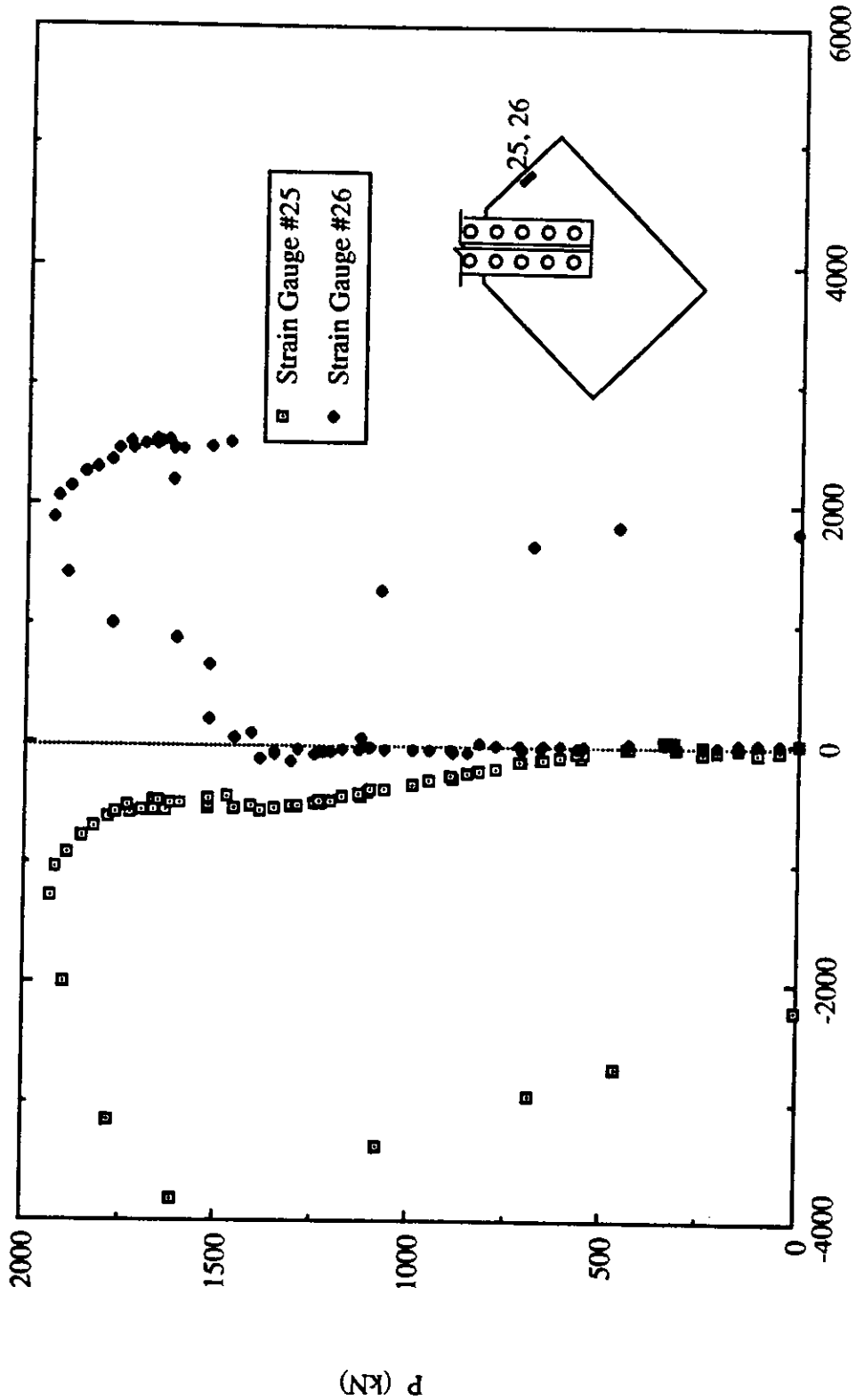

Fig. 6.24 Load vs. Strain Gauge Readings at Mid-Length of Short Free Edge for Specimen MP1

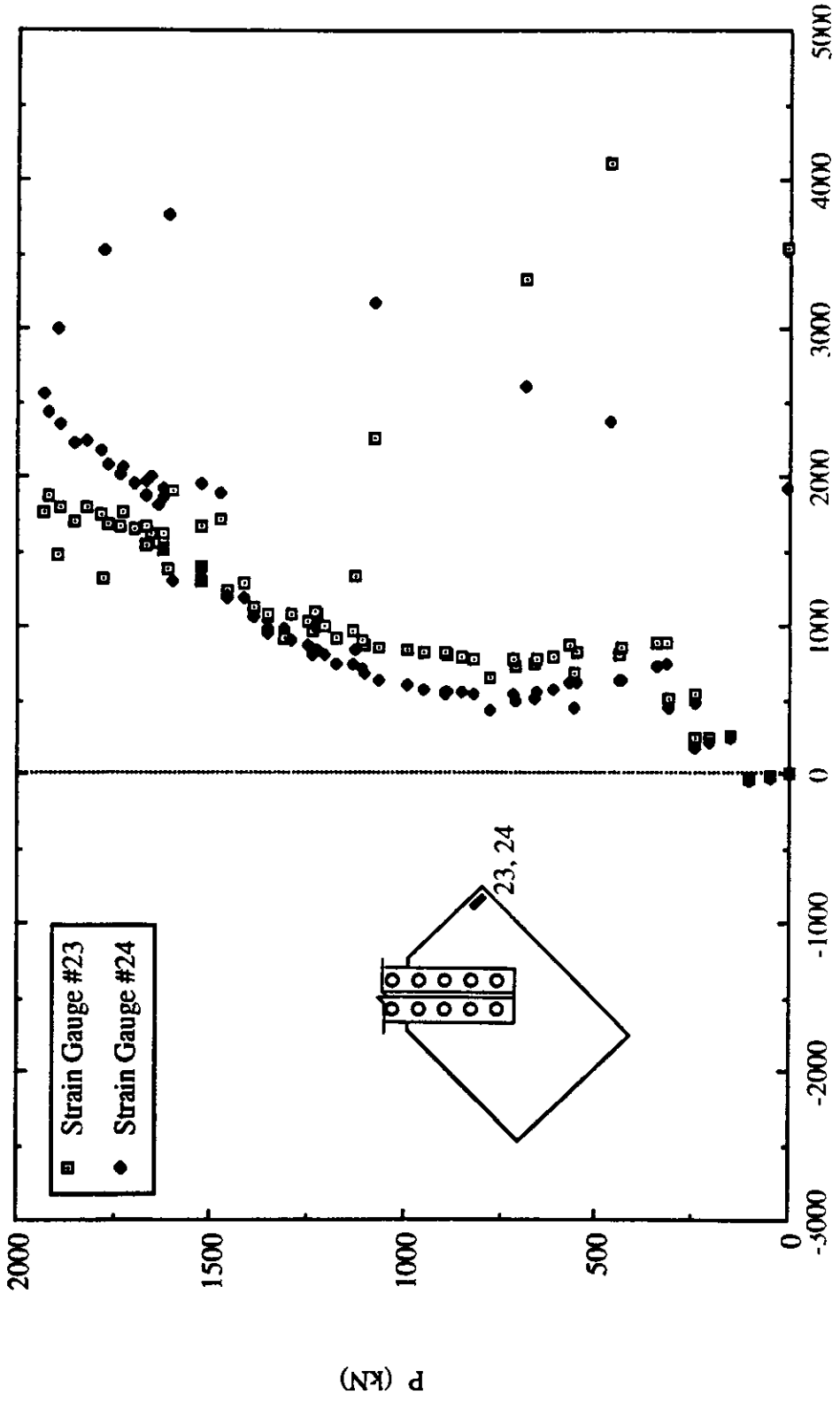

Fig. 6.25 Load vs. Strain Gauge Readings at End of Short Free Edge for Specimen MP1

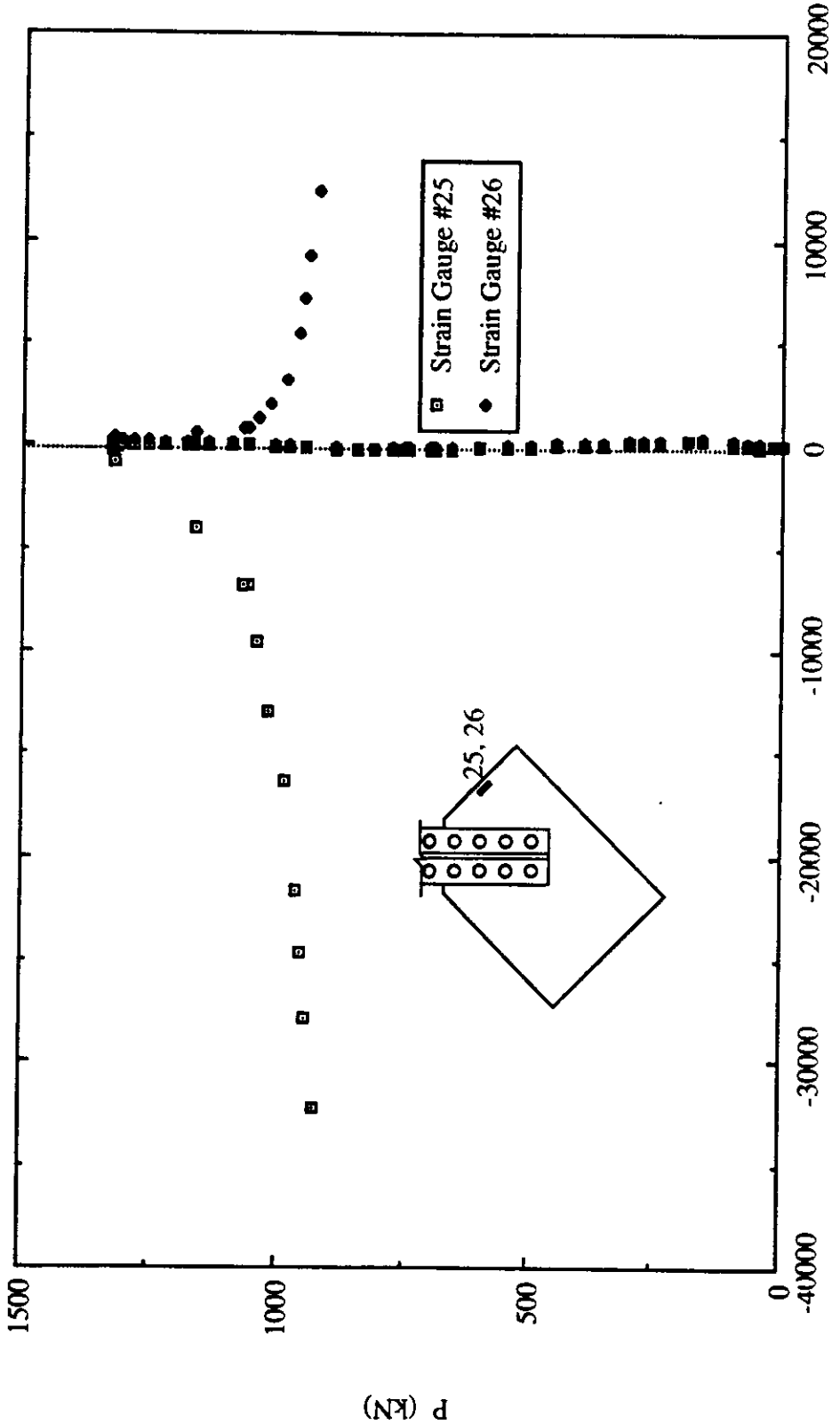

Fig. 6.26 Load vs. Strain Gauge Readings at Mid-Length of Short Free Edge for Specimen MP2

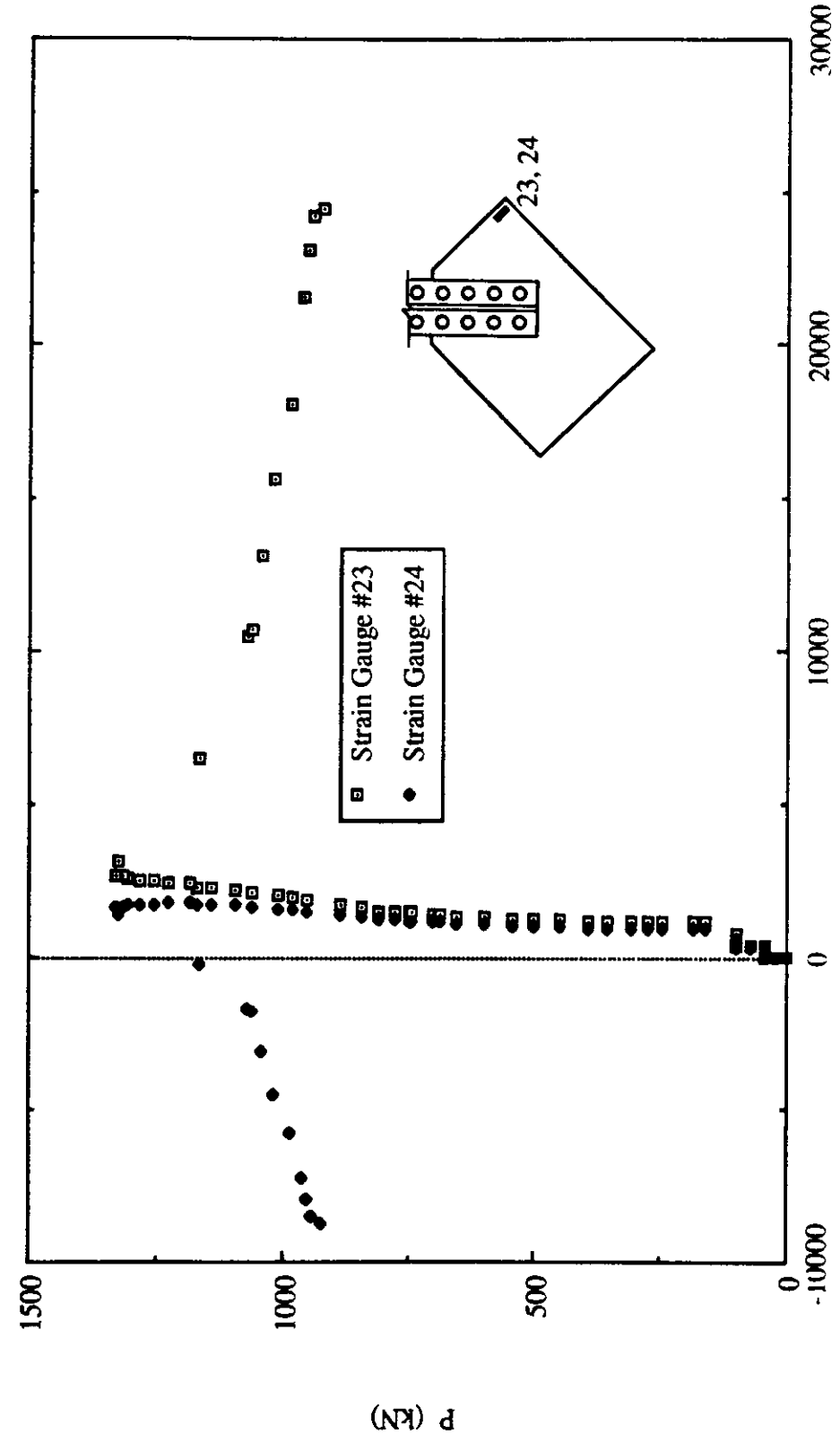

Fig. 6.27 Load vs. Strain Gauge Readings at End of Short Free Edge for Specimen MP2

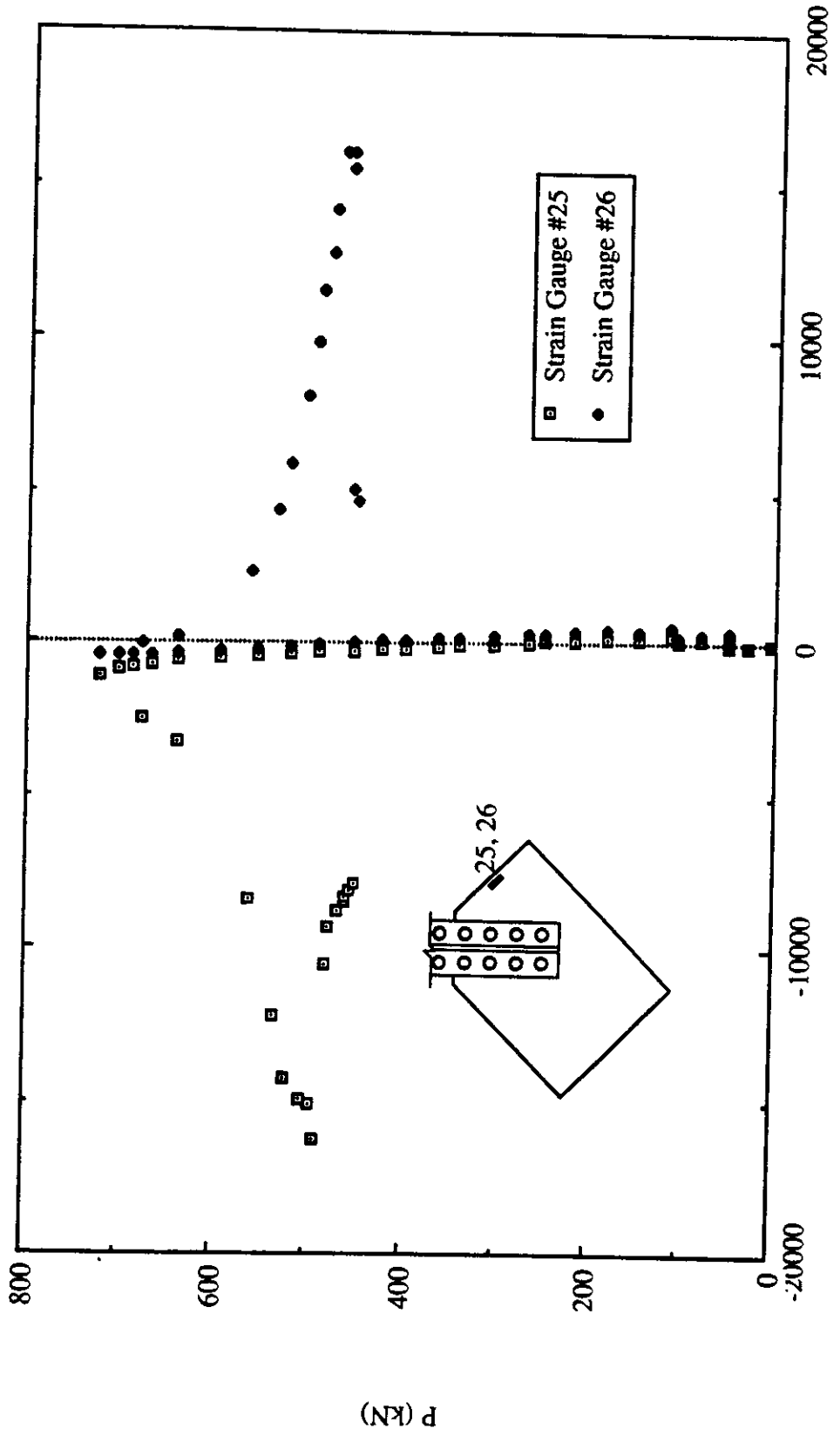

Fig. 6.28 Load vs. Strain Gauge Readings at Mid-Length of Short Free Edge for Specimen MP3

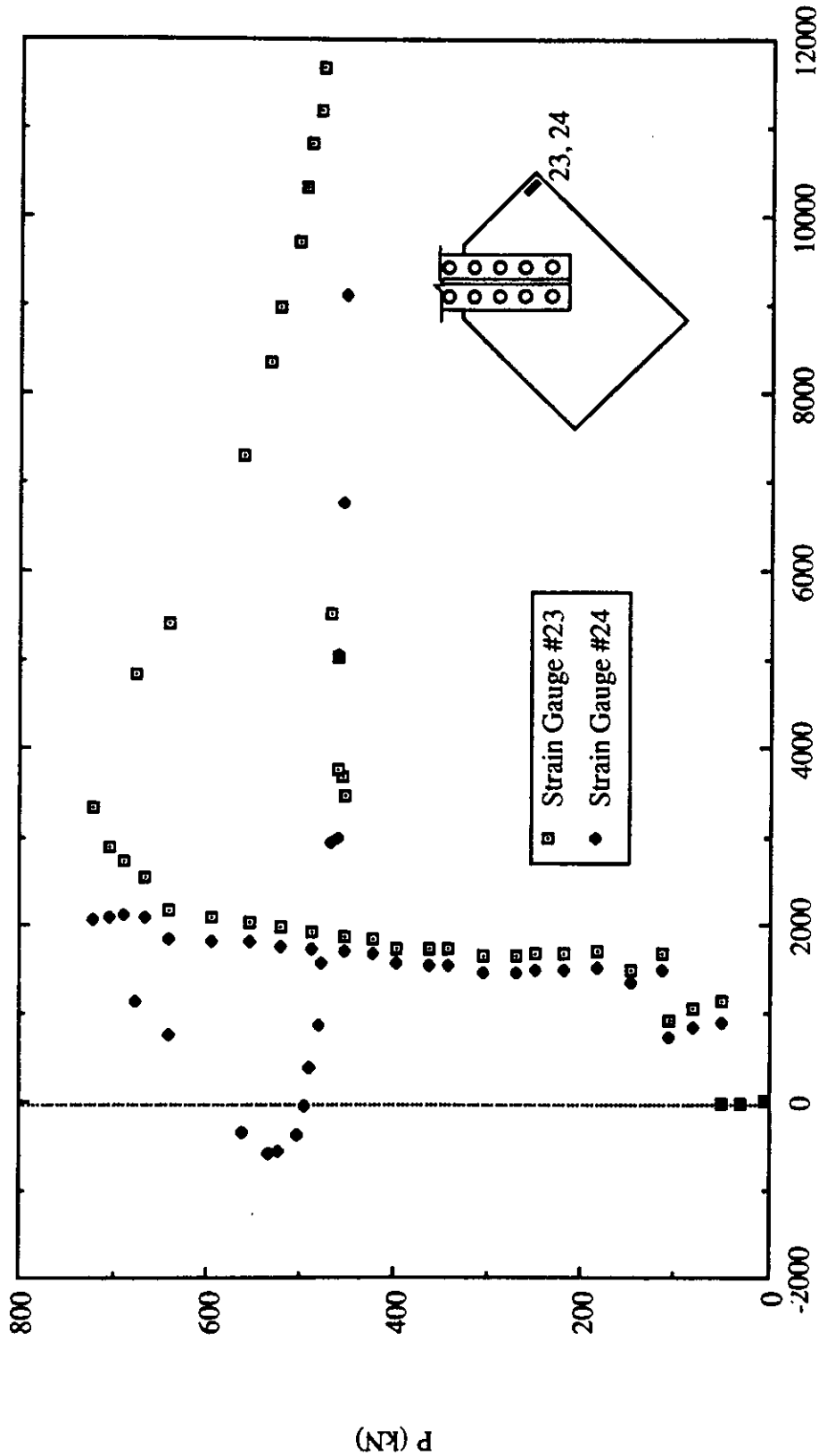

Fig. 6.29 Load vs. Strain Gauge Readings at End of Short Free Edge for Specimen MP3

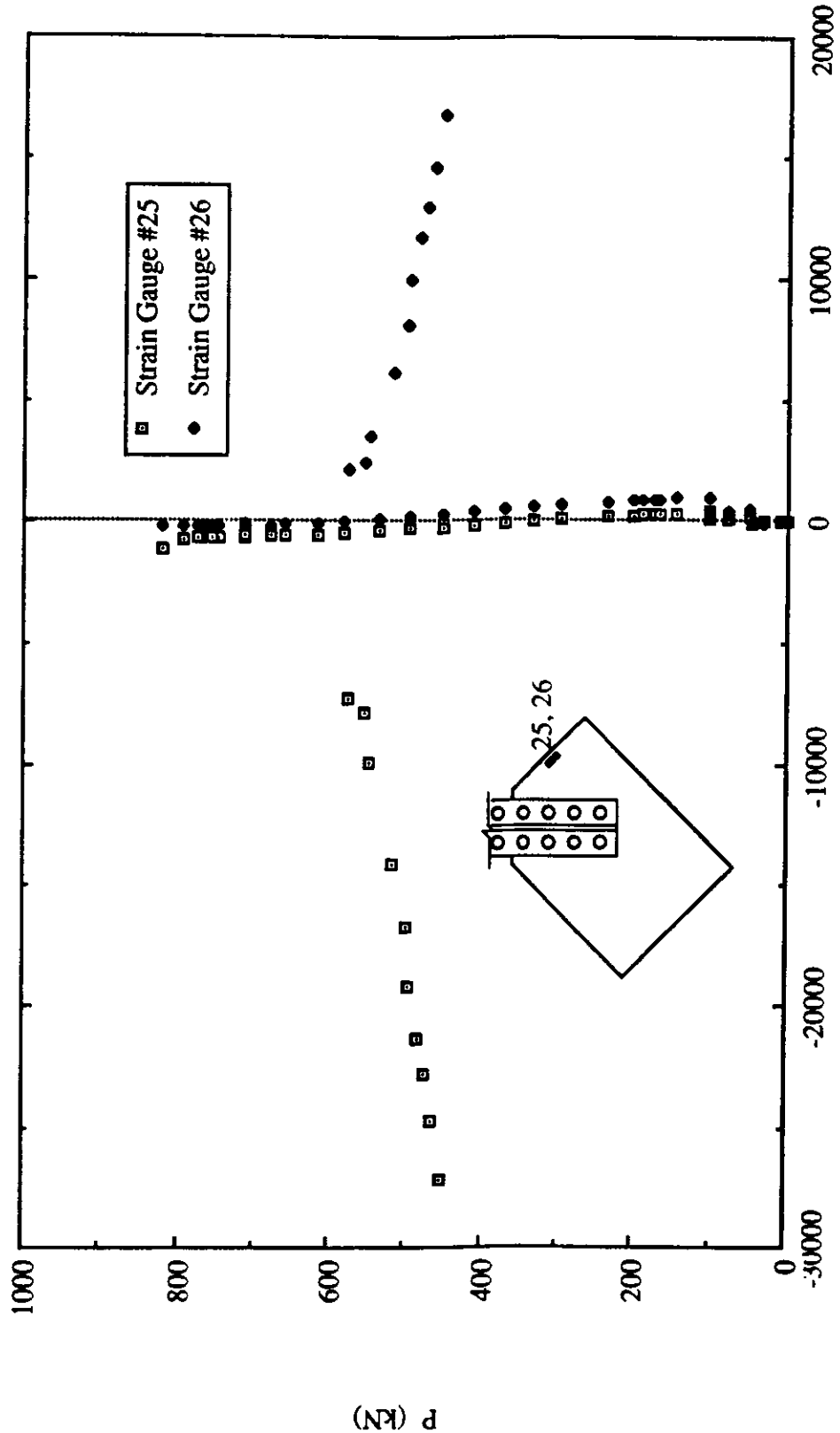

Fig. 6.30 Load vs. Strain Gauge Readings at Mid-Length of Short Free Edge for Specimen MP3A

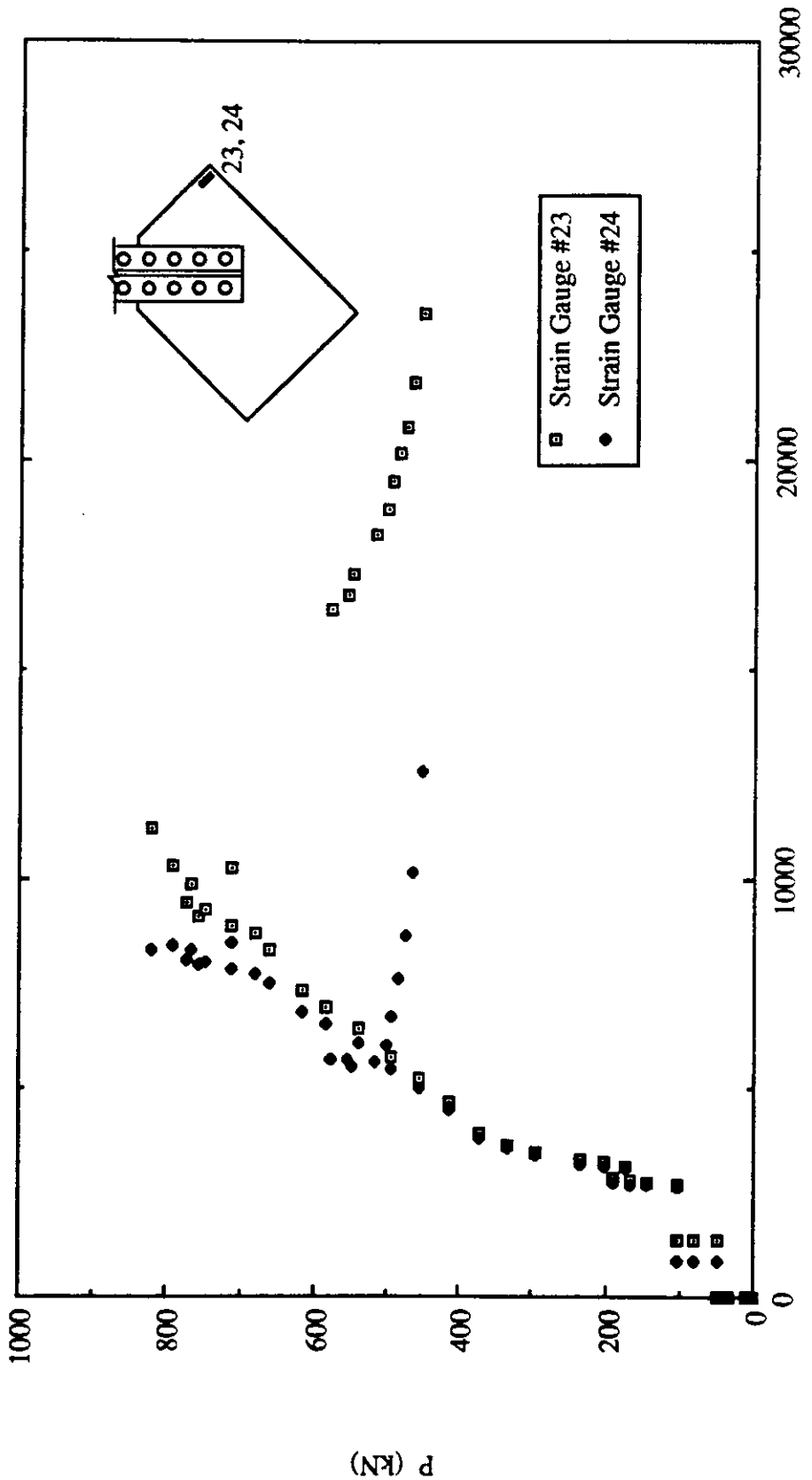

Fig. 6.31 Load vs. Strain Gauge Readings at End of Short Free Edge for Specimen MP3A

Moment Level	Beam Moment (Mb)	Column Moment (Mc)
1	80 kNm	40 kNm
2	160 kNm	80 kNm
3	250 kNm	125 kNm

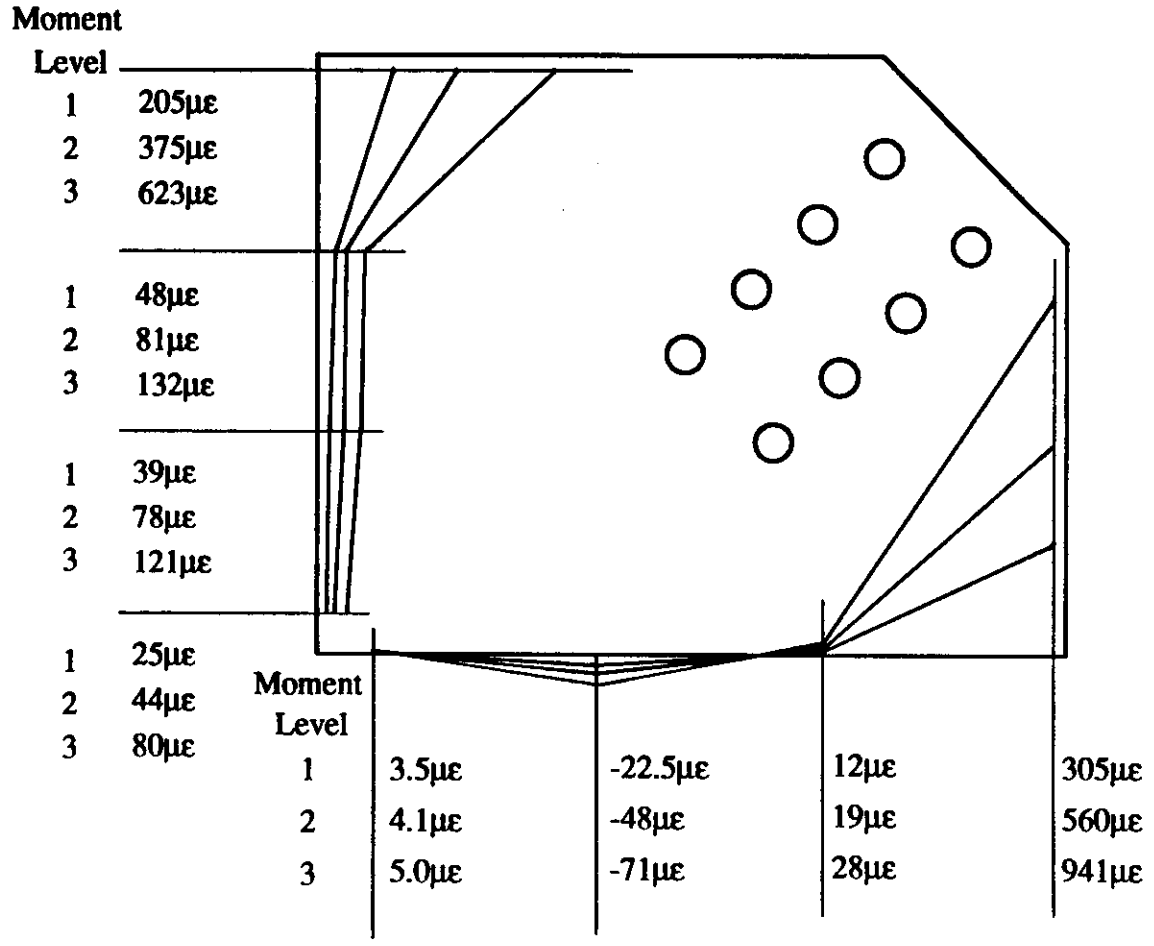

Fig. 6.32 Measured Strain Distribution Along Beam and Column Boundary at Gusset Plate for Specimen MP1

Fig. 6.33 Picture of Failed Specimen MP1

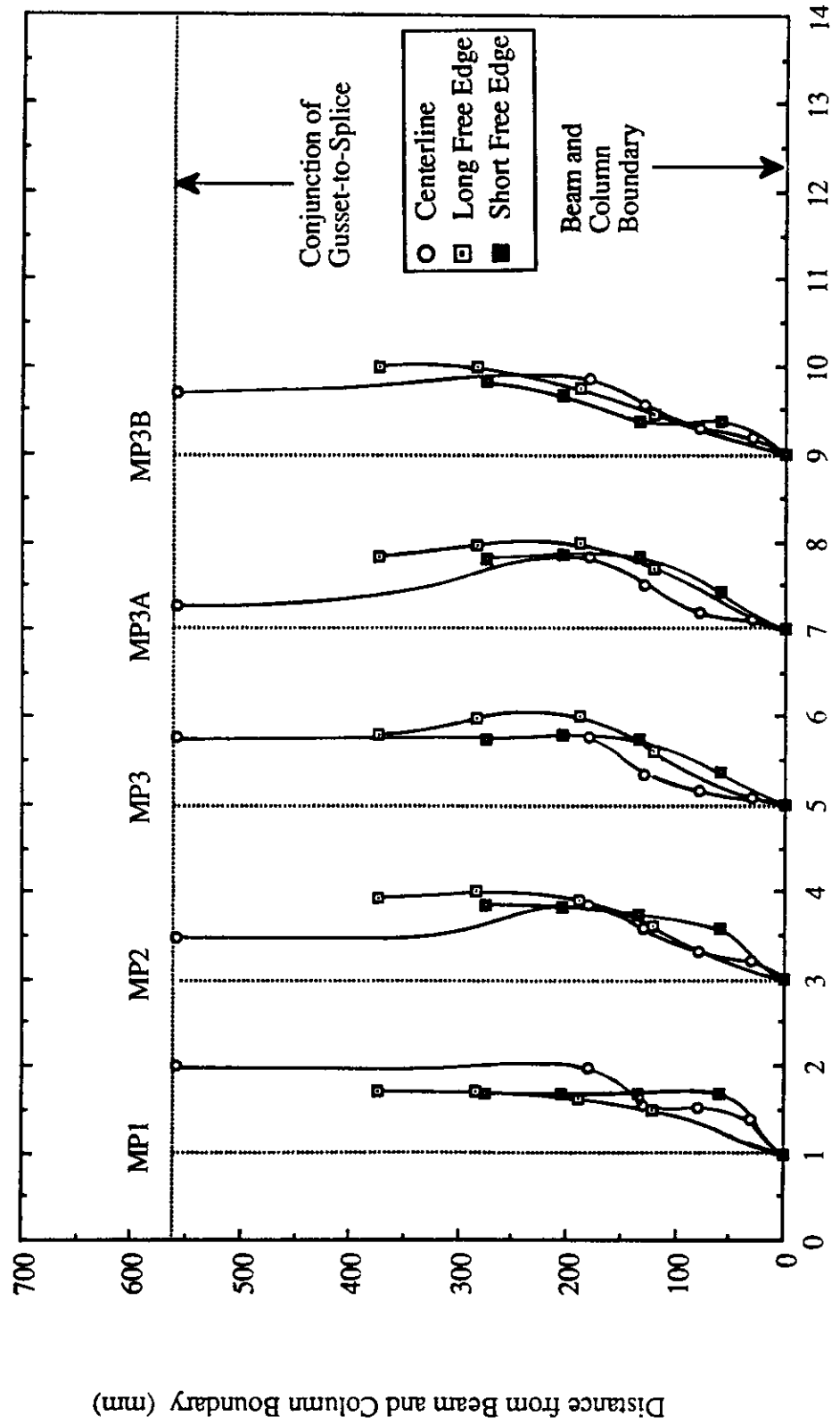

Fig. 6.34 Out-of-Plane Deflected Shapes at Free Edge and Along Centerline of Splice for MP Type Specimens

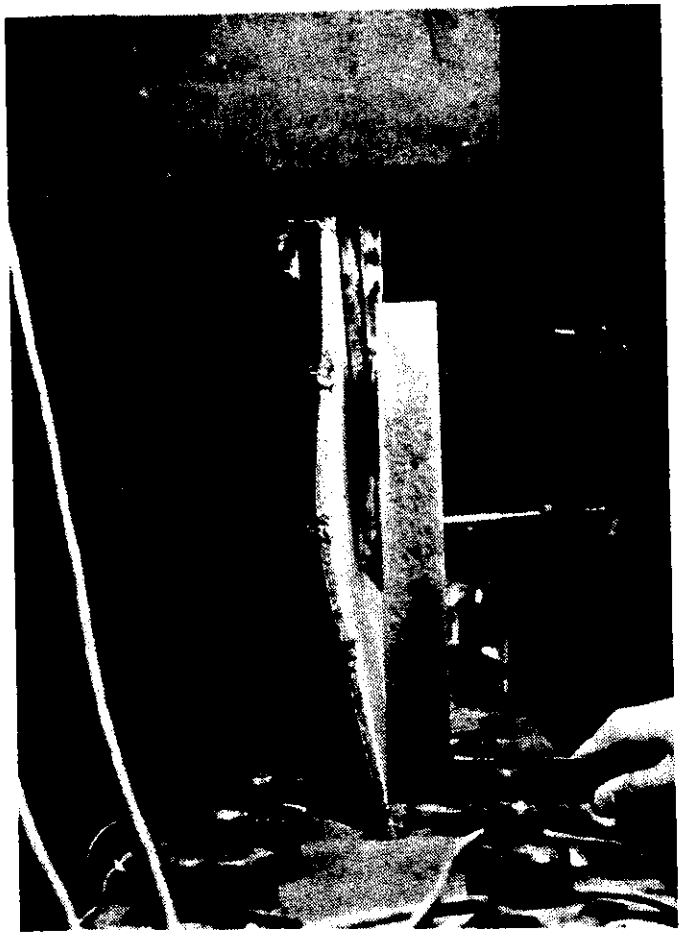

a) Long Free Edge

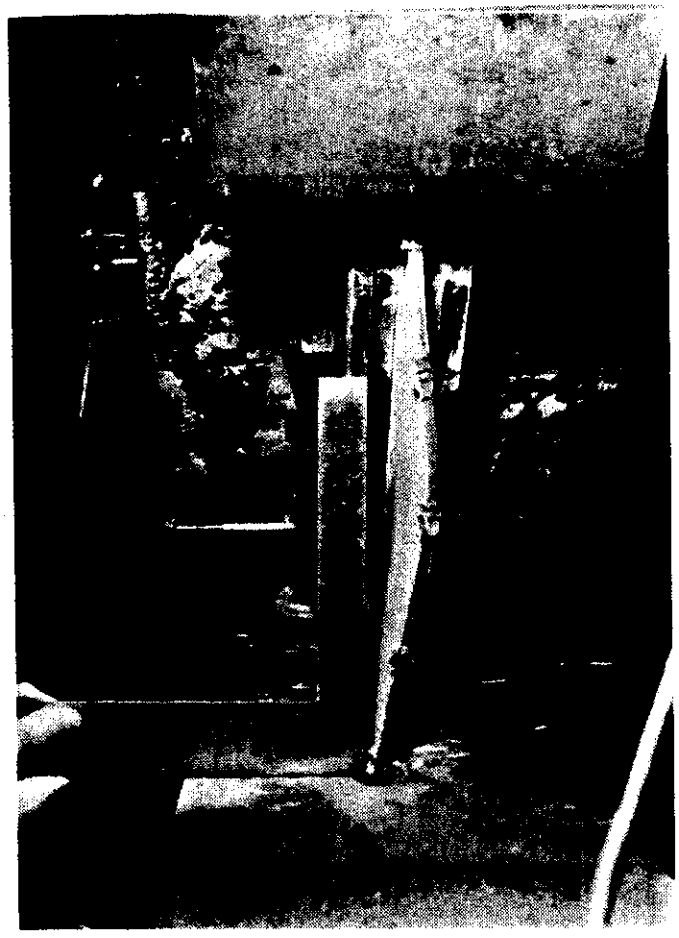

b) Short Free Edge

Fig. 6.35 Pictures of Out-of-Plane Deflected Shapes at Free Edges for Specimen MP3A

7. TEST RESULTS OF EP TYPE SPECIMENS

7.1 General

The EP type specimens were employed to study the compressive behavior of eccentrically loaded gusset plate connection. As mention in Chapter 2 that only one gusset plate thickness of 13.3 mm was used to conduct the tests. Three splice member sections were used to test the specimen as shown in Table 2.2. As a reminder, scheme I test setup was used to perform the tests. In general, specimens failed by significant yielding in splice section at the conjunction of gusset-to-splice. However, yielding in the gusset plate was also observed depending on the specimens. In particular, extensive yielding was observed underneath the splice member close to the corner of the beam and column boundary for specimen EP3 as shown in Fig. 7.1. The figure also shows that yield line mechanism was formed in specimen EP3. This mechanism originated from the end of splice member close to the beam boundary and extended towards the ends of the free edges. For specimens EP1 and EP2, yield lines were also recorded near the beam boundary close to the short side free edge. The test results of the specimens are summarized in Table 7.1.

7.2 Behavior of Load Versus In-Plane Deformation

The in-plane behavior of the specimens can be illustrated by examining the curves of load versus vertical stroke of loading head as shown in Figs. 7.2 to 7.4. In general, the specimens exhibited linear load deflection behavior until about 60 percent of the corresponding ultimate loads. Similar in-plane stiffness was observed for both specimens EP1 and EP2. However, for specimen EP3 a higher in-plane stiffness was observed. Subsequently, the curves showed nonlinear behavior and gradually turned to the ultimate loads. It can be seen from the figures that specimen EP1 showed more rapid unloading than specimens EP2 and EP3 as shown in the figures.

7.3 Behavior of Load Versus Out-Of-Plane Displacement of Test Frame

The curves of load versus out-of-plane displacement of the test frame for the specimens are shown in Figs. 7.5 to 7.7. The curve for specimen EP1 shows a typical load deflection curve for a beam column member. That is, linear behavior was observed in the initial loading stage and subsequently, the curve gradually turned to the ultimate load followed by rapid unloading. For specimens EP2 and EP3, however, the curves show a more gradual unloading path. It was also observed that specimens EP1 and EP2 reached the corresponding ultimate load at a deflection of about 20 mm. However, for specimen EP3 the ultimate load was attained at a deflection of about 10 mm which illustrated the effects of stiffening the eccentrically loaded gusset plate. It was also observed that the out-of-plane stiffness of the specimen was greatly improved by providing a stiffer splice member.

7.4 Strain Gauges Results

Since the primary failure mode of the specimens was yielding in the splice member at the conjunction of gusset-to-splice, therefore, it is important to examine the strain distribution at that conjunction and also in the gusset plate. The strain distribution and yielding pattern of each specimen will be presented individually. For specimen EP1, which employed a 9.5 mm thick splice plate, the curves of load versus strain gauges readings recorded at the conjunction of gusset-to-splice and at the splice plate 50mm above the end of bracing are shown in Figs. 7.8 and 7.9, respectively. As can be seen from the figures, bending behavior was observed from the beginning of loading due to the loading eccentricity. Yielding was first observed at gauges #19 and 20 at an applied load of about 205 kN. However, no yield line was observed from the splice member. At load level of about 275 kN, yielding was observed at strain gauge #24 as shown in Fig. 7.9 and slight flaking of the whitewash at the south side of the conjunction was found. This yielding was mainly located in splice member around the last row of bolts from the bracing member as shown schematically in Fig. 7.10. As loading continued, the yielding progressed and yield lines

were also observed at the north side of the splice plate around the first row of bolts from the gusset plate specimen. Yielding on the gusset plate specimen was only recorded at the strain gauges near the end of the splice member when the applied load was close to the ultimate load. However, yielding was observed near the beam and column boundary in the north side of the specimen as shown in Fig. 7.11. These yield lines originated from the end of the splice plate and were caused by significant bending of the gusset plate specimen. The failed splice plate for specimen EP1 is shown in Fig. 7.12. It can be seen that significant bending of splice plate was observed at the conjunction with the formation of plastic hinges near end rows of bolts, however, the ends of the splice remained quite straight. This indicated that the gusset plate and the bracing member provided relatively stiff support to the splice plate and allowed the development of plastic hinges.

For specimen EP2, which used a 13 mm thick splice plate, yielding at strain gauges was again recorded at the conjunction of gusset-to-splice at an applied load of 220 kN. The plots of strain gauges #19 and 20, which were located at the conjunction, is shown in Fig. 7.13. Figure 7.14 illustrates the curve for the strain gauge #24. Again, bending behavior was observed from the beginning of loading. At a load level of 265 kN, flaking of whitewash was observed at the south side of the conjunction. As loading continued, yielding at this region increased. When the applied reached about 334 kN yield lines were found on the gusset plate right underneath the splice plate. As out-of-plane displacement increased in the unloading stage, yielding near the beam and column boundary was observed. The failed splice plate for specimen EP2 is shown in Fig. 7.12. It can be seen from the figure that only minor bending was observed at the conjunction.

For specimen EP3, yield lines were first observed at the gusset plate in the vicinity of the corner of beam and column boundary at an applied load of about 550 kN. At this loading stage, strain gauges on the splice plate located at the conjunction of gusset-to-splice also showed yielding, however, no yield lines were detected. A plot of load versus strain

readings recorded at the web of the tee-section and on the south side of the splice plate at the conjunction is shown in Fig. 7.15. As expected, the strain reading from the web of the tee showed tension yielding while compression yielding was observed for the strain gauge at the splice plate. The strain distribution recorded at an applied load of 400 kN across the depth of tee-section and the splice plate at the conjunction is shown in Fig. 7.16. This plot shows that linear strain distribution existed across the depth of the tee-section. However, the location of the neutral axis was shifted away from the flange of the tee-section due to the compressive strain induced by the applied load. As loading continued, yielding in the vicinity of the corner of beam and column boundary progressed. When the applied load approached the ultimate load, yielding of the splice plate at the conjunction was detected and plastic hinges similar to that of specimen EP2 were observed.

7.5 Out-of-Plane Deflected Shapes of Free Edges and Along Centerline of Bracing Member

The normalized out-of-plane deflected shapes for the EP type specimens are shown in Fig. 7.17. It can be seen that similar deformed configuration was observed for the specimens. In addition, plastic hinges formed at the fixed ends of the free edges allowed rotations at the ends as shown in the figure. The figure also shows that maximum displacement occurred at about mid-height of the splice member length. The deformed shapes for specimen EP3 along the centerline of the splice indicated that the tee-section splice member provided significant out-of-plane stiffness to the connection. Slight local bending of the gusset plate underneath the splice member was observed for specimen EP3.

Table 7.1 Test Results of EP Type Specimens

Specimen Designation	Gusset Plate Size (mm x mm x mm)	Splice Member	Ultimate Load (kN)	Failure Mode
EP1	500 x 400 x 13.3	9.5 mm Splice Plate	310	Mechanism formed at Splice Plate
EP2	500 x 400 x 13.3	13.0 mm Splice Plate	334	Yielding at Conjunction
EP3	500 x 400 x 13.3	WT 125 x 22.5 + 9.5 mm Splice Plate	890	Yielding at Conjunction

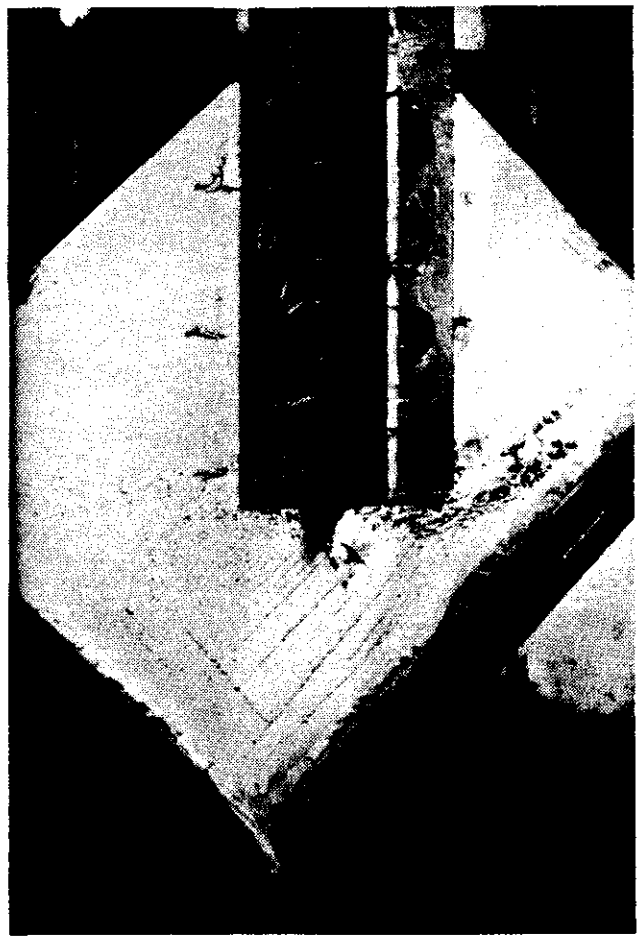

Fig. 7.1 Picture of Failed Specimen EP3

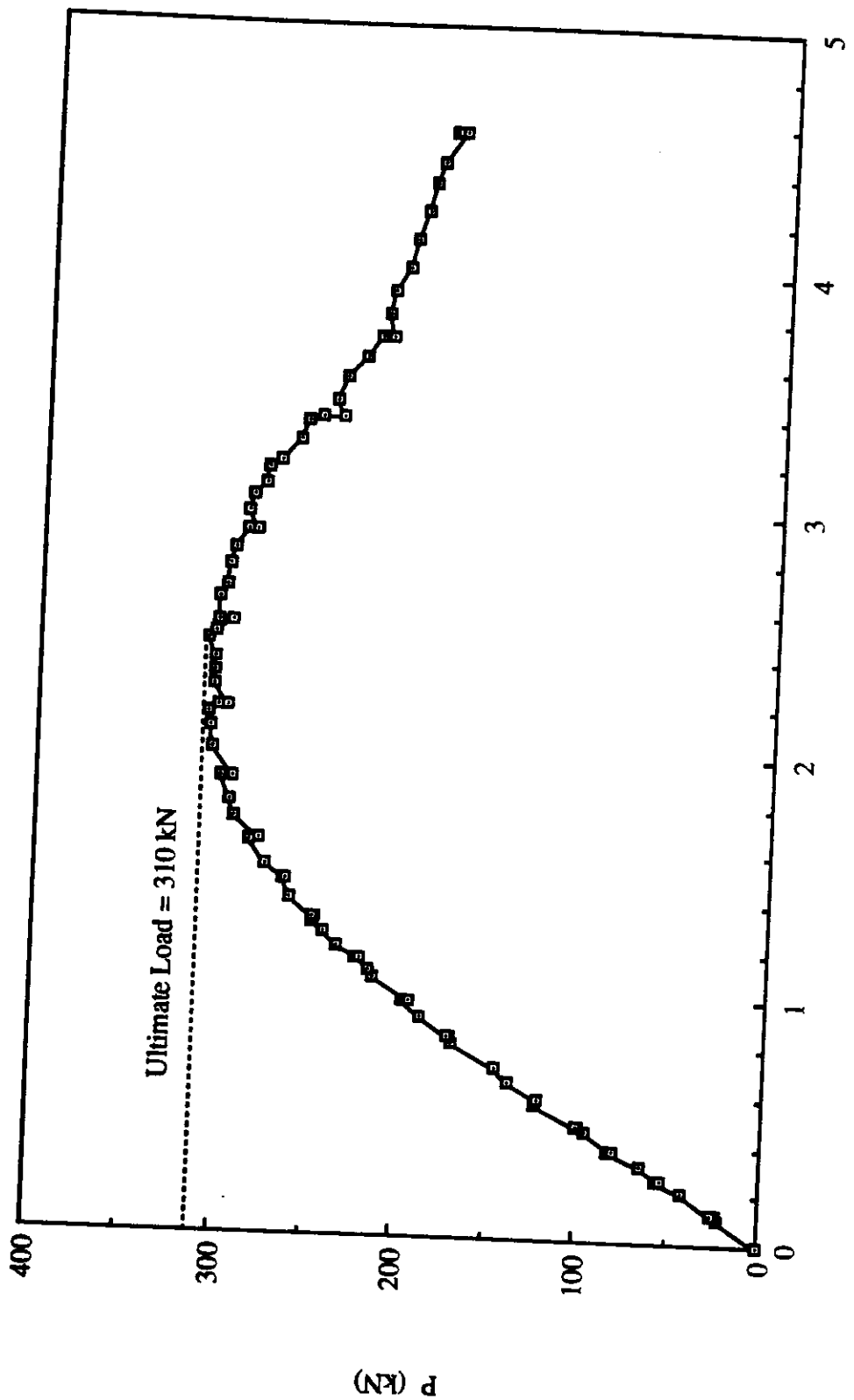

Fig. 7.2 Load vs. Vertical Stroke of Loading Head for Specimen EP1

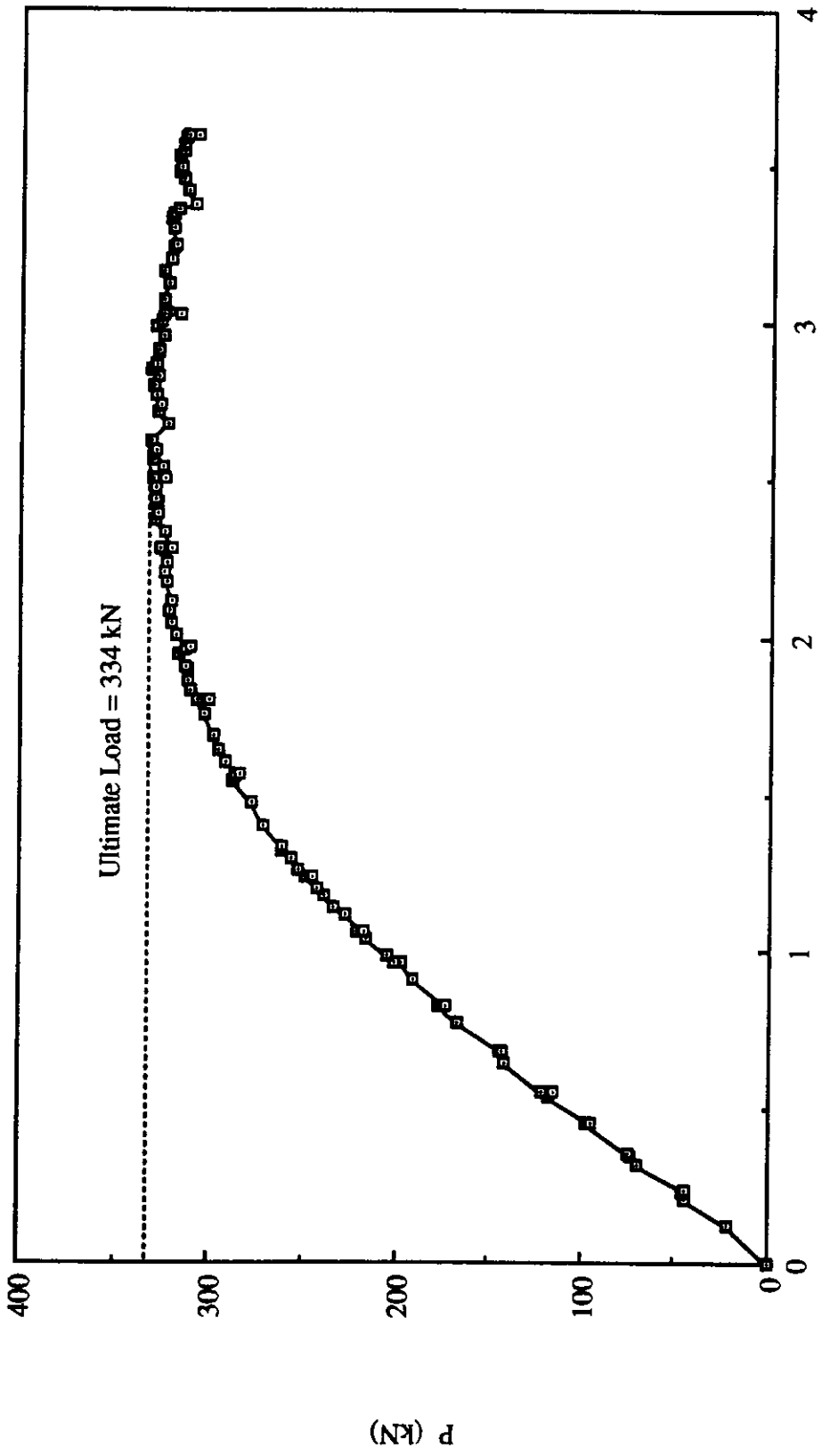

Fig. 7.3 Load vs. Vertical Stroke of Loading Head for Specimen EP2

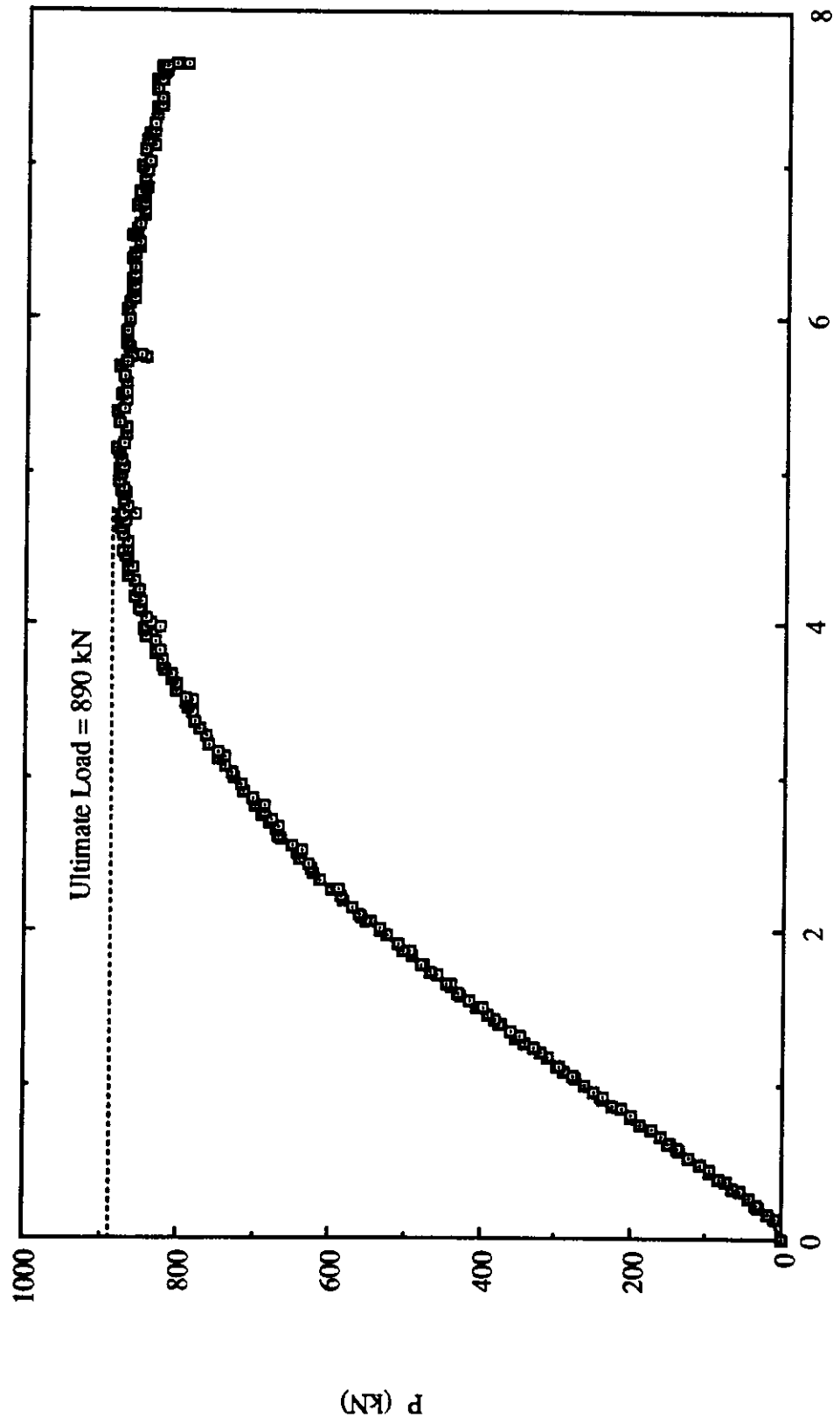

Fig. 7.4 Load vs. Vertical Stroke of Loading Head for Specimen EP3

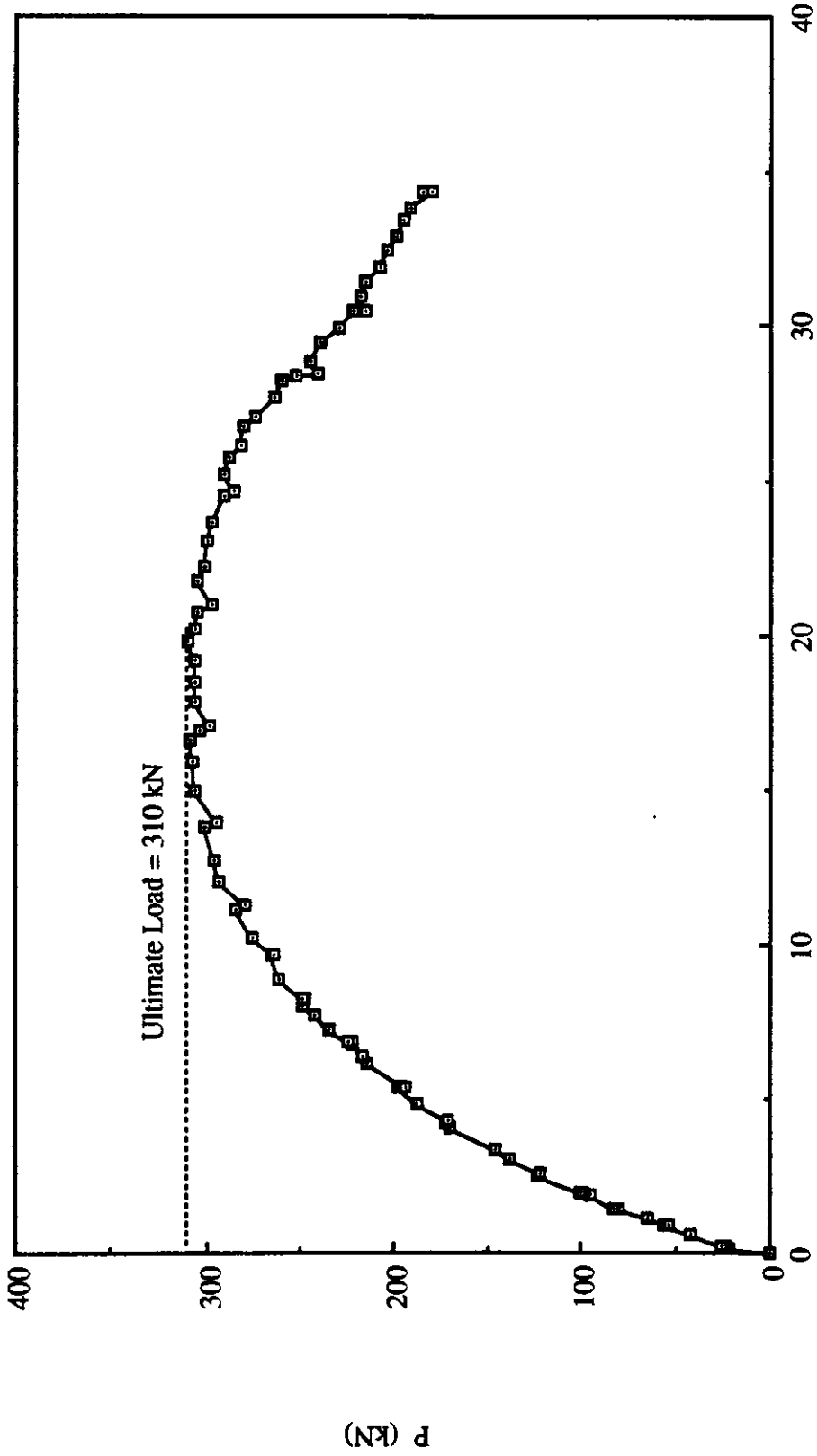

Fig. 7.5 Load vs. Out-of-Plane Displacement of Test Frame for Specimen EP1

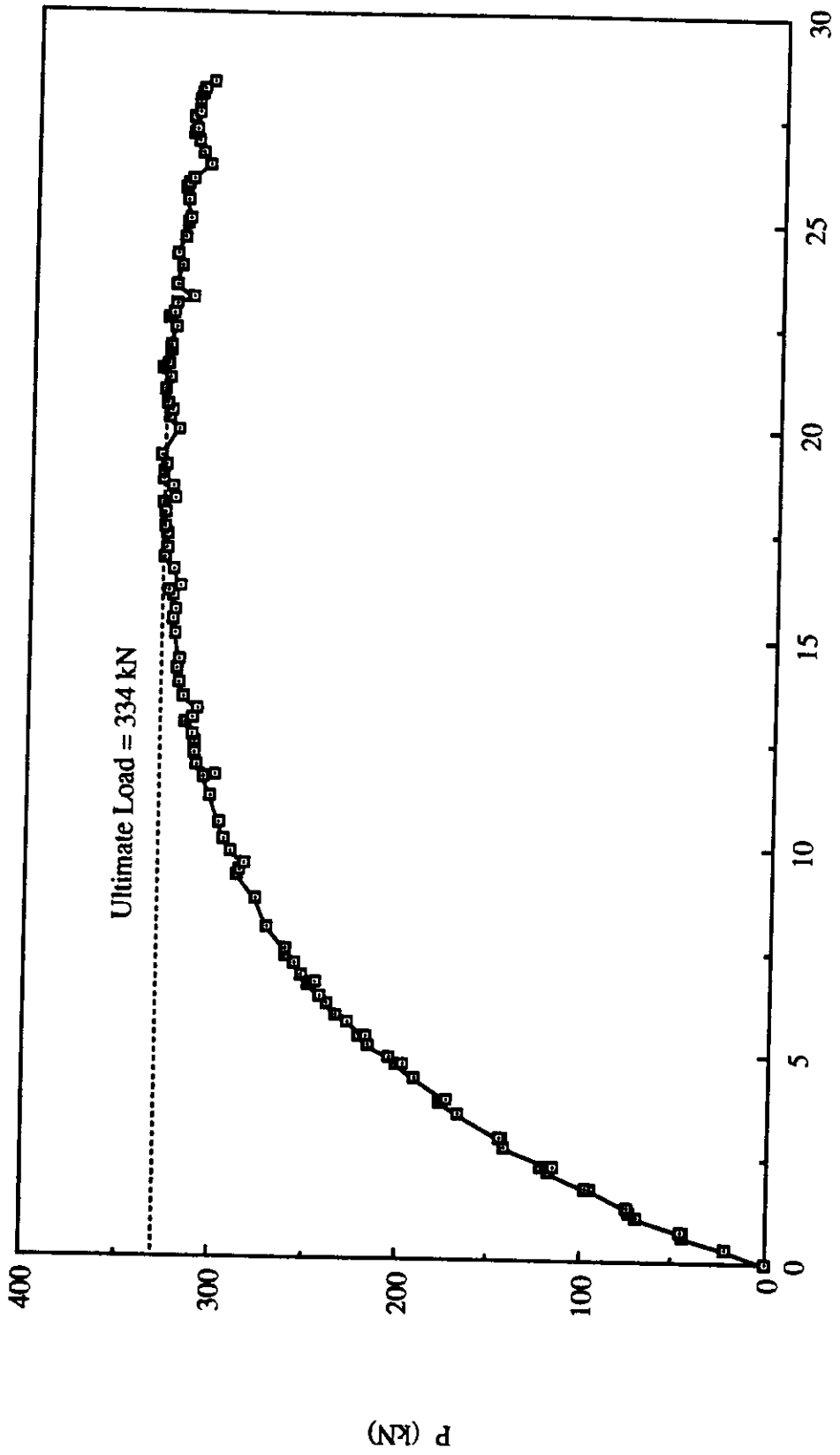

Fig. 7.6 Load vs. Out-of-Plane Displacement of Test Frame for Specimen EP2

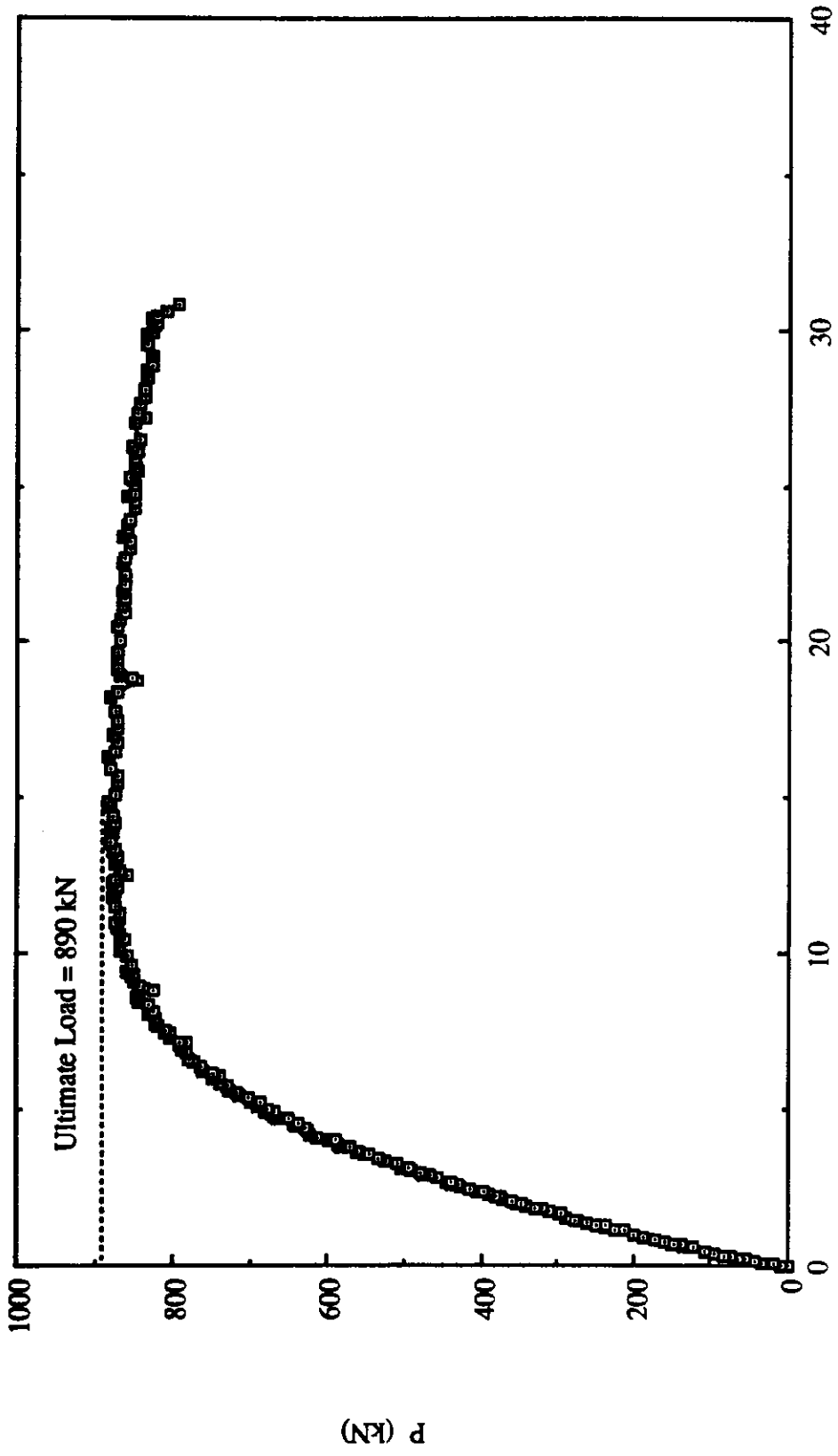

Fig. 7.7 Load vs. Out-of-Plane Displacement of Test Frame for Specimen EP3

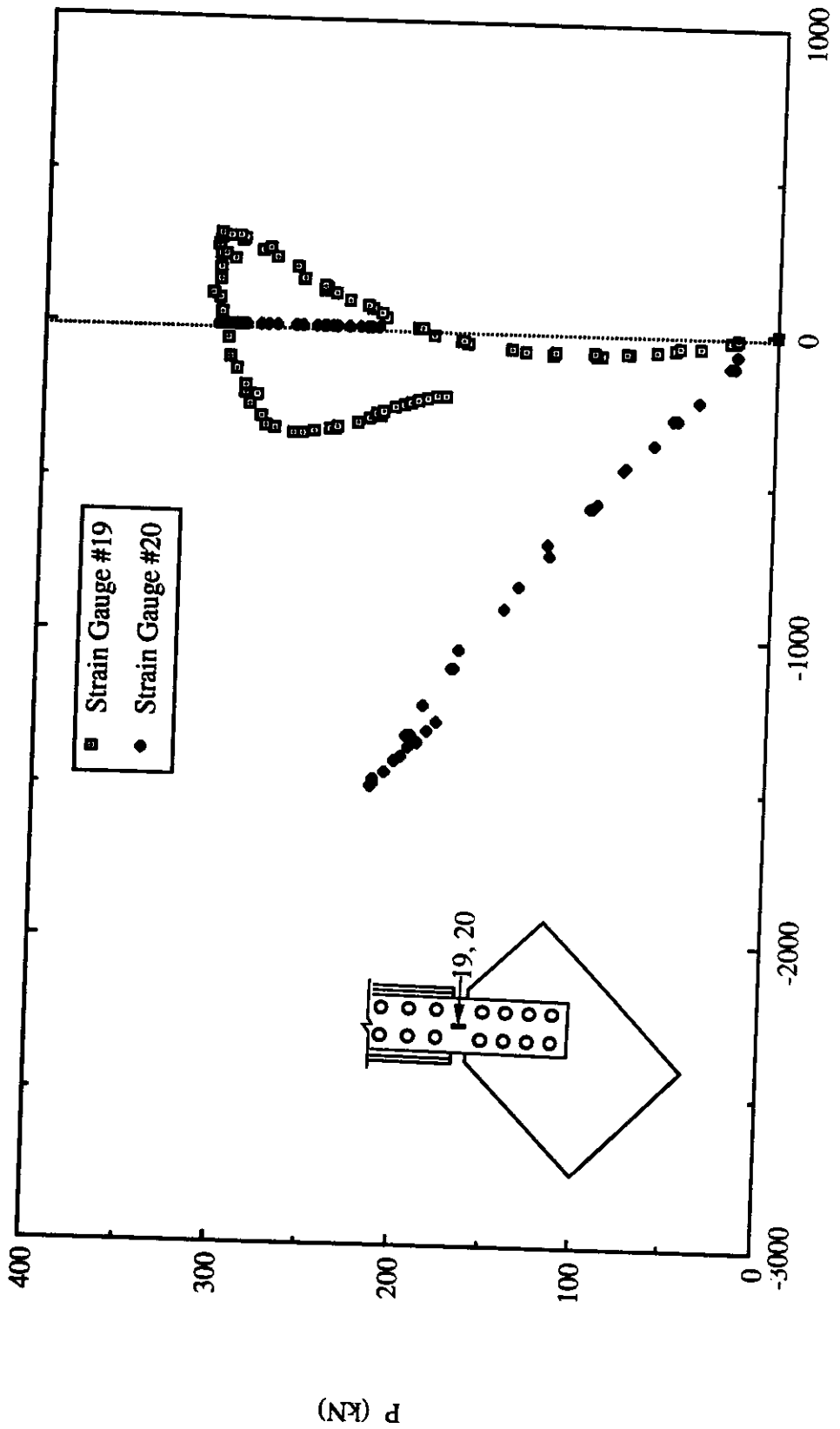

Fig. 7.8 Load vs. Strain Gauge Readings at the Conjunction of Gusset-to-Splice for Specimen EP1

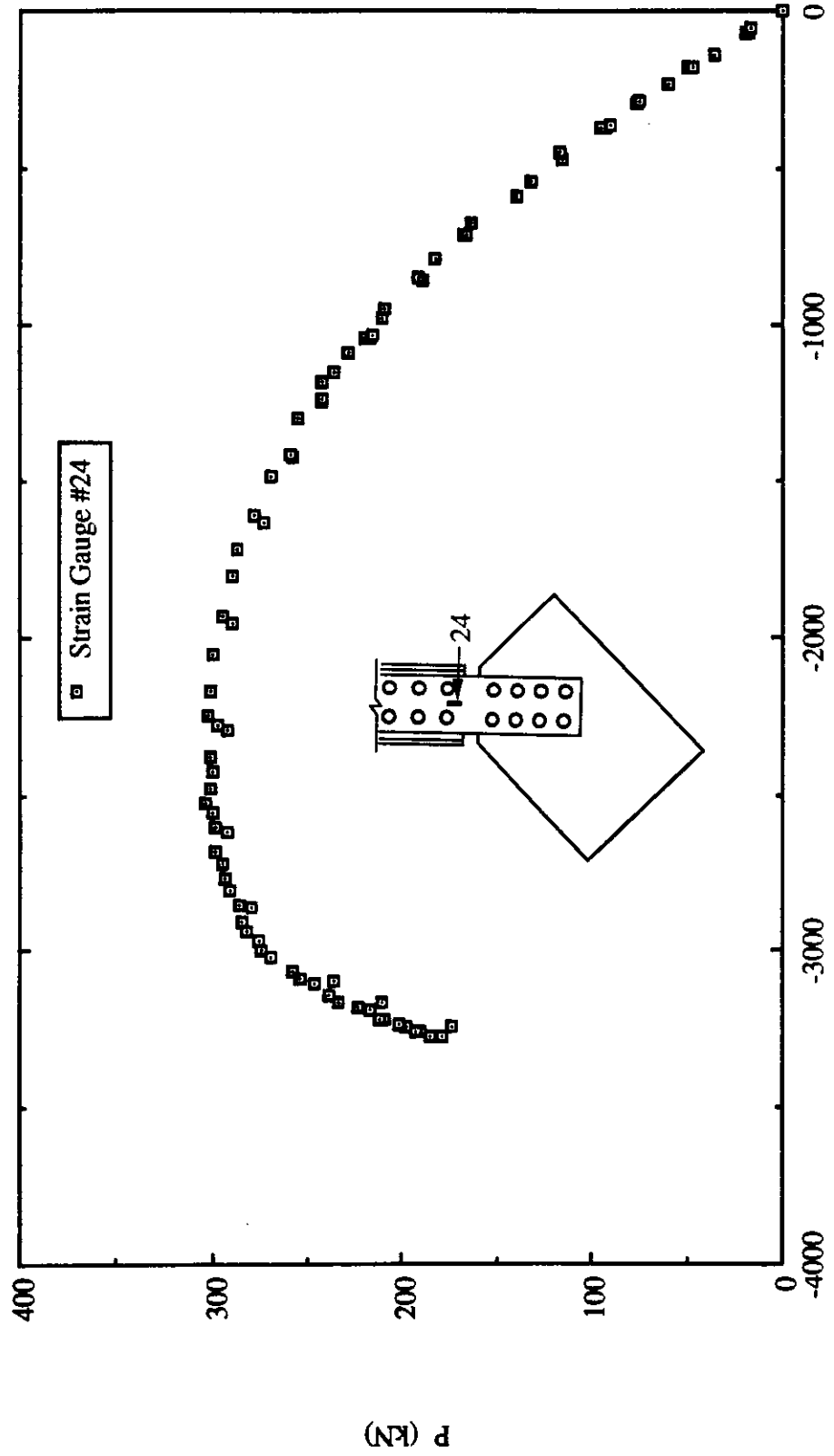

Fig. 7.9 Load vs. Strain Gauge Readings at Splice Member Near End of Brace for Specimen EP1

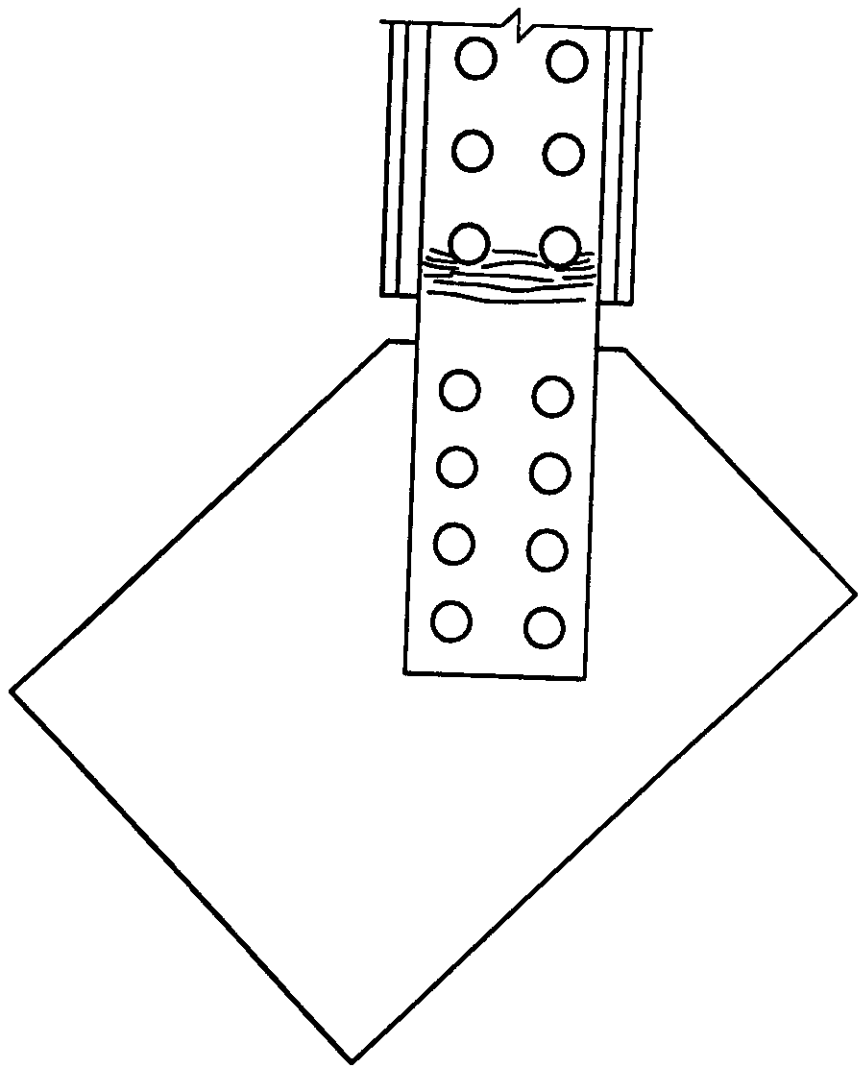

Fig. 7.10 Schematic Yield Line Pattern on Splice PLate for EP Type Specimens

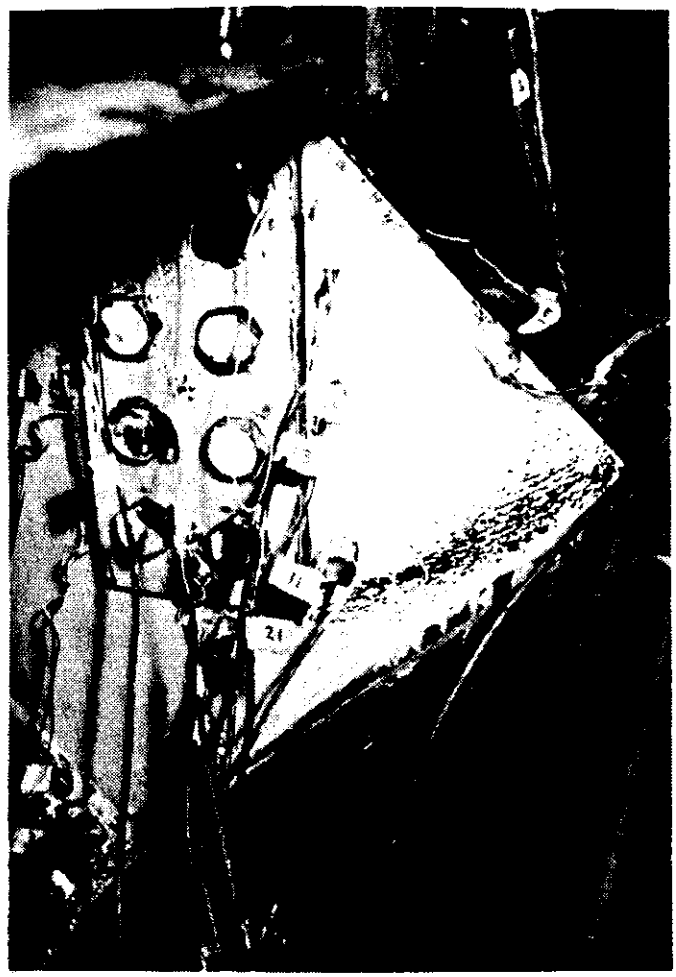

Fig. 7.11 Yielding Observed in Specimen EP1

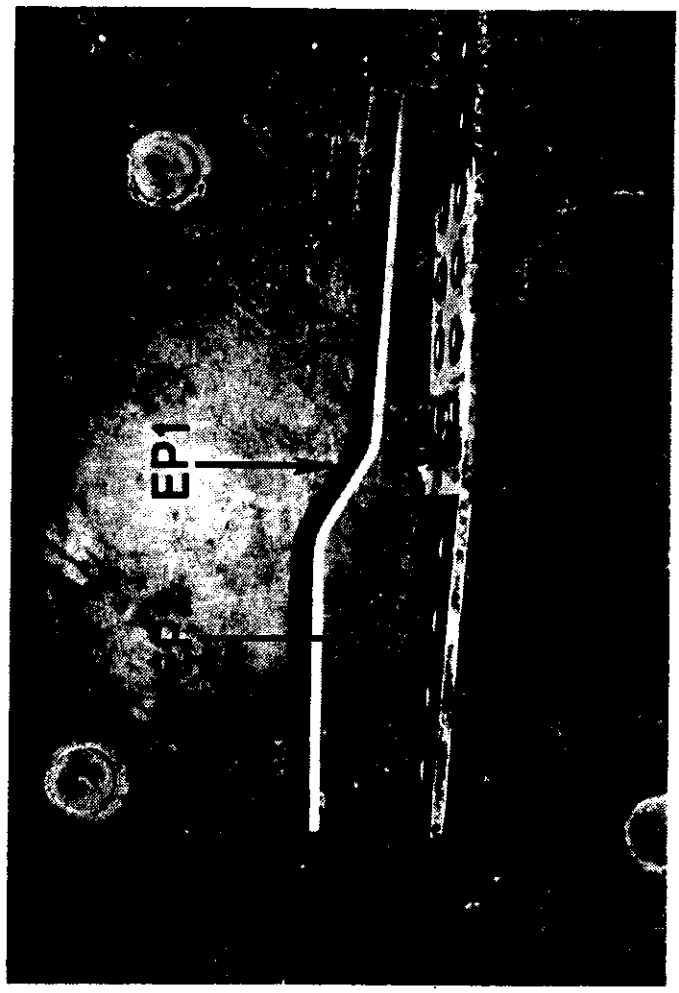

Fig. 7.12 Failed Splice Members for Specimens EP1 and EP2

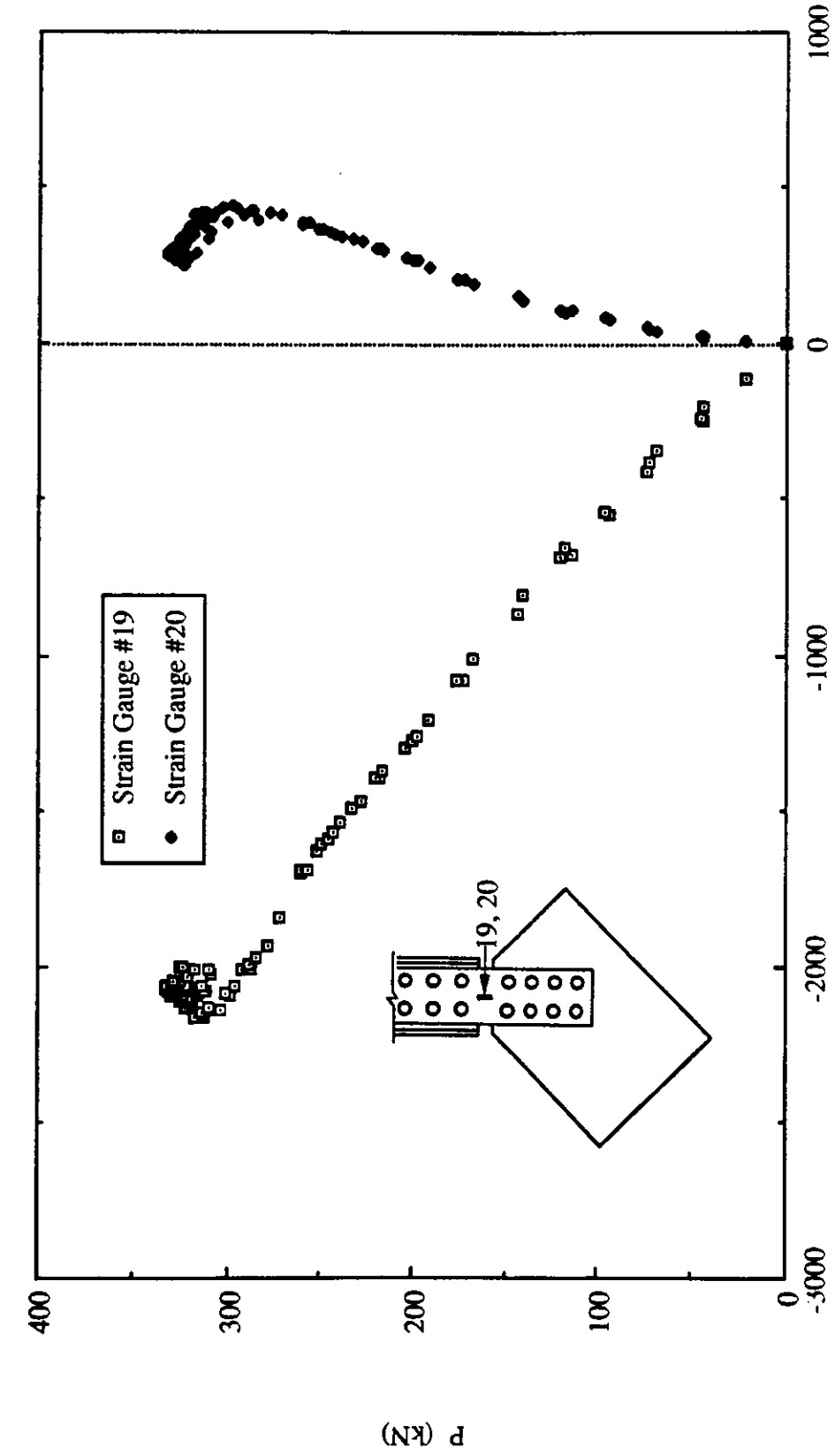

Fig. 7.13 Load vs. Strain Gauge Readings at the Conjunction of Gusset-to-Splice for Specimen EP2

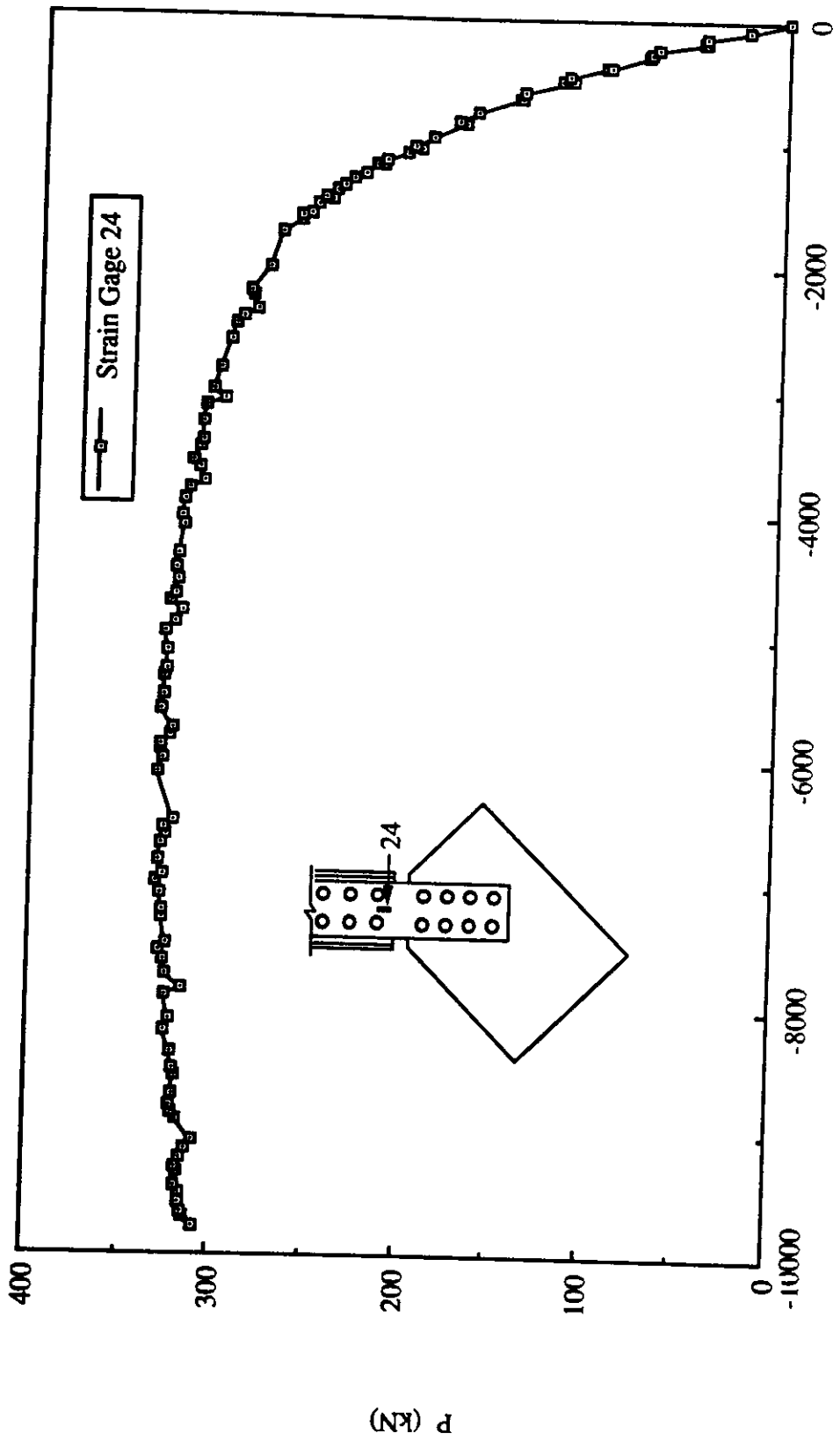

Fig. 7.14 Load vs. Strain Gauge Readings at Splice Near End of Brace for Specimen EP2

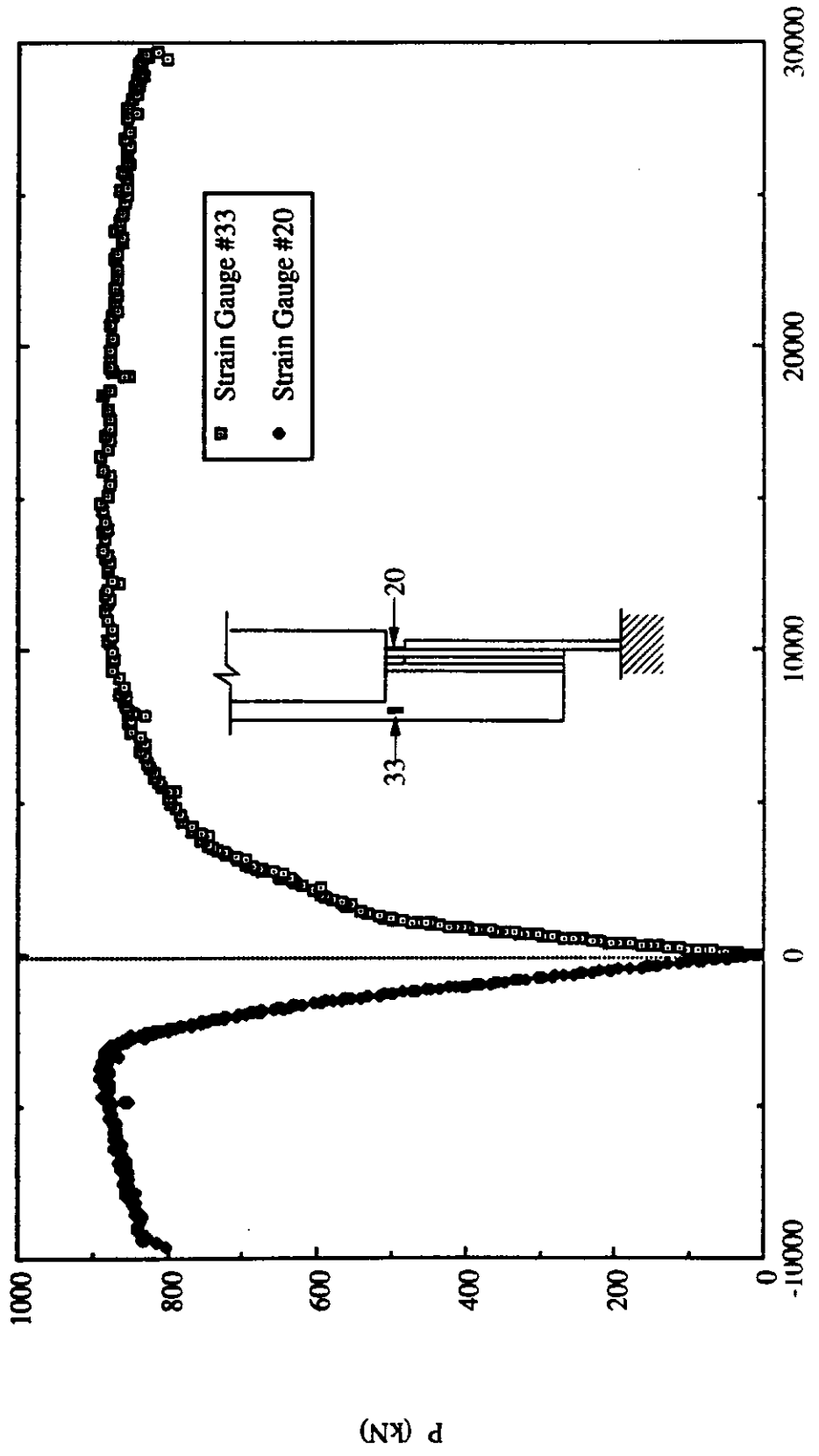

Fig. 7.15 Load vs. Strain Gauge Readings at Web of Tee-Section and Splice Plate for Specimen EP3

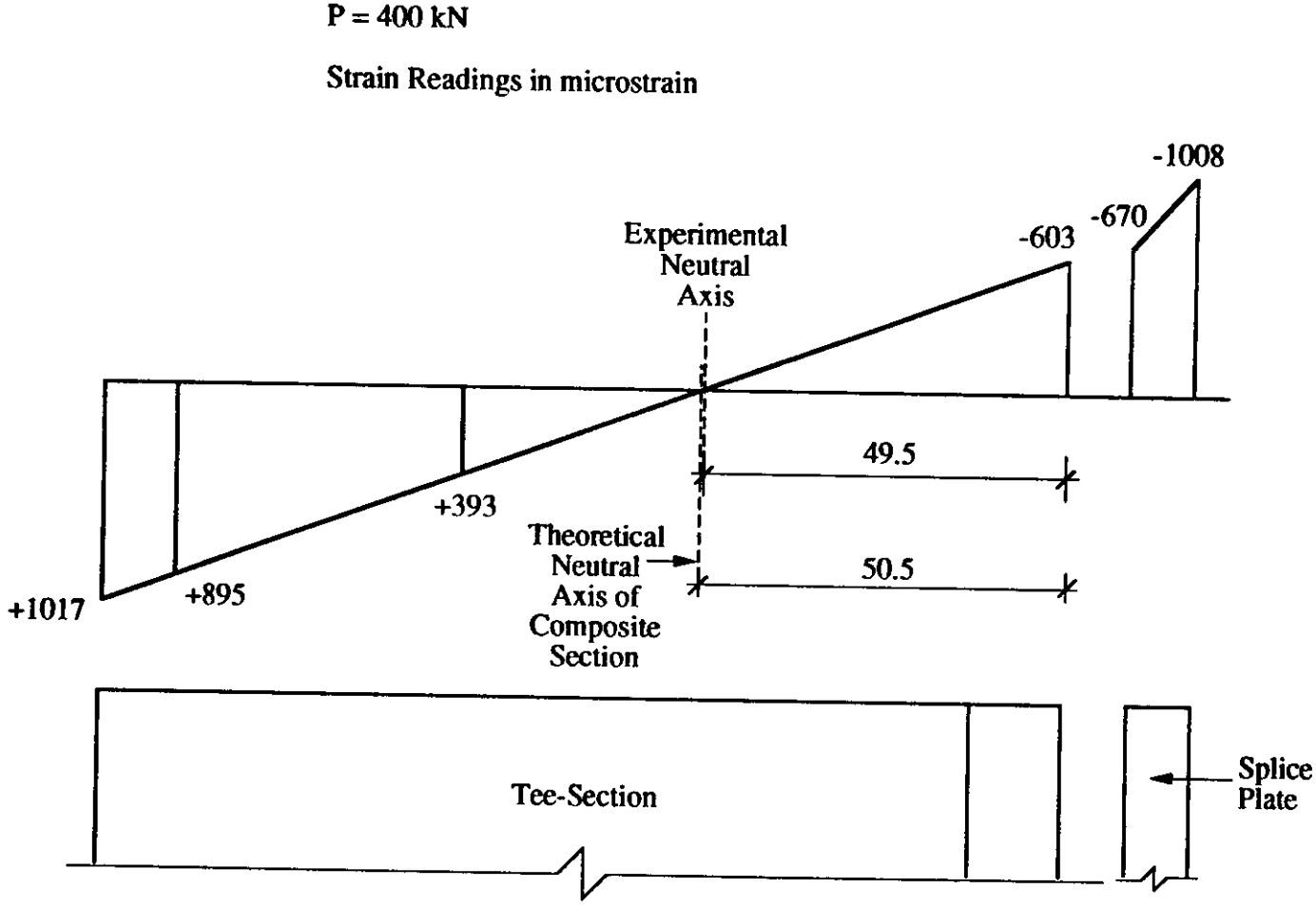

Fig. 7.16 Strain Distribution Across the Depth of the Splice Section For Specimen EP3

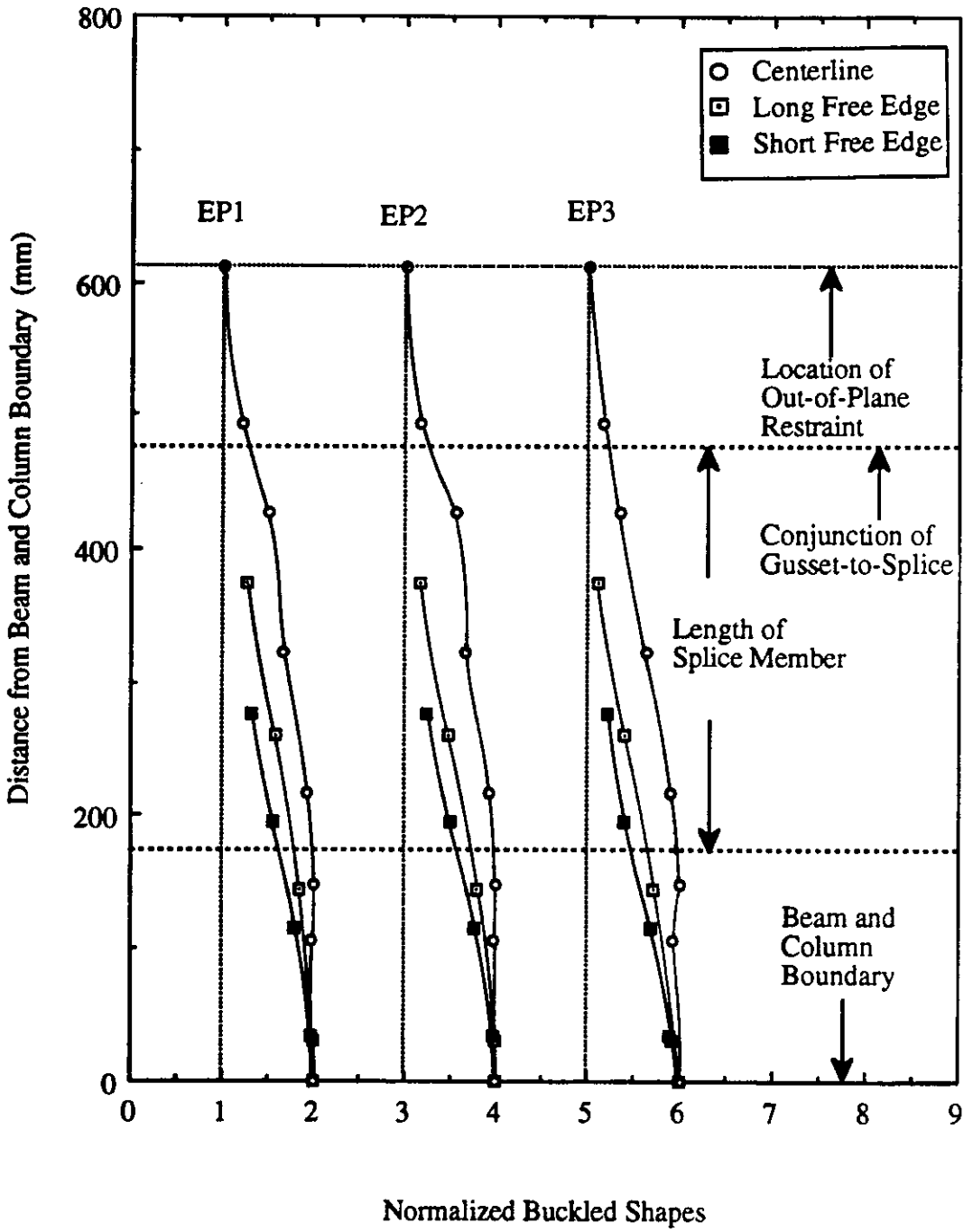

Fig. 7.17 Out-of-Plane Deflected Shapes at Free Edges and Along Centerline of Splice for EP Type Specimens

8. DISCUSSION AND COMPARISON OF TEST RESULTS

8.1 Introduction

This chapter presents the effects of the test parameters on the compressive behavior and ultimate strength of the specimens. The GP type specimens considered the general compressive behavior of a gusset plate connection with plate size of 500 x 400, a brace angle of 45° and the effects of frame action was neglected. In order to examine the effects of each variable, the test results of the GP type specimens will be used as a reference to compare with the test results of other specimens . A general discussion of the test results is included in section 8.2. The effects of each test variable on the behavior and strength of gusset plate connections will be discussed separately in each section. A summary of the test results is shown in Table 8.1.

8.2 General Discussion of Test Results

The ultimate loads of all the specimens are illustrated in Table 8.1. It should be noted that this particular discussion excludes the test results of the EP type specimens since failure of these specimens occurred in the splice member at the conjunction of gusset-to-splice. The design loads estimated by the Whitmore method and the Thornton method of all the specimens were already presented in previous chapters. Table 8.1 includes the ratios of the ultimate load to the Whitmore loads and the ratios of the ultimate load to the Thornton loads. As can be seen from the table that the Whitmore method provided a conservative estimate of the design load for the specimen except for the SP type specimens. The reason for this is that the SP type specimens, which had a plate size of 850 x 700, were relatively slender and therefore, the connection experienced stability failure before even reaching the Whitmore yield load level. Test results from Cheng et al. (1993) with gusset plate size of 850 x 700 and plate thicknesses of 6.7mm and 3.11mm also showed that the test specimens were failed by elastic buckling. The elastic buckling loads of the test specimens

were significantly lower than the corresponding Whitmore loads. The plot of the ratios of the experimental ultimate loads to the Whitmore design loads versus the gusset plate thickness for the GP, SP, AP and MP type specimens is shown in Fig. 8.1. As expected, it can be seen from this figure that the ratios are all above 1.0 except SP type specimens. Hence, in general the Whitmore method produces conservative estimates of the design load of the compact specimens. In addition, higher ratio existed for the 13.3 mm thick specimens as shown in the figure which might indicate more efficient use of the material for the compact specimens. Although the ratios for the SP type specimens were below 1.0, it can still be seen that the ratio for the specimen with larger thickness was significantly higher than the one with smaller plate thickness. However, the test data from Hu and Cheng (1987) showed that the ratio of the ultimate load to the Whitmore load did not increased with increasing plate thickness. This was probably due to the fact that postbuckling strength existed in the 3.11mm thick specimen as shown by the finite element analysis (Cheng et al. 1993). If the theoretical bifurcation buckling load was used, the ratio of the buckling load to the Whitmore load would be 0.088 instead of 0.211. Hence, the observation of the effect of gusset plate thickness to the ratio of ultimate load to Whitmore load was appropriate.

The plot of the ratio of experimental ultimate loads to the Thornton loads is shown in Fig. 8.2. It can be seen from the figure that the ratios for the specimens are all above 1.0. This ratio varied from 1.31 to 1.80 and it should be noted that the effective length factor, k, was chosen to be 0.65. For the MP type specimens, the ratio ranges from 1.62 to 1.84. Tests performed by Gross and Cheok (1988) on two gusset plate specimens subject to beam and column moments and failed by buckling showed a ratio of experimental buckling load to the Thornton load of 1.5 and 1.7. However, the effective length factor used to evaluate the Thornton load in this case was chosen to be 0.5. If a value of 0.5 was used for k in evaluating the MP type specimens, the ratio of the ultimate load to the Thornton load ranges from 1.50 to 1.71. Hence, it can be seen that the test results from two different

testing programs showed similar test to predicted ratios and Thornton method provides a simple procedure to evaluate the buckling strength of gusset plate and the estimates are conservative.

In general, similar yielding pattern was observed for the specimens. However, the final yielding pattern of each particular specimen type was influenced by the corresponding test parameter. For example, the beam and column moments caused tensile yielding at the fixed ends of the free edges for the MP type specimens, nevertheless, the general yielding pattern of the specimens was still comparable to that of the GP type specimens. The influence on the yielding pattern by various test variables will be discussed in the following sections. The general yielding pattern involved the significant yielding occurred at the plate area underneath the splice member. This area was stressed severely during loading regardless of the types of specimens. However, load redistribution occurred in most of the specimens allowing the load to transfer to the other part of the plate once the plate underneath the splice member was yielded extensively. In order for load redistribution to occur, the specimens had to be stiff enough to avoid stability failure. In addition, due to the complex boundary conditions the gusset plate connection was statically indeterminate. Hence, for the stocky specimens with a plate thickness of 13.0 mm and a plate of 500 mm x 400 mm yielding was observed almost on the entire plate due to load redistribution prior to stability failure. On the other hand, very minor yielding was observed in specimen SP2, which was quite slender, before buckling occurred. In fact, the preliminary finite element analysis indicated that specimen SP2 failed in elastic buckling.

The failure mode for the specimens without out-of-plane restraint was sway buckling of the plate and the local buckling was observed for specimens with out-of-plane restraint. The failed specimens indicated that yield line mechanism occurred in the gusset plate. These yield lines allowed the specimens to form a mechanism such that a lower load level could be maintained after the specimens reached the ultimate load. This behavior was evident

when examining the curves of load versus in-plane deformation of the MP and AP type specimens as shown typically in Figs. 6.4 and 5.4. However, this behavior was not recorded for the GP and SP type specimens since the tests were terminated before the specimens were allowed to stabilize at a lower load level. The reason for terminating the tests at that stage is that the out-of-plane displacement of the specimens had reached the physical limit of the test setup and measuring devices and the specimens were already in the unloading stage, therefore, it was decided to cease the tests. It should also be noted that specimens with smaller thickness might not be able to attain the mechanism.

8.3 Effects of Gusset Plate Thickness and Size

As can be seen from Table 8.1 that the ultimate load of the specimens increased with increasing plate thickness for the specimens tested without restraint. The plot of ultimate loads versus the plate thickness is shown in Fig. 8.3. This figure shows that the ultimate loads of the specimens increased almost linearly with respect to the plate thickness. In addition, the slope of the curves are almost parallel except for the AP type specimens. The curve for the AP type specimens show a smaller slope than the rest of the curves as shown in the figure.

For the specimens tested with restraint at the base of the test frame, specimen SP2 showed similar ultimate load to that of specimen GP2 even though specimen SP2 was more slender, as shown in Fig. 8.4. The reason for this is that for specimen SP2 the increase in ultimate load due to the restraint was significant since the specimen was predominantly failed in elastic buckling. However, specimen GP2 already showed severe yielding in the test without restraint and the ultimate load in this case might be very close to the material strength of the gusset plate. Hence, specimen GP2 might not be sensitive to the change in boundary condition whereas specimen SP2 was susceptible to the restraint.

Again, the amount of yielding decreased with increasing gusset plate size when comparing the tests results of the GP type specimens to that of the SP type specimens. Pictures of the failed specimens of GP1 and SP1 are shown in Figs. 3.15 and 4.11, respectively. Since the out-of-plane stiffness of the specimens also decreased with increasing plate size, therefore, for the SP type specimens stability failure occurred before significant yielding could be developed in the specimen. However, the general yielding pattern of the specimens was not affected much by increasing the plate size.

8.4 Effects of Out-of-Plane Restraint at Conjunction of Gusset-to-Splice

The ultimate loads of the specimens increased when out-of-plane restraint was provided at the conjunction of gusset-to-splice as shown in Table 8.1. However, it can be seen that the increase in ultimate loads for the GP type specimens due to the restraint was not significant. A maximum of about 10% increase was recorded for specimen GP2. For the SP type specimens, considerable increase was observed for specimen SP2 due to the restraint. A plot of load versus gusset plate thickness with the two restraint conditions is shown in Fig. 8.4. It can be seen from the figure that the curves for the GP type specimens are almost parallel with only minor increase in ultimate load due to the restraint.

As mentioned previously that the out-of-plane deflected shapes along the free edges and centerline of the splice member for the GP and SP types specimens without restraint at the base of test frame resembled the buckled shapes of a fixed-guided column. These deflected shapes are shown in Figs 3.16 and 4.12. However, when the restraint was applied to the base of test frame the deflected shapes were changed as shown in Figs. 3.24 and 4.20 for the GP and SP types specimens, respectively. The deflected shapes shown in these figure indicated that out-of-plane displacement was recorded at the conjunction of gusset-to-splice. This displacement, as mentioned in Chapter 3, was caused by bending of the web of the brace member about the supports of the tension rods. Hence, the restraint in the out-of-plane direction at the conjunction was reduced. Since the conjunction was not fully

fixed, therefore, the restraint at the base of the test frame might not have a significant effect on the ultimate loads of the specimens. In addition, the GP type specimens were well within the inelastic range before reaching the ultimate loads, hence the restraint might not have significant influence on the ultimate loads. On the other hand, specimen SP2 (t=9.8mm) only experienced slight yielding prior to reaching the ultimate load, therefore, the effects of the restraint might be considerable as illustrated by the increase of the ultimate loads shown in Table 8.1. In general, the restraint did not affect the yielding pattern of the specimens.

8.5 Effects of Angle of the Diagonal Brace Member

The plot of ultimate loads versus gusset plate thickness for the GP and AP type specimens is shown in Fig. 8.5. It can be seen from the figure and Table 8.1 that the ultimate loads for the specimens with 30° brace angle (AP) were slightly lower than that for the specimens with 45° brace angle. The difference in ultimate loads for these two types of specimens ranges from 2 % to 12% . Hence, it can be seen that the brace angle did not affect the ultimate load of the specimens significantly. Figure 8.5 also shows that the curve for the GP type specimens was slightly steeper than that of AP type specimens. This indicates that the rate of ultimate load increase with respect to the plate thickness for the GP type specimens was higher that of the AP type specimens. It should be noted that the test setup employed to perform the tests on the GP type specimens was different from that of the AP type specimens. However, it is believed that the test setups should not affect significantly the test results.

In general, the yielding pattern for the AP and GP types specimens was similar except yield lines were first observed near the beam and column boundary for the AP type specimens. It was observed from the tests that significant yielding was recorded in the area of the plate bounded by the beam boundary and the short side free edge. In fact, the failed AP type specimens showed that yield lines were observed in that entire area as illustrated in

Fig. 5.15. In-plane bending at the short side free edge of the AP type specimens was observed at the later stage of loading. To illustrate this, strain gauges readings recorded at the mid-length of the short side free edge for specimens GP3 and AP3 are shown in Fig. 8.6. It can be seen from the figure that average strains from the two sides of the plate were used to plot the curves. This figure shows that the strain readings from both specimens were almost identical until the load reached about 65% of the ultimate load. At this particular loading stage, strain reversal was observed for specimen AP3 which indicated that in-plane bending had occurred at the short side free edge. As loading continued, the compressive strains at the short side free edge for specimen GP3 increased, however, tensile strain was recorded for specimen AP3. This in-plane bending was probably caused by the smaller brace angle of 30° which produced a larger horizontal component of applied force to the short side free edge.

8.6 Effects of Beam and Column Moments

When comparing the test results of the GP and MP types specimens, it can be seen that beam and column moments had negligible effects on the ultimate loads of the specimens as illustrated in Table 8.1. A plot of the ratio of ultimate load for the MP type specimens to that of the GP type specimens versus the beam moment is shown in Fig. 8.7. The ratio ranges from 0.97 to 1.11. This plot shows that negligible effects of beam and column on the ultimate loads of the specimens were observed from the test results. As shown in Table 8.1 that by increasing the beam and column moments from 250 kNm and 125 kNm (MP3) to 375 kN·m and 187.5 kN·m (MP3A), the ultimate load of the specimen was increased by 14%.

Although the beam and column moment did not affect the ultimate load of the specimens significantly, early yielding in the plate area underneath the splice member was observed for the MP type specimens. As mentioned previously, yielding at the area underneath the splice occurred at a load level close to the one estimated by the Whitmore method for the

specimens without the effects of beam and column moments. However, for the MP type specimens yielding at the area underneath the splice occurred at a load level significantly lower than that estimated by the Whitmore method. To examine these behavior, a plot of load versus strain recorded at the rosette mounted underneath the splice for specimens GP3 and MP3 is shown in Fig. 8.8. It can be seen from this figure that similar strain readings were recorded for both specimens GP3 and MP3 at the initial loading stage. However, when the beam and column moment was applied to specimen MP3, sudden increase in compressive strain for this specimen was observed. For specimen MP3, full value of beam and column moment was applied at a load level of about 100 kN. It can also be seen from the figure that specimen GP3 showed yielding at approximately the load level slightly lower than the one estimated by the Whitmore method. However, for specimen MP3 yielding was observed at early loading stage after the full values of beam and column moment was applied as shown in the figure. Hence, it can seen that beam and column induced early yielding at the plate area underneath the splice. It was also discussed in the previous chapter that the beam and column moment also induced significant tensile stress at the ends of the gusset plate free edges and high tensile stress gradient was also observed along the beam and column boundary. In general, however, for the GP3 specimens compressive strain was observed along the beam and column boundary. Nonetheless, the tensile stress induced by the beam and column moment might have improved the compressive strength of the specimens. On the other hand, however, the early compressive yielding occurred underneath the splice due to presence of the beam and column moment might counteracted this beneficial effects. Hence, on the whole the ultimate loads of the specimens were not affected significantly by the beam and column moment.

The beam and column moment also affected the load deflection behavior of the specimens. To illustrate this observation, the load deflection curves of specimens MP3, MP3A and MP3B shown in Figs 8.9 and 8.10 were examined. The load versus in-plane deformation of the gusset plate specimens recorded at the end of the splice member is shown in Fig. 8.9

This figure shows that the in-plane stiffness of the specimens decreased with increasing beam and column moments. When examining the curves for specimens MP3A and MP3B, it can be seen that the curve for the specimen with zero beam and column moment (MP3B) was linear up to approximately the Whitmore yield load level, however, for the specimen with maximum beam and column moment (MP3A) nonlinearity of the curve was observed at about 350 kN which was significantly lower than the Whitmore yield load. As a reminder, it can be observed from the figure that regardless of the moment levels the specimens were all stabilized at the same lower load level after reaching the corresponding ultimate loads.

The out-of-plane load deflection behavior was also affected by the beam and column moment as shown in Fig. 8.10. This figure illustrates that as the beam and column moment increased the out-of-plane stiffness of the specimen also increased. Significant increase in stiffness was observed when comparing specimens MP3B and MP3A. However, only slight increase in stiffness was recorded when comparing specimens MP3 and MP3B. Nevertheless, this increase in out-of-plane stiffness was provided by the tensile stress due to the beam and column moment. When the gusset plate specimens deformed out-of-plane a component of the in-plane tensile stress perpendicular to the plane of the plate would act in the opposite direction of the out-of-plane deformation, hence the specimens were stiffened. This behavior is similar to membrane action, however, the in-plane tensile stress was produced by the beam and column moment.

8.7 Effect of Loading Eccentricity

As presented in the previous chapter that three tests were performed on a specimen similar to that of specimen GP1 with various splicing members to investigate the effect of loading eccentricity. Since the mode of failure for these specimens was yielding at the splice member, therefore, both the Whitmore and Thornton methods were not suitable to provide an estimate of the design load of these specimens. It can be seen from Table 8.1 that the

ultimate loads of EP type specimens were significantly lower that of the specimen GP1. The maximum load achieved by specimen EP3 was about 50% of the ultimate load of specimen GP1. When comparing the test results of specimens EP1 and EP2, it can be seen that increasing the splice plate thickness by approximately 37% the ultimate load of specimen EP2 was only improved by 8%. Although it should be noted that increasing the thickness of the splicing member, the loading eccentricity was also increased. For these specimens, the increase in loading eccentricity was 3.5 mm from specimens EP1 to EP2. However, when a tee-section was added to the 13.0mm thick splice member, the ultimate load of specimen EP3 was increased to about 2.67 times that of specimen EP2. Hence, it can be seen that significant improvement in load carrying capacity of an eccentrically loaded gusset plate connection can be attained by employing a splicing member which has higher flexural stiffness. Nevertheless, the maximum load of eccentricity loaded specimen EP3 was still much less than that of the concentrically loaded specimen GP1.

The curves of load versus out-of-plane displacement of the test frame for the specimens are shown in Fig 8.11. As expected, the out-of-plane stiffness of the specimens increased with increasing flexural stiffness of the splice member. The elastic range of the load deflection curve also increased with increasing splice member flexural stiffness. The curves were also similar to typical load deflection curve for beam-column which has an unloading path due to the effects of PΔ moments. It can be observed from the figure that the rate of unloading for the specimens decreased as the flexural stiffness of the splicing member increased.

The failure mode for specimen EP1 indicated a mechanism was formed in the splice member as shown in Fig.7.12. However, for specimens EP2 and EP3 only slight bending of the splice member was recorded although significant yield lines were observed for specimen EP2 at the splice plate around the last row of bolts from the bracing member similar to that of specimen EP1 as illustrated in Fig 7.10. In general, yielding of the gusset

plate specimen was only observed near the beam and column boundary except for specimen EP3 which showed yield lines progressed from the beam and column boundary towards the plate area underneath the splice member. In particular, this specimen showed significant yielding at the boundary. The effects of this yielding can be observed from the out-of-plane deformation of the specimen free edges which are shown in Fig. 7.15. This figure shows that the free edges of the specimen EP3 rotated about the fixed ends to the boundary. For specimens EP1 and EP2 bending deformation of the free edges was observed.

The design load of the specimens estimated by the beam-column equation are also included in Table 8.1. It should be noted that actual static yield strength of each specimen (splice member) was employed to evaluate the design load. It can be seen from this table that the beam-column equation provided conservative estimates of the strength of the specimens. The ratio of the ultimate load to the design load ranges from 1.34 (EP3) to 2.61 (EP1).

Table 8.1. Summary of Test Results

Specimen Designation	Plate Size (mm)	Ultimate Load (kN)	Beam-Column Eqn. (kN)	$\frac{P}{P_w}$	$\frac{P}{P_t}$
GP1	500 x 400 x 13.3	1956	-	1.61	1.72
GP2	500 x 400 x 9.8	1356	-	1.46	1.64
GP3	500 x 400 x 6.5	742	-	1.37	1.62
GP1R	500 x 400 x 13.3	2057	-	1.69	1.80
GP2R	500 x 400 x 9.8	1487	-	1.60	1.80
GP3R	500 x 400 x 6.5	790	-	1.42	1.72
SP1	850 x 700 x 13.3	1606	-	0.87	1.31
SP2	850 x 700 x 9.8	1010	-	0.71	1.58
AP1	500 x 400 x 13.3	1720	-	1.56	1.50
AP2	500 x 400 x 9.8	1210	-	1.55	1.45
AP3	500 x 400 x 6.5	728	-	1.31	1.55
MP1	500 x 400 x 13.3	1933	-	1.59	1.69
MP2	500 x 400 x 9.8	1316	-	1.42	1.59
MP3	500 x 400 x 6.5	721	-	1.30	1.57
MP3-A	500 x 400 x 6.5	819	-	1.48	1.78
MP3-B	500 x 400 x 6.5	821	-	1.48	1.79
EP1	500 x 400 x 13.3	310	122	0.25	0.27
EP2	500 x 400 x 13.3	334	128	0.27	0.29
EP3	500 x 400 x 13.3	890	664	0.73	0.78

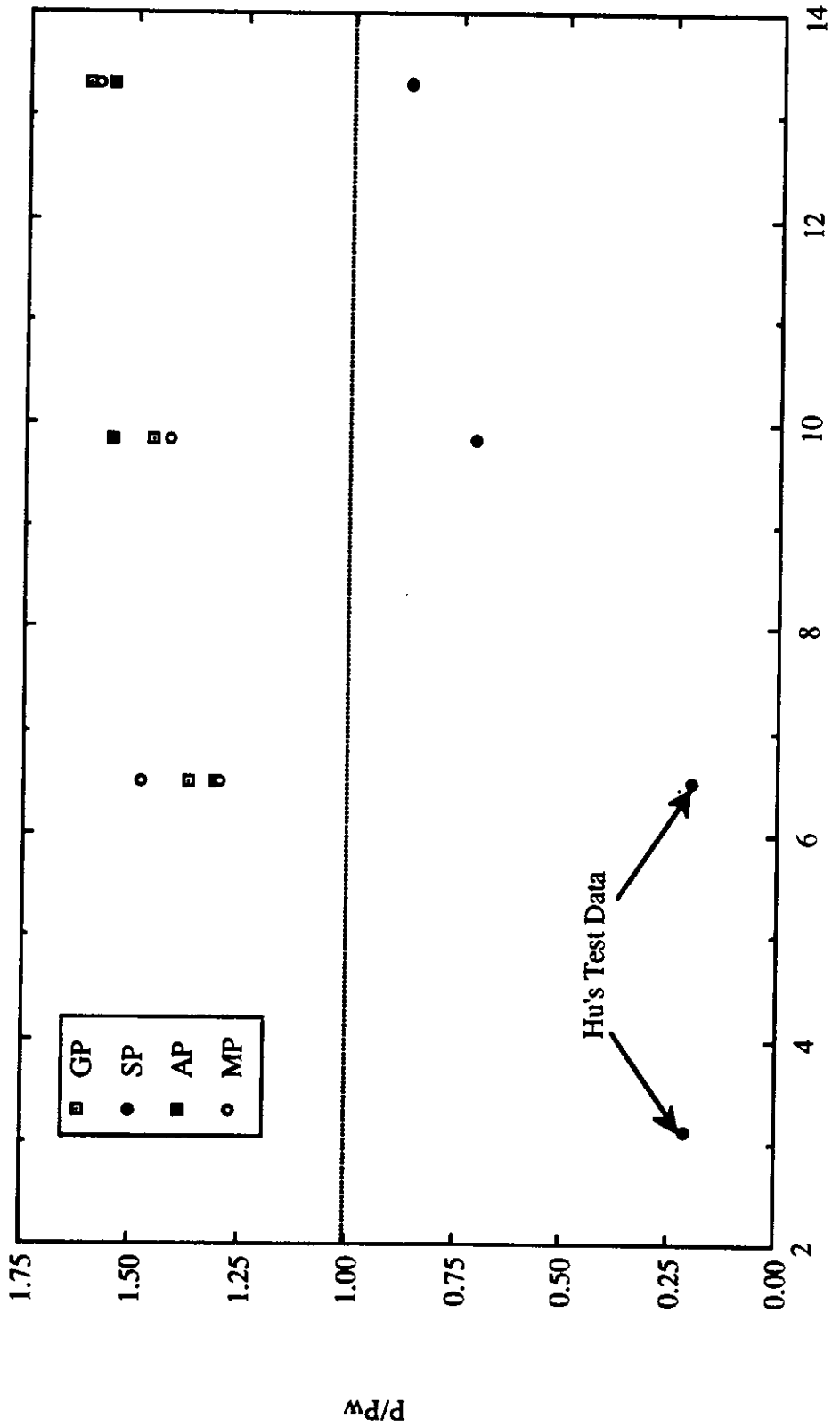

Fig. 8.1 Ratios of Ultimate Loads to Whitmore Loads vs. Gusset Plate Specimens Thickness

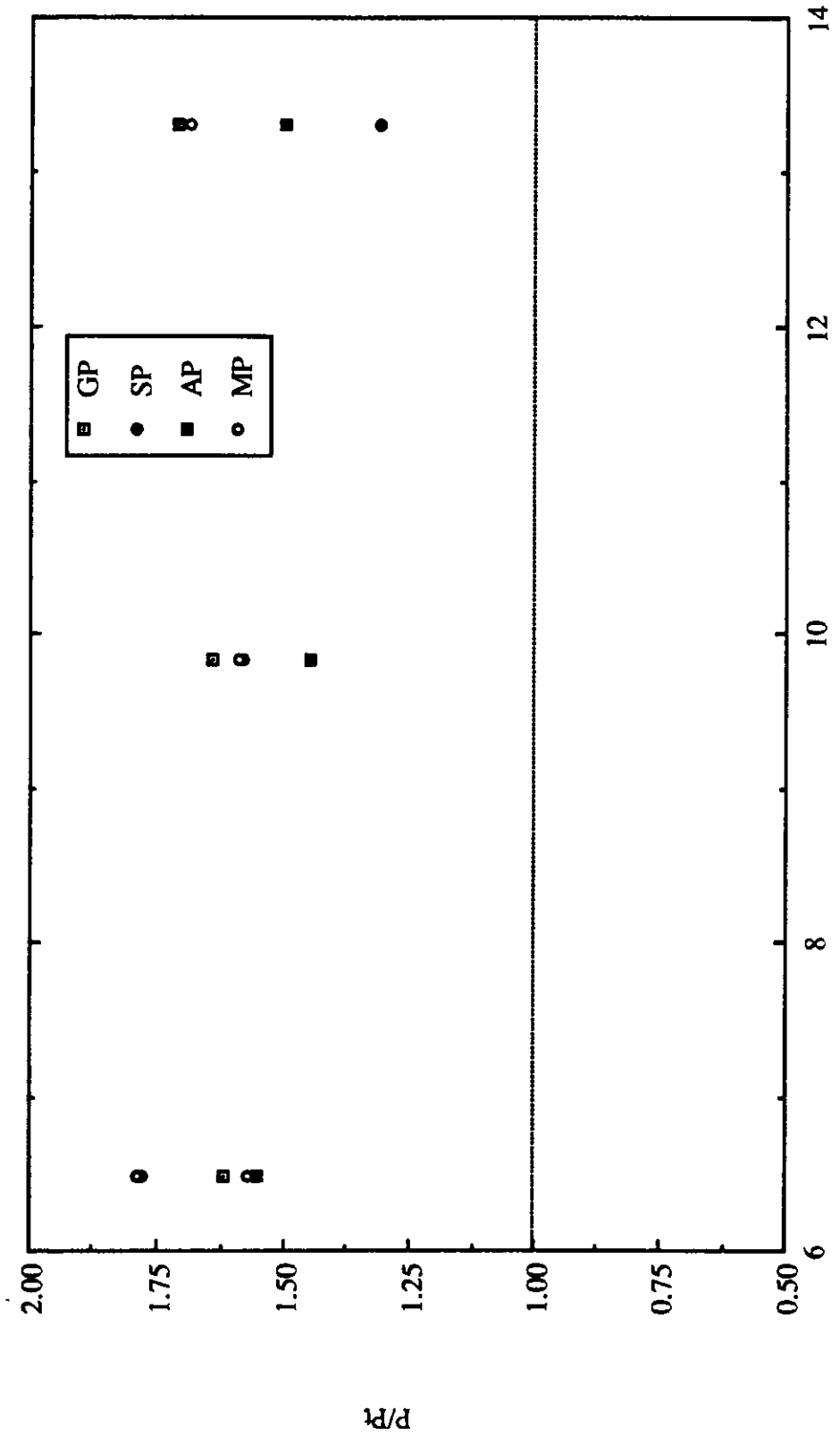

Fig. 8.2 Ratio of Ultimate Loads to Thornton Loads vs. Gusset Plate Specimens Thickness

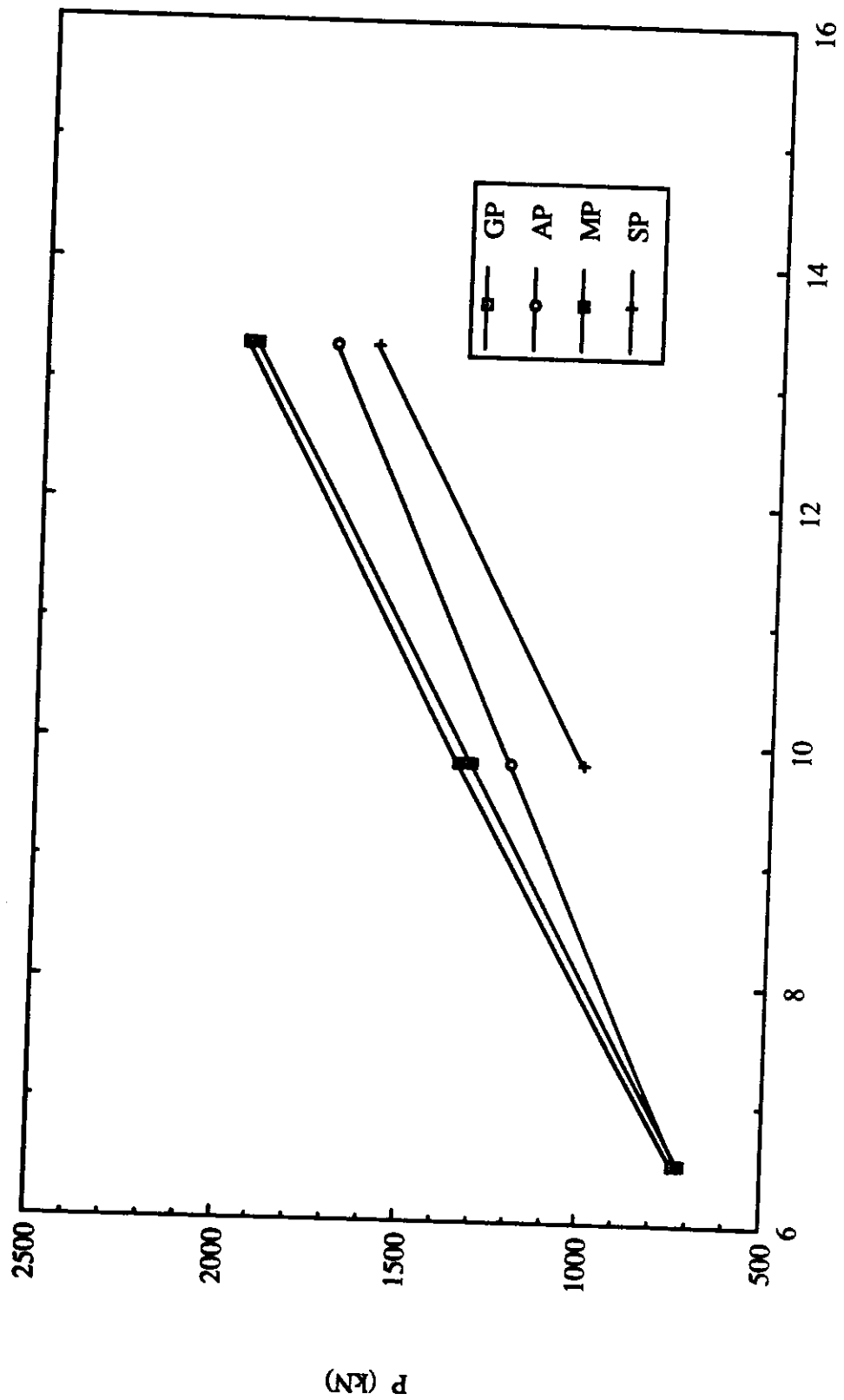

Fig. 8.3 Ultimate Loads vs. Gusset Plate Specimens Thickness

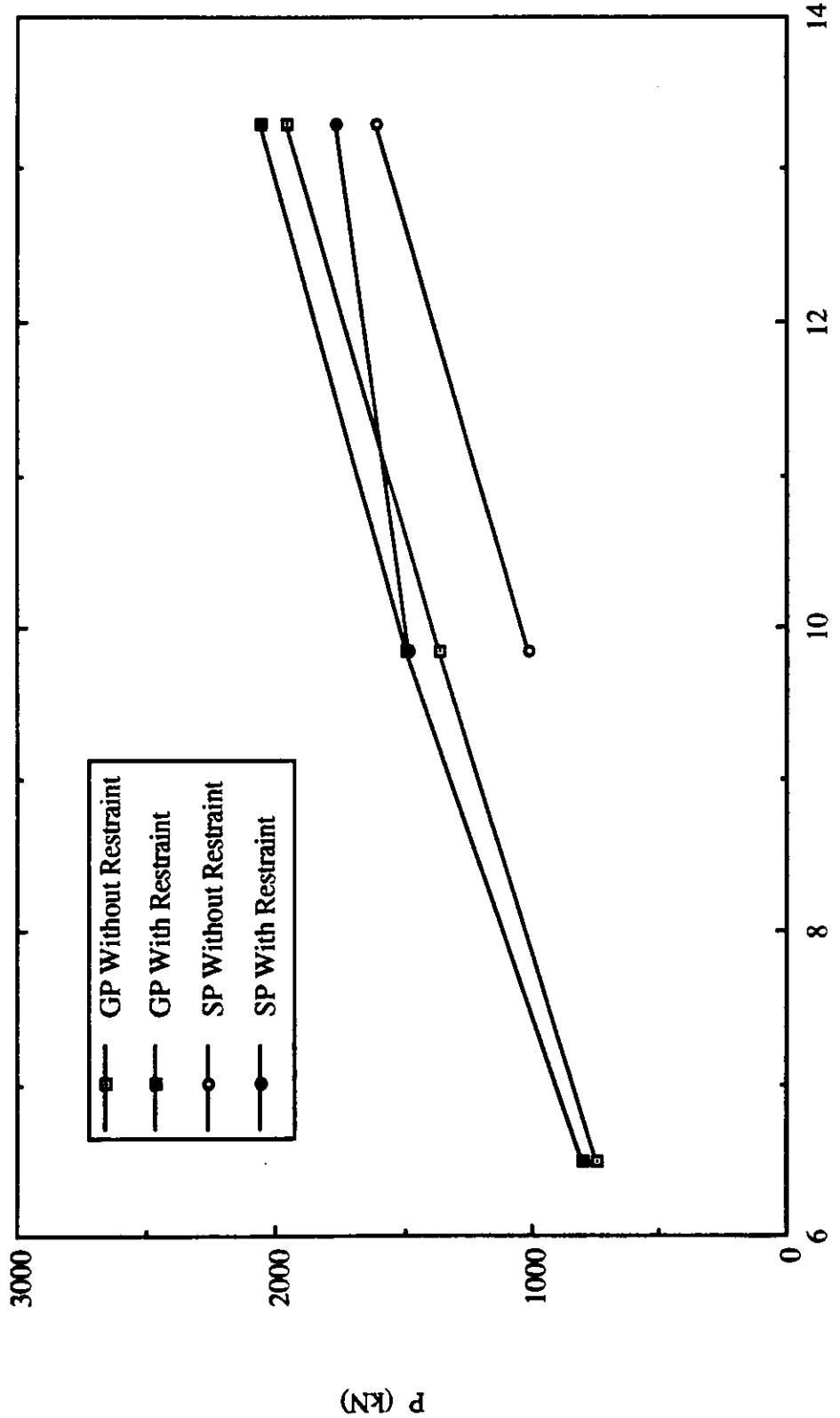

Fig. 8.4 Effects of Out-of-Plane Restraint on the Ultimate Loads of GP and SP Types Specimens

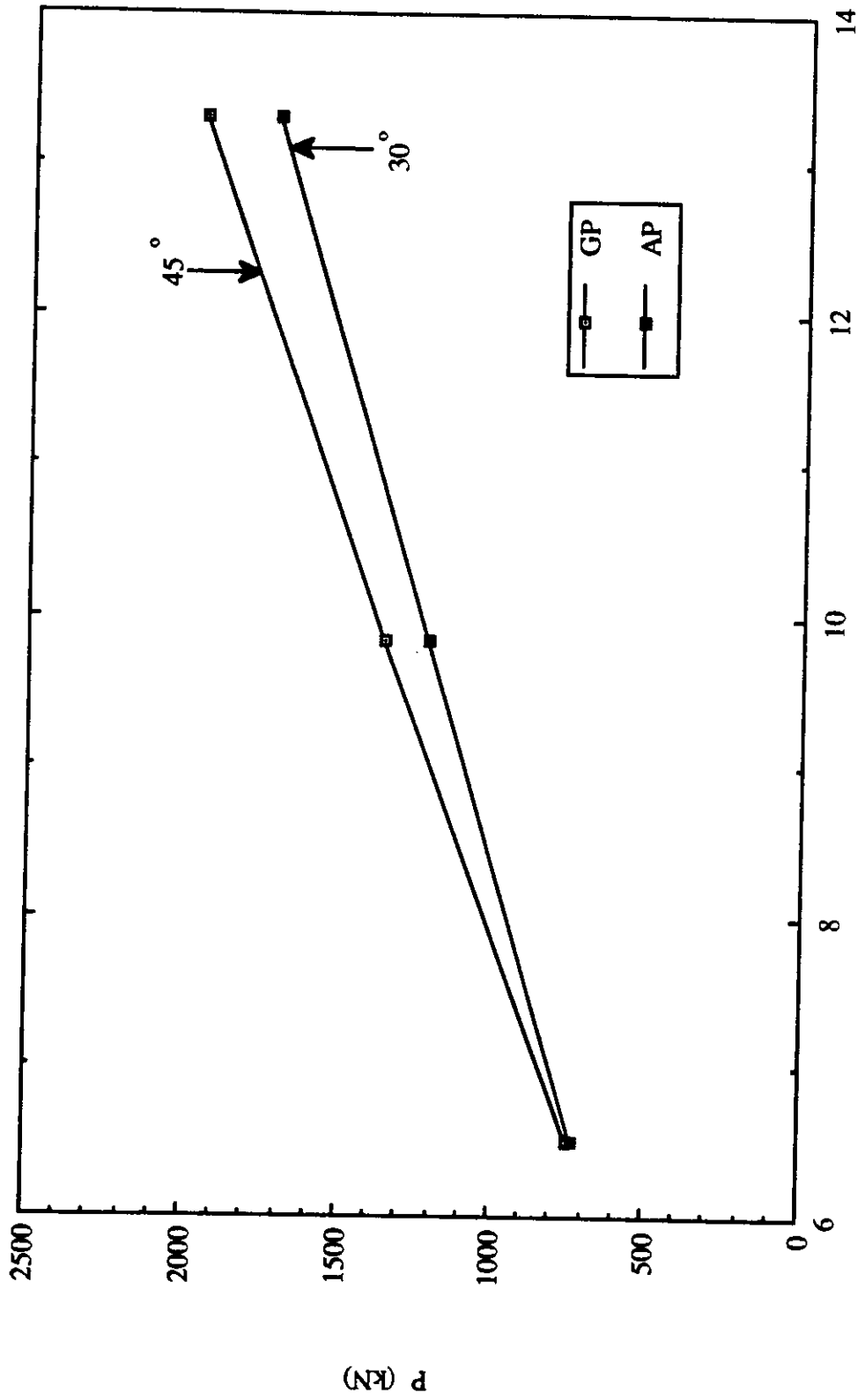

Fig. 8.5 Effects of Brace Angles on the Ultimate Loads of Specimens

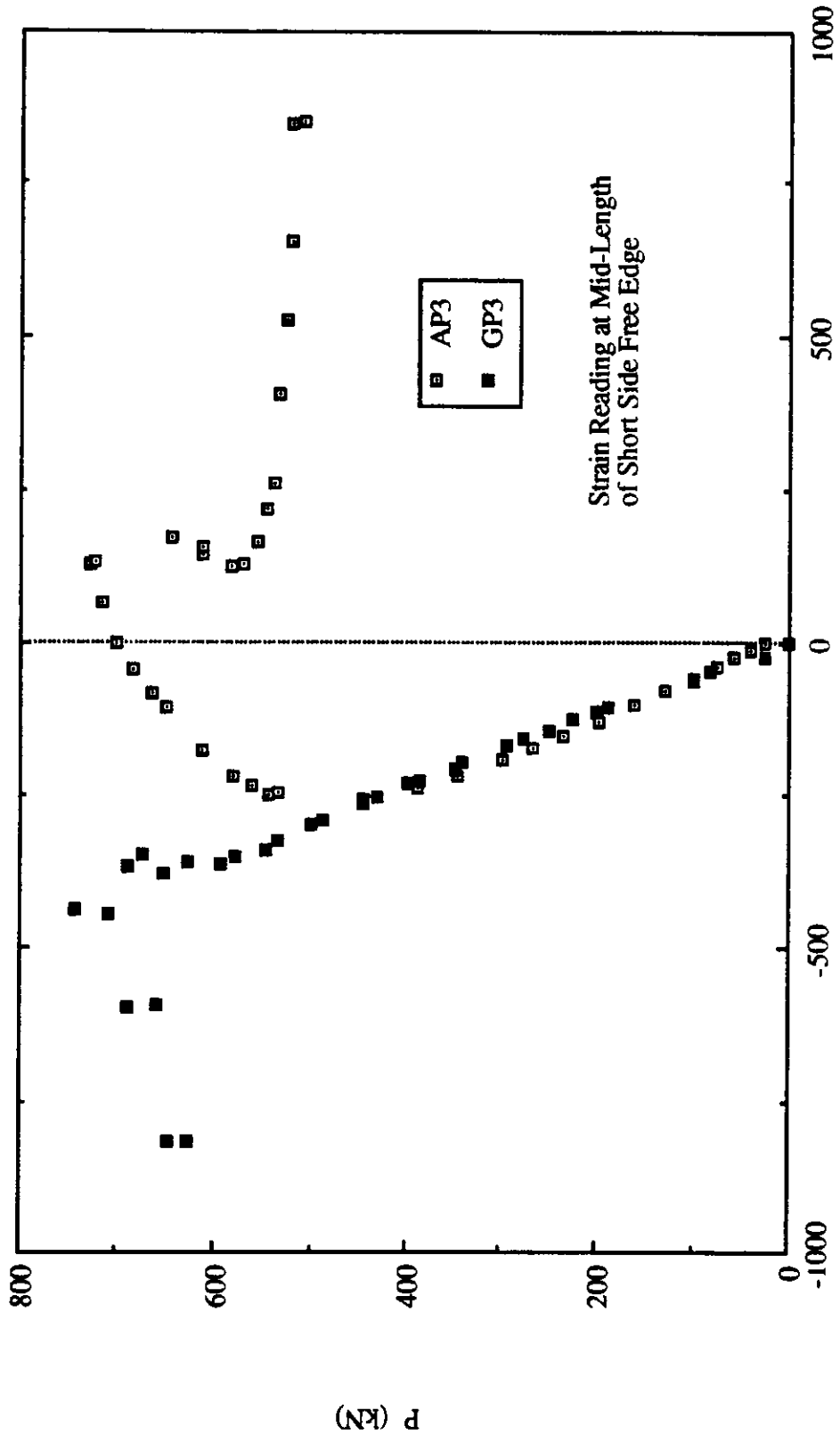

Fig. 8.6 Effects of Brace Angles on the Strain Readings Recorded at the Short Free Edge For Specimens AP3 and GP3

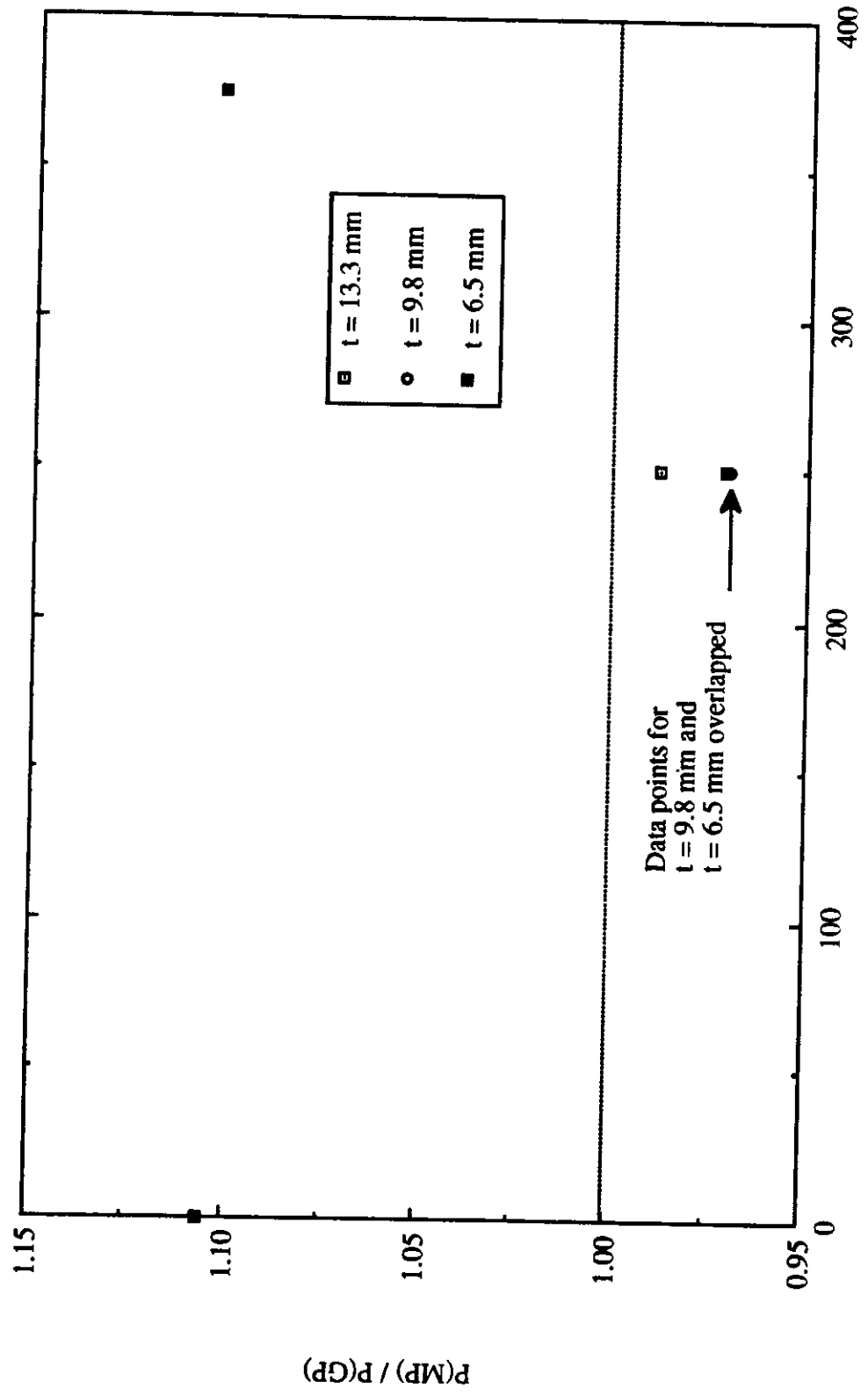

Fig. 8.7 Ratios of the Ultimate Loads of MP Type Specimens to GP Type Specimens vs. Beam Moment

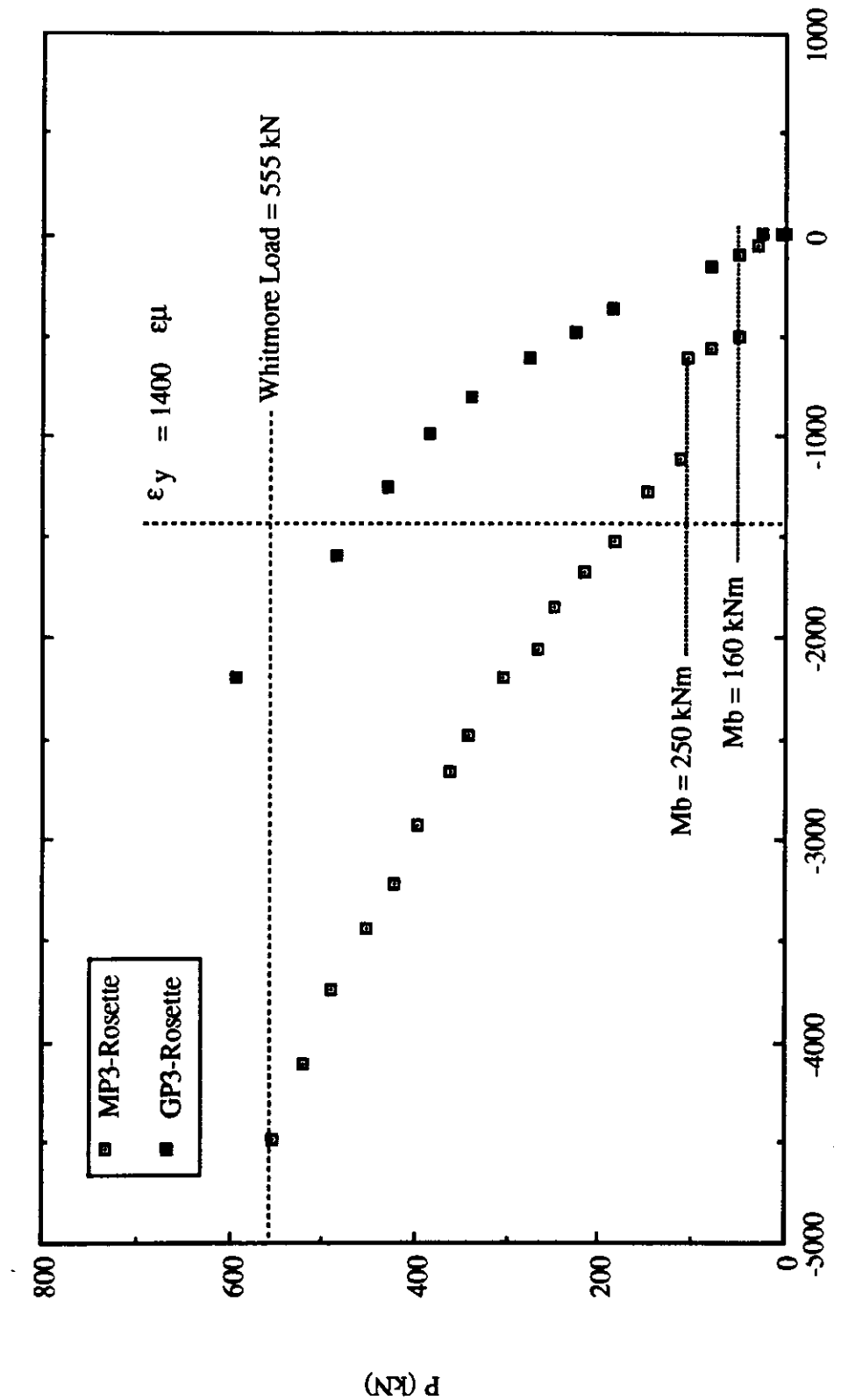

Fig. 8.8 Load vs. Strain Readings at Rosette Underneath the Splice for Specimens MP3 and GP3

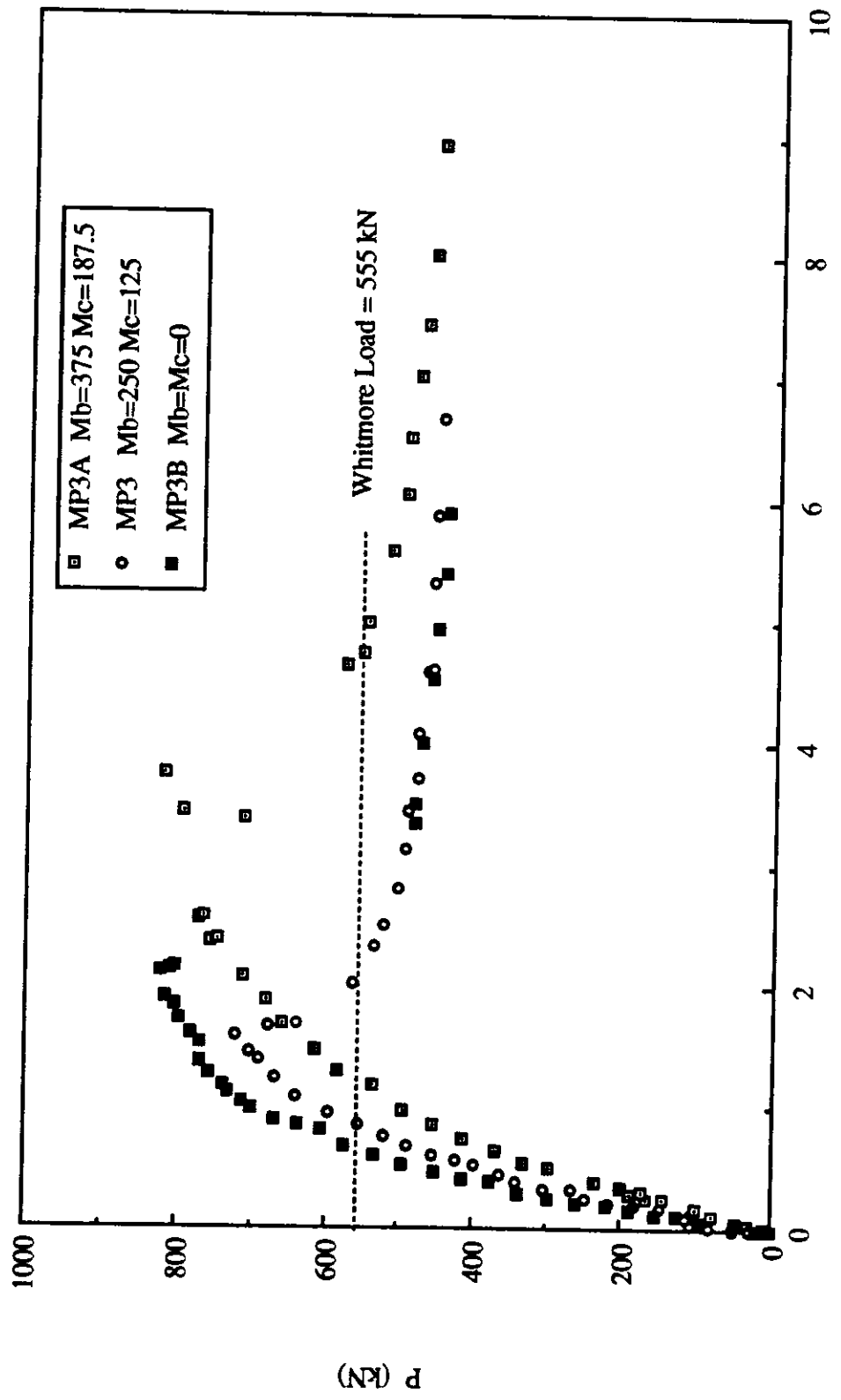

Fig. 8.9 Load vs. In-Plane Deformation Measured at End of Splice for Specimens MP3, MP3A and MP3B

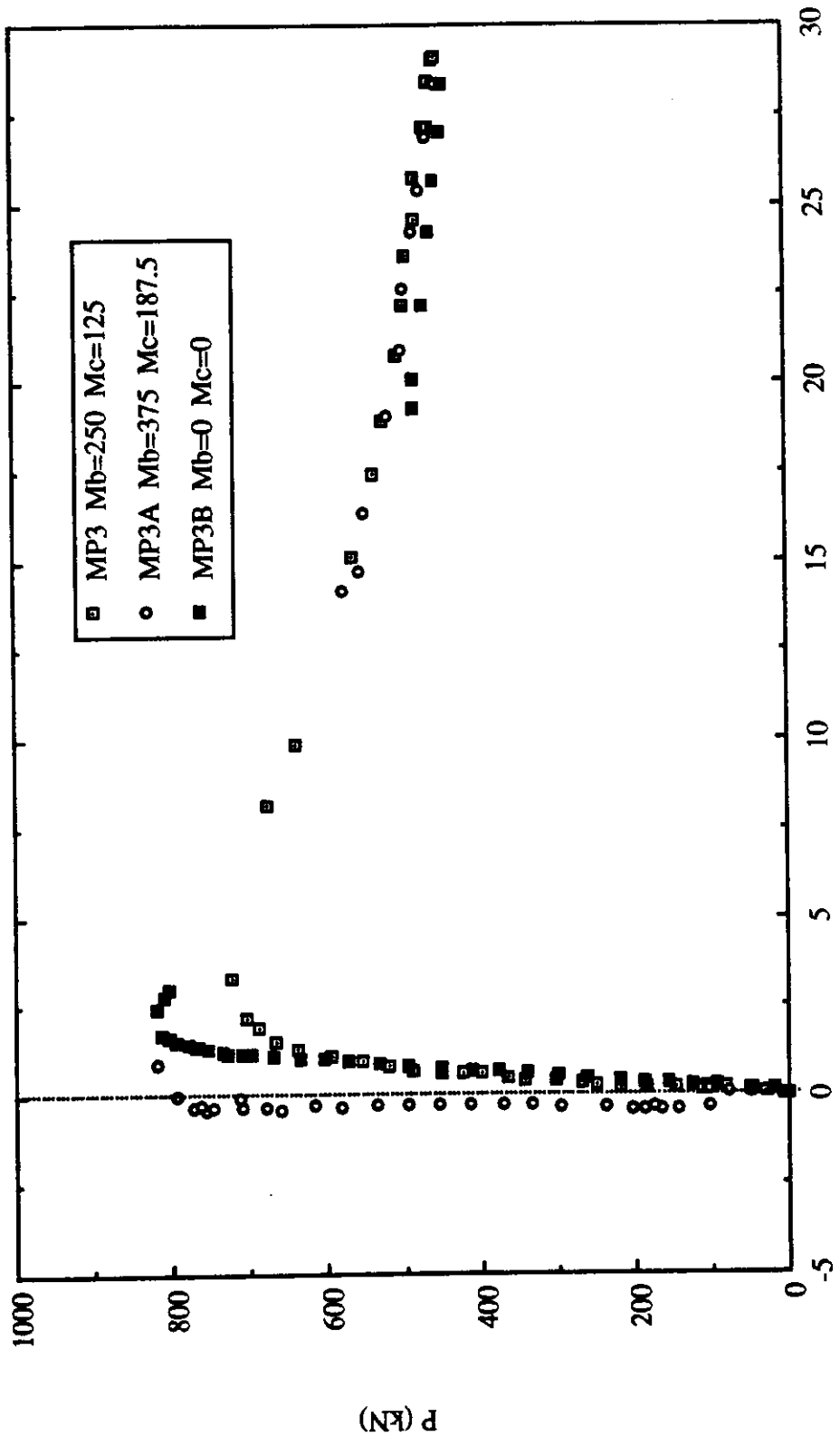

Fig. 8.10 Load vs. Out-of-Plane Displacement at Conjunction of Gusset-to-Splice for Specimens MP3, MP3A and MP3B

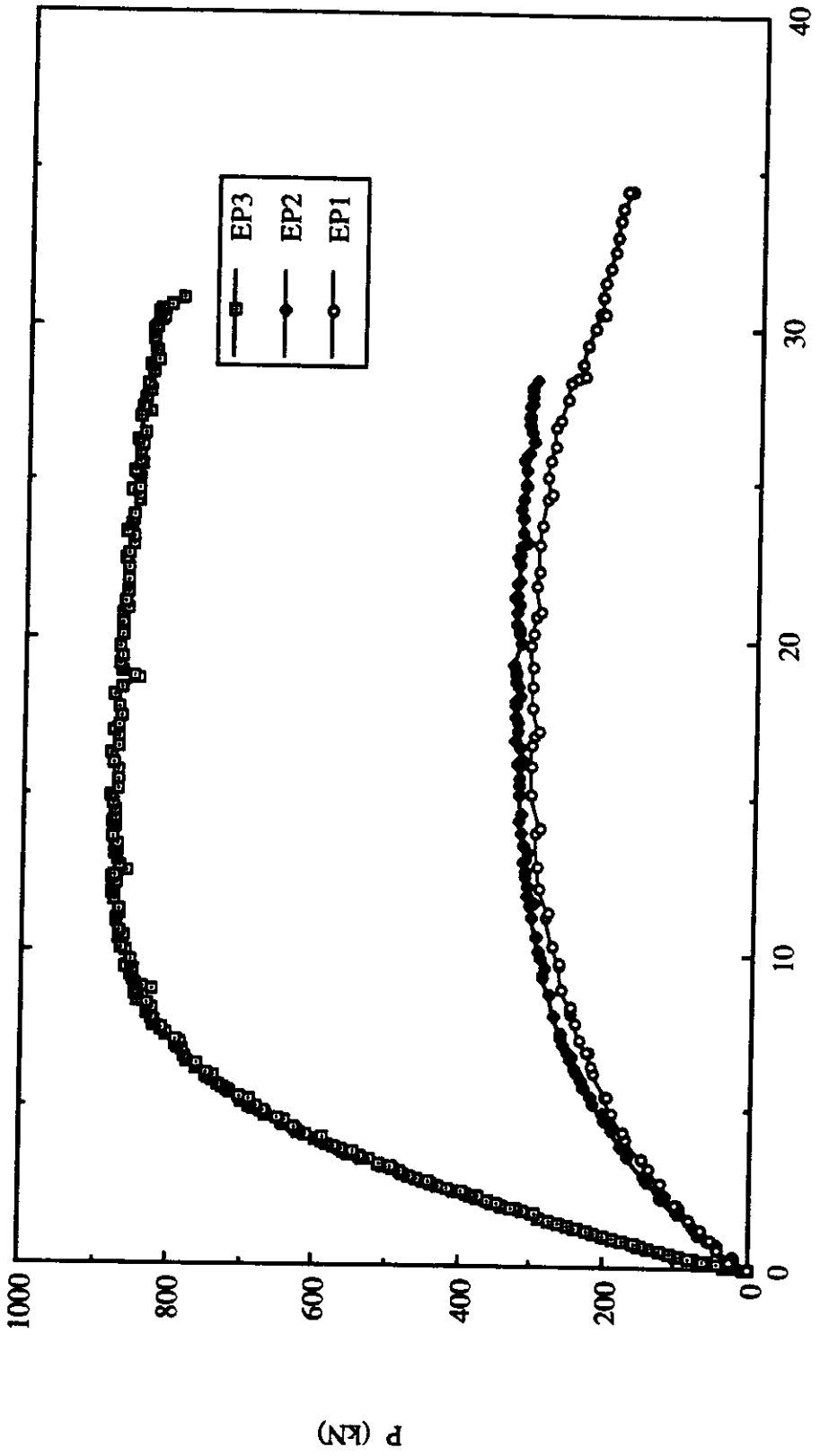

Fig. 8.11 Load vs. Out-of-Plane Displacement of Test Frame for EP Type Specimens

9. Summary and Conclusions

9.1 Summary

Twenty-one full scale tests of the compressive strength of gusset plate connections were conducted on nineteen specimens. The failure mode of the specimens without out-of-plane restraint was sway buckling of the gusset plate connection. However, local buckling of the free edges was observed for the specimens with out-of-plane restraint. For the eccentricity loaded specimens, failure was initiated on the splice member at the conjunction of gusset-to-splice due to excessive yielding. In general, yielding of the specimens was observed prior to reaching the ultimate load. For the specimens except the EP type, yielding was initiated in the plate area underneath the splice and extended first towards the beam and column boundary and finally to the free edges. The load level at which yielding was observed from the specimens agreed quite well with the Whitmore load. However, for the MP type specimens yielding at this region occurred at an early loading stage, which was significantly lower than the Whitmore load level, and tension yielding was observed at the corners of the free edges due to the applied beam and column moment. Plastic hinge mechanism was observed at the splice member of the eccentrically loaded specimens with a 9.5 mm thick splice plate.

The test results showed that the ultimate load of the specimens increased with increasing plate thickness. However, increasing the gusset plate size led to a decrease in the ultimate load of the specimens. The out-of-plane restraint boundary condition had negligible effects on the ultimate load of the compact specimens (500 x 400). However, for the slender specimens (850 x 700) the ultimate load increased when the out-of-plane restraint was applied. The ultimate load of the specimens was also decreased moderately with a 30° brace angle instead of a 45° brace. When comparing the test results of the GP and MP type specimens, it was found that beam and column moment did not affect the ultimate load of

the specimens significantly. However, as mentioned above, early yielding of the plate was observed underneath the splice and tension yielding was recorded at the corners of the free edges. It was also observed that the in-plane stiffness of the specimen decreased with increasing beam and column moment levels. For the eccentrically loaded specimens, increasing the splice plate thickness from 9.5 mm to 13.3 mm did not improve the ultimate load of the specimen appreciably. However, the ultimate load of the specimen increased significantly when a higher flexural stiffness member (tee-section) was used as the splice member (EP3). Nevertheless, the ultimate strength of the eccentrically loaded specimen EP3 was still considerably less than that of the concentrically loaded specimen GP1 which had a similar gusset plate size.

9.2 Conclusions

Based on this experimental investigation, it can be concluded that gusset plate connections subject to compression are susceptible to buckling. Yielding was observed in most of the specimens prior to inelastic buckling. The test results showed that the load carrying capacity of the compact specimens (500 x 400) was not limited to the predictions by either the Whitmore method or the Thornton method. That is, the compact specimens were able to carry additional load beyond the Whitmore load level. Hence, conservative estimate of the strength of the gusset plate can be obtained by the Whitmore method if significant yielding of the plate occurred prior to inelastic buckling. However, for slender specimens which were mainly failed in elastic buckling, Whitmore method may produce unconservative estimate of the strength of the specimens since this method only considers the material strength of the gusset plate. In general, compact specimens were sufficiently stiff to allow load redistribution to occur in the gusset plate such that the ultimate load of the specimens were significantly higher than the predictions by the Whitmore method. Conservative estimates of the strength of specimens were obtained by the Thornton method. Although the Thornton method may not provide the appropriate design model, it

does supply the designer with a stability check of the gusset plate connection. For the eccentrically loaded specimens, the beam-column formula of a rectangular section produced conservative estimates of the strength of specimens.

REFERENCES

AISC, 1986. Load and Resistance Factor Design Specification for Structural Steel Buildings. American Institute of Steel Construction (AISC), Chicago, Illinois.

Bjorhovde, R and Chakrabarti, S.K., (1985). "Tests of Full-Size Gusset Plate Connections." Journal of the Structural Division, ASCE 111(3), 667-686

Cheng, J.J.R., Yam, M., and Hu, S.Z., 1993. "Elastic Buckling Strength of Gusset Plate Connections." Accepted for publication by Journal of Structural Engineering, ASCE.

Chakrabarti, S.K. and Richard, R.M. 1990. "Inelastic Buckling of Gusset Plates." Structural Engineering Review, 2, pp. 12-29.

CSA, 1988. CAN/CSA-S6-88 - Design of Highway Bridges. Canadian Standards Association (CSA), Rexdale, Ontario.

CSA, 1989. CAN/CSA-S16.1-89 - Limit States Design of Steel Structures. Canadian Standards Association (CSA), Rexdale, Ontario.

Davis, C.S. 1967. "Computer Analysis of the Stresses in a Gusset Plate." Thesis presented to the University of Washington, at Seattle, Wash., in partial fulfillment of the requirements for the degree of Master of Science.

Fung, J.Y., and Richard, R.M. 1987. "Inelastic Finite Element Analysis of Gusset Plates." the University of Arizona.

Gaylord, E.H., Gaylord, C.H., and Stallmeyer, J.E., 1992. Design of Steel Structures. 3rd edition, McGraw-Hill, New York.

Gross, J.L. 1990. "Experimental Study of Gusseted Connections." Engineering Journal, AISC, Vol. 27, No. 3, pp. 89-97.

Hardash, S.G. and Bjorhovde, R. 1985. "New Design Criteria for Gusset Plates in Tension." Engineering Journal, AISC, Vol. 22, No. 2, pp. 77-94.

Hardin, B.O. 1958. "Experimental Investigation of the Primary Stress Distribution in the Gusset Plates of a Double Plane Pratt Truss Joint with Chord Splice at the Joint." Bulletin No.49, Engineering Experiment Station, University of Kentucky.

Hu, S.Z., and Cheng, J.J.R. 1987. "Compressive Behavior of Gusset Plate Connections." Structural Engineering Report No.153, University of Alberta.

Irvan, W.G. 1957. "Experimental Study of Primary Stresses in Gusset Plates of a Double Plane Pratt Truss." Bulletin No.46, Engineering Experiment Station, University of Kentucky.

Kulak, G.L., Fisher, J.W., and Struik, J.H.A. 1987. Guide to Design Criteria for Bolted and Riveted Joints. 2nd edition, Wiley-Interscience, New York, N.Y.

Richard, R.M., Rabern, D.A., Hormby, D.E., and Williams, G.C. 1983. "Analytical Models for Steel Connections." Behavior of metal structures, Proceedings of the W.H. Munse Symposium, ASCE, edited by W.J. Hall and M.P. Gaus, 128-155.

Struik, J.H.A. 1972. "Applications of Finite Element Analysis to Non-Linear Plane Stress Problem." Ph.D. dissertation, Department of Civil Engineering, Lehigh University, Bethlehem, Pa.

Thornton, W.A. 1984. "Bracing Connections for Heavy Construction." Engineering Journal, AISC,3rd Quarter, 139-148.

Vasarhelyi, D.D. 1971 "Tests of Gusset Plate Models." Journal of the Structural Division, ASCE, 97(2), 665-678.

Whitmore, R.E. 1952. "Experimental Investigation of Stresses in Gusset Plates." Bulletin No.16, Engineering Experiment Station, University of Tennessee.

Williams, G.C. and Richard, R.M., 1986. "Steel Connection Design Based on Inelastic Finite Element Analysis." Report to the Department of Civil Engineering and Engineering Mechanics, the University of Arizona.

Yamamoto, K., Akiyama, N., and Okumura,T. 1988. "Buckling Strength of Gusseted Truss Joints." Journal of the Structural Division, ASCE, 114(3), 575-590.

Recent Structural Engineering Reports

Department of Civil Engineering

University of Alberta

167. *Elastic Plastic and Creep Analysis of Casings for Thermal Wells* by S.P. Wen and D.W. Murray, May 1990.

168. *Erection Analysis of Cable-Stayed Bridges* by Z. Behin and D.W. Murray, September 1990.

169. *Behavior of Shear Connected Cavity Walls* by P.K. Papinkolas, M. Hatzinikolas and J. Warwaruk, September 1990.

170. *Inelastic Transverse Shear Capacity of Large Fabricated Steel Tubes*, by K.H. Obaia, A.E. Elwi, and G.L. Kulak.

171. *Fatigue of Drill Pipe* by G.Y. Grondin and G.L. Kulak, April 1991.

172. *The Effective Modulus of Elasticity of Concrete in Tension* by Atif F. Shaker and D.J. Laurie Kennedy, April 1991.

173. *Slenderness Effects in Eccentrically Loaded Masonry Walls* by Mohammad A. Muqtadir, J. Warwaruk and M.A. Hatzinikolas, June 1991.

174. *Bond Model For Strength of Slab-Column Joints* by Scott D.B. Alexander and Sidney H. Simmonds, June 1991.

175. *Modelling and Design of Unbraced Reinforced Concrete Frames* by Yehia K. Elezaby and Sidney H. Simmonds, February 1992.

176. *Strength and Stability of Reinforced Concrete Plates Under Combined Inplane and Lateral Loads* by Mashhour G. Ghoneim and James G. MacGregor, February 1992.

177. *A Field Study of Fastener Tension in High-Strength Bolts* by G.L. Kulak and K. H Obaia, April 1992.

178. *Flexural Behaviour of Concrete-Filled Hollow Structural Sections* by Yue Qing Lu and D.J. Laurie Kennedy, April 1992.

179. *Finite Element Analysis of Distributed Discrete Concrete Cracking* by Budan Yao and D.W. Murray, May 1992.

180. *Finite Element Analysis of Composite Ice Resisting Walls* by R.A. Link and A.E. Elwi, June 1992.

181. *Numerical Analysis of Buried Pipelines* by Zhilong Zhou and David W. Murray, January 1993.

182. *Shear Connected Cavity Walls Under Vertical Loads* by A. Goyal, M.A. Hatzinikolas and J. Warwaruk, January 1993.

183. *Frame Methods for Analysis of Two-Way Slabs* by M. Mulenga and S.H. Simmonds, January 1993.

184. *Evaluation of Design Procedures for Torsion in Reinforced and Prestressed Concrete* by Mashour G. Ghoneim and J.G. MacGregor, February 1993.

185. *Distortional Buckling of Steel Beams* by Hesham S. Essa and D.J. Laurie Kennedy, April 1993.

186. *Effect of Size on Flexural Behaviour of High Strength Concrete Beams* by N. Alca and J.G. MacGregor, May 1993.

187. *Shear Lag in Bolted Single and Double Angle Tension Members* by Yue Wu and Geoffrey L. Kulak, June 1993.

188. *A Shear-Friction Truss Model for Reinforced Concrete Beams Subjected to Shear* by S.A. Chen and J.G. MacGregor, June 1993.

189. *An Investigation of Hoist-Induced Dynamic Loads* by Douglas A. Barrett and Terry M. Hrudey, July 1993.

190. *Analysis and Design of Fabricated Steel Structures for Fatigue: A Primer for Civil Engineers* by Geoffrey L. Kulak and Ian F.C. Smith, July 1993.

191. *Cyclic Behavior of Steel Gusset Plate Connections* by Jeffrey S. Rabinovitch and J.J. Roger Cheng, August 1993.

192. *Bending Strength of Longitudinally Stiffened Steel Cylinders* by Qishi Chen, Alla E. Elwi and Geoffrey L. Kulak, August 1993.

193. *Web Behaviour in Wood Composite Box Beams* by E. Thomas Lewicke, J.J. Roger Cheng and Lars Bach, August 1993.

194. *Experimental Investigation of the Compressive Behavior of Gusset Plate Connections* by Michael C.H. Yam and J.J. Roger Cheng, September 1993.